Evaluation of power flow control strategies for heterogeneous battery energy storage systems

Von der Fakultät für Ingenieurwissenschaften
der Universität Bayreuth
zur Erlangung der Würde eines
Doktor-Ingenieurs (Dr.-Ing.)
genehmigte Dissertation

von

M. Sc. Markus Mühlbauer

aus

Furth im Wald

Gutachter: Prof. Dr.-Ing. Michael Danzer (Universität Bayreuth)
Prof. Dr.-Ing. Oliver Bohlen (Hochschule München)

Diese Dissertation ist im Rahmen einer kooperativen Promotion mit der
Hochschule für angewandte Wissenschaften München entstanden.

Tag der mündlichen Prüfung: 02. Februar 2022

Lehrstuhl für Elektrische Energiesysteme
Universität Bayreuth
2022

Abstract

The past decade has seen a rapid transformation of electric power systems in many countries worldwide through integrating renewable energy sources. However, the associated increase in irregular power generation and consumption forces system operators to compensate for resulting power fluctuations. Battery energy storage systems are predestined for integrating renewable energy sources smoothly but demand proper energy management. Research in this area has clearly established that coordinated control is an essential contributor to the reliable operation of energy storage systems and thus the power grid. The development of battery energy storage systems requires operating strategies to efficiently manage the power flow under rapidly and continuously changing power requirements. Therefore, this work aims to identify, quantify, and evaluate the potentials and sensitivities of power flow control strategies for heterogeneous battery energy storage systems in several applications and system designs. Moreover, it aims at developing a versatile power flow control strategy for battery energy storage systems.

The experimental research design was used to analyze the causal relationships between the inputs and the outputs of heterogeneous battery energy storage systems. In this context, a methodological framework was developed that includes a validated simulation model of a battery energy storage system and methods to systematically evaluate and visualize these causal relationships for different power flow control strategies and applications. The results showed that the trade-offs between the target indicators "performance," "efficiency," and "service life" can be quantified accurately. Furthermore, the individual influences of the power flow control strategies and applications on the target indicators were analyzed. It was shown that, for example, a heterogeneous battery energy storage system could influence the service life of the batteries in different ways depending on the applied power flow control strategy. The findings of this work show that the applied power flow control strategy, system design, and application are essential factors to consider when operating heterogeneous battery energy storage systems. These factors influence the resulting power distribution within the system, which is, in turn, a

decisive point for reliable and sustainable operation. In many cases, a trade-off between the target indicators "efficiency" and "service life" was observed, requiring a decision on a more equal or a more individual power-sharing. A more individual power-sharing, for example, might be beneficial in the case of the peak shaving scenario, especially in terms of efficiency. However, this often decreases the service life and demands a premature replacement of a single battery.

Generally, this work contributes to the body of knowledge on power flow control strategies for battery energy storage systems by incorporating a methodological framework for researchers and industries to analyze and develop battery energy storage systems. The benefits gained from the methodological framework address system operator needs across a wide range of different applications. This work focuses, among other aspects, on the successful implementation of the methodological framework for heterogeneous battery energy storage systems. However, most battery energy storage systems are included in higher-level systems, resulting in new challenges to be addressed. A further study could assess the potentials and sensitivities of operating strategies for microgrids or other higher-level systems using the methodological framework of this work.

Kurzfassung

In den vergangenen Jahren hat sich durch die Integration erneuerbarer Energien in vielen Ländern weltweit eine rasche Umgestaltung der Stromnetze vollzogen. Die damit verbundene und zunehmend volatile Stromerzeugung sowie auch der unregelmäßigere Verbrauch zwingen die Netzbetreiber zum Ausgleich resultierender Stromschwankungen. Batteriespeichersysteme sind dafür prädestiniert eine reibungslose Integration erneuerbarer Energien zu gewährleisten, erfordern aber ein entsprechendes Energiemanagement. Forschungsarbeiten in diesem Gebiet haben gezeigt, dass ein koordinierter Betrieb einen wesentlichen Beitrag zur Zuverlässigkeit von Energiespeichersystemen und somit von Stromnetzen leistet. Die Entwicklung von Batteriespeichersystemen erfordert unter anderem Betriebsstrategien zur effizienten Leistungsflusssteuerung bei sich schnell und kontinuierlich ändernden Leistungsanforderungen. Daher zielt diese Arbeit darauf ab, die Potenziale und Sensitivitäten von Betriebsstrategien für heterogene Batteriespeichersysteme in verschiedenen Anwendungen und Systemkonfigurationen zu identifizieren, zu quantifizieren und schließlich zu bewerten. Darüber hinaus verfolgt sie die Entwicklung einer vielseitigen Betriebsstrategie für Batteriespeichersysteme.

Um die Wirkungszusammenhänge von heterogenen Batteriespeichersystemen zu analysieren, wurde ein experimentelles Forschungsdesign verwendet. In diesem Zusammenhang wurde ein methodischer Rahmen entwickelt, der ein validiertes Simulationsmodell eines Batteriespeichersystems und Methoden zur systematischen Bewertung und Visualisierung der Wirkungszusammenhänge bei verschiedenen Betriebsstrategien und Anwendungen umfasst. Die Ergebnisse zeigten, dass die einzugehenden Kompromisse zwischen den Zielindikatoren „Funktionserfüllung", „Effizienz" und „Lebensdauer" genau quantifiziert werden können. Darüber hinaus wurden die einzelnen Einflüsse der Betriebsstrategien, Systemkonfigurationen und Anwendungen auf die Zielindikatoren bewertet. Es konnte gezeigt werden, dass z.B. die Heterogenität eines Batteriespeichersystems je nach verwendeter Betriebsstrategie die Lebensdauer der Batterien unterschiedlich beeinflussen kann. Die Ergebnisse dieser Arbeit legen dar, dass die genannten Faktoren wesentlich auf

einen optimierten Betrieb heterogener Batteriespeichersysteme Einfluss nehmen und für die resultierende Leistungsaufteilung innerhalb des Systems essenziell sind. Die Leistungsaufteilung wiederum ist der entscheidende Punkt für einen zuverlässigen und nachhaltigen Betrieb. In vielen Fällen wurde beispielsweise ein Zielkonflikt zwischen den Zielindikatoren „Effizienz" und „Lebensdauer" beobachtet, welcher folglich eine Entscheidung über eine gleichmäßigere oder individuellere Leistungsaufteilung erfordert. Im Hinblick auf die Effizienz ist im Anwendungsfall der Lastspitzenkappung oft eine individuellere Leistungsaufteilung vorteilhaft. Diese führt jedoch häufig zu einer geringeren Lebensdauer und somit zu einem vorzeitigen Austausch einer einzelnen Batterie.

Insgesamt leistet diese Arbeit einen wesentlichen Beitrag zum aktuellen Wissensstand von Betriebsstrategien für Batteriespeichersysteme, indem sie einen methodischen Rahmen für die Analyse und Entwicklung von Batteriespeichersystemen für Forschung und Industrie bietet. Die Vorteile, die sich aus dem methodischen Rahmen ergeben, können die Anforderungen von Systembetreibern in einem breiten Spektrum unterschiedlicher Anwendungen erfüllen. Diese Arbeit konzentriert sich unter anderem auf die erfolgreiche Umsetzung des methodischen Rahmens für heterogene Batteriespeichersysteme. Die meisten Batteriespeichersysteme sind jedoch Teil eines übergeordneten Systems, wodurch sich wiederum neue Herausforderungen ergeben. Eine nachfolgende Studie könnte die Potenziale und Sensitivitäten von Betriebsstrategien für Microgrids oder andere übergeordnete Systeme unter Verwendung des hier entwickelten methodischen Rahmens bewerten.

Vorwort und Danksagung

Die vorliegende Dissertation entstand im Rahmen meiner Tätigkeit als wissenschaftlicher Mitarbeiter an der Hochschule für angewandte Wissenschaften München in Kooperation mit dem Lehrstuhl Elektrische Energiesysteme der Universität Bayreuth. Finanziert wurde sie aus zwei Forschungsvorhaben des Bundesministeriums für Wirtschaft und Energie sowie dem Bayerischen Wissenschaftsforum (BayWISS). Mein herzlichster Dank gilt Prof. Dr.-Ing. Oliver Bohlen und Prof. Dr.-Ing. Michael Danzer, dass sie mir beide die Chance zur Promotion gegeben haben. Ihr entgegengebrachtes Vertrauen, ihr stetiges Fördern und Fordern sowie ihr reges Interesse an meinen Forschungsthemen trugen maßgeblich zum Gelingen dieser Arbeit bei. Für die zahlreichen Diskussionen, Denkanstöße und nicht zuletzt für die persönliche Weiterentwicklung durch ihren Vorbildcharakter bin ich zutiefst dankbar.

Ein großer Dank gilt Prof. Dr. Herbert Palm für die inhaltlichen und methodischen Impulse. Die Herausforderungen aus einem anderen Blickwinkel zu betrachten und zu diskutieren war stets inspirierend. Ein weiterer großer Dank gilt meinen Kollegen Daniel Goldmann und Florian Ströbl für die hervorragende Zusammenarbeit während den Forschungsprojekten. Es war mir eine große Freude und Ehre in diesen Konstellationen spannende Forschungsfragen zu beantworten und konstruktiv an einer gemeinsamen Sache zu arbeiten. Markus Spielbauer, Fabian Rang, Christian Rosenmüller und Florian Schaeufl möchte ich für die gemeinschaftlichen Projekte und Arbeiten ebenfalls recht herzlich danken. Die enge Zusammenarbeit war sehr wertvoll und den Austausch habe ich immer zu schätzen gewusst. Bedanken möchte ich mich auch bei sämtlichen Co-Autor:innen, Kolleg:innen und Studierenden am Institut für Nachhaltige Energiesysteme in München und am Lehrstuhl Elektrische Energiesysteme in Bayreuth, die in fachlicher Weise durch wertvolle Diskussionen, in den Laboren oder durch Abschlussarbeiten zum Erfolg meiner Forschung beigetragen haben. Abseits der fachlichen Aspekte bin ich auch dankbar, dass ich in München und Bayreuth eine inspirierende und tolle Zeit mit einzigartigen Menschen genießen durfte. Ob bei Festlichkeiten am Institut, bei

Ausflügen in die Bayreuther Innenstadt oder einfach nur beim gemeinsamen Kickern, für den notwendigen Ausgleich war immer bestens gesorgt. Darüber hinaus bin ich auch allen beteiligten Unterstützern sehr dankbar, dass ich einen Teil meiner Promotion an der NC State University in North Carolina, USA verbringen durfte. Diese besondere Zeit leistete einen erheblichen Beitrag für meine berufliche und persönliche Weiterentwicklung.

Zum Abschluss möchte ich mich bei den wichtigsten Menschen, meiner ganzen Familie, bedanken. Ihnen allen möchte ich für den Rückhalt, die bedingungslose Unterstützung und die Nachsicht für den zeitlichen Aufwand einer Promotion danken. Einen besonderen Dank dabei haben meine Eltern verdient, die mich unermüdlich ermutigen meinen eigenen Weg zu gehen und mich in jeder Lebenslage dabei unterstützen, sei es auch noch soweit vom Bayerischen Wald entfernt. Schließlich gilt mein letzter und größter Dank meiner Frau Julia, die mich stets mit ihrem konstruktiven Optimismus motiviert, private und berufliche Ziele zu erreichen.

Markus Mühlbauer
München, Februar 2022

Table of contents

1 Introduction and motivation

The development of battery energy storage systems involves identifying current or potential design and operating strategy gaps and developing methods to resolve these gaps. Research about power flow analysis and control, including design, operating strategies, and failure/protection issues, has clearly established that coordinated control is an essential contributor to the reliable operation of power grids and battery energy storage systems as one crucial part of future power grids. However, there are conflicting views and an overall lack of research regarding how best to manage the power flow in battery energy storage systems in which power requirements are rapidly and continuously changing due to increasing irregular power consumption and generation in the power grid. The research presented in this work aims to identify, quantify, and evaluate the potentials and sensitivities of power flow control strategies for heterogeneous battery energy storage systems since the reliable and sustainable operation of power grids and thus energy systems is becoming more critical for the future. This chapter provides an introduction to the work by first discussing the background and context, followed by the general research problem, the research aims and objectives, the significance, the overall limitations, and lastly, the structure of the dissertation.

In the new global economy, sustainability has become a central issue for several businesses. This dissertation is particularly motivated by connecting sustainability and operating strategies for battery energy storage systems. The three dimensions of sustainability, namely "economic," "environmental," and "social," have been gaining ground since the early 1990s [1]. In terms of battery energy storage systems, these three dimensions will be introduced in this work as a profitable operation of the energy system (economic), conservation of resources (environmental), and stable energy supply for residents (social). The past decade has seen a rapid transformation of electric power systems in many countries worldwide through integrating renewable energy sources. A considerable amount of renewable energy sources is indispensable on the pathway to a sustainable energy supply; however, renewable energy sources require a more flexible energy system

to integrate these technologies [2]. A recent report of the International Renewable Energy Agency (IRENA) [3] confirmed that battery energy storage systems are particularly predestined for providing a more flexible energy system, thus enabling the integration of higher shares of renewable energy sources. According to a review by Hesse et al. [4], lithium-ion-based battery energy storage systems are a promising candidate for several applications in power grids since, for example, different lithium-ion battery technologies provide individual benefits in terms of lifetime, safety, or costs. They stated that a sophisticated energy management system[1] is required to enable optimal system operation and maximize the value of an energy storage system in a given application. Operating strategies, in particular power flow control strategies, for battery energy storage systems have been an object of research in several power grid applications. Comparative reviews on power flow control strategies in different fields have been presented in the literature, such as [5–8]. However, most power flow control strategies focus on specific aspects to be analyzed and optimized [4]. This poses a problem for a system operator that faces the development process of a battery energy storage system since picking the most effective (or even most sustainable) solution is impossible without more profound analysis. As a result, the existing research provides no access to knowledge about causal relationships between the inputs and the outputs of battery energy storage systems when, for example, boundary conditions such as power requirements are subject to change, and sustainable operation should be enabled. Therefore, industries in such environments may find themselves ill-equipped in terms of methodologies to evaluate an adequate solution for their systems and problems.

Following the *Cynefin for engineers framework* [9],[2] these characteristics assign the identified problem to a *complex* problem, requesting a trade-off comparison among possible solutions. In this case, the inputs have to be influenced systematically and outputs have to become perceptible and quantifiable. Figure 1.1 illustrates the described complex problem in terms of battery energy storage system development by showing several input parameters (power flow control strategy, application, configuration), the battery energy storage system as a black-box, and output parameters (technical indicators, economic indicators).

---

[1]for, e.g., coordinated control of multiple battery energy storage systems or the consideration of battery specific parameters, application constraints, etc.

[2]This framework is based on Snowden and Boone's *Cynefin framework* [10].
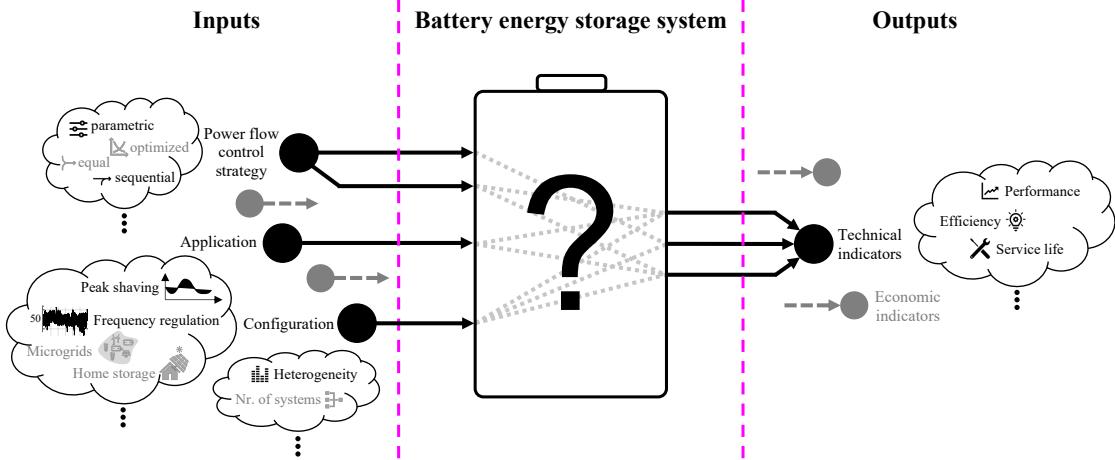
Figure 1.1: Overview of the described complex problem in terms of battery energy storage system development emphasizing the inputs and outputs on which this work is mainly focused (marked in black). Unused inputs and outputs are grayed out.

Given the lack of research regarding battery energy storage system development in terms of power flow control analysis, this work aims to identify, quantify, and evaluate the potentials and sensitivities of power flow control strategies for heterogeneous battery energy storage systems in different applications and several system designs by developing a methodological framework. Furthermore, it aims at developing a versatile power flow control strategy for battery energy storage systems. The objectives of this research are to:

1. determine reasonable input and output parameters,

2. develop a comprehensible, adequate, and validated simulation model of a battery energy storage system, and

3. gain knowledge about the potentials of power flow control strategies for battery energy storage systems and the resulting causal relationships between the inputs and the outputs.[3]

This work contributes to the body of knowledge on power flow control strategies for battery energy storage systems by incorporating a methodological framework for researchers and industries to analyze and develop battery energy storage systems. It will further help close the current research gap in this area and provide real-world value to companies operating in such environments. However, it is

---

[3]considering no complete simulation model that covers all electric, thermal, and aging characteristics of the battery energy storage system, resulting in model uncertainties

beyond the scope of this work to develop a power flow control strategy to gain information on a global optimum for a specific application and system design. Instead, it focuses on the correct setting of existent and proposed power flow control strategies that are parametrizable. Moreover, this work cannot encompass the entire field of possible applications for battery energy storage systems yet aims at achieving generalizability. Therefore, there is no guarantee that the results are fully transferable to other applications without any modifications.

In Chapter 1, the context of this work has been introduced. The research aims and objectives have been identified and the value of such research argued. The limitations of this work have also been discussed. The overall structure of this work takes the form of eight chapters, as shown in Figure 1.2.
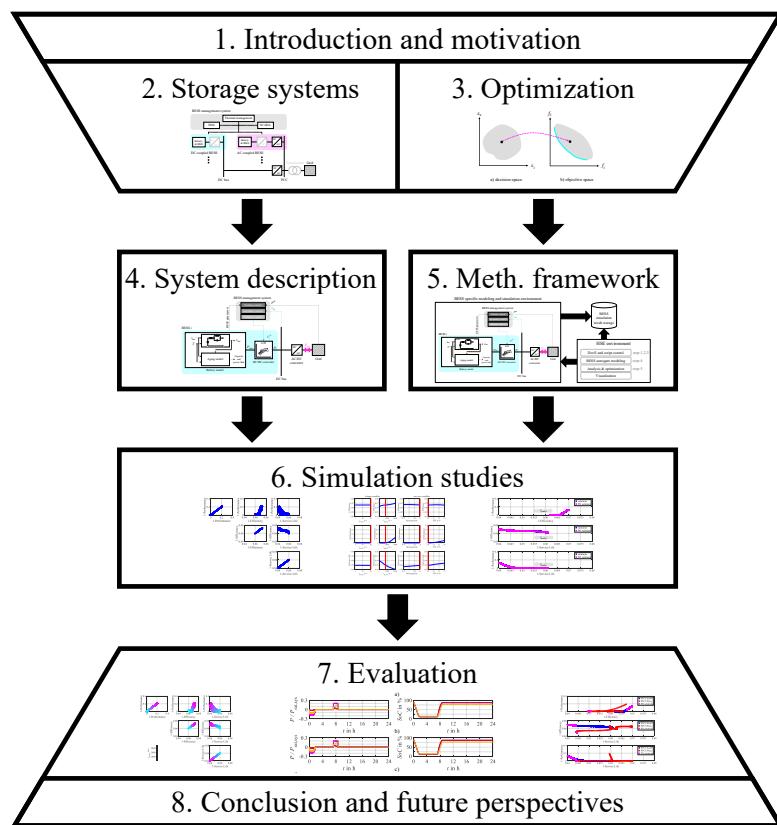
Figure 1.2: Structure of the dissertation "Evaluation of power flow control strategies for heterogeneous battery energy storage systems" emphasizing the chapters.

After the broad introduction and motivation of the research topic, Chapters 2 and 3 narrow down the topic of interest by laying out the theoretical dimensions of the research. Chapter 2 presents the fundamentals and the operation of battery

energy storage systems. In addition, battery energy storage system applications, target indicators, and power flow control strategies are identified and developed. Chapter 3 gives an overview of the fundamentals of multi-objective (black-box) optimization and the state-of-the-art approaches to solving such problems. This chapter closes with the formulation of the research question resulting from the identified research gap.

The fourth and fifth chapters are concerned with the methodology used for this work. Chapter 4 introduces the simulation model of the battery energy storage system used in this work and presents the verification and validation process of the individual submodels. Moreover, a peripheral system, including the validated simulation model, is outlined to solve the multi-objective black-box optimization problem. The fifth chapter describes the methodological framework for evaluating power flow control strategies by introducing a battery energy storage system-adapted toolchain and process flow. This chapter further addresses the implementation of the methods for evaluation and visualization of this work's results.

Chapter 6 presents the simulation studies on power flow control strategies for the two battery energy storage system applications peak shaving and frequency regulation. The results of both applications are shown with regard to the three methods for evaluation and visualization. Then, the simulation studies are summarized by comparing the results of the developed power flow control strategies with the state-of-the-art power flow control strategy.

The evaluation of the power flow control strategies is given in Chapter 7. This chapter discusses the findings in more detail by moving away from the specific presentation of the results to a broader, more general focus. Moreover, it shows how the findings relate to the research questions, fit into the research map, and lastly, affect the latter.

In Chapter 8, a conclusion is drawn, outlining the most important insights and the main contribution of this work. Then a summary is given, reflecting the key elements of each chapter. Finally, the identified limitations of this work and future perspectives are presented in detail.

2 Fundamentals of battery energy storage systems

With regard to the research aim, profound understanding of battery energy storage systems (BESSs) and the operation of them is needed to evaluate power flow control strategies (PFCSs) for heterogeneous BESSs. The necessary fundamentals, therefore, will be outlined in this chapter. An introduction to the basics of BESSs, describing such systems from the top down is given in Section 2.1. The operation of BESSs is then outlined in Section 2.2, providing an overview of applications, target indicators, control concepts, and PFCSs for such systems. Finally, Section 2.3 reveals the limitations in the current research and identifies the challenges to be tackled. It should be noted that the following sections are partly based on my published works [11–14].

2.1 Battery energy storage systems

Research into integrating batteries in grid applications has a long history. However, earlier reviews on BESSs in power systems, such as [15], focus only on lead-acid batteries due to their technical feasibility at that time. Over the past two decades, there has been an increasing amount of literature on other BESS technologies, as several reviews [16–18] over the past fifteen years have shown. According to a recent review by Stecca et al. [18], lithium-ion, sodium-sulfur, lead-acid, and redox flow batteries have become the main battery technologies used in grid applications. The authors further elaborated the performance differences among these battery technologies in terms of costs, energy density, efficiency, power density, and lifetime. They found that especially lithium-ion-based BESSs show high performances comparative to the most relevant battery technologies.

A BESS is typically composed of a battery, including its battery management system (BMS), and optionally a bidirectional inverter, depending on the system

topology (see direct current (DC) coupled BESS and alternating current (AC) coupled BESS). Batteries are built of cells connected in series and/or in parallel forming a module. These modules are then usually interconnected in series to achieve higher voltages which are necessary for grid-scale BESSs. Depending on the grid connection (cf. Section 2.1.1) and the converter topology (cf. Section 2.1.2), an additional bidirectional DC/DC converter or a transformer might be required to match the different voltage levels. DC coupled BESSs are then connected to a common DC bus, while AC coupled BESSs are connected to the point of common coupling (PCC). According to Hesse et al. [4], a BESS management system that controls the overall system often consists of a thermal management, supervisory control and data aquisition (SCADA), and an energy management system (EMS). They describe these components as follows: The thermal management regulates the heating or cooling of the system containment. The SCADA is a part of the general monitoring and the EMS is responsible for the power flow control, energy management, and distribution within the system. It further enables the execution of operating strategies. [4]

A schematic diagram of a BESS with its components indicating a DC coupled BESS and an AC coupled BESS is shown in Figure 2.1. Dashed lines indicate the communication lines and optional components are grayed out.
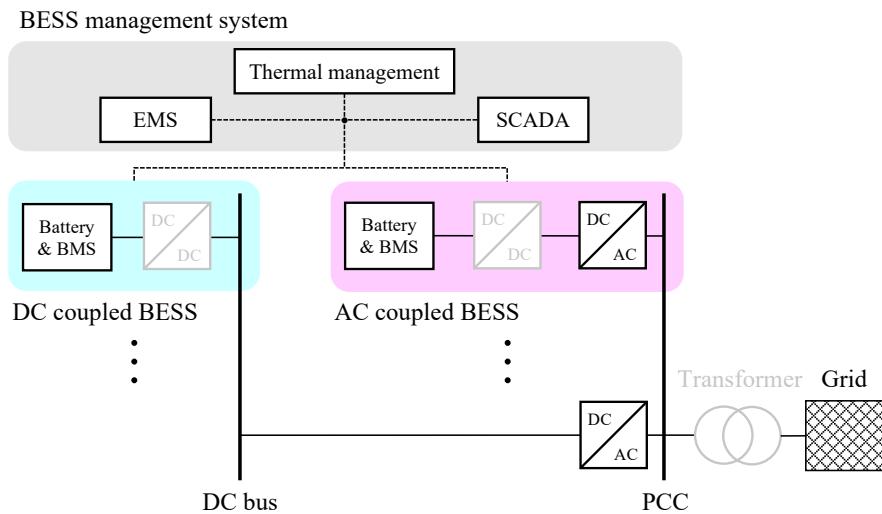

Figure 2.1: Schematic diagram of a BESS indicating a DC coupled BESS and an AC coupled BESS. The BESS management system is often composed of a thermal management, SCADA, and an EMS. Dashed lines indicate the communication lines and optional components are grayed out.

2.1.1 System design

The system design of BESSs is largely dependent on the application and thus on the connection to the specific grid level. While only few BESSs are connected to higher grid levels, such as the transmission grid or the medium voltage (MV) distribution grid, most of the BESSs that are currently installed are connected to the low voltage (LV) distribution grid (0.4 kV AC) [19]. DC voltages of BESSs, on the other hand, are usually below 1 kV due to safety issues during installation and the maximum voltages of commonly used power semiconductor devices [20]. Grid connection topologies are closely linked with the topology of the applied power converters and can be divided into transformer-based and transformerless topologies [21], suggesting the connection to the respective grid level. More specifically, they are either single-stage or double-stage topologies which indicate the structure and thus the number of applied power converters [22]. Figure 2.2 gives an overview of typical grid connection topologies of BESSs comprising batteries, DC/DC converters, DC/AC inverters, transformers, and the grid levels. AC coupled BESSs are marked in pink, DC coupled BESSs in cyan. Topologies a) and d) are single-stage topologies, b) and c) represent double-stage topologies. Each of the four topologies could be either connected to the LV distribution grid (without a transformer) or higher grid levels via a transformer [4, 20].
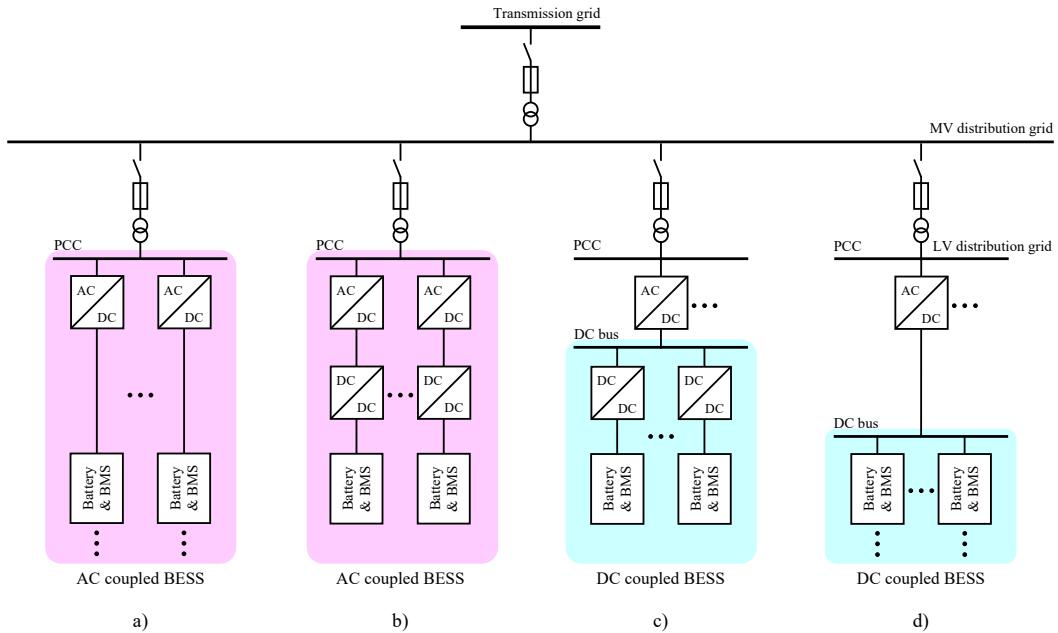

Figure 2.2: Schematic diagram of typical grid connection topologies of BESSs comprising batteries, DC/DC converters, DC/AC inverters, transformers, and the grid levels. Adapted from Bauer [23] and Schimpe et al. [20].

Topologies a), b), and c) benefit from the fact that each string of the BESS can be controlled individually. This allows using the BESS in multiple grid applications simultaneously, and individual strings can be turned off, avoiding operation under part-load conditions [4]. A clear advantage of topology d) is the reduced costs due to fewer power electronics components in the BESS. However, this topology requires matching batteries and uniform operation, as compensating currents can occur, leading to, e.g., enhanced losses. Battery matching is also a problem in topology a). Several batteries have to be connected in series to achieve the necessary voltage level of the inverter. In this case, the weakest battery determines the performance of the whole string, comprising a risk of lower efficiencies and reliability issues [23]. Topology b) and c) suffer from increased costs due to the double-stage topology which requires more power electronics components. Regardless of the topology, galvanic isolation is required at some level to, e.g., control each string of a BESS individually. Furthermore, batteries basically form an isolé-terre (IT) network in which the battery itself has no connection to Earth at all. Galvanic isolation allows preserving the safety concept of a battery that is usually connected to the IT network. Comprehensive comparisons of system designs for BESSs can be found in [20, 22, 24–26].

Batteries, power electronics devices, and consequently BESSs are subject to manufacturing tolerances and dissimilar connections between BESS components. Thus, an entirely homogeneous BESS cannot be guaranteed. However, with an increasing number of second-life electric vehicle batteries becoming available for stationary applications [27], a homogeneous BESS is in some cases deliberately not intended. Batteries with different capacities, power capabilities, or state of health (SoH) are employed in BESSs. This aspect might be challenging, as a heterogeneous system entails a heterogeneous power distribution when it comes to the operation of the BESS [23]. In this case, the operating limits of an individual BESS become more significant and it might be subject to more intense stress, affecting its performance. These aspects will be discussed later in this work. Throughout this work, the term "heterogeneity" is considered the variation of the rated capacity and internal resistance. Although the capacity of an individual battery (as defined in Section 4.4) might be subject to change, the sum of all battery capacities and the total energy of the BESSs remain unchanged by definition in this work.

2.1.2 Power electronics

Power electronics has become a key technology in the conversion of electrical power in various modern applications, such as electric vehicles, renewable energy systems, or (battery) energy storage systems. With the rise of smart grids, power electronics has established its role in power engineering [28]. Research into several fields, including the improvement of semiconductor devices, converter topologies, or digital control techniques, will help to strengthen the role of power electronics by cheaper, more efficient, and more available devices and systems [29].

Fundamental concept

The fundamental principle of a power conversion system is based on the processing of electrical power using a power converter to control the energy flow between a source and a load [30]. An electric power conversion system is composed of a power input port, power output port, and a control input port [31], as can be seen in Figure 2.3.
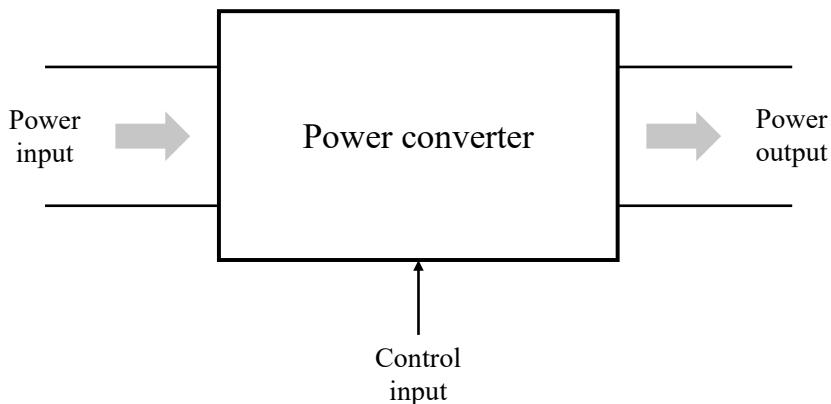
Figure 2.3: Schematic diagram for electric power conversion. Adapted from [31].

Some power systems allow power flow in only one direction (unidirectional), and some allow power flow in two directions (bidirectional). A BESS is a good example for the latter. In this case, the input and output are dependent on the direction of power flow. In general, electric power conversion can be performed in four different ways concerning the power flow: DC/DC, AC/DC, DC/AC, and AC/AC, and is described in [31] as follows: A DC/DC converter converts the input voltage to a smaller or larger output voltage. An AC/DC rectifier rectifies an AC input voltage to a DC output voltage, while each waveform of the voltages may be controlled. In a DC/AC inverter, the input voltage is transformed to an AC output voltage of controllable magnitude and frequency. The AC/AC converter converts the input

voltage to an output voltage, where the magnitude and frequency can be set arbitrarily. [31] Each power converter has to be controlled in every case, regardless of the type of power conversion, aiming to achieve high efficiency and reliability [30, 31]. Depending on the application, either one specific type of power conversion or a combination is required. In BESS applications, for example, a combination of different types of power conversion is needed, as the power flow is bidirectional and different voltage levels are present. Furthermore, the rectifier and converter are often combined in one component, as the function only depends on the direction of power flow. Thus, a suitable power converter topology must be chosen to meet application requirements.

Topologies for BESS applications

BESSs have to adapt their output voltage to the AC voltage level of the grid [32]. Power electronics enable the interconnection between batteries and the grid, using either transformer-based or transformerless topologies [21] (cf. Section 2.1.1). According to Vazquez et al. [32], the topology of the power converter is dependent on the technology and the application. They stated that power converters applied to BESSs have to primarily manage the energy flow bidirectionally to control the charging and discharging process and obtain a high level of efficiency.

In the case of transformer-based topologies, a simple three-phase two-level converter with a transformer constitutes a conventional combination for BESS applications [32]. A review by Wang et al. [21] showed that alternative topologies to the well-established two-level converter had been studied in the literature. These include a three-level neutral-point clamped converter, active neutral-point clamped converter, three-level flying capacitor converter, and five-level converter. In another review, Stecca et al. [18] concluded that such alternative topologies could guarantee better performances concerning efficiency, cost, power density, and reliability than the common two-level converter.

In the case of transformerless topologies, the voltage has to be boosted on the DC side. This can be done by either connecting more batteries in series, adding an additional DC/DC converter stage between the battery and the grid-tied inverter [21], or by directly connecting the batteries to the grid by using cascaded modular converters [33, 34]. Here, the focus is on DC/DC converter stages, as this

topology was applied in this work.[1] The most commonly used topologies are the bidirectional buck-boost converter [35] and the dual-active-bridge converter [36]. However, there are numerous other isolated and non-isolated bidirectional DC/DC converter topologies, e.g., for BESS applications, as a review by Gorji et al. [37] has shown. The two common topologies are illustrated in Figure 2.4.
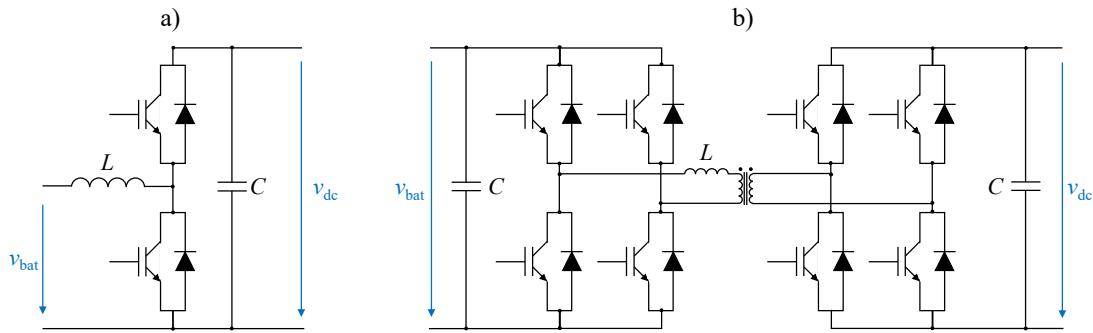
Figure 2.4: Commonly used bidirectional DC/DC converter topologies. a) buck-boost converter with the battery in the low-voltage side (boost), and b) dual-active-bridge converter. Adapted from [21].

As noted by Vazquez et al. [32], large-scale power systems based on transformer-less topologies can be built by connecting several BESS strings in parallel to a common DC bus. The common DC bus is then connected to the grid-tied inverter (cf. Figure 2.2 c)).

2.1.3 Lithium-ion batteries

Prior to the work of Whittingham [38] in the 1970s, the role of rechargeable lithium batteries was largely unknown. Serious discussions emerged when Whittingham demonstrated the first rechargeable lithium-ion battery in 1976 [39] using a metallic lithium anode and a titanium disulfide (TiS_2) cathode. However, this combination revealed numerous challenges, particularly safety concerns due to the hazard of short-circuiting. A few years later, the research group of John B. Goodenough substituted the cathode material in [40] using lithium cobalt oxide (LCO) instead of titanium disulfide. This new approach doubled the voltage and led to an increased energy density. In 1985, the US patent of Yoshino et al. [41] laid the

---

[1]A synchronous buck-boost converter was applied in this work, and the dual-active-bridge converter was used in the *UnABESA* research project. *UnABESA* was a joint project of the partner Bayerische Motoren Werke AG (Coordinator), University of Applied Sciences Munich, Inductron Inductive Electronic Components GmbH, and Munich Electrification GmbH. It was funded by the Federal Ministry for Economic Affairs and Energy (03ET6126B).

foundations for commercial rechargeable lithium-ion batteries by producing the first prototype of a safer and more stable lithium-ion battery. They used carbonaceous materials as the anode and LCO as the cathode in a non-aqueous electrolyte, eliminating the safety problems of metallic lithium. The revolutionary groundwork of all these researchers[2] led to the lithium-ion battery, which is currently used in several applications, such as consumer electronics, electric vehicles, or BESSs.

Fundamental concept

The working principle of a lithium-ion battery is based on the galvanic cell or voltaic cell, respectively, converting chemical energy into electrical energy and vice versa. A lithium-ion battery is composed of two electrodes connected to an electric circuit, the electrolyte, and the separator, as can be seen in Figure 2.5. Electrochemical reactions take place in the two electrodes, namely the anode and cathode. The electrolyte serves as an ionic conductor and simultaneously as an electronic insulator to enable only ionic charge transfer between the electrodes. The separator constitutes a barrier material that impedes the physical (electric) contact of the two electrodes.
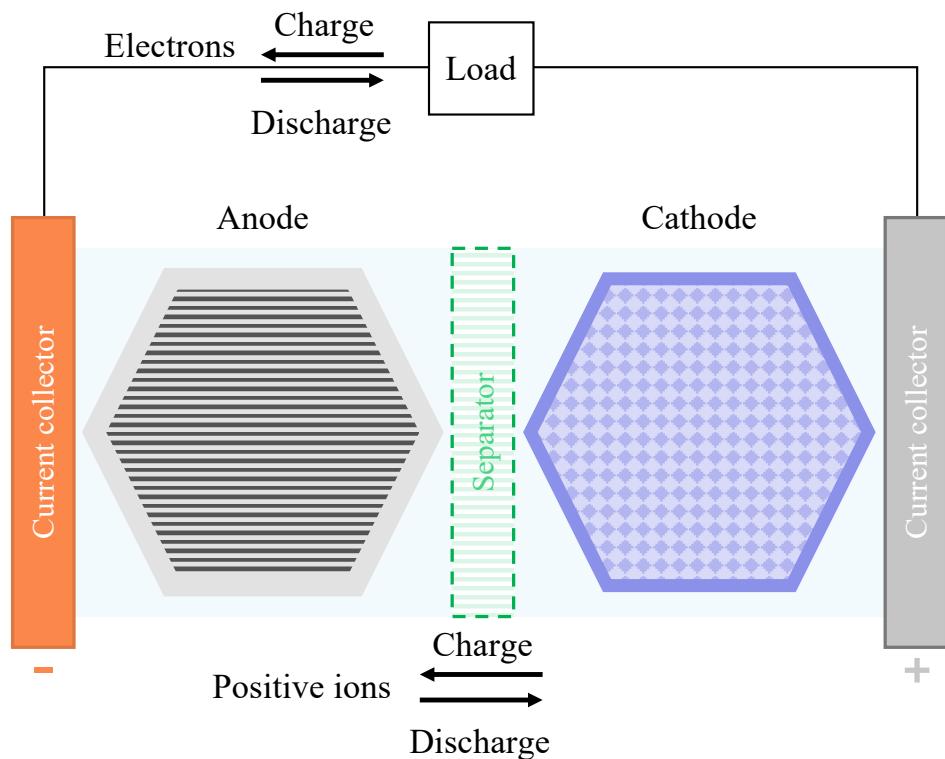

Figure 2.5: Schematic diagram of a lithium-ion battery. Adapted from [42, 43].

[2]Nobel Prize winners in Chemistry 2019

During discharge, the oxidation process at the anode releases electrons into the electric circuit. The remaining positive ions move into the electrolyte and enter the crystal structure of the cathode to compensate for the electron flow. This process is called intercalation. At the cathode, electrons recombine with positive ions, forming neutral lithium atoms. Consequently, the lithium-ion battery discharges its energy through the load, converting chemical energy into electrical energy. For secondary batteries, i.e., rechargeable ones, the electrochemical reactions can take place in reverse order. For a more detailed description of the inner workings of a lithium-ion battery, please refer to [42].

The performance of lithium-ion batteries is strongly dependent on the choice of the materials for all components as, for example, electrical, thermal, or mechanical characteristics are directly affected. In the case of anode materials, carbon-based materials can be found in most lithium-ion batteries due to their impressive electrical and thermal conductivity [44] and the good reversibility of lithium intercalation. Regarding cathode materials, two groups of active materials are considered state of the art due to their high operating voltage and the resulting higher energy storage capability: layered transition metal oxides, such as LCO, lithium nickel cobalt aluminium oxide (NCA), or lithium nickel manganese cobalt oxide (NMC), and polyanion compounds, such as lithium iron phosphate (LFP) [44]. Further information on key technological developments and challenges of lithium-ion battery electrodes can be found in, for example, [45]. Besides electrodes, numerous studies on electrolytes and separators have been conducted to overcome, for example, safety concerns of current lithium-ion batteries. A profound review on state-of-the-art electrolytes can be found in [46] and on recent developments of separators in [47]. Although the described processes and characteristics will not be modeled exactly in this work, they influence the electrical and aging behavior. Therefore, they are important to understand in order to interpret the obtained results in Chapter 6 correctly.

Degradation

Degradation of lithium-ion batteries has been extensively and intensively studied over the past two decades, for example, in [43, 48–51]. In more general terms, a battery degrades both over time (calendar aging) and due to operation loads (cycle aging). Calendar aging represents aging without load. In contrast, cycle aging is described by the number of cycles until the end of a battery's life. The degradation is mainly caused by physical and chemical properties and causes the

two main effects of degradation: capacity fade and power fade [43]. While capacity fade means a reduction in the amount of energy that can be stored, power fade represents a reduction in the power that can be provided due to resistance increase.

The main degradation modes include loss of lithium inventory and loss of active material. Loss of lithium inventory describes the reduction of the amount of cyclable lithium, and loss of active material represents the reduction of available sites for lithium intercalation [52]. The processes and degradation mechanisms responsible for it need to be investigated and understood in order to limit degradation or extend it in time. Degradation occurs mainly at the anode, cathode, and inactive materials, such as the binder, current collector, or separator. However, studying these effects proves difficult because individual effects happen on the same time scales or interact with each other [48]. A graph by Birkl et al. [43] shows the main degradation mechanisms of lithium-ion cells illustratively, as can be seen in Figure 2.6.
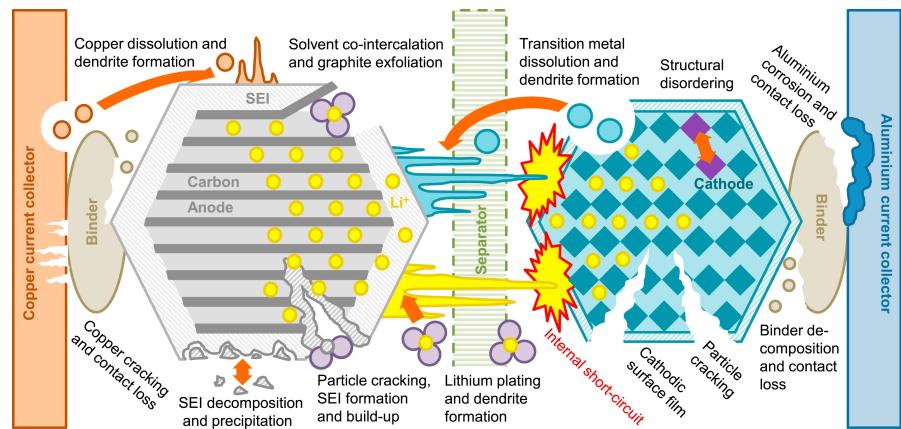
Figure 2.6: Schematic overview of degradation mechanisms in lithium-ion cells (CC BY 4.0 Birkl et al. [43]).

The main degradation mechanisms include solid electrolyte interphase (SEI) formation and lithium plating (all in the anode) [48], loss of active material, electrolyte degradation, and SEI growth (all in the cathode) [51], and decomposition, corrosion, metal dissolution, and electrical or mechanical contact losses (all in the inactive materials) [52]. These degradation mechanisms are subject to complex processes that occur during storage and operation loads and are related to specific degradation variables. A literature review by Dubarry et al. [53] showed that time, temperature, and state of charge (SoC) are considered to be the most crucial degradation variables for calendar aging, regardless of the cell chemistry.

They found that for all chemistries with a carbon-based anode, high temperatures and high SoCs are detrimental in terms of a battery's service life and the capacity loss is mainly driven by the loss of lithium inventory. Another study by Gewald et al. [54] concluded that for cyclic aging, temperature, charge or discharge current, average SoC, depth of discharge (DoD), and charge throughput were found to be the variables with the most substantial influence on degradation. However, the authors stated that controversy on relevant stress factors exists and especially the relevance of the discharge current is controversially discussed in the literature. Different stress factors or combinations of stress factors are applied in the literature depending on the specific battery. They further expressed that the continuous development of lithium-ion batteries makes it impossible to generalize the quantitative effects of the individual stress factors.

Modeling

The reasons for modeling lithium-ion batteries are highly diverse, ranging from design purposes to the optimization and operation of BESSs. Battery models can be evaluated according to their accuracy, computational complexity, configuration effort, and analytical insight [55]. Consequently, the intended purpose of the battery model is the most decisive factor for its selection, meaning that, for example, the most accurate model may not always be the best choice. The existing literature on lithium-ion battery models is extensive and focuses particularly on electrical, thermal, and aging models. Here, the focus is on electrical and aging models for lithium-ion batteries, as both play a vital role in this work. Thermal models would increase the accuracy of the electrical and aging model but are not part of this work to reduce the complexity and computational effort. For more information on thermal modeling of lithium-ion batteries, see the review of Bandhauer et al. [56]. In the case of electrical and aging models, several models have been developed to model the states (mainly SoC and SoH) of lithium-ion batteries. They can be further categorized into three categories relative to their physical interpretation: mechanistic white-box models, phenomenological gray-box models, and data-driven black-box models [57, 58].

White-box models

Mechanistic models, or synonymously electrochemical models, aim at modeling prevailing chemical and physical processes and thus the resulting states inside a battery [58]. For accurate predictions, continuum models that take into ac-

count electrochemical kinetics and transport phenomena are commonly used in this field [59]. An accepted and widely used model for single cells is the pseudo-two-dimensional (P2D) model of Doyle, Fuller, and Newman [60]. It is based on the principles of the porous electrode theory, concentrated solution theory, and kinetics equations [60]. However, the P2D model and some of its variations, such as the single particle model, are typically not real-time capable [61] which constitutes a major drawback for their use in BESS applications. Therefore, simplified P2D models have been proposed in the literature, leading to, e.g., lower computation complexity. An extensive review of simplified P2D models can be found in [61]. In [62], for example, a physics-based (electrochemical) model, including a degradation model, has been used in an energy trading application showing that both an increased revenue and decreased degradation can be achieved by applying such models. However, the models are still computationally more expensive than, for example, gray-box models, and require model parameters that are difficult to extract (cf. Ecker et al. [63, 64]).

Gray-box models

An equivalent circuit model (ECM) consisting of simple electrical elements that represent the dominating electrochemical processes is a common phenomenological (gray box) approach to model a battery's behavior [58]. According to Plett [42], the majority of battery management systems use some form of ECMs due to its simplicity and robustness. However, ECMs vary in their accuracy and computational complexity. Simple models only contain a SoC-dependent controlled voltage source to represent the open-circuit voltage (OCV) and a resistance in series to model instantaneous polarization. By adding resistor-capacitor (RC)-circuits in series, additional polarization effects that develop and decay over time, such as diffusion processes, can be modeled [42]. However, the ambiguity of the individual circuits might lead to a misinterpretation of the effects, even if the terminal behavior is correctly reproduced [57]. The characterization of the elements can take place either in the frequency domain or in the time domain using impedance or pulse measurement.

One approach to model degradation when using gray-box approaches is to keep track of the impedance spectra [65, 66]. The impedance spectra are subject to change over time and due to operation loads, allowing the aging behavior to be concluded. Another approach is to extend the electric model by a separate aging model, as shown in several studies [67–72]. In this case, aging experiments at,

e.g., different temperatures or SoCs are carried out beforehand, providing insights into the capacity fade and resistance increase as a function of time and cycles. Gray-box models are usually implemented by adapting model parameters relative to the current operating point.

Black-box models

Data-driven black-box models take an empirical approach to modeling a battery. They require a large amount of historical, operational, or experimental data, yet no knowledge about the underlying physicochemical processes [58]. A mathematical function of the input-output correlations is trained and provides feedback and predictions of the states of the battery. This approach results in less computational complexity and a low configuration effort. However, this function has mostly no physical significance, meaning that no analytical insights can be provided and no conclusions can be drawn about the underlying cause of a particular behavior. Furthermore, black-box models are not suited for extrapolation beyond the measured data. Several approaches, such as artificial neural network algorithms, fuzzy-logic, or regression algorithms, for data-driven state estimation have been studied and summarized in the literature for both SoC estimation [73] and SoH estimation [74].

Definition of parameters

Most battery parameters are not directly accessible by measurement, as shown in the last subsection. Only the current, voltage, and temperature are measurable. Thus, a proper definition of battery parameters, and particularly non-measurable parameters, is indispensable.

Sign convention

In this work, the battery current i_{bat} is considered positive for charging and negative for discharging the battery. Unlike what was stated in ISO 12405-1 [75], this is in line with the vast majority of scientific works.

Terminal voltage and open-circuit-voltage

The terminal voltage v_{bat} of a battery describes the potential difference measured across its positive and negative terminal under load. If no current is being drawn from the battery for a sufficiently long time, dynamic processes are no longer present. In that case, the OCV of a battery is measured, and the battery is in electrochemical equilibrium.

Battery capacity

Following the definitions of Plett [76], two different definitions of the capacity are used in this work: First, the rated (or nominal) capacity C_{rat} of a battery is defined as a manufacturer-specified quantity (determined by the anticipated application of the cell) indicating the charge a battery is rated to hold. Second, the actual discharge capacity (here C_{act}) is defined as the quantity of charge removed during discharge at a defined temperature, the charging method defined in the data sheet, and a specified and constant discharge current from $100\,\%$ SoC until the terminal voltage reaches the defined cut-off voltage. The unit of both the rated and actual capacity is ampere-hours (Ah).

Coulombic efficiency

The coulombic efficiency η_{c} describes the ratio between the discharge capacity and the charge capacity of a battery resulting from an entire cycle. In [77], the coulombic efficiency was found slightly lower than unity ($\eta_{\mathrm{c}} > 0.98$) for commercial lithium-ion batteries. They further stated that coulombic efficiency becomes closer to unity for decreasing temperatures and at higher C-rates. Therefore, it is defined as equal to unity in this work as enhanced temperatures and very low C-rates will not be the standard case.

C-rate

The C-rate defines the rate at which a battery is charged or discharged relative to its rated capacity [75]. A C-rate of one means that the battery will be entirely charged or discharged in one hour.

Full equivalent cycle

Following the definition of Naumann [78], a full equivalent cycle (FEC) is defined as the ratio of the cumulative capacity throughput to twice the battery capacity.

$$FEC(t) = FEC(t_0) + \frac{1}{2 \cdot C_{\mathrm{act}}} \int\limits_{t_0}^{t_0+t} \eta_{\mathrm{c}} \cdot |i_{\mathrm{bat}}(\tau)| \, d\tau \tag{2.1}$$

In this work, the actual discharge capacity C_{act} is applied, and the cumulative capacity throughput is calculated by the integral of the absolute battery current i_{bat} over the time t. $FEC(t_0)$ is the initial FEC and η_{c} the coulombic efficiency.

State of charge

The SoC is defined in this work using current integration to determine the change in battery capacity over time (coulomb-counting method), as given by

$$SoC(t) = SoC(t_0) + \frac{1}{C_{\text{act}}} \int\limits_{t_0}^{t_0+t} \eta_{\text{c}} \cdot i_{\text{bat}}(\tau) \, d\tau \, , \qquad (2.2)$$

where $SoC(t_0)$ is the initial SoC, t the current time, η_{c} the coulombic efficiency (which is equal to unity), and C_{act} the actual discharge capacity.

Depth of discharge

The DoD refers to the amount of charge added to or removed from the battery in relation to the actual capacity. In particular, the DoD as used for the aging model is defined as the absolute difference between the SoC at the beginning of a charging or discharging process (SoC_{start}) and the SoC at the end of the identical charging or discharging process (SoC_{end}). Thus, the DoD is recalculated in the event of a change of sign and is valid for a monotonic charging or discharging process.

$$DoD = |SoC_{\text{start}} - SoC_{\text{end}}| \qquad (2.3)$$

2.2 Operation of battery energy storage systems

The economic, environmental, and social benefits of a BESS are primarily dependent on an optimal design and operation. Efficient operation, multi-level collaborative optimization control, and the achievement of multiple objectives are essential goals in the future development of centralized or distributed BESSs [8]. The operation of BESSs concerns a variety of different aspects, such as applications, objectives of the operator, control concepts, and operating strategies. The following subsections provide information about the state of the art of these aspects and improvements undertaken in the course of this work.

2.2.1 Applications

The selection of suitable BESS applications contributes significantly to the evaluation of PFCSs for heterogeneous BESSs. BESS applications can be identified at various sites in the electricity grid. According to a study by Fitzgerald et al. [79], the value proposition of BESSs is dependent on where they are deployed and the

respective stakeholders. Thus, they divided the grid into three levels for BESS deployment: transmission level, distribution level, and behind the meter (cf. Section 2.1.1). The authors further identified three main stakeholder groups: customers, system operators, and utilities, and described their benefits as follows: Customer services provide benefits to end-users in monetary form when the BESS is deployed behind the meter (e.g., time-of-use bill management). Simultaneously, benefits are provided to system operators as the demand side is much easier and less costly to match up with the generation side. System operators further benefit from ancillary services, such as regulating the frequency or voltage required to ensure grid stability. BESSs are capable of providing these ancillary services. Utility services help utilities to a) defer investments in transmission and distribution infrastructure and b) meet system peaking requirements on a day-to-day basis. [79] Figure 2.7 gives an overview of BESS applications with respect to stakeholder groups.
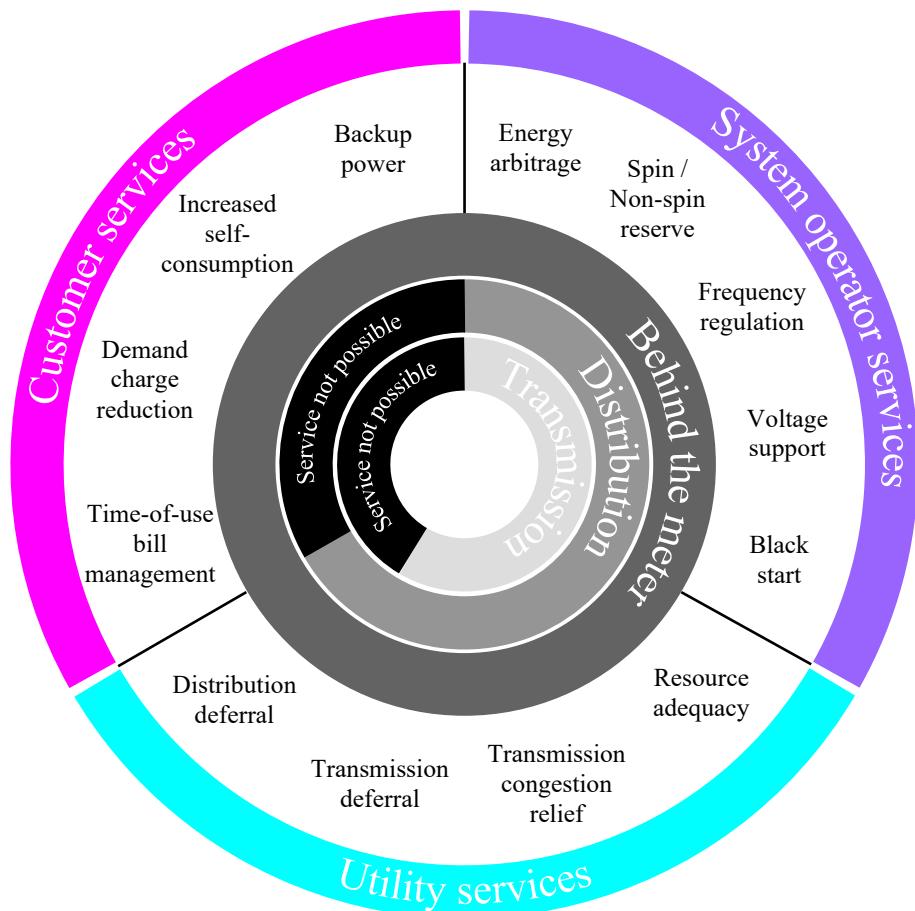

Figure 2.7: BESS applications with respect to stakeholder groups. The circles indicate the range of individual services considering the stakeholder (outer ring) and the grid level (inner rings). Adapted from [79].

BESSs can provide a wide range of individual services to meet the interests of the stakeholders, as shown in the figure. However, only some of them are technically and economically attractive in a standalone application [79, 80]. Therefore, the focus is on two common BESSs applications: peak shaving and frequency regulation.

Peak shaving is one form of time-of-use bill management. Commercial and residential customers reduce the power drawn from the grid by using BESSs during times of peak demand to reduce the demand charge component of the electricity bills [80]. A considerable amount of literature has been published on sizing, evaluating, and managing BESSs for peak shaving applications. By focusing on control strategies, in [81] for example, a peak shaving algorithm in combination with a continuous battery peak power estimation algorithm for a BESS is proposed. Tests on a real-time microgrid (MG) suggested that the proposed algorithm allows limiting power exchanges between the MG and the grid. Uddin et al. [82] introduced an algorithm for peak load management, facilitated by BESSs, and tested it in a real MG. The results showed that substantial savings could be achieved for MG utility while reducing the peak demand of the MG. An extensive review of peak load shaving strategies can be found in [83].

Frequency regulation services, on the other hand, deal with grid stability issues by keeping the frequency of the grid within an acceptable tolerance band [80]. In this case, an immediate and automatic response to frequency deviations is required to match demand and generation [79]. Much of the current literature pays particular attention to the operation of BESSs for frequency regulation services. In [84], the impact of operation strategies on different parameters, such as FEC or SoC, was investigated in a case study for a 2 MWh BESS under the German regulatory framework. Optimization methods are suggested to ensure the BESS's operability during primary control supply. Stroe et al. [85] investigated from a battery lifetime perspective the suitability of five strategies for frequency regulation. The results showed that depending on the control strategy, different success ratios and expected lifetimes occurred. In [86], a profit-maximizing BESS control strategy with a focus on both the frequency regulation and SoC recovery phase is proposed. Findings suggest that the proposed control scheme is optimal and the runtime complexity is low. A review of frequency control in future power systems is provided by Obaid et al. [87].

In a joint publication [88], a method was presented to generate and analyze standardized BESS load profiles. These profiles relate to a self-consumption increase, peak shaving, and frequency regulation service. Based on the approaches presented in [88], two artificial application-oriented profiles for peak shaving and frequency regulation were generated within the scope of this work. These profiles are shown later in Figure 4.6.

The artificial peak shaving profile was derived from the German standard load profile G0 and covered an operating period of one day with a 15 minute sampling time. In order to obtain a higher resolution (one second) and a more realistic load profile, its values were interpolated in the first place and then replaced by random numbers at equidistant intervals. Arbitrary values remained inside the standard deviation of 0.0025 of the normal distribution with a mean of the interpolated value. Then, the load profile was normalized to the maximum value and transformed into a profile suitable for BESS applications. For this reason, the peak load time window defined by the respective distribution system operator in Germany was extracted,[3] a threshold for peak shaving was selected, and the remaining profile was set to zero. The user could select the free parameters of the profile: the amplitude, energy throughput, peak shaving threshold, and the time and intensity of the recharging. Thus, both technical and time factors were adjustable. The profile was characterized by a high energy throughput between sign changes and long resting periods, resulting in only a few sign changes.

The profile for the frequency regulation service was derived from frequency measurements (December 2018) in Munich. The measurement data covered one day and was on a per-second basis. The frequency profile was decreased by the nominal frequency of $50\,\mathrm{Hz}$ and normalized to the maximum value. For reasons of simplicity, the desired power follows the normalized frequency deviation. In this case, the user can only manipulate the amplitude. This profile is characterized by many sign changes and a low energy throughput between sign changes.

The artificial application-oriented profiles are considered scenarios and constitute one part of the use case. Throughout this dissertation, the term "use case" will be used to refer to a combination of a specific BESS application and a specific system design.

---

[3]The peak load time window depends on the season and the distribution system operator. It refers to a forecast period in which the loads are highest and is calculated by the respective distribution system operator.

2.2.2 Target indicators

Target indicators are figures designed to reflect the current status of a BESS. With the aim of evaluating PFCSs in BESS applications, quantitative target indicators are required. Target indicators for BESSs should follow the widely accepted "SMART criteria," introduced by Doran [89] as a guide for setting objectives in management processes. In the figurative sense, target indicators for BESSs should be specific, measurable, assignable, realistic, and time-related when following his statements. Here, the target indicators should additionally represent the three dimensions of sustainability: social, economic, and environmental, as described in Chapter 1. Therefore, three target indicators, namely "performance," "efficiency," and "service life" are applied in this work and have already been introduced in a previous collaborative work [90].

The performance criterion (PE) indicates the fulfillment of the power requirements and provides information on the operating times of the BESS. It assesses the difference between the requested and the supplied energy. In terms of sustainability, it represents the stable energy supply for residents (social benefit) and is defined as

$$PE = 1 - \frac{\int (|P^*(t) - P_{\text{sys}}(t)|)\, dt}{\int |P^*(t)|\, dt} \, , \qquad (2.4)$$

where P^* is the requested power from the grid and P_{sys} the output power of the system. The limits of integration are the start point and endpoint of the simulation or operation.

For most applications, a system would be designed and operated in a way to achieve full performance. However, in home storage applications, for example, a performance of less than one might also be reasonable as the main goal is to enhance the self-sufficiency. A system where $PE = 1$ indicates an uninterrupted operation of the BESS. However, limitations such as rounding errors or latencies have to be considered in real applications. Obviously, the performance criterion would not be a distinctive indicator in cases of a full performance. Instead, parameters correlated with the system size or the application can be varied to find the minimum system size or maximum amplitude at which full performance can be achieved.

The efficiency criterion (η_{rt}) shows the round-trip efficiency η_{rt} of the system to evaluate the system's lost energy. It aims to indicate a profitable operation of the energy system (economic benefit) and is defined as follows:

$$\eta_{\text{rt}} = 1 - \frac{\int (P_{\text{sys}}(t) - P_{\text{bat}}(t))\,dt}{\int P_{\text{ref}}(t)\,dt} \quad \text{with} \quad P_{\text{ref}}(t) = \begin{cases} P_{\text{sys}}(t) & \text{for} \quad P^*(t) \geq 0 \\ |P_{\text{bat}}(t)| & \text{for} \quad P^*(t) < 0 \end{cases} \tag{2.5}$$

P_{bat} constitutes the output power of the battery, P_{sys} the output power of the entire system, P^* the requested power from the grid, and P_{ref} represents a variable that changes with respect to the operation mode. The target indicator considers the losses of each battery and each converter stage inside the system. The limits of integration are again the start point and the endpoint of the simulation or operation. Definitions of the performance and efficiency criteria might look similar but apply to two distinct target indicators. A system with high power losses will have a poor efficiency but still covers full performance if it is sufficiently oversized. For underdesigned systems, the two criteria might correlate but are affected differently by the PFCS.

The service life criterion (SL) represents a battery's estimated remaining life before reaching a defined end-of-life (EOL) criterion. Conservation of resources (environmental benefit) is paramount for this indicator, which is formulated as follows:

$$SL = 1 - \frac{Q^*_{\text{loss}} - \int q_{\text{loss,min}}(t)\,dt}{Q_{\text{loss,max}} - \int q_{\text{loss,min}}(t)\,dt} \quad \text{with} \tag{2.6a}$$

$$Q^*_{\text{loss}} = Q^{*\text{cal}}_{\text{loss}} + Q^{*\text{cyc}}_{\text{loss}}, \tag{2.6b}$$

$$Q_{\text{loss,max}} = BOL_{\text{C}} - EOL_{\text{C}}, \tag{2.6c}$$

$$q_{\text{loss,min}} = q^{\text{cal}}_{\text{loss,min}}(T, SoC, t^*), \tag{2.6d}$$

where Q^*_{loss} is the accumulated value of the differential capacity losses of both calendar and cycle aging, $Q_{\text{loss,max}}$ is the maximum permitted capacity loss defined by the beginning-of-life (BOL) and EOL criteria, $q_{\text{loss,min}}$ is the minimum differential capacity loss due to calendar aging, BOL_{C} is the initial capacity of a battery at BOL, and EOL_{C} is the remaining capacity at EOL. Note that all pa-

rameters are normalized to the initial capacity. Thus, Equations (2.6a)–(2.6d) are expressed per unit. The limits of integration are also the start point and endpoint of the simulation or operation. It should be further noted that the target indicator "service life" could be considered differently. One way is to take into account all batteries' accumulated service life (i.e., the accumulated capacity loss as shown in Equation (2.6a)). This means the overall deterioration of the BESSs should be minimized, which could lead to premature replacement of a single BESS. Alternatively, only the most degraded battery is decisive for the service life criterion. This might lead to a more balanced deterioration among the BESSs, presumably leading to longer service intervals. The first alternative was implemented in this work, as this constitutes a more critical assessment of the service life.

The introduced target indicators follow the "SMART criteria" as mentioned previously. The target indicators serve a specific purpose (specific), indicate the current status of the BESS (measurable), specify which BESS is affected (assignable), indicate what realistically can be achieved using a specific PFCS (realistic), and provide feedback at any time (time-related). Additionally, the target indicators reflect the three dimensions of sustainability, as previously mentioned. Even if these target indicators are somewhat technical, economic target indicators could be derived if necessary. For example, these could be penalties for non-fulfillment of performance requirements, lost revenues through energy losses, or maintenance costs caused by enhanced degradation of the components. However, economic target indicators depend on many legal conditions, some of which are outside the system operators' scope of action and are thus not considered in this work.

2.2.3 Control concepts

The control concepts presented in this subsection are usually from other engineering areas, such as control engineering. In recent years, however, several researchers have also repurposed these concepts in fields of modern power systems like smart grids or MGs, as reviews have shown [5, 91–94]. The operation of an MG or BESS using such control concepts can be realized by operating the interfacing power converters properly [93]. However, the selection of an appropriate control concept for a BESS depends on its topology and the application. Figure 2.8 gives an overview of basic control concepts, namely centralized, decentralized, and distributed control. Dashed lines indicate the communication lines.
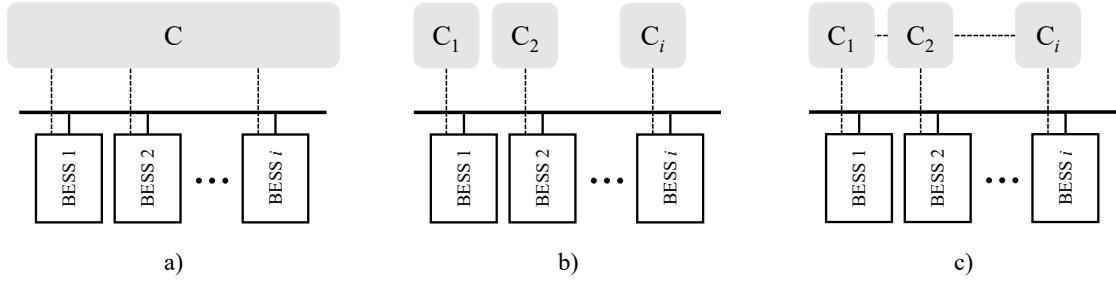
Figure 2.8: Overview of basic control concepts. a) centralized, b) decentralized, and c) distributed. Dashed lines indicate the communication lines between the BESSs and the controllers (abbr. C). Adapted from [93].

In the context of MGs, or more specifically BESSs, these three control concepts, their advantages and their disadvantages can be described as follows: Centralized control (a) describes a control concept in which a central controller collects and processes data sent from BESSs and transmits information back to them [94]. While a clear advantage of this concept constitutes strong observability and controllability, it suffers from reduced reliability, flexibility, and expandability [93]. Decentralized control (b) provides no communication link between the individual BESS controller, and BESSs are controlled rather by their own local variables [94]. This has the advantage of simplicity and independence from communication technologies but is limited in its performance due to the lack of information from other BESSs [92]. Distributed control (c) combines the concepts of centralized and decentralized control. As indicated in Figure 2.8, BESSs communicate only with their neighbors through communication lines, sharing important information in order to achieve coordinated control among all BESSs [93]. In case of a failure, the systems remain fully functional [92]. However, one main challenge is to achieve the consensus to fulfill, e.g., optimization objectives [93].

With MGs becoming more important in the 2000s, in 2009, Guerrero et al. [95] proposed a general approach towards standardization: a general hierarchical multi-level control for DC and AC MGs. This constitutes a special form of control concept and has gained much attention in the literature. The hierarchical control can be implemented to either replicate a centralized, decentralized, or distributed control concept. According to Guerrero et al. [95], the hierarchical multi-level control is divided into three levels: primary, secondary, and tertiary control, and interacts as follows: Primary control adjusts the voltage reference provided by upper-level controllers to local parameters, such as those for the inner current and voltage con-

trol loop. As a result, it enables the parallel operation between the converters and improves the dynamic performance of the output voltage. However, this yields a load-dependent voltage deviation. For this reason, secondary control appears on top of primary control and restores the load-dependent voltage deviation by sensing and comparing the actual voltage level with the voltage reference. The compensation of the resulting voltage error is done via a controller and ensures that the system is operated within its approved operating limits. Tertiary control appears on top of all control levels and manages the power flow. [95] At this level, the PFCSs are usually implemented.

2.2.4 Power flow control strategies

In general, power-sharing defines how the requested power of the grid will be distributed among the BESSs. The calculation of the power-sharing within the system can be expressed as shown in Equation (2.7) regardless of the applied PFCS. It varies according to the power-sharing factor α.

$$P_i^* = P^* \cdot \alpha_i \,, \tag{2.7}$$

where P_i^* is the desired output power of the ith BESS and P^* is the requested power from the grid. It should be noted that for the power at the battery's input, the efficiency of the converter stage must be considered. Moreover, each α_i ranges between zero and one, whereby the sum of all power-sharing factors equals one.

However, two special cases exist when implementing Equation (2.7). First, the system's maximum output power might be lower than the requested power. In this case, P_i^* is calculated as stated in Equation (2.7) but only the maximum output power of the respective BESS is provided. Second, in the case of reaching a battery's limit, the maximum output power of one BESS could be lower than the calculated share even if it is within the nominal power limits. This means the system output power is reduced accordingly. As a remedy, some PFCSs redistribute the power, forcing other BESSs to take over a larger share. In both cases, the output power of a BESS is calculated as follows:

$$|P_i| = \min(|P^*| \cdot \alpha_i, |P_{\max,i}|) \,, \tag{2.8}$$

where P_i is the output power of the ith BESS and $P_{\text{max},i}$ is the maximum output power of the respective BESS (regardless of the operating mode) when battery limits are reached.

PFCSs for an efficient and reliable operation of BESSs have been widely studied in several fields of BESS applications, such as MGs, grid applications, or electric vehicles. They aim to meet certain requirements given by, e.g., the application or the system operator. The existing literature on PFCSs is extensive and has revealed that different levels of implementation effort and operating parameters can be identified. Consequently, PFCSs can be classified into three distinctive categories, namely *static*, *dynamic*, and *optimization-based* PFCSs, as previously mentioned in a collaborative work [90].

Static PFCSs apply constant power-sharing factors during operation and are based on nominal values of the battery, e.g., the number of utilized BESSs or the rated capacity of these. In terms of complexity, computing power, and implementation effort, static PFCSs are the most straightforward approach. *Dynamic* approaches, in contrast, adapt power-sharing factors during operation, yielding a more efficient operation. Battery state variables, such as SoC or available energy/power, can be considered, and the implementation effort is nearly as low as for static PFCSs given that the state variables are available. Power-sharing factors of *optimization-based* PFCSs are changing during operation relative to the output of a specified objective function. Several optimization methods can be applied and specific optimization goals can be addressed. However, in terms of complexity and computing power, optimization-based PFCSs are costly.

Only a few studies on static PFCSs can be found in the literature. Jiang and Dougal [96], for example, presented a static PFCS for active power-sharing among multiple battery branches in which the charging currents were equally distributed. In my published work [11], two static PFCSs were applied to analyze different PFCSs in heterogeneous BESSs systematically. The first one shares the requested power relative to the number of utilized BESSs and the second one takes into account the rated capacity.

A common dynamic PFCS in the field of MGs is to balance the SoC of participating BESSs, ensuring a reliable and coordinated operation [93]. There is a large volume of published studies [97–108] describing the role of SoC balancing in MGs

by using the well-known droop method. This method is based on the concept of changing the droop coefficients of the interfacing DC/DC converters according to the respective SoCs of participating BESSs. Besides the standard droop method, Ali et al. [109] proposed a dynamic coordinated control strategy that takes into account the SoC, SoH, and capacity of the batteries, aiming to improve battery life. Apart from the research area of MGs, dynamic PFCSs have also been investigated in the field of grid applications and electric vehicles. Instead of balancing the SoC, other BESS parameters were taken into account in these areas. Li et al. [110] proposed a SoH-balancing PFCS in order to equalize the degradation during the long-term operation. In [111], a PFCS for the provision of primary control reserve in combination with intraday trading was proposed, aiming to reduce the power electronics' losses by minimizing their in-operation time. One of the presented PFCSs by Choi et al. [112] shares the requested power according to the available energies of each battery with the aim of improving the energy efficiency of the entire system. Jiang and Dougal [96] further presented a dynamic PFCS in which the charging current of a battery is proportional to the fraction of its DoD. In [113], a PFCS based on the state of the available power (SoAP) for a hybrid energy storage system was proposed, yielding performance improvements in terms of battery lifetime, vehicle range, and regenerative braking energy recovery.

Beyond static and dynamic PFCSs, researchers have assessed the efficacy of PFCSs using optimization-based approaches. In this respect, several studies have been published in the research area of MGs. Morstyn et al. [114] proposed a model predictive control (MPC) PFCS with receding time horizon optimization that considers line losses and voltage drops. In [115] a particle swarm optimization (PSO)-based PFCS was established, which balances the SoC and reduces power losses in an island DC MG. Meng et al. [116] applied an optimization-based approach considering the SoC and the overall system efficiency at the same time. The results showed that the SoC balancing was successfully implemented into the system efficiency optimization problem. In [117], a multi-dimensional droop surface (parameter map) was developed determining optimal droop parameters based on different capacities and SoCs to optimize a global cost function. The work of Wang et al. [118] presents a distributed method of minimizing the difference between the SoC values and their reference values and minimizing the controlling power consumption. Apart from the research area of MGs, optimization-based PFCSs have also been investigated in the field of grid applications. In [119], a

multi-agent PSO for large-scale BESSs was presented. Fluctuations of a wind power station were stabilized and the SoC imbalance of the BESS was gradually reduced in a one-day operation. In [120], PSO was used to minimize the multiple operation costs of a BESS. The BESS was composed of retired batteries with a different SoH and its economical operation was optimized by applying a use case with shifting peak loads. Fortenbacher et al. [121, 122] proposed a MPC framework for power system applications to maximize the battery life and provide optimal control of multiple battery sets in real-time. Optimal scheduling of a small-scale photovoltaic-battery hybrid system has been proposed by Wu et al. [123]. They used an optimal control method to schedule the hybrid system's power flow to minimize electricity costs. In the work of Kim et al. [124], an optimal operation framework for BESSs was implemented for load management of a large-scale customer under time-based pricing, proving the reliability and effectiveness of the PFCS. An optimization-based MPC approach for controlling a stationary energy storage system is presented in [90]. The proposed approach provides the flexibility to design a PFCS that enables the trade-off between multiple objectives to be managed. Besides PSO and MPC, other PFCSs based on optimization techniques have been proposed. Zhu and Zhang [86] considered a profit-maximization PFCS that coordinates a distributed BESS to provide primary frequency control service. Kang et al. [125] proposed a distributed multi-objective power management scheme, in which economic power dispatch objectives, dissatisfaction costs, and system voltage loss are optimized using a Nash bargaining solution. Recent studies also consider machine learning approaches to control energy storage systems in different applications, such as grid applications [126] or electric vehicles [127, 128]. Figure 2.9 gives an overview of PFCSs for BESS applications categorized into static, dynamic, and optimization-based PFCSs.
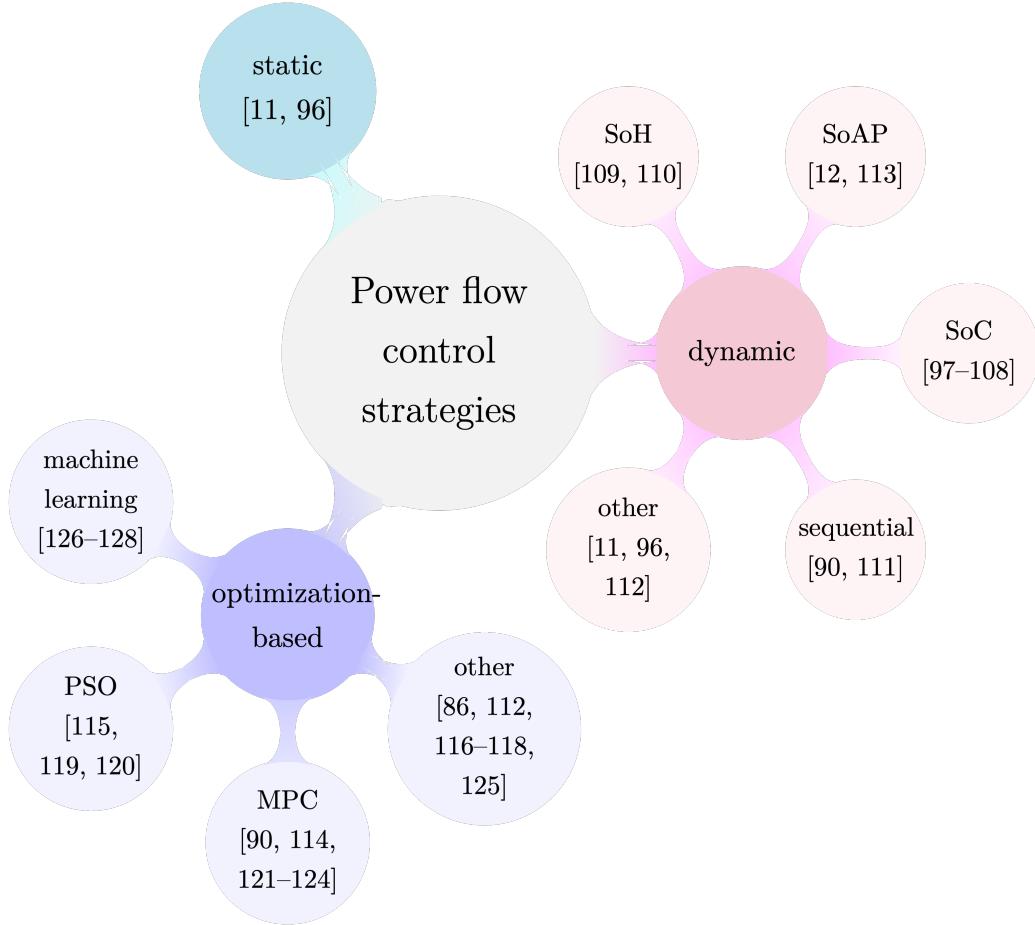
Figure 2.9: Overview of power flow control strategies for BESS applications.

2.3 Summary of the review

The studies presented thus far provide evidence that the optimal operation of BESSs depends on three key criteria: system design, application, and objectives of the operator. As mentioned by Hesse et al. [4], most PFCSs focus on specific aspects to be analyzed and optimized. Consequently, there are some conflicting views regarding how best to manage the power flow in BESSs while considering multiple objectives. Achieving multiple objectives in BESS applications, such as fulfilling power requirements, increasing the BESS's overall efficiency, and reducing battery degradation necessitates solving a multi-objective optimization (MOO) problem [90]. Moreover, each MOO process demands decision-making at some point to achieve the optimal operation of a BESS. Therefore, the vast majority of published works on PFCSs consider optimization-based approaches, for example [90, 118–122, 125]. However, two crucial challenges emerge from the studies discussed

so far: First, there is only a limited thorough analysis of the multiple objectives mentioned in these studies. In most MOO problems, no single solution exists that concurrently optimizes multiple objectives and adequately satisfies the operator's objective. Thus, rational decision-making cannot be guaranteed since there is no set of solutions to quantify the trade-offs and provide information about conflicting objectives. Second, the existing research provides no access to general knowledge about causal relationships between the inputs and the outputs of BESSs when, for example, boundary conditions such as power requirements are subject to change and sustainable operation should be enabled. By bringing together the challenges of providing information about conflicting multiple objectives and knowledge about causal relationships, new opportunities arise to analyze and consequently operate BESSs more efficiently and sustainably. In this case, a systematic and concurrent optimization for multiple objectives is required, classifying the resulting problem into a MOO problem.

In this work, a special focus is placed on three dynamic PFCSs as the implementation effort and computation complexity is low: the state-of-the-art PFCS for several homogeneous and heterogeneous BESS applications (PFCS SoC), a parametric PFCS (PFCS SoAP), and a sequential PFCS (PFCS Pseq). Although the calculation method of the parameters used in the following (e.g., SoC or predicted power) may vary, the calculation of the power-sharing factors could be equally considered. Furthermore, each PFCS can be implemented in a MOO framework.

State-of-the-art PFCS

A well-known and state-of-the-art PFCS for several BESS applications constitutes SoC balancing. This PFCS has been investigated by several researchers, e.g., Lu et al. [97] or Marcelino et al. [106]. The basic idea is to share the requested power proportional to the SoC. Concerning the operation mode, α_i can be calculated for the charging/discharging case by

$$\alpha_{\text{SoC},i} = \frac{f(SoC_i, p)}{\sum\limits_{n=1}^{n_{\text{BESS}}} f(SoC_n, p)} \, , \tag{2.9}$$

where n_{BESS} represents the number of applied BESSs and SoC the state of charge of the respective battery. $f(SoC, p)$ and p represent the compensation function (see Table 2.1) and the convergence factor, both as proposed in [106]. The SoC is typically determined by the coulomb-counting method as defined in Equation (2.2).

The compensation function and the convergence factor are considered design variables. According to Marcelino et al. [106], typical compensation functions[4] are as follows:

Table 2.1: Compensation functions $f(SoC, p)$ to calculate the power-sharing factor [106].

Function	Charging mode	Discharging mode
Power	SoC^{-p}	SoC^{p}
Exponential	$e^{-p \cdot (SoC-1)}$	$e^{p \cdot (SoC-1)}$
Linear	$p \cdot (1 - SoC) + 1$	$p^{-1} \cdot (SoC - 1) + 1$
Hyp. sine	$\sinh(-p \cdot (SoC - 1)) + 1$	$\sinh(p^{-1} \cdot (SoC - 1)) + 1$
Logarithmic	$-p \cdot \ln(SoC) + 1$	$p^{-1} \cdot \ln(SoC) + 1$

Parametric PFCS

The parametric PFCS shares the requested power relative to the maximum available power of the batteries. This quantity changes during operation concerning the current status of the battery. Masih-Tehrani and Dahmardeh [113] proposed such an algorithm in a hybrid energy storage system consisting of a battery and an ultracapacitor. This approach was further developed within my published works [12, 13]. For each BESS, the power-sharing factor

$$\alpha_{\text{SoAP},i} = \frac{|P_{\text{pred},i}|}{\sum\limits_{n=1}^{n_{\text{BESS}}} |P_{\text{pred},n}|} \tag{2.10}$$

is calculated, where $P_{\text{pred},i}$ is the maximum available charging/discharging power of the ith battery. The respective share of each BESS can be adjusted applying Equation (2.10). If one BESS hits its operating limits, other BESSs take over a larger share of the required power as long as their limits are not exceeded.

The maximum available power P_{pred} is calculated by voltage limits, current limits, and the maximum available charging and discharging energy of a BESS. For both charging and discharging, P_{pred} is defined as

$$|P_{\text{pred}}| = \min(|P_{\text{pred,I}}|, |P_{\text{pred,V}}|, |P_{\text{pred,E}}|) , \tag{2.11}$$

where $P_{\text{pred,I}}$, $P_{\text{pred,V}}$, and $P_{\text{pred,E}}$ are the maximum available power for the current, voltage, and energy limit of the battery. Their calculation is based on an ECM of

---

[4]Charging and discharging mode are reversed compared to [106].

a battery (see Section 4.2) and subject to current, voltage, and energy/capacity limitations for a predefined time frame of a few seconds to a few hours. The maximum available charging and discharging power for current and voltage limits ($P_{\text{pred,I}}$ and $P_{\text{pred,V}}$) can be predicted by, for example, the method proposed in [129] and Equations (2.12) and (2.13). The prognosis of the maximum available power is based on a predefined prediction horizon $t_{\text{pred,p}}$ of usually a few seconds. Here, i_{lim} and v_{lim} are the current and voltage limits of the battery.

$$P_{\text{pred,I}}(t) = v_{\text{pred,I}}(t) \cdot i_{\text{lim}} \tag{2.12}$$

$$P_{\text{pred,V}}(t) = i_{\text{pred,V}}(t) \cdot v_{\text{lim}} \tag{2.13}$$

In the simplest case, the maximum available charging and discharging energy E_{pred} can be predicted by applying the following equations under the assumption that dynamic processes are neglected:

$$E_{\text{pred,ch}}(t) = C_{\text{act}}(T, SoH) \cdot \int_{SoC(t)}^{SoC_{\text{max}}} OCV(SoC, T, SoH) \, dSoC \,, \tag{2.14}$$

$$E_{\text{pred,dch}}(t) = C_{\text{act}}(T, SoH) \cdot \int_{SoC_{\text{min}}}^{SoC(t)} OCV(SoC, T, SoH) \, dSoC \,, \tag{2.15}$$

where C_{act} is the capacity subject to temperature and SoH of the battery, and OCV is the open-circuit voltage which depends on the battery's SoC, temperature, and SoH. The limits of the integration are the actual SoC and the SoC limits of the battery. By neglecting the impact of dynamic processes, a prediction error of the maximum available energy has to be accepted.

In order to improve the predicted value of the maximum available energy, dynamic processes in batteries can be modeled using a more detailed ECM. Consequently, the charge and discharge cut-off voltage will be reached earlier. This leads to a reduced maximum available charging and discharging energy of the battery during operation, reducing the capacity relative to the load. Moreover, integration limits have to be adjusted concerning the minimum and maximum SoC. In general, the maximum available charging and discharging power for the energy limit

is calculated by

$$P_{\text{pred,E}}(t) = \frac{E_{\text{pred}}(t)}{t_{\text{pred,e}}} \, , \qquad\qquad (2.16)$$

where $t_{\text{pred,e}}$ is an arbitrary prediction horizon of usually minutes or hours. The prediction horizons are considered design variables. In the case of the more detailed predicted value of the maximum available energy, Equation (2.16) might not be simply solvable as the maximum available energy is dependent on the predicted charging/discharging power.

Sequential PFCS

The sequential PFCS (PFCS Pseq) shares the requested power based on a predefined power limit while using the BESSs sequentially. A similar PFCS was investigated by Bauer [23]. The BESSs are arranged in a fixed ascending (BESS 1, BESS 2, BESS 3) or descending (BESS 3, BESS 2, BESS 1) order considering the size (i.e., rated capacity) of the BESSs (cf. Appendix Table C.6). The first BESS will be charged/discharged as long as predefined power and SoC limits are not exceeded. If the limits are exceeded, the next BESS takes over the residual power. It should be noted that the last BESS in the sequence might be charged/discharged with a higher power than the predefined power limit (if possible). The variables to set the power limit (P_{max}) and the order of the BESSs (*Sorting*) applied are considered design variables. Other methods to arrange the BESSs, such as dynamic sorting relative to the SoC, are possible but will not be considered in this work.

3 Fundamentals of multi-objective optimization

The identified optimization problem mentioned in Section 2.3 is characterized by simultaneously optimizing the three defined target indicators, which could be expressed as nonlinear objective functions over a set of variables, such as the previously mentioned design or use case variables. This defines the given problem as a nonlinear MOO problem. In order to solve this problem, appropriate methods and processes are necessary. Thus, this research field has to be reviewed academically and suitable approaches have to be selected. For this reason, the basic scientific knowledge about nonlinear multi-objective (black-box) optimization is presented in this chapter. Section 3.1 gives an overview of the fundamentals of MOO and its terminology. In Section 3.2, an overview of black-box optimization is given and the state-of-the-art methods currently used in black-box optimization are then presented. In Section 3.3 an appropriate tool to solve the black-box optimization problem is described. Section 3.4 summarizes relevant findings from the current literature and manifests the research gap. Finally, in Section 3.5 the research questions of this work are outlined.

3.1 Multi-objective optimization

Optimization is basically concerned with finding an optimal, i.e., a feasible decision from a set of possible alternatives (subject to several constraints) that optimize an objective function [130]. However, real-world optimization problems are often nonlinear and have multiple conflicting objectives [131]. The process of optimizing more than one objective function at the same time is referred to as MOO. In this context, optimization means finding a maximum or a minimum of an objective function, whereby a maximization problem can always be transformed into a minimization problem. Following the notation of Ehrgott [132], a MOO problem can

be formulated as

$$\begin{aligned} \min f(x) = \quad & \min(f_1(x), ..., f_p(x)) \\ \text{s.t.} \quad & x \in X \, , \end{aligned} \tag{3.1}$$

where $f(x)$ is the objective vector, p the number of objective functions, x a vector of feasible decisions, and X the feasible decision space.

MOO problems give rise to a set of solutions in the objective space and aim at identifying all the feasible decisions that simultaneously optimize each objective function value. These solutions are defined as Pareto-optimal (PO) or non-dominated. In this case, no accessible decision of the feasible decision space is capable of improving any specific objective function value without causing a simultaneous deterioration to at least one other objective function value [133]. The set of all non-dominated solutions, in turn, forms the Pareto-front. Figure 3.1 shows the decision and objective space indicating non-dominated solutions (cyan), i.e., the Pareto-front.

a) decision space   b) objective space
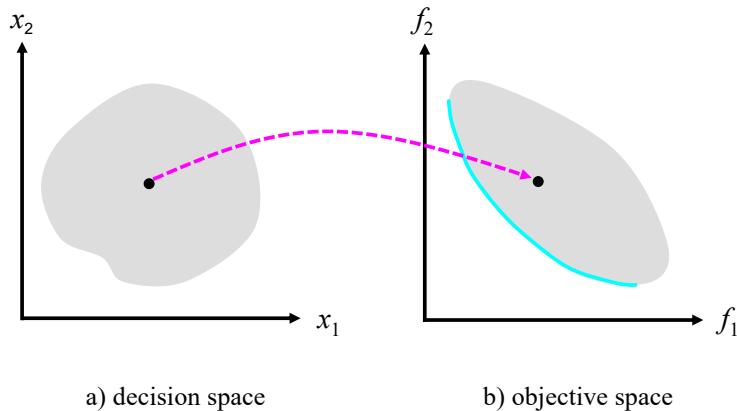
Figure 3.1: Representation of the decision and objective space indicating non-dominated solutions (cyan), i.e. the Pareto-front. Adapted from [131].

However, function evaluations to optimize one or multiple objective functions may be computationally expensive due to, e.g., complex simulation models. Especially in industrial optimization problems, where complex computer simulations are used, expensive-to-evaluate functions are often existent [134]. In general, computationally expensive refers to an optimization problem where a single run (function evaluation) takes a few minutes to hours or even days [135]. In the case of computationally expensive function evaluations, a careful and adaptive selection

of values to evaluate is reasonable [136]. Proper methods for that are explained in the next section.

Moreover, each MOO process necessitates decision-making at some point. Marler and Arora [137] divide the methods to model the preference of a decision-maker into three major categories: *a priori*, *a posteriori*, and *no articulation of preferences*, and describe them as follows. Methods with a priori articulation of preference allow the user to specify preference information in terms of goals or the importance of different objectives before a solution that satisfies these preferences is found [137]. In this case, the MOO problem is often transformed into a single-objective optimization problem. Common a priori methods are, e.g., scalarizing methods, goal programming, or the lexicographic method. A posteriori methods allow the decision-maker to choose from a set of PO solutions that were found beforehand [137]. Well-known a posteriori methods are mathematical programming-based approaches, such as the Normal boundary intersection method or the Normal constraint method. Methods with no articulation of preference do not require any preference information as they identify solutions independently [137]. The most common methods are global criterion methods and the Nash arbitration scheme. Considering the third research aim, the a posteriori articulation of preferences could be a reasonable approach in this work. The identified set of PO solutions can be investigated afterward, which allows analyzing the causal relationships between the inputs and the outputs.

3.2 Black-box optimization

Black-box optimization describes the optimization of an objective function where the budget for evaluations is limited [136]. Reasons for such black-box optimization may be diverse. For example, there is no structure to exploit any analytical or derivative information of the problem [135], or input-output relationships are simply not known. In particular, the inner workings of the system under observation will be treated as a black-box function, for which only inputs and outputs are known [138]. Such a black-box function problem can be formulated as shown in Equation (3.1). In contrast, the function here refers to a function of the input-output relationship that has no analytical form.

Suitable methods to solve such problems and evaluate the given function are limited to mainly derivative-free methods and surrogate-based methods. Nevertheless, these methods can be used to identify the best operating parameters for systems where the output is measurable and the input parameters are customizable [136]. Additionally, proper performance metrics are required to quantify the error between the real (measured or virtually derived) and the predicted output.

Function evaluation methods

Heuristics, such as evolutionary algorithms, simulated annealing, or tabu search, are the most common way to solve black-box optimization problems, as they are easy to implement and only rely on function evaluations [135]. Such stochastic algorithms are easy to parallelize, avoid becoming stuck in a local minimum, and help to optimize the objective function globally [139]. Bayesian optimization is another common approach for global optimization of black-box functions in which the function is expensive to evaluate. This method is high performant for continuous objective functions with typically less than 20 dimensions [140]. A comprehensive review of Bayesian optimization is provided by Shahriari et al. [141]. Another way is to use classic derivative-free methods. For example, random search constitutes the most straightforward method, selecting possible decisions arbitrarily. Direct-search methods, such as the Nelder-Mead algorithm [142], or model-based methods like the trust region method perform a local search of points maintaining either a search pattern or a simple model of the objective function [136]. These methods are often deterministic and are advantageous when the objective function is expected to have a single global optimum. A review of these and other derivative-free optimization methods can be found in [143].

According to Wang and Shan [138], for MOO problems involving expensive to evaluate simulations, the use of surrogate approximation can be helpful. In this case, a functional approximation term for output dependencies as a function of inputs x is required, replacing the computationally expensive model by a less expensive approximate (surrogate) model $\hat{f}$ [144]. The surrogate model is a functional approximation term for target indicator dependencies as a function of design and use case variables, as can be seen in the following equation:

$$\hat{f} := \hat{f}(x) \approx f(x) \tag{3.2}$$

Surrogate-based methods seek to iteratively build a surrogate model to approximate the black-box function and use the functional approximation to search for optimal solutions [145]. Surrogate models differ primarily in their mathematical base of approximation. Besides the well-studied polynomial functions [146], several other approaches like radial basis functions (RBFs) [147, 148], Kriging models [149], or Gaussian Processes in general [150] have been thoroughly discussed. Surrogate models could be an interesting candidate for this work, as they are rather smooth and inexpensive to evaluate allowing efficient optimization [139]. A review of surrogate-based methods can be found in [135].

Sampling

Regardless of the preferred surrogate model, the first step in surrogate-based methods is to find a set of starting points uniformly spread over the feasible decision space [135]. This step is called sampling or design of experiments [151]. The most straightforward method to obtain a design in terms of space-filling is to sample the points uniformly, considering all possible combinations of the feasible decisions [135]. This is called a full factorial design. However, with a growing number of decision/design variables, a full factorial design becomes logistically infeasible [139]. Consequently, only a fraction of the feasible decisions (fractional factorial design) can be considered. Another approach is to use algorithms that rely on random sampling. A well-known random sampling method is the Latin hypercube sampling method introduced by McKay et al. [152]. One advantage is that this method can be applied to multiple decision variables without becoming logistically infeasible. An overview of experimental designs can be found in [135, 139].

Performance metrics

Relying on model-based outputs requires knowledge of a model's confidence level. For this purpose, the role of performance metrics has been intensively studied in regression analysis evaluation. The most common performance metrics are the mean square error (MSE), root mean square error (RMSE), mean absolute error (MAE), mean absolute percentage error (MAPE), and the coefficient of determination R^2. While the error measures express the distance between the data points and the regressor, the coefficient of determination expresses the relation between the dependent variables and the independent variables [153]. A general overview of regression analysis can be found in [154]. A recent comparative overview of regression analysis evaluation was provided by Chicco et al. [153]

Tools

Besides proper methods for function evaluation, sampling strategies, and performance metrics, tools are required to solve the MOO black-box optimization problem efficiently and effectively.[1] In the literature, the Design Space Exploration has become established as an appropriate tool for that [155–157]. It refers to a systematic exploration of design alternatives (i.e., feasible decisions) before implementation [158]. Another approach is the Hyper Space Exploration (HSE) presented by Palm and Holzmann [159]. This methodology develops the Design Space Exploration further and is an appropriate tool for multi-criterial quantitative trade-off analysis for black-box optimization problems.

3.3 Hyper Space Exploration

The HSE significantly extends the Design Space Exploration approach. It constitutes a system design methodology in complex environments and combines methods of virtual prototyping with methods of design of (virtual) experiment-based studies for statistical learning [159]. According to the authors, the hyperspace consists of three different spaces: the design space, use case space, and target indicator space as spanned by design, use case, and target indicator variables within their parameter value definition sets. As shown in the following equations, the HSE methodology demands phrasing the optimization problem as a minimization problem:

$$d(u) \quad = \quad \mathrm{argmin}\,(t(d,u)) \tag{3.3a}$$

$$s.t. \quad \begin{cases} d = & (d_1, \dots d_i)^T \in D, \\ u = & (u_1, \dots u_j)^T \in U, \\ t = & (t_1, \dots t_k)^T \in T, \end{cases} \tag{3.3b}$$

where d spans the i-dimensional design space D, u the j-dimensional use case space U, and t the k-dimensional target indicator space T.

---

[1] In this context, efficiency is characterized by a minimum number of required function evaluations to statistically learn on functional input-output dependencies and to identify the set of PO solutions; the identification and trade-off quantification of PO solutions characterizes efficacy [12].

The HSE methodology aims at identifying all the parameter value combinations for design space vectors that simultaneously optimize each of the target indicators for a given use case combination. In the context of MOO, such identified solutions are defined as PO or non-dominated (cf. Section 3.1). The set of all non-dominated target indicator vectors for a given use case forms the Pareto-front $P(u)$:

$$P(u) := \{t \in T \mid \nexists \, t'(d', u) : t(d, u) \prec t'(d', u) \, \forall \, d, d' \in D\}, \qquad (3.4)$$

where D represents the set of all parameter value combinations for design space vectors d.

3.4 Summary of the review

To recap the main challenges carved out in the previous chapter, there is only a limited thorough analysis of the trade-offs between the multiple objectives, and the existing research provides no access to general knowledge about causal relationships between the inputs and the outputs of BESSs. Considering all of the studies reviewed here, a time series problem, as present in this work, aggravates the solution-finding for these two challenges and has to be treated specially. In this case, decision-making must occur after a predefined number of time steps, ranging from at least once in the period considered to after each time step. As noted by Deb [131], once a set of PO solutions is found, the set can be investigated as a post-optimality analysis, presumably revealing interesting knowledge on the trade-offs between the objectives. However, this entails three significant aspects to be considered: First, not every method mentioned in Section 3.1 is practicable in terms of a post-optimality analysis. Second, depending on the frequency of decision-making and the method applied, the evaluation of the MOO problem can become costly concerning computing complexity. Third, due to the presence of a complex problem (cf. Chapter 1), the correlations between the inputs and outputs of the BESS are only available through expensive to evaluate simulations which characterize the MOO problem as a MOO on a black-box function problem [138].

Consequently, it might be favorable to postpone the decision-making process and analyze the set of PO solutions (in terms of trade-offs between the objectives and causal relationships) after the considered period. This also tackles the problem

when an analytically closed form of the functional correlation between the outputs and the inputs is not accessible. By using black-box optimization, one benefit is that any PFCS can be applied for analysis, and optimization-based PFCSs, such as evolutionary algorithms, are not necessary to obtain a set of PO solutions. For this reason, the HSE methodology in combination with the surrogate-based method (cf. Section 3.2) can be a valuable approach to achieve the research aims.

3.5 Research questions

In view of all that has been mentioned in Chapters 2 and 3, existing approaches in the literature are not sufficient to a) perform comparative trade-off analyses between the multiple objectives and b) gain access to general knowledge about causal relationships between the inputs and the outputs of BESSs. Based on these findings and in consideration of the research aims, the following research question and five subordinate research questions emerge:

How can the potentials and sensitivities of power flow control strategies for heterogeneous battery energy storage systems be quantified?

1. *How can the Hyper Space Exploration methodology be applied to perform a potential analysis for power flow control strategies?*

   By performing a potential analysis, existing trade-offs between the defined objectives (cf. Section 2.2) should be gained, and a functional approximation term of the causal relationships between the inputs and the outputs derived. This creates the opportunity to learn how different power flow control strategies affect, e.g., the aging behavior.

2. *How can the trade-offs of the applied target indicators be quantified?*

   Technical target indicators usually have different units and are thus hardly comparable due to the lack of a common basis for comparison. Reasonable features should be identified to quantify and analyze the trade-offs adequately.

3. *What are the sensitivities of the target indicators with regard to the design variables?*

Trivial solutions for choosing the design variables of the power flow control strategies to maximize, e.g., the efficiency of the system, are not immediately evident. By performing a sensitivity analysis, these correlations should become apparent.

4. *What are the sensitivities of the target indicators with regard to the use case variables?*

   The same applies to the fourth subordinate research question. The effects of use case variables on, e.g., the system's performance, are not immediately evident. By performing a sensitivity analysis, these correlations should become apparent.

5. *What are the design rules that can be derived to support operators of battery energy storage systems?*

   The design rules are sets of recommendations on how to enable sustainable and reliable operation of battery energy storage systems. Based on the findings made in this work, generally valid recommendations should be given.

4 System description and toolchain

In order to quantify the potentials and sensitivities of PFCSs for heterogeneous BESSs, an appropriate simulation model is required. This work's simulation model was first introduced in my published work [11] and has been further extended in my published works [12, 14]. Its basic topology was derived from the concept proposed within the *UnABESA* research project, in which the incorporation of PFCSs for heterogeneous BESSs was a main part of the research conducted. The basic idea of this chapter is to introduce the simulation model used here, confirm the validity of the individual submodels, and extend the simulation model by a peripheral system to solve the MOO on a black-box function problem.

The general system overview is presented in Section 4.1. Next, the model design, including submodels for the batteries, power electronics, and control scheme, is described in detail. In Section 4.3, the extension of the simulation model by an appropriate process flow and toolchain is shown. After that, the verification and validation of each submodel are provided. Finally, general difficulties and their effects are explained. The following sections are mainly based on my published works [11, 12, 14].

4.1 System overview

The system's basic topology was derived from the concept and ideas proposed within the *UnABESA* research project. In this context, different system topologies were intensively reviewed in advance by Bauer [23] to identify a suitable topology for investigating PFCSs for heterogeneous BESSs. The defining characteristic of the chosen system topology (see Figure 4.1) is constituted by the parallelization of strings denoted as BESSs (batteries and DC/DC converters) at the DC bus level, allowing to expand the number of BESSs arbitrarily. Another advantage of using this topology is that, due to the DC/DC converters, the freedom to control the power flow of each participating BESS individually is provided. Consequently, the

smallest possible configuration to distribute the power inside the system reasonably is two BESSs connected in parallel. In this work, the number of BESSs connected in parallel was set to three since this configuration constituted a reasonable system size to investigate PFCSs systematically.
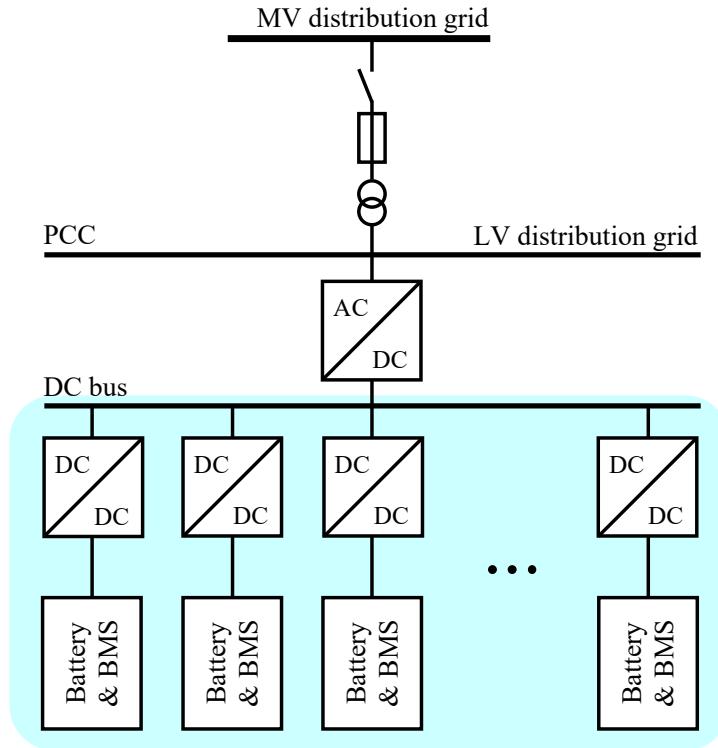

Figure 4.1: Schematic diagram of the applied topology comprising multiple batteries and DC/DC converters, one AC/DC converter, and the grid connections. Adapted from Bauer [23].

The virtual experiments (simulations) were conducted, developing a simulation model based on the chosen topology. The basic architecture of the simulation model is composed of a BESS, including a battery and a bidirectional DC/DC converter, a common DC bus, an AC/DC converter which is also bidirectional and connected to the LV distribution grid, and a BESS management system. All these submodels are coupled either via power lines or communication lines, allowing modular development and modeling of the respective submodel. The system is controlled based on the requested power at the grid side's power electronics. The requested charge/discharge power is represented by P^* and is dependent only on the investigated scenario (cf. Section 4.2). P^* is considered positive for charging and negative for discharging the system (cf. Section 2.1.3). The resulting power at the battery terminals is then computed by implementing efficiency models of the

converter stages. The total charged/discharged power of the system is indicated by P_{sys} and considers the efficiencies of each converter stage and the direction of the power flow. In more detail, the charged/discharged power P_i of each of the three strings (BESS 1–3) adds up to the total system power. According to this, the output power provided by a single battery $P_{\text{bat},i}$ is considered higher than the output power of the entire BESS P_i in discharging mode. In contrast, in charging mode, the battery's input power is considered lower than the input power of the entire BESS. The battery's input power is further used to calculate the battery's specific parameters, such as the terminal voltage or the capacity fade. Note that a linear power derating starts at 5 % SoC and 95 % SoC, respectively, reducing the charged/discharged power P_i of the concerned string. In the case of the communication lines, the BESS management system controller is implemented to collect data (e.g., P^*, v_{dc}, or BESS parameters) of the entire system. Here, the hierarchical control scheme is located (cf. Section 4.2). The collected data is used to control the system in a centralized manner by calculating the respective power share P_i^* of each BESS and keeping the voltage at the DC bus stable. Figure 4.2 shows the schematic diagram of the utilized BESS simulation model.
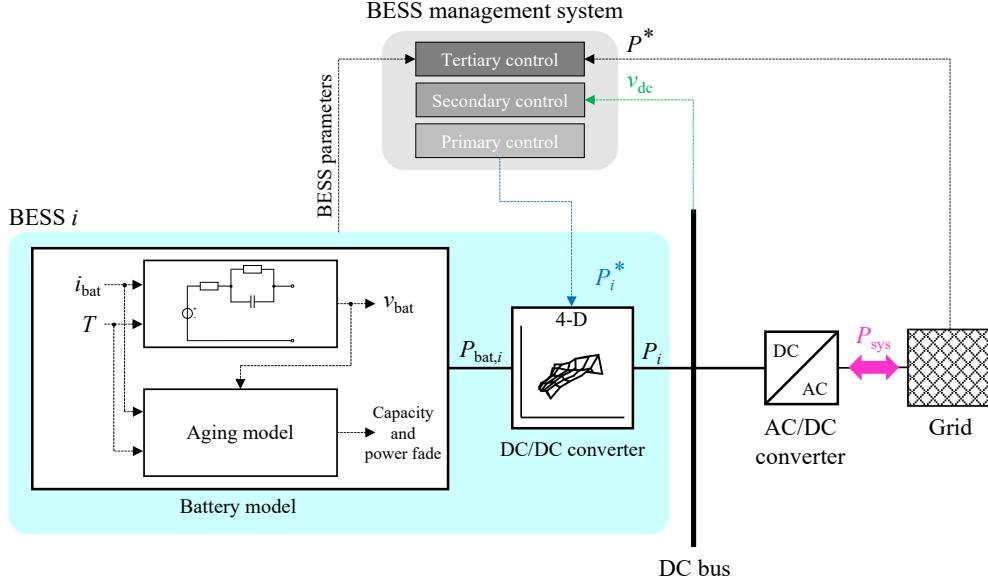

Figure 4.2: Schematic diagram of the utilized BESS simulation model comprising a BESS, a common DC bus, an AC/DC converter, the grid connection, and the BESS management system. Adapted from my published work [14].

The software that simulates the described system must enable the variation of different input parameters since it is essential when quantifying the potentials and sensitivities of PFCSs for heterogeneous BESSs. The simulation model was programmed using *MathWorks MATLAB® and Simulink®* software. This software provides a suitable environment for designing, simulating, and analyzing dynamical BESS systems rapidly and allows for programmatically running multiple simulations with varying input parameters. Both the BESS model and the BESS management system were realized in the discrete-time domain (fixed-step discrete solver and a fixed-step size of 1 s) to decrease the simulation time and to enable a fast implementation on a microcontroller target. The latter is of particular importance for verifying or validating individual submodels, which constitutes an essential part to confirm the validity of this work's results.

4.2 Model design

The different submodels were established based on the system shown in Section 4.1 and the assumptions presented in the following. The basic concept of quantifying the potentials and sensitivities of PFCSs for heterogeneous BESSs relies on multiple simulations with varying input parameters and a defined period (here 24 h). Consequently, a simulation step-size of 1 s was used to reduce computational costs and keep the time for a simulation run at around one minute. A lower simulation step-size would increase the computational costs disproportionately and multiple simulations with varying input parameters would be infeasible. However, the level of detail of each submodel was limited in this case yet sufficiently accurate (cf. Section 4.4). This means, for example, high dynamic effects of the battery and converter models could not be modeled. At the system-level, further assumptions were made. Instead of using current and voltage values, the DC power flow was simulated. The advantage of using the DC power flow is that the simulation model is less complex and less computation-intensive since the different voltage levels are considered implicitly and algebraic loops can be avoided. At the same time, the maximum system power was limited to the power limitations of the battery and the DC/DC converters. This approach is one way to avoid states of the submodels which are not validated. Furthermore, line losses were neglected due to short cable lengths. They are assumed to be low compared to the losses of the power electronics.

4.2.1 Battery model

In this work, the battery model is based on a lithium-ion battery pack typically designed for low power, low energy, and low voltage applications. Even though common BESSs designed for stationary applications are different regarding the voltage level or the rated capacity, for simpler testing under laboratory conditions and the validation of the battery model, the low power, low energy, and low voltage battery pack was used here. Nevertheless, the transferability of the results to real-world systems is still given due to similar operational behavior. For example, operating parameters such as the C-rate or the DoD can be aligned accordingly, and a comparable energy density or power density can be assumed due to similar cell chemistry. The battery model is separated into an electric model and an aging model. Because of the basic concept of quantifying the potentials and sensitivities of PFCSs for heterogeneous BESSs mentioned above, no thermal model, no model for self-discharge, and no feedback loop for the aging parameters are mandatory. Although, for example, self-discharge and degradation occur within the defined period of 24 h, the effects on the results can be assumed to be low. However, slight improvements concerning the efficiency and the aging behavior of the batteries might occur.

One main assumption of the battery model is that a SoC-dependent OCV and diffusion voltages, calculated using an ECM, adds up to the battery terminal voltage. Here, an ECM consisting of the OCV as a voltage source, the ohmic resistance R_s, and one RC-circuit was used. In a sensitivity analysis (see Appendix C Table C.2), the difference between an ECM with zero RC-circuits, one RC-circuit, and two RC-circuits regarding the used battery packs and the verification case (cf. Section 4.4) was investigated. It was found that the median absolute model error of the terminal voltage decreases with adding more RC-circuits. However, the simulation speed was increased disproportionately. Therefore, an ECM with one RC-circuit was applied here as a compromise. This is also in general agreement with studies on modeling lithium-ion batteries for mobile and stationary applications [160, 161]. Note that the ECM parameters exclusively depend on the SoC, current, and battery temperature. Furthermore, the shortest time constant of the RC-circuit values was constrained to values higher than 1 s to meet the requirements of the simulation step-size. Using such a model, instantaneous polarization and additional polarization effects, such as diffusion processes, can be modeled [42, 58]. Even though a hysteresis effect can be measured for lithium-ion

batteries [162], a hysteresis model was not considered in this work as the effects are considered small, especially for NMC cells[1] [163]. The determination process of the parameters[2] is presented in Section 4.4. The applied ECM is shown in Figure 4.3.
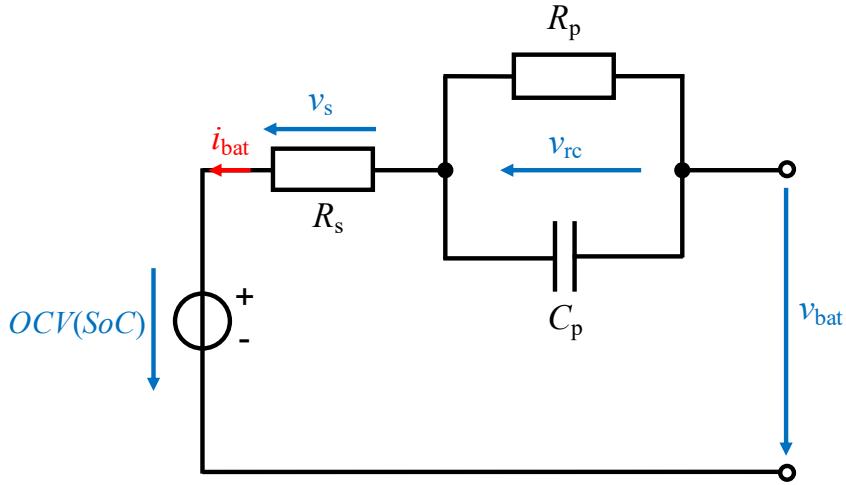

Figure 4.3: Equivalent circuit model of the used lithium-ion battery pack consisting of the OCV as a voltage source, the ohmic resistance, and one RC-circuit. Adapted from my published work [11].

As illustrated in this figure and previously mentioned in Section 2.1.3, the current i_{bat} is considered positive for charging and negative for discharging (cf. Section 2.1.3). The respective elements of the applied battery model were parameterized by the two batteries described in Section 4.4. Applying Kirchhoff's laws results in the following (differential) equations:

$$\frac{d}{dt}v_{\mathrm{rc}} = -\frac{v_{\mathrm{rc}}}{R_{\mathrm{p}}C_{\mathrm{p}}} + \frac{i_{\mathrm{bat}}}{C_{\mathrm{p}}}, \tag{4.1a}$$

$$v_{\mathrm{bat}} = OCV(SoC) + R_{\mathrm{s}} \cdot i_{\mathrm{bat}} + v_{\mathrm{rc}}, \tag{4.1b}$$

where the OCV is implemented as a look-up table using the SoC as breakpoints, v_{s} is the instantaneous ohmic voltage drop ($v_{\mathrm{s}} = R_{\mathrm{s}} \cdot i_{\mathrm{bat}}$), v_{rc} is calculated by the differential equation of the RC-circuit, and i_{bat} is the battery's output current. The SoC is determined by the coulomb-counting method presented in Section 2.1.3.

---

[1]In the study of Barai et al. [163], the hysteresis voltage for the NMC cell was lower than $20\,\mathrm{mV}$ across the whole SoC range.
[2]Detailed look-up table values are presented in Appendix C Tables C.3–C.5.

An aging model, as introduced in my published work [14], further extends the battery model. However, analyzing the potentials and sensitivities of PFCSs on a higher level of abstraction requires a replicable and valid aging model to comprehend individual correlations independently from, e.g., a specific battery type. Thus, a more generic modeling approach[3] with a focus on capacity fade as proposed by Motapon et al. [164] was further developed and implemented within this work. The underlying assumption that capacity loss due to calendar and cycle aging is linearly independent is a common simplification of more complex interdependencies and is used in many publications [69, 70, 72, 165]. The applied aging model incorporates all relevant stress factors concerning calendar and cycle aging. The individual aging effects due to calendar and cycle aging, Q_{loss}^{cal} and Q_{loss}^{cyc}, are then superimposed to create a combined aging model calculating Q_{loss}, as shown in Equation (4.2).

$$Q_{loss} = Q_{loss}^{cal} + Q_{loss}^{cyc} \tag{4.2}$$

The calendar and cycle aging models' basic concept is that of weighted time and charge throughput, respectively. This approach can often be found in the literature [69–72]. Weighting factors are multiplied with a function of time and FECs at each time step. For the sake of simplicity, higher-order interdependencies were not considered, and the calculation of Q_{loss} is expressed per unit, indicating the percentage loss of the initial capacity. The structure itself allows eliminating stress factors individually, e.g., for sensitivity analysis, and can get adjusted to the most relevant lithium-ion batteries. However, this generic approach suffers from some slight limitations due to the equations of the stress factors. If operating limits are exceeded, occurring aging effects cannot be considered anymore. For example, lithium plating may occur outside the defined operating range, especially at low temperatures and high charge currents. In such cases, aging effects cannot be covered by the aging model. Nevertheless, the generic aging model is applicable to evaluate the potentials and sensitivities of PFCSs for heterogeneous BESSs as long as the system is operated within the defined operating limits. Figure 4.4 shows the general overview of the combined generic aging model.

[3]based on physical equations from fatigue theory
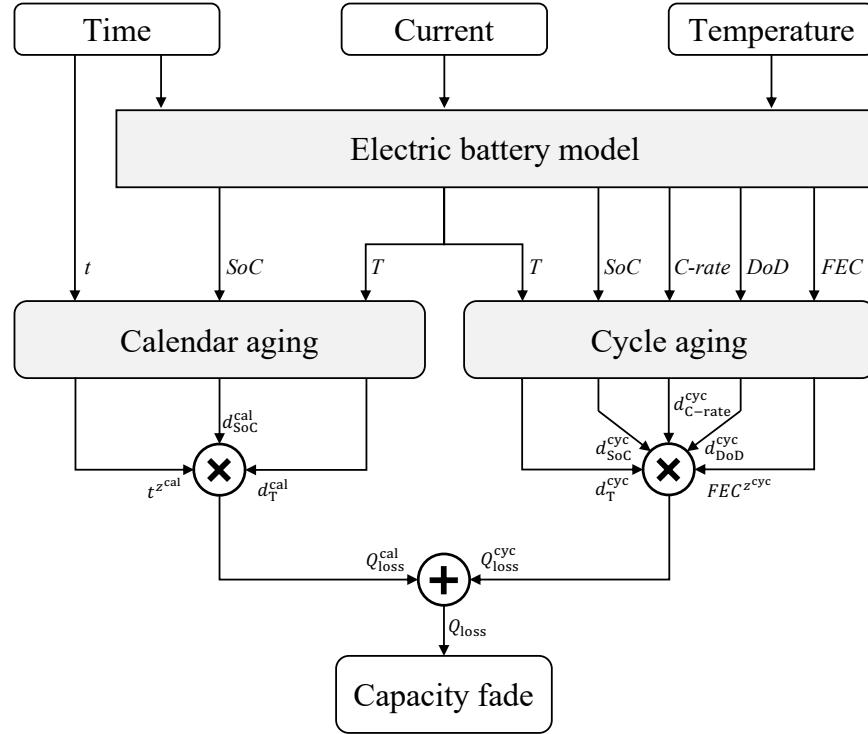
Figure 4.4: General overview of the generic aging model according to my published work [14].

A literature review by Dubarry et al. [53] showed that time, temperature, and SoC are regarded as the most important stress factors of calendar aging regardless of cell chemistries. They stated that in the literature, the capacity fade due to calendar aging follows a power law with time, and most studies suggest a square root dependence over time due to the SEI growth. According to the authors, temperature effects are commonly modeled using the Arrhenius equation, while the modeling of the SoC effects is limited in the examined models. Similar findings have also been reported in a review by Gewald et al. [54]. In accordance with these findings and reference [164], in this work, the capacity fade $Q_{\text{loss}}^{\text{cal}}$ caused by calendar aging was calculated by

$$Q_{\text{loss}}^{\text{cal}}(T, SoC, t) = d_{\text{T}}^{\text{cal}}(T) \cdot d_{\text{SoC}}^{\text{cal}}(SoC) \cdot t^{z^{\text{cal}}}, \tag{4.3a}$$

$$d_{\text{T}}^{\text{cal}}(T) = x_{11} \cdot e^{-\gamma_{\text{T}}^{\text{cal}} \cdot \left(\frac{1}{T} - \frac{1}{T_{\text{ref}}}\right)}, \tag{4.3b}$$

$$d_{\text{SoC}}^{\text{cal}}(SoC) = x_{12} \cdot \left(\frac{SoC}{SoC_{\text{ref}}}\right)^{\frac{1}{\gamma_{\text{SoC}}^{\text{cal}}}}, \tag{4.3c}$$

where z^{cal} is the exponential factor for the time, x_{11} and x_{12} are the calendar aging pre-factors, and $\gamma_{\text{T}}^{\text{cal}}$ and $\gamma_{\text{SoC}}^{\text{cal}}$ are the stress exponents. T and SoC are the temperature in Kelvin and the SoC during operation, and T_{ref} and SoC_{ref} are the reference values for the temperature in Kelvin and the SoC, respectively. It should be noted that the aging pre-factors in combination with the reference values are somewhat redundant. However, they were separated into two parameters for reasons of clarity.

In the case of cycle aging, a review by Gewald et al. [54] has revealed that the most relevant stress factors are temperature, charge/discharge current (or C-rate), average SoC, DoD, and charge throughput. However, the authors stated that the relevance of some stress factors is controversially discussed in the literature and depends on the specific battery type (cf. Section 2.1.3). Consequently, the capacity fade $Q_{\text{loss}}^{\text{cyc}}$ due to cycle aging was implemented as a customizable function in this work:

$$Q_{\text{loss}}^{\text{cyc}}(T, SoC, C\text{-}rate, DoD, FEC) =$$
$$d_{\text{T}}^{\text{cyc}}(T) \cdot d_{\text{SoC}}^{\text{cyc}}(SoC) \cdot d_{\text{C-rate}}^{\text{cyc}}(C\text{-}rate) \cdot d_{\text{DoD}}^{\text{cyc}}(DoD) \cdot FEC^{z^{\text{cyc}}}, \tag{4.4a}$$

$$d_{\text{T}}^{\text{cyc}}(T) = x_{13} \cdot e^{-\gamma_{\text{T}}^{\text{cyc}} \cdot \left(\frac{1}{T} - \frac{1}{T_{\text{ref}}}\right)}, \tag{4.4b}$$

$$d_{\text{SoC}}^{\text{cyc}}(SoC) = x_{14} \cdot \left(\frac{SoC}{SoC_{\text{ref}}}\right)^{\frac{1}{\gamma_{\text{SoC}}^{\text{cyc}}}}, \tag{4.4c}$$

$$d_{\text{C-rate}}^{\text{cyc}}(C\text{-}rate) = x_{15} \cdot \left(\frac{C\text{-}rate}{C\text{-}rate_{\text{ref}}}\right)^{\frac{1}{\gamma_{\text{C-rate}}^{\text{cyc}}}}, \tag{4.4d}$$

$$d_{\text{DoD}}^{\text{cyc}}(DoD) = x_{16} \cdot \left(\frac{DoD}{DoD_{\text{ref}}}\right)^{\frac{1}{\gamma_{\text{DoD}}^{\text{cyc}}}}, \tag{4.4e}$$

where $d_{\text{T}}^{\text{cyc}}$, $d_{\text{SoC}}^{\text{cyc}}$, $d_{\text{C-rate}}^{\text{cyc}}$, and $d_{\text{DoD}}^{\text{cyc}}$ are the average stress factors for temperature, SoC, C-rate, and DoD, z^{cyc} is the exponential factor for the FEC, x_{13}, x_{14}, x_{15}, and x_{16} are the cycle aging pre-factors, and $\gamma_{\text{T}}^{\text{cyc}}$, $\gamma_{\text{SoC}}^{\text{cyc}}$, $\gamma_{\text{C-rate}}^{\text{cyc}}$, and $\gamma_{\text{DoD}}^{\text{cyc}}$ are the stress exponents. T_{ref}, SoC_{ref}, $C\text{-}rate_{\text{ref}}$, and DoD_{ref} are the reference values for temperature in Kelvin, SoC, C-rate, and DoD, respectively.

Different approaches such as the rainflow cycle-counting algorithm [165] or half-cycle detection [72, 166] have been applied in the literature to detect a cycle event. For the sake of simplicity, the half-cycle detection algorithm was used in this work to determine the mean values of the stress factors for each half-cycle. However, this

simplification implies some limitations. According to Magnor et al. [166], it has to be assumed that, e.g., aging during a cycle is independent of previous events, and aging occurs in the same way during the charging and discharging process.

The aging pre-factors for both calendar and cycle aging depend on the chosen EOL criteria, and the weighting between calendar aging and cycle aging. It is also assumed that the values of the stress factors equal their reference values. With respect to the EOL criteria mentioned in Table 4.2, Equation (4.5a) and Equation (4.5b) were mathematically derived from Equation (4.3a) and Equation (4.4a), respectively.

$$x_{1k} = \left(\omega \cdot \frac{1 - EOL_{\mathrm{C}}}{t_{\mathrm{end}}^{z^{\mathrm{cal}}}} \right)^{\frac{1}{n_{\mathrm{cal}}}} \cdot \lambda(k) \tag{4.5a}$$

$$\text{with } \prod_{k=1}^{n_{\mathrm{cal}}} \lambda(k) = 1 \,,$$

$$x_{1j} = \left(\frac{(1 - \omega) \cdot (1 - EOL_{\mathrm{C}})}{FEC_{\mathrm{end}}^{z^{\mathrm{cyc}}}} \right)^{\frac{1}{n_{\mathrm{cyc}}}} \cdot \lambda(j) \tag{4.5b}$$

$$\text{with } \prod_{j=n_{\mathrm{cal}}+1}^{n_{\mathrm{cal}}+n_{\mathrm{cyc}}} \lambda(j) = 1 \,,$$

where ω is the weighting factor between calendar aging and cycle aging, EOL_{C} is the relative remaining capacity at EOL, t_{end} and FEC_{end} are the EOL criteria for the time in seconds and FECs, n_{cal} and n_{cyc} are the number of applied stress factors, and λ are the weighting factors for the aging pre-factors. It should be noted that the exponent and λ influence the weighting between the aging pre-factors, i.e., stress factors, and are therefore somewhat redundant. For reasons of clarity, they were separated into two parameters.

The generic aging model can be used for both static and dynamic applications, in which stress factors are subject to change during operation. The latter especially is of substantial interest for most BESS applications. In [71, 72], Naumann et al. presented an appropriate approach for that and confirmed its validity. They suggested deriving a differential form of Equation (4.3a) and Equation (4.4a). A virtual time t^{*} and a virtual full equivalent cycle FEC^{*} to determine the differential capacity loss are also required, as stress factors are time-dependent. Therefore,

three actions are to be repeated in each step n for using the generic aging model for dynamic applications[4]:

1. The virtual values have to be derived by solving Equation (4.3a) and Equation (4.4a) for t or FEC, respectively (see Equations (4.6a) and (4.7a)).

2. These values are then used to calculate differential capacity loss in the next interval (Δt and ΔFEC) using the differential form of Equation (4.3a) and Equation (4.4a) (see Equations (4.6b) and (4.7b)). It should be noted that (average) stress factors are assumed to be constant in the respective interval.

3. The accumulated differential capacity loss due to calendar aging $Q_{\text{loss}}^{*\text{cal}}$ is calculated by
   $Q_{\text{loss}}^{*\text{cal}}(n+1) = Q_{\text{loss}}^{*\text{cal}}(n) + q_{\text{loss}}^{\text{cal}}(n) \cdot \Delta t$,
   and the accumulated differential capacity loss due to cycle aging $Q_{\text{loss}}^{*\text{cyc}}$ by
   $Q_{\text{loss}}^{*\text{cyc}}(n+1) = Q_{\text{loss}}^{*\text{cyc}}(n) + q_{\text{loss}}^{\text{cyc}}(n) \cdot \Delta FEC$,
   respectively.

Equations (4.6a) and (4.6b) present the calculation of the virtual time t^* and the differential form of Equation (4.3a), respectively.

$$t^*(T, SoC, Q_{\text{loss}}^{*\text{cal}}) = \left(\frac{Q_{\text{loss}}^{*\text{cal}}}{d_{\text{T}}^{\text{cal}}(T) \cdot d_{\text{SoC}}^{\text{cal}}(SoC)} \right)^{\frac{1}{z^{\text{cal}}}} \tag{4.6a}$$

$$q_{\text{loss}}^{\text{cal}}(T, SoC, t^*) = d_{\text{T}}^{\text{cal}}(T) \cdot d_{\text{SoC}}^{\text{cal}}(SoC) \cdot z^{\text{cal}} \cdot t^{*z^{\text{cal}}-1} \tag{4.6b}$$

With respect to cycle aging, Equations (4.7a) and (4.7b) present the calculation of the virtual full equivalent cycle FEC^* and the differential form of Equation (4.4a).

$$FEC^*(T, SoC, C\text{-}rate, DoD, Q_{\text{loss}}^{*\text{cyc}}) =$$
$$\left(\frac{Q_{\text{loss}}^{*\text{cyc}}}{d_{\text{T}}^{\text{cyc}}(T) \cdot d_{\text{SoC}}^{\text{cyc}}(SoC) \cdot d_{\text{C-rate}}^{\text{cyc}}(C\text{-}rate) \cdot d_{\text{DoD}}^{\text{cyc}}(DoD)} \right)^{\frac{1}{z^{\text{cyc}}}} \tag{4.7a}$$

$$q_{\text{loss}}^{\text{cyc}}(T, SoC, C\text{-}rate, DoD, FEC^*) =$$
$$d_{\text{T}}^{\text{cyc}}(T) \cdot d_{\text{SoC}}^{\text{cyc}}(SoC) \cdot d_{\text{C-rate}}^{\text{cyc}}(C\text{-}rate) \cdot d_{\text{DoD}}^{\text{cyc}}(DoD) \cdot z^{\text{cyc}} \cdot FEC^{*z^{\text{cyc}}-1} \tag{4.7b}$$

---

[4]Step n might be different regarding calendar and cycle aging.

The aging parameters could be determined by fitting the model to measured data of a specific battery type. This has successfully been tested with data from [68, 71, 72] (cf. Section 4.4) to confirm the validity. However, the task here is to find a typical parameter set for a more generic approach to maintain a replicable and comprehensible aging model. Thus, the aging parameters were determined through parameterizing the model using definitions, certain assumptions, or parameters supported by the relevant literature. The generic aging model was parameterized to reproduce monotonic behavior for battery aging. The reference values for each stress factor were based on values that typically occur in application-oriented scenarios, further described in this section. The exponential factors z were set to 0.5 since numerous studies observed a square root dependence for different batteries over both time or cycles [53, 67, 69, 71, 72]. While the freely adjustable stress exponents γ are based on assumptions to reproduce comprehensible aging effects, the aging pre-factors x resulted from the values outlined in Table 4.2. In this work, each stress factor was represented by a nearly linear behavior with increasing values. A linear aging behavior might not represent the actual aging behavior of all stress factors exactly. However, this will not affect the results in qualitative terms but strengthens their comprehensibility. Table 4.1 summarizes the parameters used for the generic calendar and cycle aging model.

Table 4.1: Definitions and assumptions for the generic calendar and cycle aging model. The aging pre-factors x resulted from the values outlined in Table 4.2.

Stress factor	Calendar aging		Cycle aging	
	Parameter	Value	Parameter	Value
T	T_{ref}	298.15 K	T_{ref}	298.15 K
	$\gamma_{\text{T}}^{\text{cal}}$	1000	$\gamma_{\text{T}}^{\text{cyc}}$	1000
	x_{11}	2.907e-03	x_{13}	5.689e-01
SoC	SoC_{ref}	0.5	SoC_{ref}	0.5
	$\gamma_{\text{SoC}}^{\text{cal}}$	1	$\gamma_{\text{SoC}}^{\text{cyc}}$	1
	x_{12}	1.937e-03	x_{14}	2.099e-01
C-rate	-	-	C-$rate_{\text{ref}}$	1
	-	-	$\gamma_{\text{C-rate}}^{\text{cyc}}$	1
	-	-	x_{15}	5.172e-02
DoD	-	-	DoD_{ref}	0.8
	-	-	$\gamma_{\text{DoD}}^{\text{cyc}}$	1
	-	-	x_{16}	7.241e-01
t	z^{cal}	0.5	-	-
FEC	-	-	z^{cyc}	0.5

A widely accepted definition of the relative capacity at BOL and EOL is 1 and 0.8, respectively, and was therefore applied in this work. According to a recent study on the degradation of commercial lithium-ion cells by Preger et al. [167], the results suggest that a few hundred to a few thousand FECs constitute a reasonable cycle life for NMC cells until a cell reaches 80 % of its initial capacity. Furthermore, a comprehensible aging behavior can be expected in this operating range. The EOL criteria for time and FEC, however, depend mainly on the operation of the battery. With regard to this work's use cases, a total operating time of ten years (t_{end}), which can often be found as the warrantied life, and 500 full equivalent cycles (FEC_{end}) was assumed before the battery reaches its EOL. All of the described stress factors were applied for both the calendar and cycle aging model. However, the weighting factor between calendar and cycle aging ω was set to 0.5 since no consistent observations have been made in the literature [72, 168, 169]. The weighting λ between the stress factors is based on assumptions that are supported by the literature. In the case of calendar aging, the impact of the temperature on aging is higher in many cases than the impact of the SoC [69, 71].

In the case of cycle aging, the DoD and the temperature often have a stronger influence on aging than the SoC or the C-rate [54]. Note that the absolute value of the parameters mentioned above is of subordinate interest for this work, as the product of the stress factors d is not subject to change for varying weighting factors λ. Nevertheless, reasonable weighting factors were selected with regard to the findings made in the literature. Table 4.2 shows the chosen EOL criteria and weighting factors.

Table 4.2: EOL criteria, definitions, and weighting factors for the generic aging model.

Parameter	Value
t_{end}	$10\,\mathrm{a}$
FEC_{end}	500
BOL_{C}	1
EOL_{C}	0.8
n_{cal}	2
n_{cyc}	4
ω	0.5
$\lambda(k)$	$1.225,\ 1.225^{-1}$
$\lambda(j)$	$2.2,\ 0.812,\ 0.2,\ 2.8$

4.2.2 Power electronics

Connecting batteries to the public grid require at least one converter stage to technically match these components, as the applied topology reveals. In the case of discharging the system, a DC/DC converter transforms the DC battery voltage into a higher DC voltage before conversion from DC to AC voltage takes place. This means different sources of possible losses, points of failure, and factors directly affecting the power distribution are present due to the chosen topology. However, the implementation of detailed power electronics models is not the focus of this work since most DC/DC converters and inverters are considered highly dynamic compared to the rest of the submodels, i.e., the battery model. Consequently, dynamic effects of the converter stages can be neglected, and a static implementation of those is sufficient in this case. Furthermore, the inverter was considered a nondissipative converter stage as the focus of this work is on quantifying the potentials of PFCSs. Thus, only the bidirectional DC/DC converters were implemented as look-up tables.

The DC/DC converter model takes into account different voltages levels on both the primary (45–52 V) and secondary side (25–42 V) as well as different power values (0–400 W) (see Figure 4.5). Consequently, the resulting look-up table shows the efficiency over the power at different voltage levels on both the primary and secondary side. Note that the calculation of the transformed power inside the BESS depends on the operation mode due to the converter's efficiency. 500 W was defined as $P_{rat} = 1$ in this work and P/P_{rat} related to the rated power of one BESS.
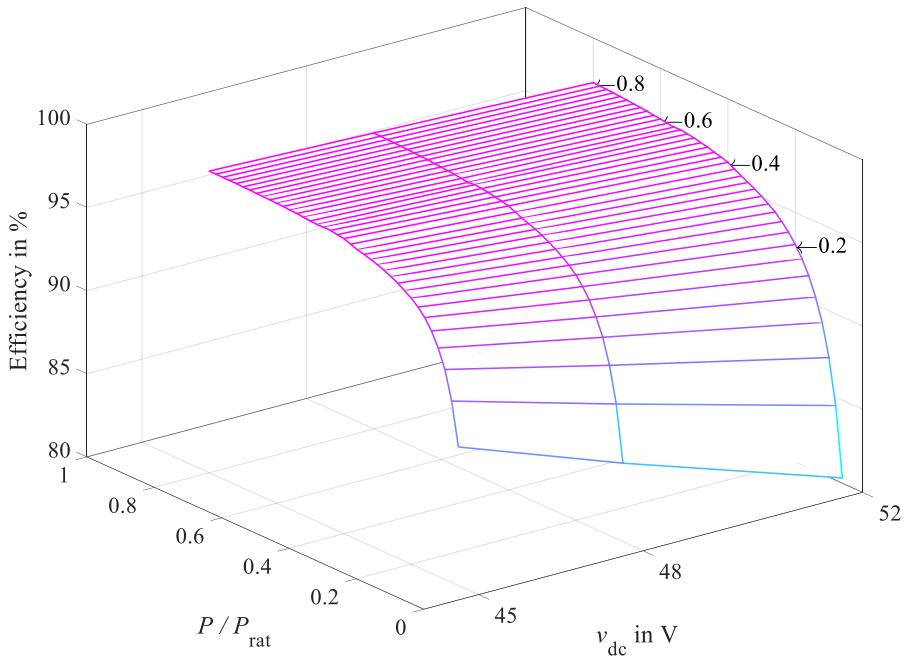

Figure 4.5: Efficiency map of the DC/DC converter showing the efficiency over the power at different DC bus voltage levels and a battery voltage of 36 V, as an example.

4.2.3 Hierarchical control

The concept of hierarchical control extends the simulation model to control the individual system components properly. As shown in a review by Meng et al. [93], hierarchical control has been successfully implemented in different DC microgrids, in which BESSs play a key role. It consists of the three levels mentioned in Section 2.2: primary, secondary, and tertiary control.

A linear droop-control was implemented at the primary control level to specify a setpoint for the desired output power P_i^* of the individual BESS. The droop control can be defined as

$$P_i^* = \frac{v_{\text{ref}}^* + \delta v - v_{\text{dc}}}{m_i}, \tag{4.8}$$

where P_i^* represents the desired output power of the ith BESS, v_{dc} the voltage at the common DC bus, δv the control signal of the proportional integral (PI)-controller of the secondary control, v_{ref}^* the reference DC voltage, and m_i the droop coefficient. The reference DC voltage was set to 48 V in this work. 48 V constitutes a reasonable voltage level to enable boost operation of the DC/DC converters, as the maximum voltage of the battery packs is 42 V. To calculate the droop coefficients, the desired output power shares were normalized to $m_{\text{min}} = 0.25$ V/kW. This value was chosen to keep the load-dependent voltage deviation below 1 %. Consequently, the maximum desired output power at each time step calculates to $m = 0.25$ V/kW. For simulation reasons, the desired output power P_i^* was directly calculated based on the applied PFCS. Equation (4.8) was only used to emulate the droop voltage due to the load-dependent voltage deviation.

Secondary control was implemented via a PI-controller that restores the load-dependent voltage deviation to the reference DC bus voltage v_{ref}^*. The computed control signal δv acts as an input parameter for the primary control. The resulting DC bus voltage v_{dc} is used for the power electronics look-up table, respectively. In this simulation model, the PI-controller was implemented as a discrete-time PI-controller with a trapezoidal integrator method and can be defined as

$$\delta v(z) = \left[k_{\text{p}} \left(1 + k_{\text{i}} \frac{T_{\text{s}}}{2} \frac{z+1}{z-1} \right) \right] (v_{\text{ref}}^* - v_{\text{dc}}), \tag{4.9}$$

where δv indicates the control signal, k_{p} the proportional gain coefficient, k_{i} the integral gain coefficient, and T_{s} the sampling period. Here, the gains of the secondary controller ($k_{\text{p}} = 0.00061$ and $k_{\text{i}} = 7.5\,\frac{1}{s}$) were chosen to meet a reasonable compromise between the overshoot and the settling time. A detailed study on this was the main part of a bachelor thesis [170] in the *UnABESA* research project.

Tertiary control appears on top of both primary and secondary control and manages the power flow in the system. At this level, the PFCSs are usually implemented. In more detail, the parametric PFCS (PFCS SoAP) and the sequential PFCS (PFCS Pseq) were implemented at this control level, and the power-sharing factors concerning the applied PFCS were calculated.

4.2.4 Scenarios

The scenarios used in this work are similar to those described in Section 2.2. The advantage of these two scenarios is that the profile characteristics such as the length of the resting periods, the number of sign changes, or the energy between sign changes are completely different. Thus, this work is based on two distinct application-oriented scenarios suitable for BESS applications. Both profiles cover an operating period of one day with a one-second sampling period. Each profile is normalized to the rated system power for the simulations and can be scaled up arbitrarily.

In the peak shaving scenario, a certain threshold can be set to precisely shave the peak load (see pink line in Figure 4.6a)). The amount of the potentially discharged energy is then recharged at an arbitrary time outside of the peak load time window to assure comparability when quantifying the potentials and sensitivities of different PFCSs. In this work, the discharged energy was recharged seven hours after the beginning of the scenario with a total maximum charging power of 20 % of the rated system power. Regardless of the peak shaving process, these values ensure that the recharging is finished in time and that they intend to cause just a low impact on the degradation of the batteries. The time for recharging, in turn, depends on the discharged energy and is therefore variably, as indicated with the gray arrow. In practice, the load profile might vary on different days. However, the described scenario is an exemplary use case and could be replaced by any other desired scenario.

In the frequency regulation profile, the energy throughput is also equalized for comparability reasons regardless of the scaling factor. Figure 4.6 shows both utilized application-oriented scenarios.
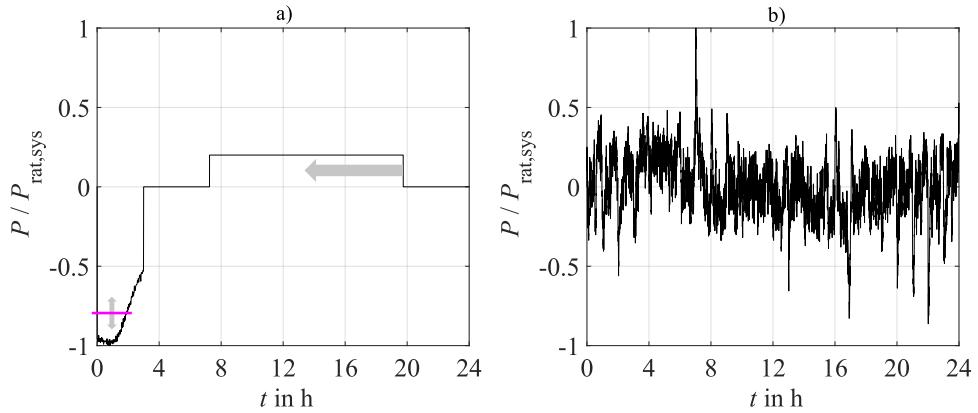
Figure 4.6: Utilized application-oriented scenarios according to my published works [11, 12]. a) peak shaving scenario, b) frequency regulation scenario.

4.3 Peripheral system

In this work, each of the applied PFCSs is characterized by two freely selectable parameters (design variables), as shown in Section 2.2. BESS applications are characterized by the system design, e.g., the rated capacity of the batteries and the use case scenario as defined by the profile scaling factor (use case variables). From a BESS operator's point of view, parametric design variables for a given scenario should be chosen concerning simultaneously maximizing the efficiency, performance, *and* service life of the BESS, i.e., optimizing the three independent target indicators. However, an analytically closed form of the functional correlation between the target indicators and the design and use case variables is not accessible, as some parts of the BESS model are nonlinear. This characterizes the problem as a MOO on a black-box function problem [138] (cf. Section 3.2). Furthermore, the correlations are only available through expensive to evaluate simulations. Solving this problem by using the HSE methodology requires (among other things) modifying the toolchain presented in [159] to a BESS-specific environment, including the presented simulation model.

According to Palm and Holzmann [159], different requirements should be met to execute the HSE work flow. First, the simulation model should run domain or cross-domain specific simulations individually. Second, for further processing, the results of the individual simulations should be stored in a simulation result storage. And third, the implemented HSE environment should run a five-step process

flow (see Chapter 5). To meet these requirements, a BESS-specific HSE toolchain, including the BESS simulation result storage and the five-steps process flow, was programmed using the programming language *Python*™. An interface between *MathWorks MATLAB®/Simulink®* and *Python*™ was set up to automatically run *Simulink®* simulation models via a script. Finally, the HSE toolchain was modified by implementing the BESS simulation model as a modeling and simulation environment. The complete BESS-specific HSE toolchain is shown in Figure 4.7.
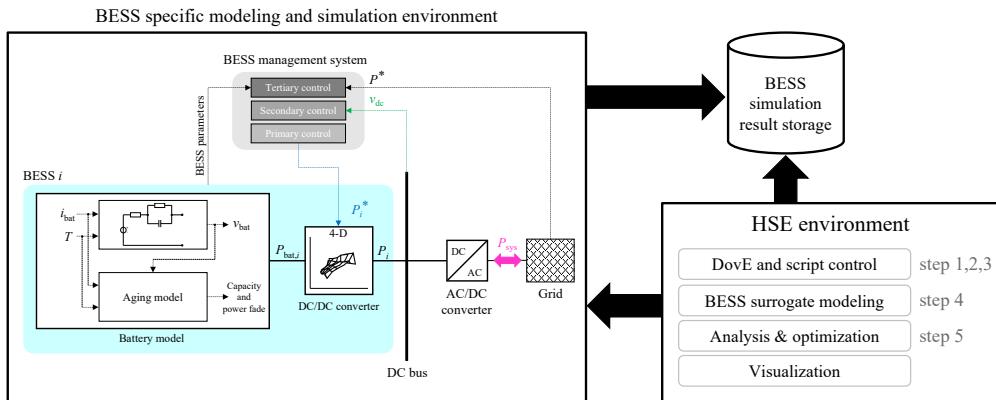

Figure 4.7: Modified mutli-objective BESS optimization HSE toolchain according to [159]. Adapted from my published work [12].

As a result, the peripheral system to quantify the potentials and sensitivities of PFCSs is formed, and a solid basis for answering the research questions is provided. In the following, verification and validation of the submodels are presented to prove the validity of the simulation model.

4.4 Model verification and validation

In this section, the model design, i.e., the submodels battery, power electronics, and control scheme described in the previous sections, was tested in terms of a verification and validation process.[5] As shown in Figure 4.2, the utilized BESS simulation model (system) is composed of different submodels, and each submodel consists of individual units. Dating back to the ideas of Boehm [171], such a process is ideally done by using a bottom-up approach. Therefore, the units, e.g., the generic aging model, are tested before the submodels, e.g., the entire battery. Finally, the validation on a system-level shall prove the validity of the entire sim-

---

[5]For the sake of completeness, a formal verification of the target indicators can be found in Appendix C Figures C.20 and C.21.

ulation model and confirm whether the simulation model is suitable to solve the given problem. For the latter, it would be necessary to validate each simulation run by performing the corresponding measurement in this work. However, the time and resources required for validations to this extent are not available due to the extensive parameter variation when applying the HSE methodology. Furthermore, such an approach would implicitly assume that, e.g., each battery configuration is available and could be either measured in terms of the electric or aging behavior. To overcome this difficulty, one approach to ensure the validity of the results in this work is to examine the transferability of each submodule (battery, DC/DC converter, and control scheme) when design and use case variables are changing. Another benefit of this approach is that sensitivities can be evaluated, and consequently, the external validity is strengthened.

According to the IEEE Standard for System, Software, and Hardware Verification and Validation [172], verification is defined as "*the process of evaluating a system or component to determine whether the products of a given development phase satisfy the conditions imposed at the start of that phase*" and validation as "*the process of evaluating a system or component during or at the end of the development process to determine whether it satisfies specified requirements.*" Consequently, verification and validation can be interpreted as follows in the context of this work: The verification confirms that the developed model is correctly implemented and its output matches a defined measurement. The validation checks whether the accuracy of the model is satisfactory in its intended application.

Verification and validation of the battery model
The verification and validation of the electric battery model were carried out on a battery test system from ScienLab (SL80/100/8BT6C), providing up to 100 A per channel. They were based on an analysis of the model error between the simulated and measured voltage. Since the heterogeneity (use case variable) was considered the variation of the rated capacity and internal resistance in this work, two Samsung 18650 25R lithium-ion battery packs in 10s2p and 10s1p configuration were analyzed to examine the battery model's transferability when this use case variable is changing. The applied battery pack (battery 1) comprised 20 Samsung 18650 25R lithium-ion cells with a rated capacity of 5 Ah and a rated voltage of 36 V. The other battery pack (battery 2) consisted of ten Samsung 18650 25R lithium-ion cells with a rated capacity of 2.5 Ah and a rated voltage of 36 V. Note

that the current measurement error of the battery test system was not considered within the simulation model. However, simulations with the maximum specified current measurement error of the battery test system were carried out, identifying the boundaries of possible inaccuracies. The respective elements of the chosen electric battery model were parameterized at 20 °C.

At first, the actual capacities of both battery packs were measured by discharging the full battery packs at a C-rate of 1 C. For battery 1 the discharge capacity amounted to 4.98 Ah, and for battery 2 the discharge capacity was 2.49 Ah. The static behavior was identified by measuring the OCV in both charging and discharging mode at a constant C-rate of 0.05 C. The average value of both curves was then used as the OCV curve. Since the OCV curves of battery 1 and battery 2 were almost similar over a broad SoC range, the OCV curve of battery 1 was applied for the battery model (see Appendix Figure C.1). The dynamic behavior was characterized by a hybrid pulse power characterization (HPPC) test [173], in which five different charging and discharging currents at eleven SoCs were applied. The HPPC test is a common method to determine the dynamic behavior of lithium-ion batteries [174, 175] and was therefore used within this work. Consequently, the voltage responses of the batteries during the pulses (20 s) were analyzed, and the values of R_s and the RC-circuit were determined. Figure 4.8 shows the comparison of the simulated and the measured voltage of battery 1 in a voltage-time diagram.[6]

---

[6]The comparison of the simulated and the measured voltage of battery 2 can be found in Appendix C Figure C.2.

a)

b)
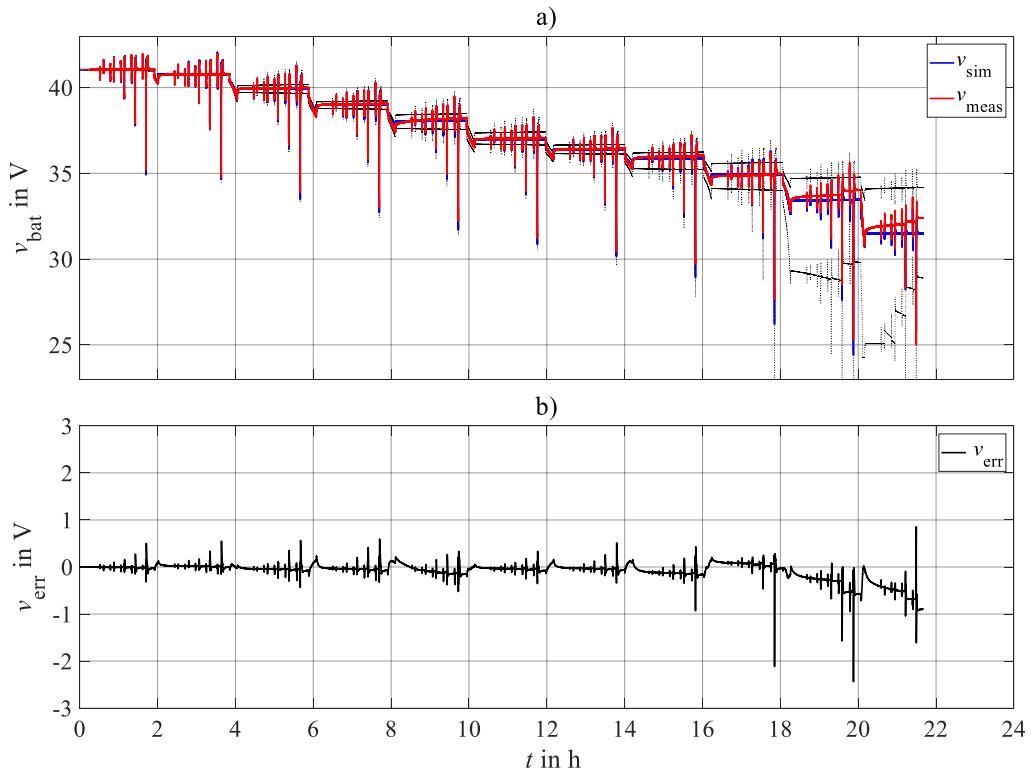
Figure 4.8: Comparison of the simulated terminal voltage (blue) and the measured terminal voltage (red) of battery 1. The dotted lines show exemplary simulations with the maximum specified current measurement error of the battery test system. a) terminal voltages, b) model error. Adapted from my published work [12].

As can be seen, the simulated terminal voltage showed a similar behavior as the terminal voltage of the real battery, indicating a successful verification. The simulated voltage was following the measured one during almost the whole pulse profile. Difference up to -2.4 V occurred only for a low SoC ($\leq 10\%$). Since the voltage dropped disproportionately in this area, the difference between the simulated and measured voltage, especially at the end of the highest discharge current, was comparably high at SoCs less than or equal to 10%. Similar results were obtained for battery 2. More detailed results are shown in Figure C.3 in Appendix C, in which boxplots represent the model errors for both batteries. The inaccuracies can be attributed to at least two effects. First, the approximated OCV curve showed a slight asymmetry between the charge and discharge curve leading to deviations when applying the average values of both curves. Second, no current measurement error of the battery test system was considered within the simulation model. However, the dotted lines show exemplary simulations with the maximum specified current measurement error (± 20 mA) of the considered battery test sys-

tem. The resulting interval defines the range of possible simulation results for a constant current measurement error. In general, the median model error of battery 1 was approximately -35 mV, and the median model error of battery 2 was at around 41 mV. The peak value of outliers reached -2.4 V for battery 1 and 2.8 V for battery 2, whereas, in the area $> 10\%$, the model error of both batteries was considerably smaller.

Since the model parameters were determined using the HPPC test, and thus only short and defined pulses were applied, the battery model was further validated by two data sets that represent the scenarios as presented in Section 4.2. The advantage of using these two distinct scenarios is that the effects of the battery model and the parameterization method on the applied scenarios can be investigated thoroughly. Consequently, the model behavior can be examined for a profile with either low and high dynamics. By way of example, the simulation model with the parameters of battery 1 was applied in the following.[7]

In the case of the frequency regulation scenario, a slight difference between the simulated and measured terminal voltage was observed (median model error of approximately -282 mV). Outliers of up to -1 V were observed only at the end of the test for low SoCs. This is consistent with the results obtained in the verification case and could be attributed to the increasingly inaccurate OCV curve at low SoCs and the current measurement error of the battery test system.

---

[7]The results of the validation case for battery 2 can be found in Appendix C Figures C.4 and C.5.
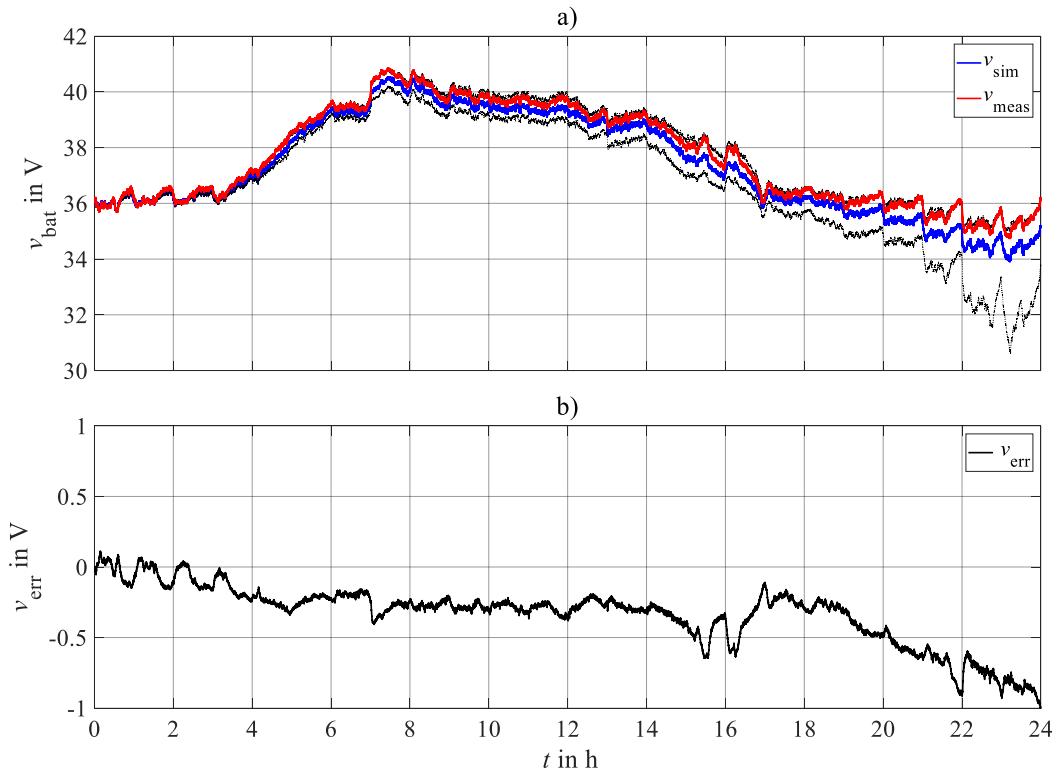
Figure 4.9: Comparison of the simulated terminal voltage (blue) and the measured terminal voltage (red) of battery 1 for the frequency regulation scenario. The dotted lines show exemplary simulations with the maximum specified current measurement error of the battery test system. a) terminal voltages, b) model error.

However, Figure 4.10 reveals that another drawback of the battery model and the parameterization method could be identified. Covering the effects of the recovery phases remains difficult using the described ECM (see Figure 4.10 at around 8 h). It is apparent that this effect implicates measurable voltage deviations due to a faster decay behavior. Consequently, there is room for improvement concerning the battery model and the parameterization method. More detailed results are shown in Figure C.6 in Appendix C, in which boxplots represent the model errors for both batteries. Nevertheless, considering the advantage of the gained computation speed and the research questions, a median model error of roughly $\pm 280 \, \text{mV}$ is acceptable. The battery model is valid and can be used to quantify the potentials of different PFCSs.
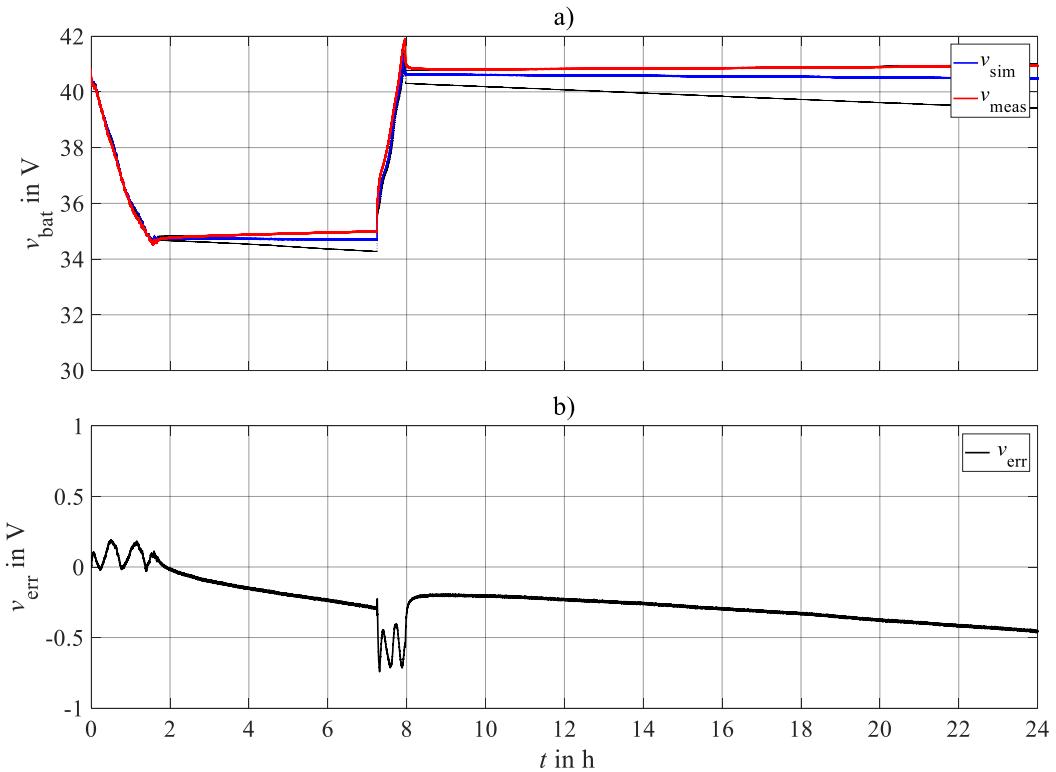
Figure 4.10: Comparison of the simulated terminal voltage (blue) and the measured terminal voltage (red) of battery 1 for the peak shaving scenario. The dotted lines show exemplary simulations with the maximum specified current measurement error of the battery test system. a) terminal voltages, b) model error.

In the case of the battery aging model, verification was done based on different literature data sets. Validation was not part of this work since aging experiments would be considerably time-consuming, especially for the different battery configurations resulting from the extensive parameter variation. Furthermore, a more generic approach was chosen intentionally in this work to model common aging effects regardless of the specific battery type or format. The generic aging model, however, is based on assured knowledge of the aging effects of lithium-ion batteries through only representing common aging effects that have already been investigated thoroughly in the literature. Thus, the obtained results are supposed to be transferable, too.

The verification was performed by comparing the output of the fitted aging model with measured data from the literature. For this reason, two specific battery types—a 26650 LFP/C cell and an 18650 NMC/C cell—were successfully tested for both calendar and cycle aging with data from [68, 71, 72]. By way of example,[8] the results of the generic aging model using the data of the aging experiment (26650 LFP/C cell - calendar aging) presented in [71] are given in Figure 4.11. In more detail, a comparison between the measured values for Q_{loss} and the results of the generic aging model with a static SoC of 100 % for three different temperatures was performed.
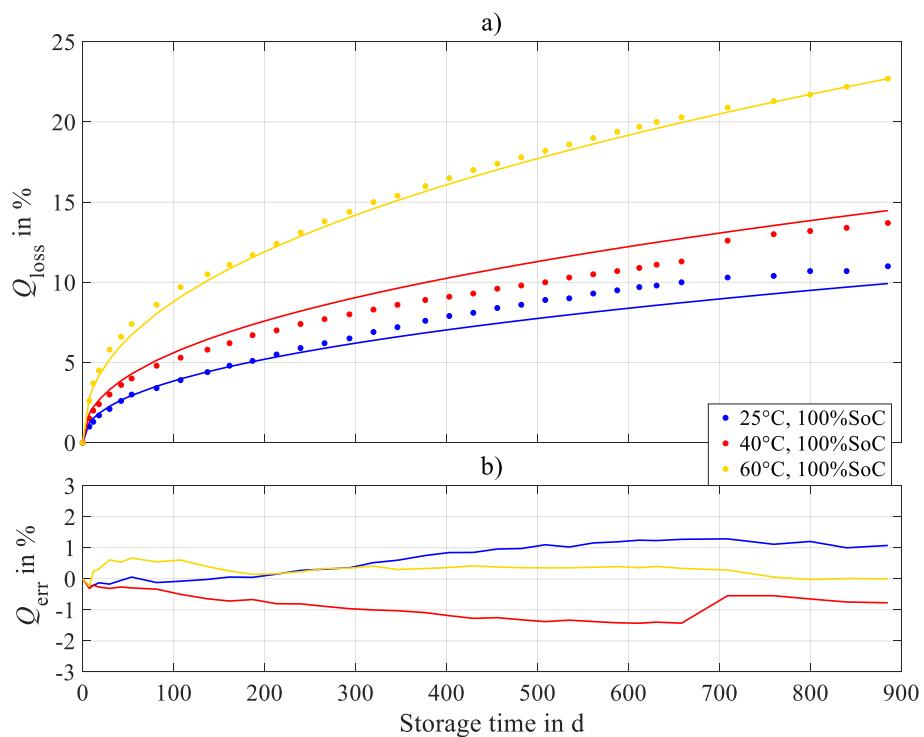

Figure 4.11: Results of the generic aging model using the data of the aging experiment presented in [71]. a) loss of relative discharge capacity, b) model error.

As shown in Figure 4.11, the obtained results indicated a slight difference between the measured and the fitted loss of the relative discharge capacity Q_{loss}. Consequently, the model error ranged between ± 2 %. However, this is consistent with the results obtained in [71]. Similar results were obtained when using the data of the cycle aging experiments presented in [72] and were also in good agreement with the results there. However, the data presented in [72] showed an atypical

---

[8]Further results of the verification can be found in Appendix C Figures C.7–C.9.

behavior resulting in a recovery of the capacity (cf. Appendix C Figure C.7). The generic aging model used in this work cannot model such effects. In the case of the 18650 NMC/C cell, in most test points, the comparison revealed a similar behavior with a model error lower than $\pm 3\%$. However, the difference at some test points was higher than $\pm 3\%$, especially when the loss of the relative discharge capacity was above 20%. Nevertheless, losses of more than 20% are not expected in this work. Generally, the choice of the test points is crucial when modeling the aging behavior of batteries. Even though the generic model cannot consider each aging effect of a battery, the correct implementation and applicability of the presented aging model was shown by the verification.

Verification and validation of the power electronics model
The verification and validation of the DC/DC converter model were performed by using a bidirectional dynamic synchronous buck-boost converter as a reference. This DC/DC converter was developed at the *Institute for Sustainable Energy Systems (ISES)* to build a reference system for the simulation model similar to the system described in Section 4.1. Thus, the applied converter is specified to provide a voltage range from 12–60 V on both the primary and secondary side (depending on the application) with a rated power P_{rat} of at least 500 W. Measurements were carried out using a high-precision power analyzer from Zimmer (LMG670) to accurately determine the input and output power of the DC/DC converter.

The verification was done by comparing the measured with the simulated efficiency at different voltage levels for the primary and secondary sides. This approach was intended to check that the output of the simulation model correlates with the real converter's results and test the model's response on varying input parameters. The latter is of great interest to ensure the transferability of the results of this work, especially when use case variables or primary side voltage levels are changing. As an example,[9] the efficiency curves of the applied DC/DC converter at a primary side voltage of 48 V are shown in the following.

---

[9]Efficiency curves at different primary side voltage levels can be found in Appendix C Figures C.10 and C.11.
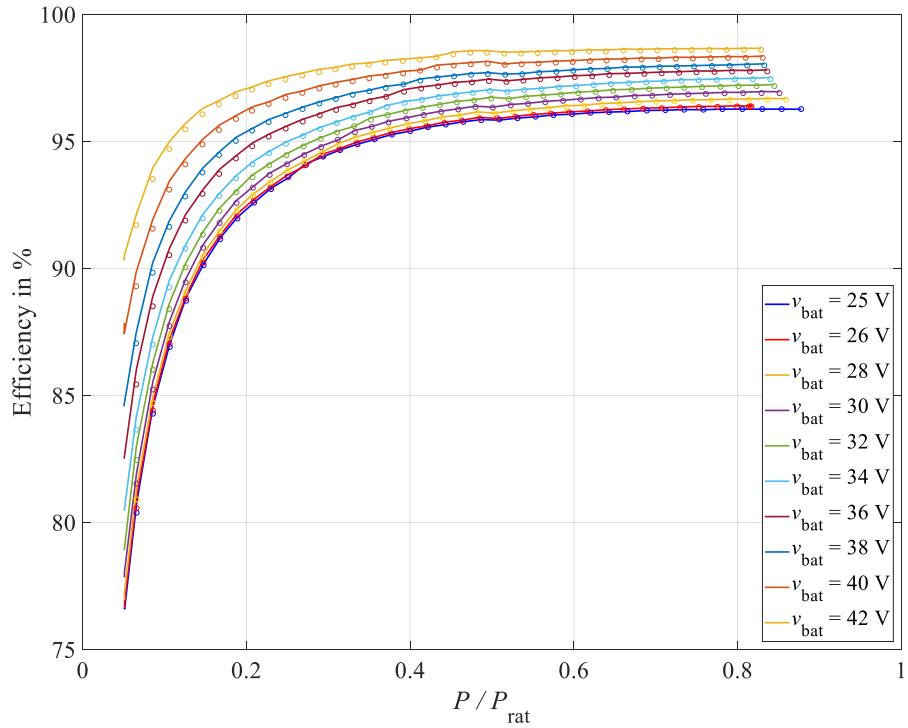
Figure 4.12: Efficiency curves of the applied bidirectional dynamic synchronous buck-boost converter at a primary side voltage of 48 V. The solid lines show the measured efficiencies at different secondary side voltages, and the markers represent the corresponding simulated efficiencies.

The measured and simulated efficiencies in Figure 4.12 show a successful verification of the DC/DC converter model, as both are similar. The measured efficiency curves demonstrated the typical characteristics of such a DC/DC converter. It should, however, be noted that at around 0.3–0.5 P/P_{rat} slight steps in the efficiency curves were observed. These little steps are attributable to the switching between two different current measurement ranges. Nevertheless, comparing the measured and simulated efficiencies shows that the simulation model calculated the efficiency for different power steps and secondary side voltages (v_{bat}) correctly, and only slight differences occurred. In particular, the model error was lower for increasing values of P/P_{rat}. These slight differences resulted from the discrepancy between the measured values (P, v_{bat}, and v_{dc}) and the values stored in the look-up table. The median model error of all measured and simulated test points amounted to -0.039 %. However, when the primary side voltage was set to 45 V, the median model error was -0.042 %, and in the case of a primary side voltage of 52 V, the median model error amounted to -0.033 %. Since these errors are considered small

76

and hardly measurable, the model was correctly implemented. Furthermore, the median model error for changing primary side voltages remains almost constant which indicates the transferability of the results for changing input parameters.

The DC/DC converter was further validated to ensure that the simulation model is valid for the scenarios used in this work and operational needs can be met. For this purpose, the converter was connected to battery 1 on the secondary side and the battery test system from ScienLab (SL80/100/8BT6C) on the primary side. Measurements were again performed using the high-precision power analyzer from Zimmer (LMG670) to accurately determine the input and output power on both sides of the DC/DC converter. The converter was operated in boost-mode at a primary side voltage of 48 V. The goal of this approach was to compare the measured battery power P_{bat} with the simulated one to check the simulation models's accuracy. The first 20 min of the peak shaving scenario were applied in a first test, as illustrated in Figure 4.13.
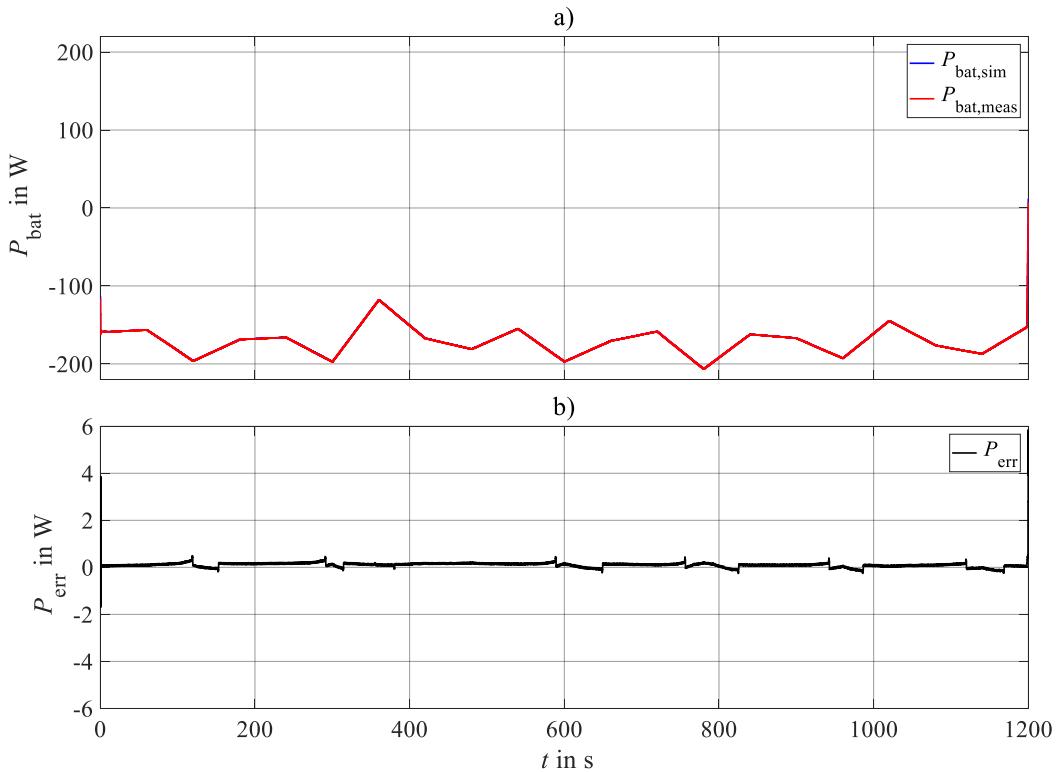

Figure 4.13: Comparison of the simulated and measured battery power P_{bat} for the peak shaving scenario. The bidirectional dynamic synchronous buck-boost converter was operated in boost-mode and at a primary side voltage of 48 V. a) battery power, b) model error.

77

The upper graph a) shows the comparison of the simulated and measured battery power P_{bat} and indicates that both are almost congruent for the whole testing period. In the lower graph b), the model error concerning the power is displayed. As can be seen in this graph, the model error was minimal in this case. Slight differences occurred at the beginning and the end of the test, where outliers of up to almost 6 W were observed. These errors are attributable to the switch-on/off processes, where a short time delay between input and output power occurred. Furthermore, the median model error amounted to 0.12 W for the peak shaving scenario. It can be concluded that the model's accuracy is very high for comparable scenarios since the simulation model was parameterized accurately in these operating ranges. However, a more dynamic scenario with various sign changes and the minor output power led to a higher model error, as evident in Figure 4.14.
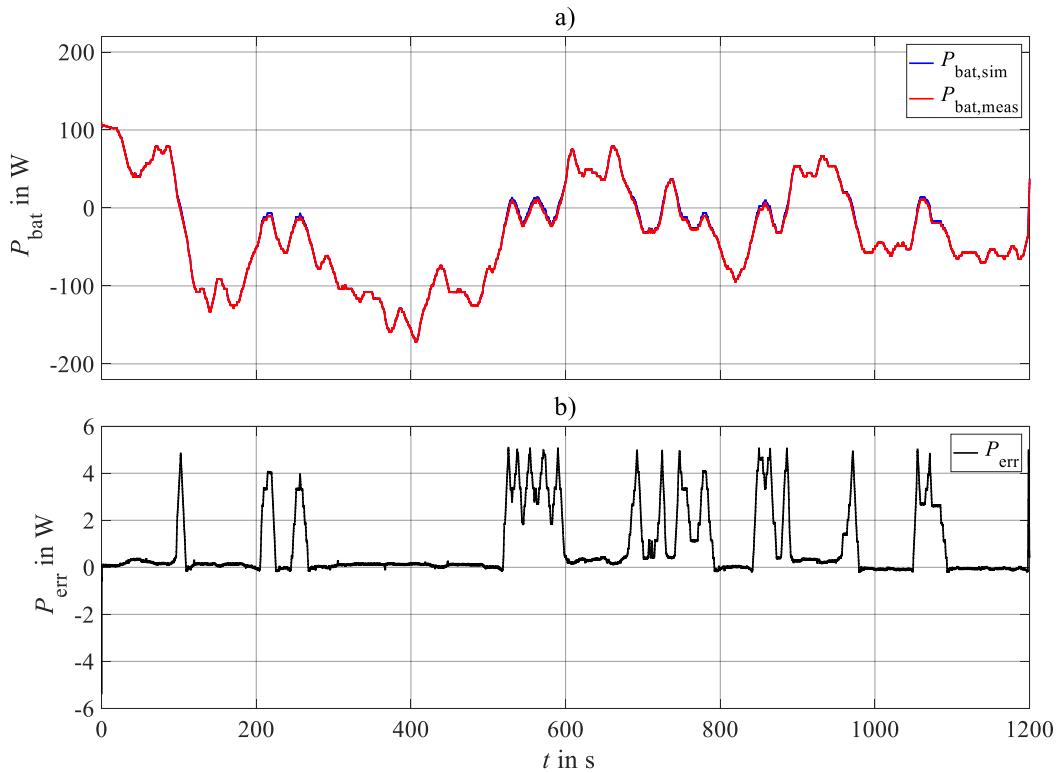
Figure 4.14: Comparison of the simulated and measured battery power P_{bat} for the frequency regulation scenario. The bidirectional dynamic synchronous buck-boost converter was operated in boost-mode and at a primary side voltage of 48 V. a) battery power, b) model error.

Especially at an output power below 20 W, differences between the simulated and measured battery power P_{bat} were observed, as shown in the upper graph of Figure 4.14. Outliers of up to 5 W arose. This is consistent with the results

obtained during verification. In these operating ranges, the simulation model was hardly parameterized as power values were too small. Therefore, the efficiency values of the last measured values were applied, accepting the resulting inaccuracies.[10] The median model error was, however, small with 0.16 W. More detailed results are shown in Figure C.12 in Appendix C, in which boxplots represent the model errors of the output power of the battery model. Nevertheless, the energy losses in these operating areas are relatively small compared to the overall energy throughput. Thus, the simulation model is considered accurate and suitable when quantifying the potentials and sensitivities of different PFCSs for heterogeneous BESSs. Note that the range of validity is limited to power electronics with similar characteristics such as the curve shape or the mainly monotonically increasing efficiency. In this case, the transferability of the results obtained in this work should be preserved, even if absolute efficiency values change for different systems.

Verification of the control scheme

For verification of the control scheme, in particular, the tertiary control, simulation results of eight different combinations of load profiles, use case variables, PFCSs, and design variables were compared to its corresponding measurements. The measurements were carried out on a battery test system from ScienLab (SL80/100/8BT6C) with three batteries (2x battery 1 and 1x battery 2) connected to separate channels. The BESS management system was implemented on a central controller to calculate the power share of each battery concerning the four criteria mentioned previously. Two generic load profiles were used, a static one and a dynamic one, to check the tertiary control under very diverse conditions. This further involved the variation of the profile scaling factor (use case variable). In addition, the two presented PFCSs were tested for changing design variables. As an example,[11] the test case comprising the static load profile with a requested power P^* of 40 % of the rated BESS power and the sequential PFCS (PFCS Pseq) with the two design variables $P_{\max} = 150$ W and *Sorting* $= 0$ is shown in Figure 4.15. $P_{\max} = 150$ W means that the maximum power share of each battery is limited to 150 W by the PFCS, and *Sorting* $= 0$ means that the batteries are used in ascending order.

---

[10]The extrapolation mode was set to "clip," and therefore, the last table value for inputs at or above the last breakpoint was used.

[11]Further tests of the verification of the control scheme can be found in Appendix C Figures C.13–C.19.
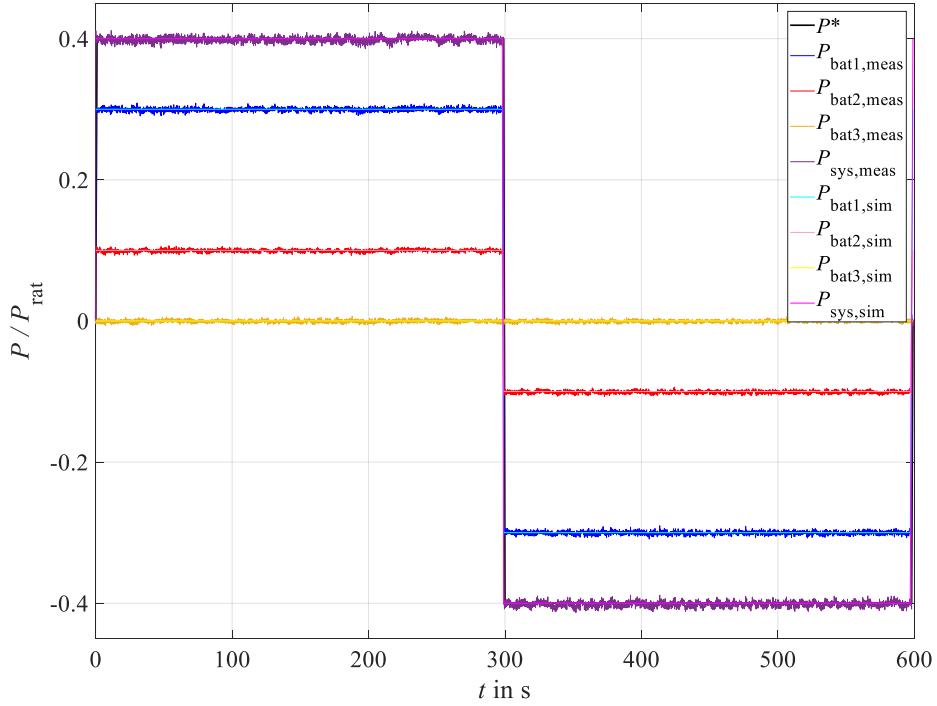
Figure 4.15: Test case for verification of the control scheme. Static load profile with a requested power P^* of 40 % of the rated BESS power and the sequential PFCS (PFCS Pseq) with the two design variables $P_{\text{max}} = 150\,\text{W}$ and *Sorting* $= 0$, indicating that the batteries were used in ascending order.

From Figure 4.15 it can be seen that a good match between simulation and measurement was achieved for both the charging and discharging mode. The requested power was shared as intended, where the first battery provided a maximum of $150\,\text{W}$ (equivalent to $0.3\,P/P_{\text{rat}}$) and the second battery took over the rest of the requested power. Here, the median error of the power was $0.19\,\text{W}$ for the first battery and $0.27\,\text{W}$ for the second battery. Similar results were obtained when testing other combinations of load profiles, use case variables, PFCSs, and design variables, as can be seen in Appendix C. These slight differences between the simulation and measurement results can be attributed to the inaccuracies of the measurement. Nevertheless, the results demonstrate that the control scheme, especially the tertiary control, fits well into BESSs and can be used within the simulation model. Consequently, when design and use case variables change, the transferability of the simulation results is still given.

Conclusions for the verification and validation

Referring back to the ideas at the beginning of this section, one crucial point when applying the HSE methodology is to ensure validity of this work's results when design and use case variables change during the simulations. The verification and validation in this way helped overcome this problem generally. Furthermore, it proved that the simulation model implemented in the HSE toolchain constitutes an appropriate approach to answer the research questions adequately. However, and as previously stated in the respective sections, some minor challenges are associated with the submodels. For example, inaccuracies of the electric battery model at very high or low SoCs slightly impact the target indicator "performance" since battery limits are reached differently compared to the actual battery pack, as can be seen in Figures 4.9 and 4.10. Furthermore, the parameterization of the generic aging model affects the target indicator "service life" in quantitative terms. Quantitative mismatches on a small scale concerning the target indicator "efficiency" are also present, e.g., for divergent efficiency curves of the power electronics (see evaluation of different primary voltage levels). Continuing research could explore how to a) quantify model inaccuracies of, e.g., the aging model concerning the stress factors and b) develop the target indicators further to compensate for such model inaccuracies.

Nevertheless, the difficulties mentioned above do not significantly affect this work's qualitative results as the focus here is on evaluating PFCSs and not on detailed modeling of the systems' submodels. Even if absolute values may change for different battery types, power electronics, or parameters applied, the key points remain the same for the specified validity ranges of the submodels. Thus, the advantages when using the HSE methodology outweigh potential model inaccuracies by far. In the following chapter, the methodological framework to execute the intended investigations is explained in detail.

5 Methodological framework for evaluating power flow control strategies

The BESS-adapted HSE toolchain, including the validated BESS simulation model, provides the necessary foundation to quantify the potentials and sensitivities of different PFCSs for heterogeneous BESSs both effectively and efficiently. In the context of BESSs, this toolchain was first introduced in my published work [12], in which it has been proven to successfully solve MOO problems for simulation accessible environments and has since been used in my published work [14]. An evolved version of it was utilized in this work to solve the MOO on a black-box function problem and analyze the correlations between input variables and target indicators more profoundly. Therefore, a methodological framework for evaluating PFCSs is introduced by means of the HSE process flow as part of the BESS-adapted HSE toolchain. The methodological framework enables quantifying the potentials and sensitivities of PFCSs in different use cases and system designs. Consequently, it improves the understanding of the correlations between the PFCSs, use cases, and target indicators by systematically analyzing them. The content of this chapter is built on my published work [14].

Accordingly, this chapter addresses the implementation of the HSE process flow and the methods for evaluation and visualization of this work's results. In general, the generic HSE process flow is separated into five steps and explained in detail by Palm and Holzmann [159]. Detailed information about the HSE process flow and the parameters and optimization algorithms used within this work is provided in the following sections. In Section 5.1, a comprehensive definition of the BESS hyperspace is provided as this constitutes the first step of the process flow. Based on the defined hyperspace, an initial experimental test plan is created by suitable algorithms in step two before the simulations are executed according to this plan,

and the results are filed in the BESS simulation result storage in step three. The parameters and algorithms used for the design of virtual experiments (DovE) (i.e., experimental test plan) are described in Section 5.2. In step four, the BESS surrogate models are built based on the results of the previous step. The surrogate models are further optimized in step five, enabling a conclusive analysis of different PFCSs for heterogeneous BESSs. Steps two to five are executed in a loop. The chosen surrogate models and their characteristics are also explained in Section 5.2. Finally, the different evaluation and visualization methods complete the methodological framework and are presented in Sections 5.3–5.5. An overview of the methodological framework, including the HSE process flow, is given in Figure 5.1.
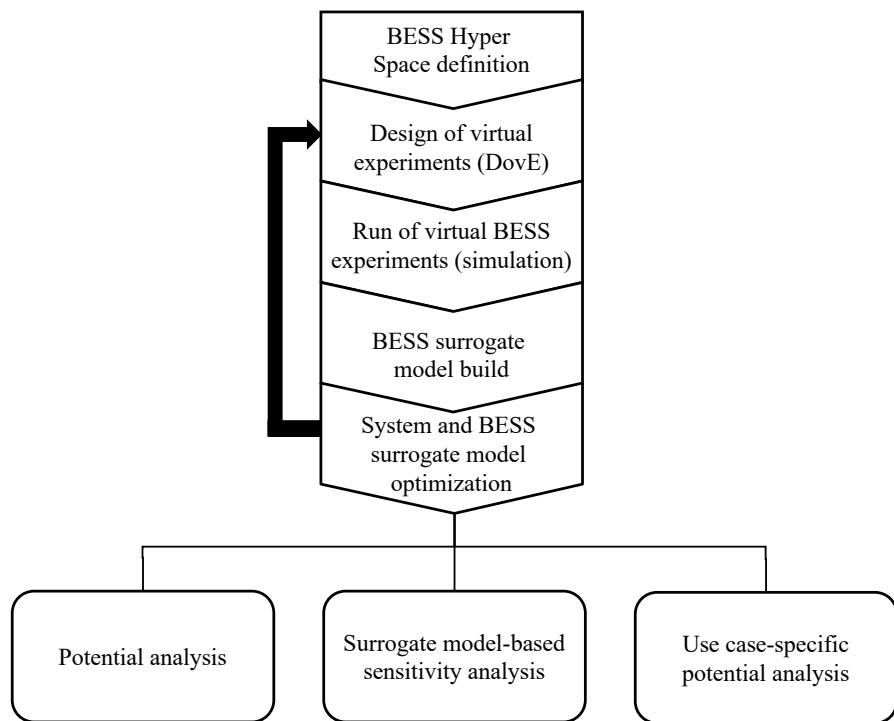
Figure 5.1: Methodological framework for evaluating PFCS, including the HSE process flow according to [159] and the methods for evaluation and visualization. Adapted from my published work [12].

5.1 Hyperspace definition

The BESS hyperspace consists of three different spaces: design space, use case space, and target indicator space, as previously mentioned in Section 3.3. As a preliminary point, however, fixed parameters of the BESS simulation model were specified. As defined in Section 4.1, the number of BESSs was set to three in this work, resulting in a rated system power of 1500 W. In the case of the peak shaving

scenario, the initial SoC of each battery was set to 90 %, and for the frequency regulation scenario, the initial SoC of each battery was set to 50 %. These SoCs are typical for BESSs deployed in such scenarios. Moreover, the ambient temperature was specified at a constant value of 25 °C for both scenarios, suggesting a tempered system containment. All these parameters were entirely fixed and did not change during the virtual experiments.

However, design variables and use case variables changed within a specified range during the virtual experiments. The design variables were further linked to the PFCSs, which have already been presented in Section 2.2. Note that different PFCSs could be used interchangeably since the PFCS is independent of the premises stated in this section. In this work, the virtual experiments were carried out using two distinct PFCSs. The first PFCS (PFCS SoAP) copes with the transition between power balancing and state of energy (and similarly state of charge) balancing due to the two freely selectable prediction horizons $t_{\mathrm{pred,p}}$ and $t_{\mathrm{pred,e}}$ and is therefore well suited for this work. Both were considered continuous design variables. The second PFCS (PFCS Pseq) allows operating BESSs sequentially, which is a significant difference from the first PFCS. Here, the two arbitrary parameters, namely P_{max} and Sorting S, are decisive for each individual BESS's maximum allowed charge/discharge power and the merit order of the BESSs.[1] P_{max} was considered a continuous design variable and S a discrete design variable.

Regarding the use case variables, the arbitrary parameters were linked to the system design (*heterogeneity*) and the scenario (*profile scaling factor*). The heterogeneity H_{C} was considered the variation of the batteries' rated capacity and internal resistance. In particular, it constituted a vector of four discrete values, each representing one specific system design (cf. Appendix C Table C.6). In this case, the heterogeneity is not bijective, meaning that another system design could result in the same heterogeneity. A heterogeneity of zero would be the equivalent of a completely homogeneous system. In this work, however, the values were chosen to consider more heterogeneous system designs. The profile scaling factor PSF was used to scale up the normalized profiles regarding the rated system power of 1500 W. Therefore, the maximum value of the specific normalized profile corresponds to the proportion of the rated system power defined by the profile scaling factor. Note that 1500 W was defined as $P_{\mathrm{rat,sys}} = 1$ in this work and $P/P_{\mathrm{rat,sys}}$

---

[1] 0 = ascending order, 1 = descending order

relates to the rated system power. Both use case variables were considered discrete.

The target indicators have already been presented in Section 2.2. The target indicator "performance" T_{P} indicates the difference between the requested and the supplied energy by way of reminder. In contrast, the target indicator "efficiency" T_{E} evaluates the system's energy losses. The third target indicator, namely "service life" T_{SL}, represents a battery's estimated remaining life until it reaches a defined EOL criterion. Table 5.1 sums up the specification of the entire hyperspace.

Table 5.1: Specification of the design space for the parametric (D_{SoAP}) and sequential (D_{Pseq}) PFCS, use case space for the peak shaving (U_{UC1}) and frequency regulation (U_{UC2}) scenario, and target indicator space.

Space	Parameter	Value
Design space D_{SoAP}	$t_{\mathrm{pred,p}}$	$[1,\,20]\,\mathrm{s}$
	$t_{\mathrm{pred,e}}$	$[1,\,3600]\,\mathrm{s}$
Design space D_{Pseq}	P_{max}	$[1,\,400]\,\mathrm{W}$
	S	$\{0,\,1\}$
Use case space U_{UC1}	H_{C}	$\{0.75,\,1,\,1.25,\,1.5\}$
	PSF	$\{20,\,21,\,22,\,23\}\,\%$
Use case space U_{UC2}	H_{C}	$\{0.75,\,1,\,1.25,\,1.5\}$
	PSF	$\{25,\,26,\,27,\,28,\,29,\,30,\,31\}\,\%$
Target indicator space T	T_{P}	$[0,\,1]$
	T_{E}	$[0,\,1]$
	T_{SL}	$[0,\,1]$

The results presented in my published works [11, 12] show that the chosen value ranges for the design and use case variables are reasonable for analyzing the impact of these variables on the target indicators.

5.2 Multi-objective optimization implementation

Further information about the problem formulation, chosen parameters, and utilized algorithms is required in order to implement the remaining steps of the HSE process flow appropriately. First of all, the optimization problem to quantify PFCSs for heterogeneous BESSs must be formulated correctly. In general, the optimization problem is characterized by simultaneously optimizing the three target indicators "performance," "efficiency," and "service life," defining it as a MOO problem. Since an analytically closed form of the functional correlation between the target indicators and the design and use case variables was not accessible in

this work (cf. Section 4.3), the MOO problem is further characterized as a MOO on a black-box function problem. The HSE methodology enables solving such problems, as outlined in Sections 3.2 and 3.3. Moreover, it aims at identifying all the parameter value combinations for PFCS parameters that simultaneously optimize each of the target indicators for a given use case combination. This approach allows exposing the maximum potential of each PFCS applied. For this purpose, the design variables, use case variables, and target indicators described in Table 5.1 have to be considered as follows in this work when applying Equation (3.3):

$$d = (t_{\text{pred,p}},\, t_{\text{pred,e}})^T \text{ or } (P_{\max},\, S)^T, \tag{5.1a}$$

$$u = (H_{\text{C}},\, PSF)^T, \tag{5.1b}$$

$$t = (1 - T_{\text{P}},\, 1 - T_{\text{E}},\, 1 - T_{\text{SL}})^T \tag{5.1c}$$

Following the process flow given in Figure 5.1, the initial experimental test plan was created as one part of step two. By using a full factorial design,[2] the test plan for the peak shaving scenario consisted of 16 different use case combinations. For the frequency regulation scenario, the test plan was composed of 28 different use case combinations. Furthermore, for each use case combination 100 simulation runs were carried out. The number of simulation runs was obtained from preliminary analysis (see Appendix C Figure C.22) evaluating the hypervolume[3] for several simulation runs. It should be noted that this part of the test plan was updated iteratively during the experiments to identify PO solutions based on the previous results. Consequently, the entire test set for each PFCS amounted to 1600 and 2800 simulation runs, respectively.

For the 100 simulation runs per use case combination, however, a suitable MOO underlying search method is required to identify PO solutions for the given use case. Besides random search algorithms such as Latin hypercube sampling [152], adaptive sampling approaches may improve the search performance. In my published work [12], a genetic algorithm in the implementation form of an NSGA-II [177] was applied for most of the simulation runs. This approach tended to be robust but required a substantial amount of simulation runs to achieve acceptable

---

[2]Each possible combination of the two discrete use case variables was included in the test plan.
[3]The hypervolume indicator [176] is a performance metric for indicating the quality of the approximated Pareto-fronts generated by multi-objective optimizers.

results when applying the computationally expensive simulation. To tackle this problem, surrogate model-based approaches are gaining popularity due to an increased search efficiency [178]. Therefore, the computationally expensive model $t = t(d, u)$ was replaced here by an analytically accessible and approximated surrogate model $\hat{t}$. The BESS surrogate model $\hat{t}$ is a functional approximation term for target indicator dependencies as a function of design and use case variables (cf. Section 3.2).

Surrogate model-based search algorithms vary concerning their effectiveness and efficiency depending on the mathematical behavior of the black-box function [144, 179]. In this work, one primary requirement is high accuracy for the training points to guarantee good model predictions. Comparative studies have shown that the RBF-based surrogate model [147, 148] performs well in different test problems and engineering applications and can achieve high accuracies [180]. Thus, the RBF-based surrogate model was chosen due to its general applicability, easily adjustable smoothness, and powerful convergence properties [181]. In particular, the surrogate optimization toolbox (pySOT) from Eriksson et al. [182] was used utilizing their RBF surrogate model.[4]

Steps two to five were carried out following the multi-objective surrogate optimization algorithm proposed by Müller [183]. Thus, the initial DovE sets (20/100 simulation runs) per use case combination were defined by the standard Latin hypercube sampling approach as described before. The number of initial DovE sets was derived from the Pareto principle, i.e., the 80/20 rule, which is a widely accepted approach in optimization. After performing the 20 expensive function evaluations (simulation runs) at the selected points, the three surrogate models (one for each target indicator) were computed based on the identified non-dominated points. Then, an iterative sampling process took place using information from the surrogate models to select the next sampling points. This means the experimental test plan was updated after each simulation run depending on the results obtained until the 100 simulation runs were completed. Within the iterative process, function evaluations were performed, non-dominated points were identified, and surrogate models were updated. More detailed information about the optimization algorithm and its sampling strategies is provided in [183].

---

[4]Parameters of the RBF surrogate model during optimization: kernel = cubic, tail = linear, eta = 1e-06.

For further analysis, the surrogate models were used to evaluate and quantify the potentials and sensitivities of different PFCSs. In contrast to my published work [14], in which the BESS-adapted HSE toolchain and HSE process flow were used to implement a PO-PFCS, decision-making is not covered in the methodological framework of this work, as the focus is on the analysis of the causal relationships between the inputs and the outputs of BESSs. Furthermore, some limitations regarding the implementation and the interpretation of the subsequent results exist. The presumably most important limitation is that the applied methodology cannot guarantee to identify the global optimum for the $t(d, u)$ system behavior since both the accuracy of the simulation model (i.e., the surrogate models) and the utilized PFCSs restrict it. However, this methodological framework provides the basis to systematically quantify the potentials and sensitivities of different PFCSs. In the following sections, the methods for evaluation and visualization of this work's results are presented.

5.3 Potential analysis

The purpose of the potential analysis is twofold. First, an overview of existing target indicator trade-offs is gained to analyze the correlations between the different target indicators "performance," "efficiency," and "service life." Second, full access to the analytical surrogate models of the $t(d, u)$ system behavior is granted as the entire hyperspace is investigated systematically. The HSE process flow is capable of providing both results. Therefore, the space of potential solutions was built up systematically in steps two to five, and the surrogate models were trained to approximate the $t(d, u)$ behavior of the BESS simulation model based on efficient search strategies, as discussed in Section 5.2. Especially steps four and five involved the identification of the set of PO target indicator trade-offs. In these two steps, various surrogate models $\hat{t}$ to approximate $t(d, u)$ were assessed and compared to each other concerning their prognosis power. Moreover, these surrogate models can be used for further processing and analysis (see Sections 5.4 and 5.5). Examining the target indicator space for all accessible PFCS layout alternatives by varying the design variables within the given parameter boundaries allowed identifying possible PO configurations. The Pareto-front in this context may be considered to prove the potential of the utilized PFCSs. The potential analysis is illustrated using a matrix plot.

5.4 Surrogate model-based sensitivity analysis

Knowing PO target indicator trade-offs as a result of the potential analysis does not yet provide information about the input-output relationship of the BESSs. Moreover, even if dominated solutions are sorted out, different correlations between, e.g., the design variables of the PFCS and the target indicators might exist. Consequently, trivial solutions for, e.g., how to chose the design variables to minimize the degradation of the batteries, are not immediately evident. For this purpose, knowledge of the target indicator versus design or use case variables sensitivities is required. The surrogate model-based sensitivity analysis was carried out, enabling a thorough investigation of these correlations and sensitivities. However, relying on surrogate model-based decisions requires knowledge of the surrogate model's confidence level. For this purpose, the surrogate models derived within the potential analysis and a K-fold cross-validation-based mean coefficient of determination R^2 [184, 185] were used for analysis (cf. Section 3.2). The K-fold cross-validation constitutes a state-of-the-art machine learning methodology to evaluate a surrogate model's prediction power quality [186] by estimating a model's *accuracy*. Furthermore, it is a proven performance metric without adding computational expenses.

$$accuracy := \frac{1}{K} \sum_{k=1}^{K} R_k^2 \,, \tag{5.2}$$

where K is the number of entire folds, i.e., groups of data sets, R_k^2 are the individual coefficients of determination, and $k = 1, ...K$ is the data set used for validation. According to Kuhn and Johnson [187], K is usually set to 5 or 10. However, the difference between the estimated and true values becomes smaller for larger K's [187].

The surrogate model-based sensitivity analysis is usually considered an interactive plot to experience the sensitivities by changing the values of the design and use case variables independently. Here, it is visualized by plotting each target indicator versus each design and use case variable for only one given design and use case combination.

5.5 Use case specific-potential analysis

Finally, the use case-specific potential analysis expands on using surrogate models for a fixed use case. Therefore, surrogate models with a sufficient confidence level were used and allowed identifying PO solutions for the fixed use case within a computationally inexpensive algorithm. Assigning fixed values to the use case variables "heterogeneity" and "profile scaling factor" limits the target indicator trade-off degrees of freedom to the design space dimension. Thus, the potential of the applied PFCS for the fixed use case was calculated on a surrogate model basis for all design variable parameters within the given boundaries. These results (dominated and non-dominated solutions) are presented within a pairwise target indicator trade-off analysis.

6 Simulation studies on power flow control strategies

Results obtained in my published works [11, 12] analyzing different PFCSs indicated that the selection of the PFCS depends on the chosen use case and the objectives of the system operator. However, in the field of DC MGs, by way of example, in which BESSs play a key role, a SoC-balancing PFCS is often applied (cf. Section 2.2) without any proof of whether this PFCS is the most reasonable one. Understanding the causal relationships in complex BESSs to enable sustainable operation requires analyzing different PFCS systematically. Thus, the goal of the simulation studies in this work is to quantify the potentials and sensitivities of different PFCSs for heterogeneous BESSs, which constitutes the main research question of this work. The methodological framework presented in the previous chapter provides an appropriate setting for this. Moreover, the methods for evaluating and visualizing this work's results are closely related to the subordinate research questions outlined in Section 3.5.

Therefore, in Sections 6.1 and 6.2 the results of the parametric and the sequential PFCS are presented for both scenarios. Following the structure of the methodological framework, a threefold analysis for each PFCS is carried out to answer the research questions thoroughly. First, an overview of existing target indicator trade-offs is gained by applying the potential analysis. Second, the surrogate model-based sensitivity analysis is performed, analyzing the sensitivities and correlations between target indicators and design or use case variables. Third, the use case-specific potential analysis is conducted using the surrogate models for a fixed use case to identify a set of PO solutions. Finally, a comparison between the two distinct PFCSs applied here and the SoC-balancing PFCS, as well as a summary of the simulation studies, are provided in Section 6.3. It should be noted that the presentation of the results in Section 6.1 is partly based on my published work [14].

6.1 Use case I: Peak shaving

In this section, the results of the parametric and the sequential PFCS for the peak shaving scenario are presented to quantify the potential of these two computationally inexpensive PFCSs in variable use cases, i.e., system designs and applications. As mentioned earlier, the test set consisted of 1600 independent simulations in the case of the parametric PFCS (PFCS SoAP). In the case of the sequential PFCS (PFCS Pseq), the test set also amounted to 1600 simulation runs. Regarding the interpretation of the target indicators' value, zero is the optimal value a target indicator could achieve. For example, in the case of the performance criterion zero means the entire system can fulfill the power requirements at any time. This is in contrast to the definitions in Section 2.2. However, the MOO problem was formulated as a minimization problem, resulting in a different interpretation. Referring back to the ideas in Section 2.2, the target indicator "service life" was considered the accumulated service life (i.e., the accumulated capacity loss) of all batteries in this work's results. This means the overall deterioration of the BESSs should be minimized.[1]

6.1.1 Potential analysis

The first two subquestions of the research questions were tested by means of the potential analysis. The entire test set was used to quantify the overall potential of the parametric PFCS (PFCS SoAP) concerning the three target indicators. Note that each data point represents one possible design alternative for the peak shaving use case. In general, trade-offs between the different target indicators were observed and the maximum potential of the applied PFCS was exposed. The results obtained from the potential analysis are shown in Figure 6.1. The potential analysis is illustrated using a matrix plot showing the potential of a specific target indicator on its main diagonal. The upper triangular matrix shows the target indicator trade-offs. It can be observed from the data in the matrix plot's main diagonal that each target indicator was limited (Performance $= 100\,\%$, Efficiency $= 94.0\,\%$, Service life $= 96.0\,\%$). Consequently, better results cannot be expected regarding the specified design space and the use case space. The most interesting aspect of the potential analysis can be seen in the upper triangular matrix, where the trade-offs between the three target indicators are presented.

---

[1]However, this might lead to an increased deterioration of a single BESS. Nevertheless, no significant differences regarding the correlations of the target indicators were found as, for example, a comparison between Figure 6.1 and Figure C.23 reveals.

These plots are very revealing in several ways. First, pseudo-grouped data sets can be observed, e.g., in the upper right plot. Second, the correlations between the target indicators are indicated. A positive correlation was found between the target indicators "performance" and "efficiency," whereas a negative correlation was observed between the service life criterion and the other target indicators. The interpretation of these results is given in Section 7.1.
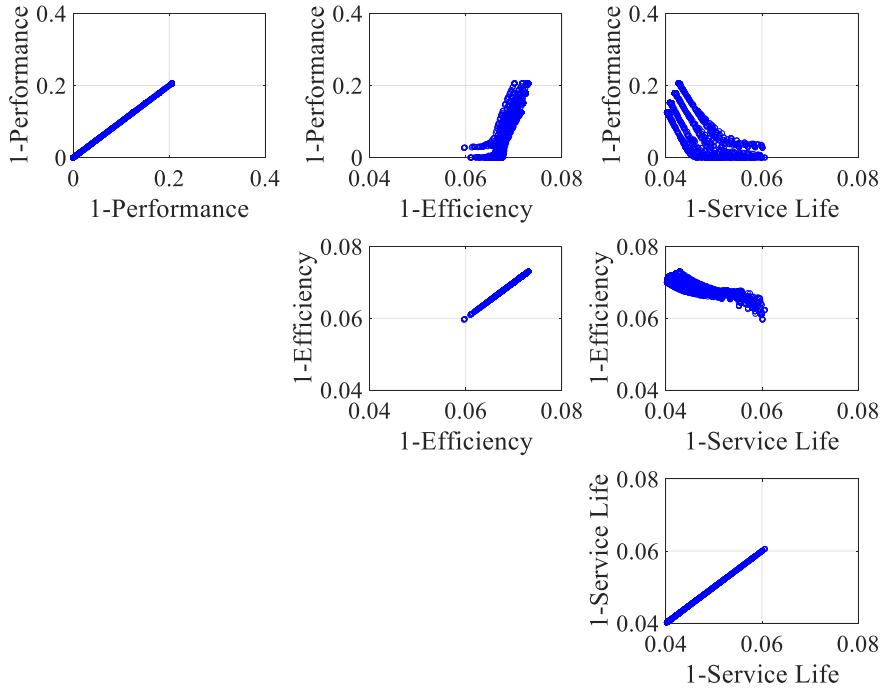

Figure 6.1: Results of the parametric PFCS (PFCS SoAP) potential analysis for the peak shaving scenario within the specified design space, use case space, and target indicator space. Adapted from my published work [14].

Turning now to the potential analysis of the sequential PFCS (PFCS Pseq), it is evident from the results that the correlations and the maximum potentials are different from the results obtained using the parametric PFCS (PFCS SoAP). The upper triangular matrix in Figure 6.2 indicates that strong positive or strong negative correlations between the target indicators were not present. Only a low positive correlation was noticed between the target indicators "efficiency" and "service life." However, comparing the matrix plot's main diagonal in Figures 6.1 and 6.2 reveal that the maximum potentials of the target indicators "efficiency" and "service life" had changed to some extent. Interestingly, in as many as 56 % of cases, increased

efficiency was observed compared to the parametric PFCS (PFCS SoAP), and the maximum efficiency amounted to 95.0 %. The maximum service life was equal to 95.8 % using the sequential PFCS (PFCS Pseq), which is about 0.2 percentage points lower when compared with the parametric PFCS (PFCS SoAP). In other words, in 32 % of cases using the parametric PFCS (PFCS SoAP), service life was even higher than the maximum obtainable service life when using the sequential PFCS (PFCS Pseq).
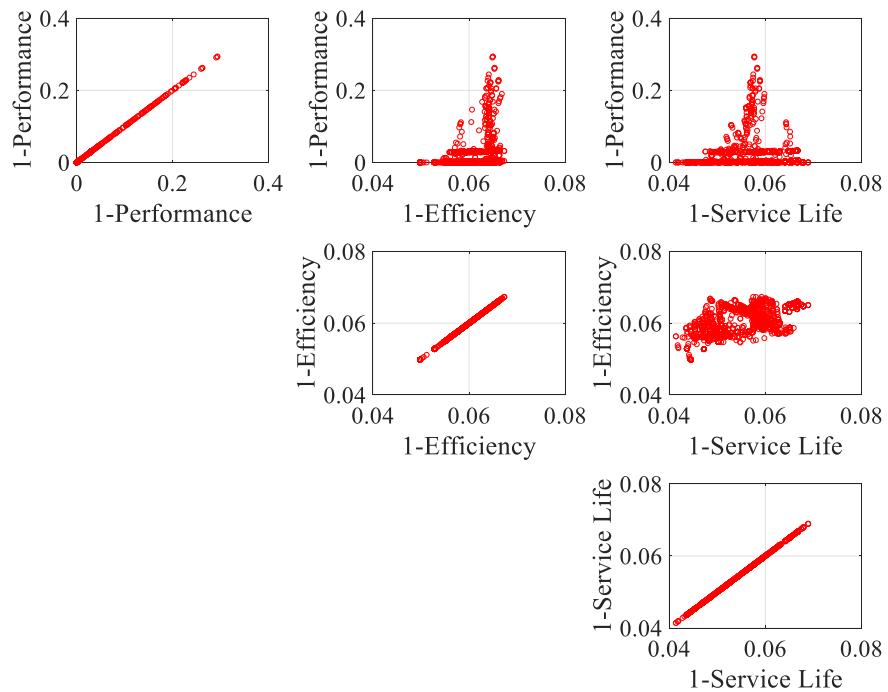
Figure 6.2: Results of the sequential PFCS (PFCS Pseq) potential analysis for the peak shaving scenario within the specified design space, use case space, and target indicator space.

6.1.2 Sensitivity analysis

Regarding the subordinate research questions about sensitivities, this subsection deals with the sensitivity analysis of the target indicators, design variables, and use case variables. The results of the surrogate model-based sensitivity analysis are divided into two parts as follows: First, the results of the K-fold cross-validation described in Section 5.4 are presented. Second, the results of the surrogate model-based sensitivity analysis are shown for both PFCSs. In general, the K-fold cross-validation was used to evaluate the quality of the surrogate model,

i.e., the confidence level and its predictions. A surrogate model represented each target indicator's relations to design and use case variables. For the simulation results of both PFCSs, the data were randomly split into 20 folds of equal size due to a lower bias (cf. Section 5.4). This means, in the case of the parametric PFCS (PFCS SoAP), 80 simulation results (one fold) were retained as the validation set for testing the model, and the remaining 1520 simulation results (19 folds) were used as training data. In the case of the sequential PFCS (PFCS Pseq), 80 simulation results also represented one fold and were retained as the validation set for testing reasons. The remaining 19 folds, i.e., 1520 simulation results, were used as training data. In each case, this process was repeated 20 times and, therefore, precisely once for each fold. Table 6.1 shows the accuracy (cf. Equation (5.2)) of each of the six surrogate models.

Table 6.1: Results of the K-fold cross-validation. The accuracy of each surrogate model was higher than 91.2 %

Model	Folds	Validation set	Training set	accuracy
parametric PFCS				
Efficiency	20	80	1520	0.994
Performance	20	80	1520	0.999
Service life	20	80	1520	0.999
sequential PFCS				
Efficiency	20	80	1520	0.941
Performance	20	80	1520	0.912
Service life	20	80	1520	0.946

The applied RBF surrogate models were represented by a cubic kernel with a linear tail and a regularization parameter of 1e-03 in the case of the parametric PFCS (PFCS SoAP). Regarding the sequential PFCS (PFCS Pseq), a cubic kernel with a linear tail and a regularization parameter of 7e-03 were applied as hyperparameters for the subsequent evaluation. These are common hyperparameters and are partly defined as the default, i.e., for the kernel and the tail. The validation showed that there was a high accuracy ($> 99.4\,\%$) for the surrogate models in the case of the parametric PFCS (PFCS SoAP). The accuracy of the surrogate models in the case of the sequential PFCS (PFCS Pseq) was somewhat less, with values higher than 91.2 %. The lower accuracy can be attributed to slightly too few simulation runs in specific design space areas and the discrete use case variable. Moreover, it should be noted that there was a discrepancy between the selection of the hyperparameters during optimization and the subsequent evaluation. Since hyperparameters were

not being optimized during the simulations, the default parameters mentioned in Section 5.2 were used in the first place. Thus, slight deviations in accuracy might occur between the surrogate models used during optimization and the subsequent evaluation. Nevertheless, reasonable accuracies were obtained, and the surrogate models could be used to analyze the sensitivities further.

The surrogate model-based sensitivity analysis was carried out to enable a thorough analysis of the impact of design and use case variables on the target indicators. In the case of the parametric PFCS (PFCS SoAP), the sensitivities were exemplified using an arbitrary design and use case combination.[2] Both the set values of the design and use case variables were chosen to achieve full performance. The results of this sensitivity analysis are provided in Figure 6.3.
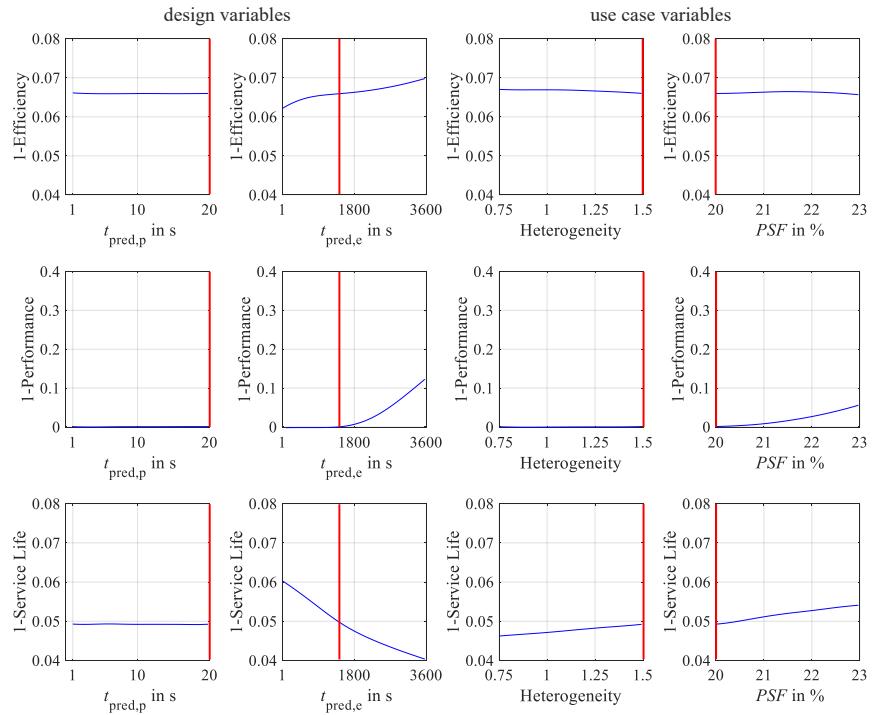

Figure 6.3: Sensitivity analysis of the target indicators "efficiency," "performance," and "service life" concerning the design variables of the parametric PFCS (PFCS SoAP) and the use case variables of the peak shaving scenario. The set values of the design and use case variables are shown in red. $t_{\mathrm{pred,p}} = 20\,\mathrm{s}$, $t_{\mathrm{pred,e}} = 1500\,\mathrm{s}$, Heterogeneity $= 1.5$, and $PSF = 20\,\%$. Adapted from my published work [14].

---

[2] $t_{\mathrm{pred,p}} = 20\,\mathrm{s}$, $t_{\mathrm{pred,e}} = 1500\,\mathrm{s}$, $H_{\mathrm{C}} = 1.5$, and $PSF = 20\,\%$

Surprisingly, the impact of the design variable $t_{\mathrm{pred,p}}$ on each target indicator was negligible. In contrast, the influence of the design variable $t_{\mathrm{pred,e}}$ on the target indicators was severe. A positive correlation was noticed between $t_{\mathrm{pred,e}}$ and both the target indicators "efficiency" and "performance" on the one hand. On the other hand, a negative correlation was observed between $t_{\mathrm{pred,e}}$ and the target indicator "service life." In the case of the use case variable "heterogeneity," only a slight impact on the target indicators was present. A more homogeneous system led to a marginally lower efficiency of up to 0.1 percentage points and higher service life of roughly 0.3 percentage points. The impact on the target indicator "performance" was negligible for the specified use case combinations; however, a higher profile scaling factor reduced performance by about six percentage points and service life by roughly 0.5 percentage points. Here, the impact on efficiency was minimal. The interpretation of these results is given in Section 7.2.

From the sensitivity analysis of the sequential PFCS (PFCS Pseq), it is apparent that in most cases, different correlations were observed. Figure 6.4 shows the results obtained from the sensitivity analysis of the target indicators "efficiency," "performance," and "service life" concerning the design variables of the sequential PFCS (PFCS Pseq) and the use case variables. In this figure, the sensitivities were exemplified using a design and use case combination with $P_{\mathrm{max}} = 400\,\mathrm{W}$, Sorting $= 1$, $H_{\mathrm{C}} = 1.5$, and $PSF = 20\,\%$. These values were chosen to provide comparability between Figures 6.3 and 6.4.
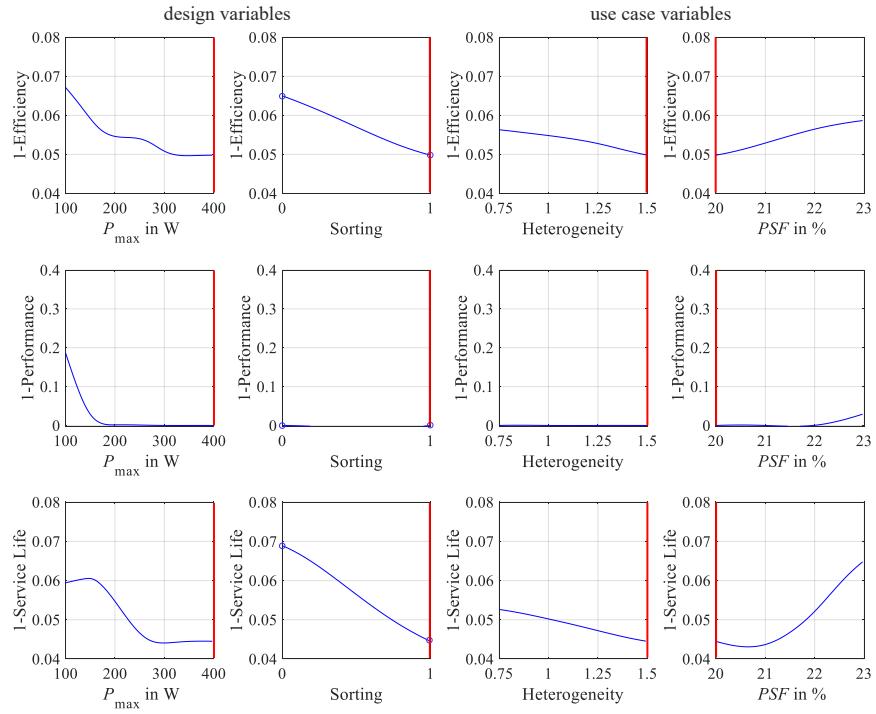
Figure 6.4: Sensitivity analysis of the target indicators "efficiency," "performance," and "service life" concerning the design variables of the sequential PFCS (PFCS Pseq) and the use case variables of the peak shaving scenario. The set values of the design and use case variables are shown in red. $P_{\max} = 400\,\text{W}$, Sorting $= 1$, Heterogeneity $= 1.5$, and $PSF = 20\,\%$.

It can be seen in Figure 6.4 that there was a significant negative correlation between the design variable $P_{\max}$ and each target indicator. Efficiency and service life were enhanced by almost two percentage points and performance by up to 20 percentage points with an increasing design variable. Interestingly, negative correlations were also found in the case of the other design variable. Efficiency and service life could be worsened by 1.5–2.5 percentage points when changing the merit order of the BESSs, i.e., using the smallest battery first. In agreement with the parametric PFCS (PFCS SoAP), the results indicated that a less heterogeneous system decreased the target indicator "efficiency," and no significant correlation was found concerning the target indicator "performance." However, contrary observations were made regarding the service life criterion. A less heterogeneous system reduced service life by about 0.8 percentage points using the sequential PFCS (PFCS Pseq). The impact of the profile scaling factor on the target indicators showed a positive correlation. Each target indicator could be reduced by about 1–3 percentage points with an increasing profile scaling factor.

6.1.3 Use case-specific potential analysis

The use case-specific potential analysis was carried out in the final part to test the last subquestion (design rules). For this reason, an exemplary use case was defined, setting the heterogeneity to 1.5 and the profile scaling factor to 20 %. The use case variables were selected to make the results more comparable with those of the sensitivity analysis. The sorted surrogate model-based results of both PFCSs are presented within a pairwise target indicator trade-off analysis (see Figures 6.5 and 6.6). It should be noted that the blue/red data points represent all surrogate model-based solutions for the specific use case and the pink ones show PO solutions. In general, the surrogate models tend to give predictions that are parallel to the experimental data from corresponding simulations (cf. Figures 6.1 and 6.2). Figure 6.5 illustrates the results of the parametric PFCS (PFCS SoAP).
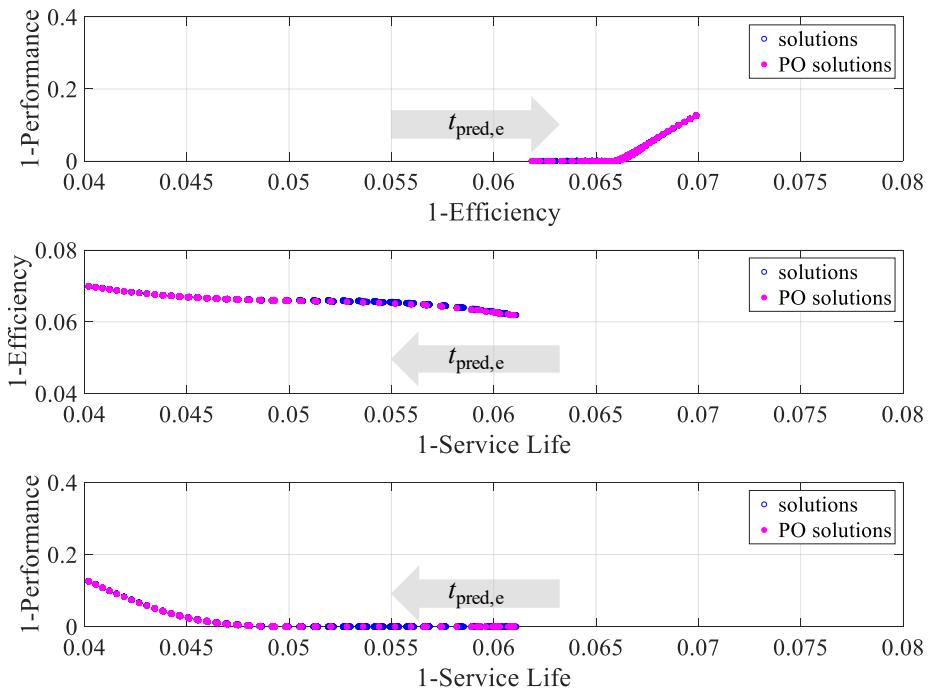
Figure 6.5: Pairwise target indicator trade-off analysis for the specified peak shaving use case emphasizing PO solutions concerning the parametric PFCS (PFCS SoAP). The heterogeneity was set to 1.5 and the profile scaling factor amounted to 20 %. Adapted from my published work [14].

In accordance with the results of the potential analysis, in which no surrogate models were used, it can be observed from Figure 6.5 that the same correlations between the target indicators occurred. An interesting aspect of this figure is that

both all solutions and PO solutions lay close together. However, considerable differences between the minimum and maximum values of each target indicator were noticed. In the case of the target indicator "performance," the difference amounted to 12.6 percentage points, and for the target indicator "service life," the highest difference was 2.1 percentage points. The range between the highest and lowest efficiency was roughly one percentage point. In these ranges, PO solutions were identified. Furthermore, the effect of the most influential design variable $t_{\text{pred,e}}$ is illustrated by the arrows. There is evidence to indicate that an increasing value of $t_{\text{pred,e}}$ led to lower performance, lower efficiency, but higher service life. This is also consistent with the results of the sensitivity analysis (cf. Figure 6.3). The interpretation of these results is given in Section 7.3.

In the case of the sequential PFCS (PFCS Pseq), an overall concordance between the surrogate models and the experimental data from corresponding simulations can be observed when comparing Figures 6.6 and 6.2.
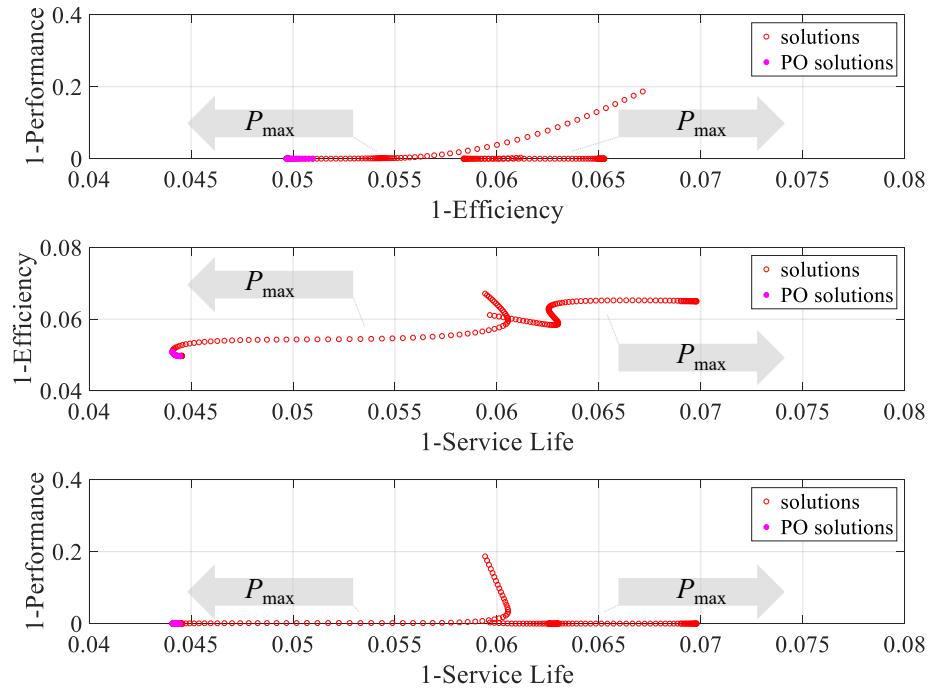

Figure 6.6: Pairwise target indicator trade-off analysis for the specified peak shaving use case emphasizing PO solutions concerning the sequential PFCS (PFCS Pseq). The heterogeneity was set to 1.5 and the profile scaling factor amounted to 20 %.

The pairwise target indicator trade-off analysis indicates that two disconnected solution spaces existed due to the discrete use case variable "sorting." This is in line with the results of the potential analysis. On the right-hand side of each plot, the solutions for an ascending order of the BESSs (Sorting = 0) can be found. In contrast, the solutions for a descending order of the BESSs are shown on the left-hand side of the plots. Interestingly, the design variable $P_{\max}$ influenced both solution spaces in different ways, as illustrated by the arrows in the plots. However, the results suggest that only the descending order is of importance when seeking PO solutions. Therefore, an increasing value of $P_{\max}$ yielded higher performance, higher efficiency, and higher service life in this case. Consequently, PO solutions were observed for this design variable combination. The interpretation of these results is given in Section 7.3.

6.2 Use case II: Frequency regulation

Similar to the previous section, the results of the parametric and the sequential PFCS for the frequency regulation scenario are presented to quantify the potentials and sensitivities of these two PFCSs. In both cases, the entire test set consisted of 2800 independent simulation runs. Again, zero is the optimal value a target indicator can achieve since the MOO problem was formulated as a minimization problem.

6.2.1 Potential analysis

In the first step, the first and the second subquestion were again tested by means of the potential analysis. The potential analysis was applied to the parametric PFCS (PFCS SoAP) to quantify the potentials of this PFCS. It is evident from the results that correlations were existent, as can be seen from Figure 6.7.
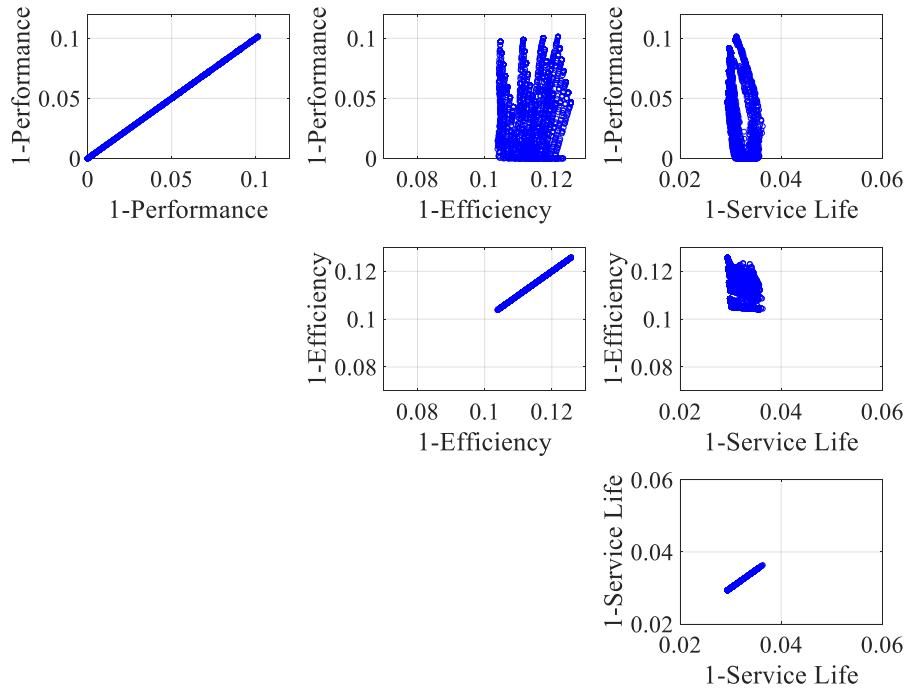
Figure 6.7: Results of the parametric PFCS (PFCS SoAP) potential analysis for the frequency regulation scenario within the specified design space, use case space, and target indicator space.

However, only closer inspection of the upper triangular matrix reveals the individual correlations between the target indicators adequately. What is striking about the correlations of the target indicators is that these correlations changed in most cases depending on the design and use case variable combinations. A positive correlation was found between the target indicators "performance" and "efficiency." However, the correlation changed within a specific range of the design variable $t_{\mathrm{pred,e}}$ depending on the use case variables. In contrast, a negative correlation was observed between the target indicator "service life" and the other target indicators. However, in both cases positive correlations were noticed for specific design and use case variable combinations. Furthermore, the matrix plot's main diagonal shows the limits of each target indicator. For the target indicator "performance" the limit was 100 %, whereas the target indicator "efficiency" was limited to 89.6 %. In the case of the target indicator "service life," the limit amounted to 97.1 %. As far as the potential analysis of the sequential PFCS (PFCS Pseq) is concerned, the correlations and the maximum potentials differ from the parametric PFCS (PFCS SoAP) in several aspects.
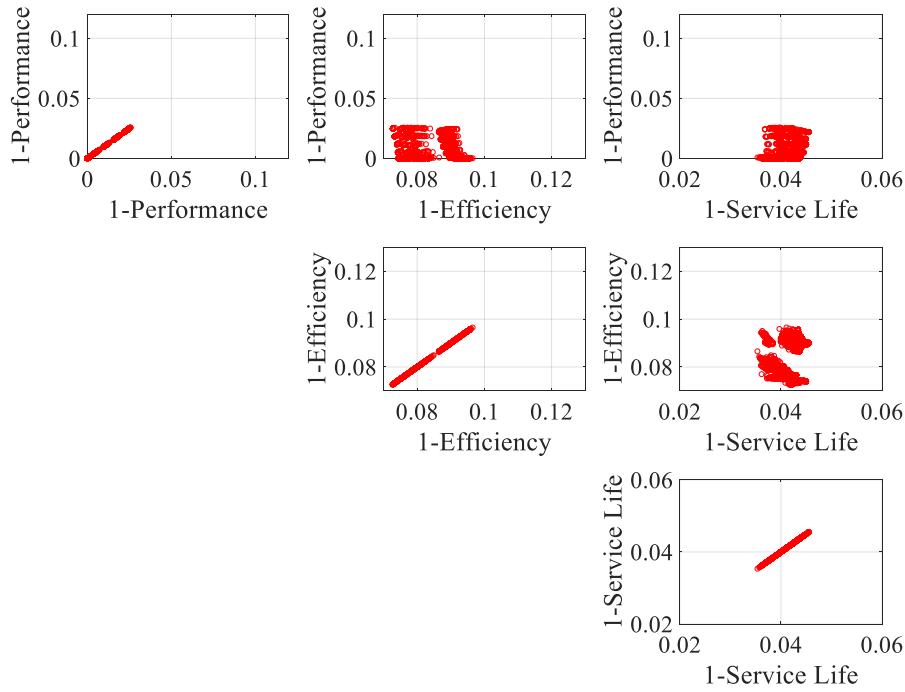
Figure 6.8: Results of the sequential PFCS (PFCS Pseq) potential analysis for the frequency regulation scenario within the specified design space, use case space, and target indicator space.

From the upper triangular matrix in Figure 6.8 it can be seen that strong positive or strong negative correlations between the target indicators were non-existent. However, a low negative correlation was observed between efficiency and the other two target indicators. Moreover, between the target indicators "performance" and "service life," a low positive correlation was found. The most striking result to emerge from the data is that the maximum potentials of the target indicators changed significantly. In contrast to the maximum efficiency using the parametric PFCS (PFCS SoAP), here, the lowest efficiency amounted to 90.4%. Thus, increased efficiency was noticed in each case, as can be seen in the matrix plot's main diagonal in Figures 6.7 and 6.8. When using the sequential PFCS (PFCS Pseq), a maximum service life of 96.5% could be achieved. Interestingly, in 95.3% of cases using the parametric PFCS (PFCS SoAP), service life was even higher than the maximum service life here.

6.2.2 Sensitivity analysis

Similar to Section 6.1, the surrogate model-based sensitivity analysis results concerning the frequency regulation scenario are separated into two parts and aim to answer the subquestions about sensitivities. Starting with the results of the K-fold cross-validation, the quality of the surrogate models was evaluated. For the 2800 simulation results of the parametric PFCSs (PFCS SoAP), the data were randomly split into 20 folds of equal size due to a lower bias (cf. Section 5.4). This means 140 simulation results (one fold) were retained as the validation set for testing the model and the remaining 2660 simulation results (19 folds) were used as training data. Thus, this process was repeated 20 times and consequently exactly once for each fold. In the case of the sequential PFCS (PFCS Pseq), the data were randomly split into only 18 folds of equal size as the accuracy was enhanced in this case. Therefore, 155 simulation results represented one fold and were retained as the validation set for testing reasons. The remaining 2645 simulation results, were used as training data. Here, this process was repeated 18 times and thus once for each fold. Table 6.2 provides the accuracy (cf. Equation (5.2)) of each surrogate model.

Table 6.2: Results of the K-fold cross-validation. The accuracy of each surrogate model was higher than 48.1 %

Model	Folds	Validation set	Training set	accuracy
parametric PFCS				
Efficiency	20	140	2660	0.996
Performance	20	140	2660	0.999
Service life	20	140	2660	0.946
sequential PFCS				
Efficiency	18	155	2645	0.999
Performance	18	155	2645	0.481
Service life	18	155	2645	0.962

In the case of the parametric PFCS (PFCS SoAP), the applied RBF surrogate models were represented by a cubic kernel with a linear tail and a regularization parameter of 9e-03. The validation showed high accuracy ($> 94.6\,\%$) for these surrogate models. Regarding the sequential PFCS (PFCS Pseq), a TPS kernel with a linear tail and a regularization parameter of 1e-09 were applied as hyperparameters for the subsequent evaluation. Here, the accuracy of at least two surrogate models was also high ($> 96.2\,\%$). However, the surrogate model of the target indicator "performance" showed somewhat less accuracy, with a value of 48.1 %. As previ-

ously mentioned in Section 6.1, the lower accuracy can be attributed to slightly too few simulations in specific design space areas, the discrete use case variable, and the discrepancy between the selection of the hyperparameters during optimization and the subsequent evaluation. Nevertheless, the surrogate model was used for further analysis of the sensitivities since no significant deviations were expected (cf. Figure C.24).

In the second part of the surrogate model-based sensitivity analysis, the impact of the design and use case variables on the target indicators was analyzed using the validated surrogate models. Regarding the parametric PFCS (PFCS SoAP), the sensitivities were exemplified using an arbitrary design and use case combination with $t_{\mathrm{pred,p}} = 5\,\mathrm{s}$, $t_{\mathrm{pred,e}} = 700\,\mathrm{s}$, $H_{\mathrm{C}} = 0.75$, and $PSF = 27\,\%$. In this case, for both the design and use case variables, entirely different values were selected compared to the peak shaving scenario. The design variables were chosen to achieve full performance, and the use case variables to show a sensitivity analysis for a less heterogeneous system. The results of the sensitivity analysis are given in Figure 6.9.
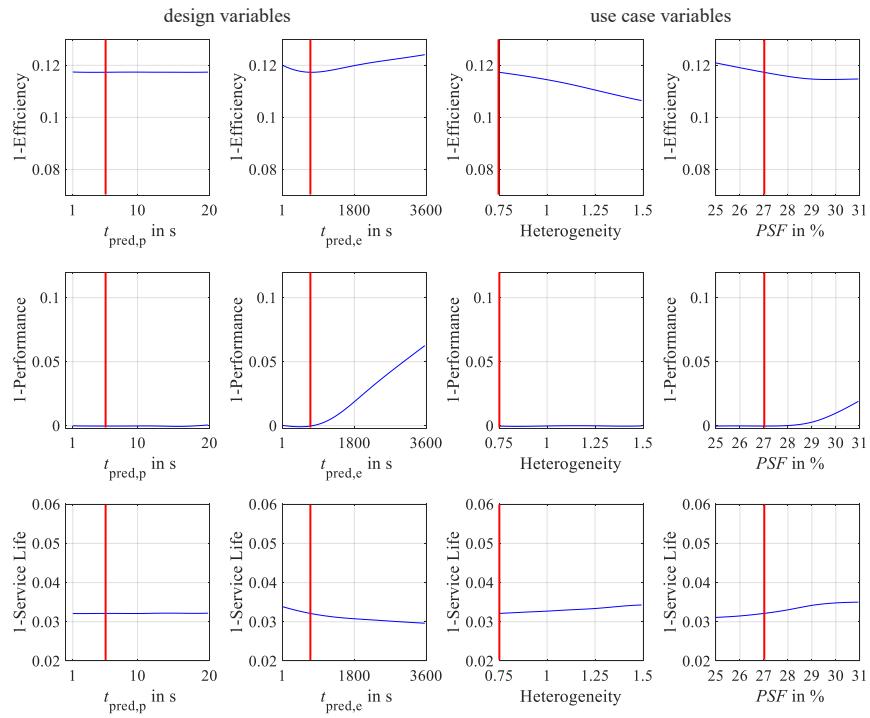
Figure 6.9: Sensitivity analysis of the target indicators "efficiency," "performance," and "service life" concerning the design variables of the parametric PFCS (PFCS SoAP) and the use case variables of the frequency regulation scenario. The set values of the design and use case variables are shown in red. $t_{\mathrm{pred,p}} = 5\,\mathrm{s}$, $t_{\mathrm{pred,e}} = 700\,\mathrm{s}$, Heterogeneity $= 0.75$, and $PSF = 27\,\%$.

The effects of the design variables $t_{\mathrm{pred,p}}$ and $t_{\mathrm{pred,e}}$ on each target indicator were similar to those of the other use case. No significant correlation was found between $t_{\mathrm{pred,p}}$ and the target indicators. However, a positive correlation was found between $t_{\mathrm{pred,e}}$ and the target indicators "efficiency" and "performance," and a negative correlation was noticed between $t_{\mathrm{pred,e}}$ and the target indicator "service life." The impact of the use case variable "heterogeneity" on the target indicator "efficiency" was noticeable. An increasing heterogeneity led to higher efficiency of up to one percentage point. In addition, a more heterogeneous system worsened service life slightly by as much as 0.2 percentage points. The target indicator "performance" appeared to be unaffected by the heterogeneity in this case. In contrast, a significant positive correlation was found between the profile scaling factor and the target indicator "performance" leading to a two percentage point worse performance with an increasing profile scaling factor. Moreover, a higher profile scaling factor reduced service life by about 0.4 percentage points but enhanced efficiency

by roughly 0.7 percentage points within the specified parameter range.

Regarding the surrogate model-based sensitivity analysis of the sequential PFCS (PFCS Pseq), the sensitivities were exemplified using a design and use case combination with $P_{\max} = 400\,\mathrm{W}$, Sorting $= 1$, $H_{\mathrm{C}} = 0.75$, and $PSF = 27\,\%$. This example aligns with the ideas mentioned before, achieving full performance and representing a less heterogeneous system. The results obtained from the sensitivity analysis of the target indicators "efficiency," "performance," and "service life" concerning the design variables of the sequential PFCS (PFCS Pseq) and the use case variables are shown in Figure 6.10.
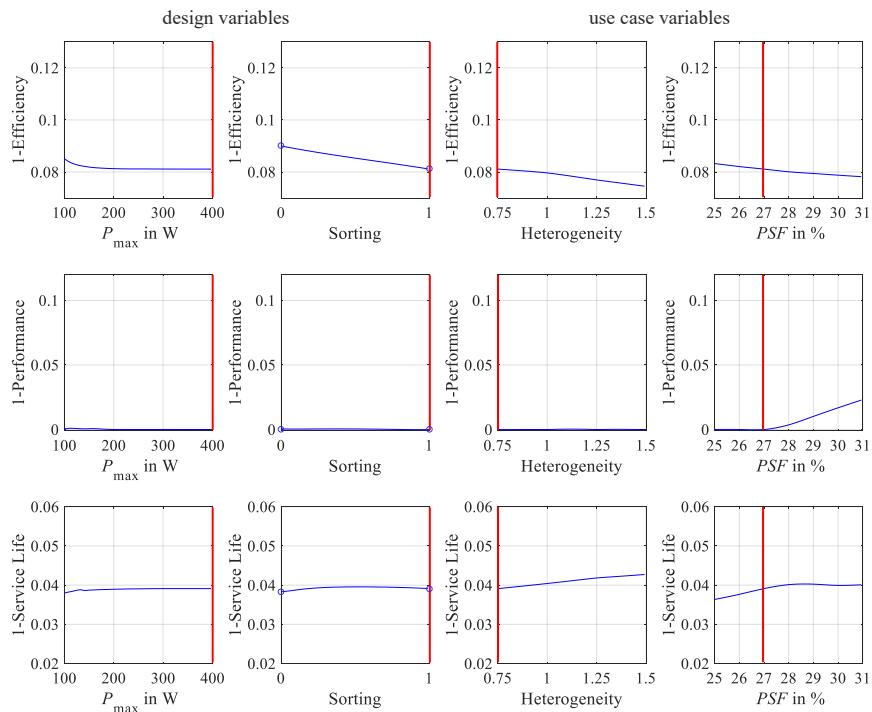
Figure 6.10: Sensitivity analysis of the target indicators "efficiency," "performance," and "service life" concerning the design variables of the sequential PFCS (PFCS Pseq) and the use case variables of the frequency regulation scenario. The set values of the design and use case variables are shown in red. $P_{\max} = 400\,\mathrm{W}$, Sorting $= 1$, Heterogeneity $= 0.75$, and $PSF = 27\,\%$.

From Figure 6.10 it can be seen that there were different correlations between the design variable $P_{\max}$ and each target indicator. While a negative correlation was found between the design variable $P_{\max}$ and the target indicator "efficiency,"

a positive correlation was observed between $P_{\max}$ and the target indicator "service life." No significant correlation was noticed regarding the performance criterion. Furthermore, efficiency could be enhanced by one percentage point when changing the merit order of the BESSs from ascending to descending, i.e., using the largest battery first. An impact on the target indicators "performance" and "service life" was not found. Another negative correlation was observed between efficiency and the use case variables "heterogeneity" and "profile scaling factor." In both cases, efficiency could be enhanced by about 0.5–0.7 percentage points with increasing values of the use case variables. Whereas no significant correlation between the target indicator "performance" and the use case variable "heterogeneity" was observed, positive correlations were found between performance and the profile scaling factor and between the target indicator "service life" and the two use case variables. A higher profile scaling factor worsened performance by roughly two percentage points and service life by roughly 0.4 percentage points. A more heterogeneous system reduced service life by about 0.4 percentage points using the sequential PFCS (PFCS Pseq). The interpretation of these results is given in Section 7.2.

6.2.3 Use case-specific potential analysis

The use case-specific potential analysis moves on to describe an exemplary use case in more detail and again tests the last subquestion (design rules). Therefore, the use case as defined above was applied for analysis. The heterogeneity was set to 0.75 and the profile scaling factor to 27 %. These use case variables were selected to make the results more comparable with those of the respective sensitivity analysis. Similar to the previous section, the sorted surrogate model-based results of both the parametric and the sequential PFCS are presented within a pairwise target indicator trade-off analysis (see Figures 6.11 and 6.12). Again, it is evident that the surrogate model-based results obtained were in good agreement with existing data from corresponding simulations. Figure 6.11 presents the results of the parametric PFCS (PFCS SoAP).
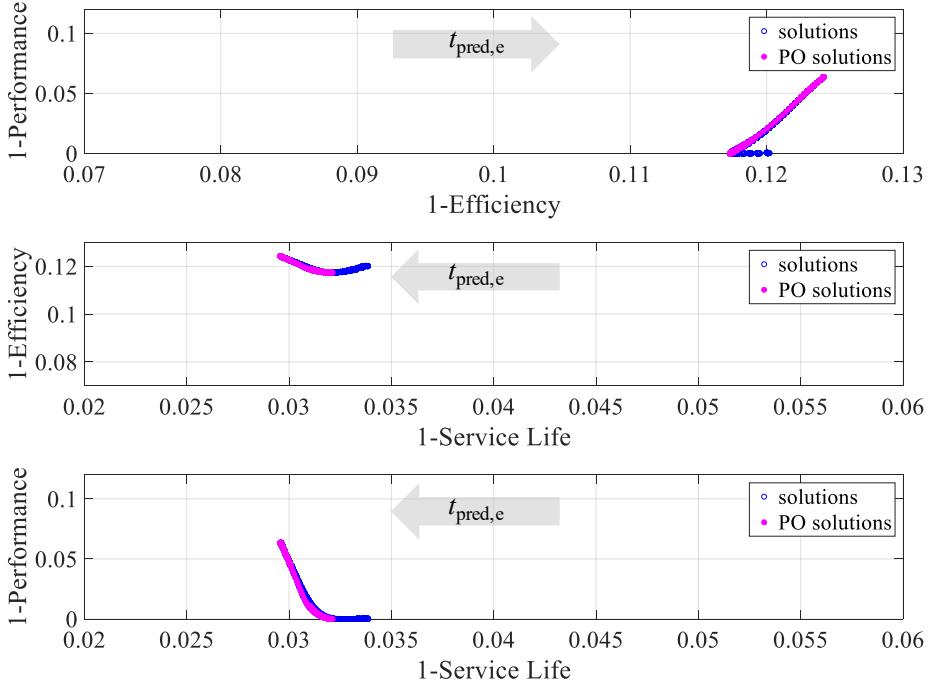
Figure 6.11: Pairwise target indicator trade-off analysis for the specified frequency regulation use case emphasizing PO solutions concerning the parametric PFCS (PFCS SoAP). The heterogeneity was set to 0.75 and the profile scaling factor amounted to 27 %.

The main finding of the corresponding potential analysis was that the correlations between the target indicators changed in most cases depending on the design and use case variable combinations. This is in line with the findings here for a specific use case variable combination. As shown in Figure 6.11, changing correlations between the target indicators were observed. Consequently, the resulting PO solutions were directly affected. In the case of the target indicator "performance," PO solutions were obtained in the range between 93.0 % and 100 %, and for the target indicator "service life," PO solutions ranged from 96.8 % to 97.1 %. Regarding the target indicator "efficiency," PO solutions were obtained for efficiencies higher than approximately 87.6 %. Moreover, the impacts of the design variable $t_{\mathrm{pred,e}}$ on the target indicators are displayed by the arrows. An increasing value of $t_{\mathrm{pred,e}}$ led to significantly lower performance, slightly lower efficiency, but higher service life. These results are qualitatively similar to those of the sensitivity analysis. The interpretation of these results is given in Section 7.3.

Regarding the sequential PFCS (PFCS Pseq), the results were similar to those of the potential analysis, as can be seen when comparing Figures 6.12 and 6.8.
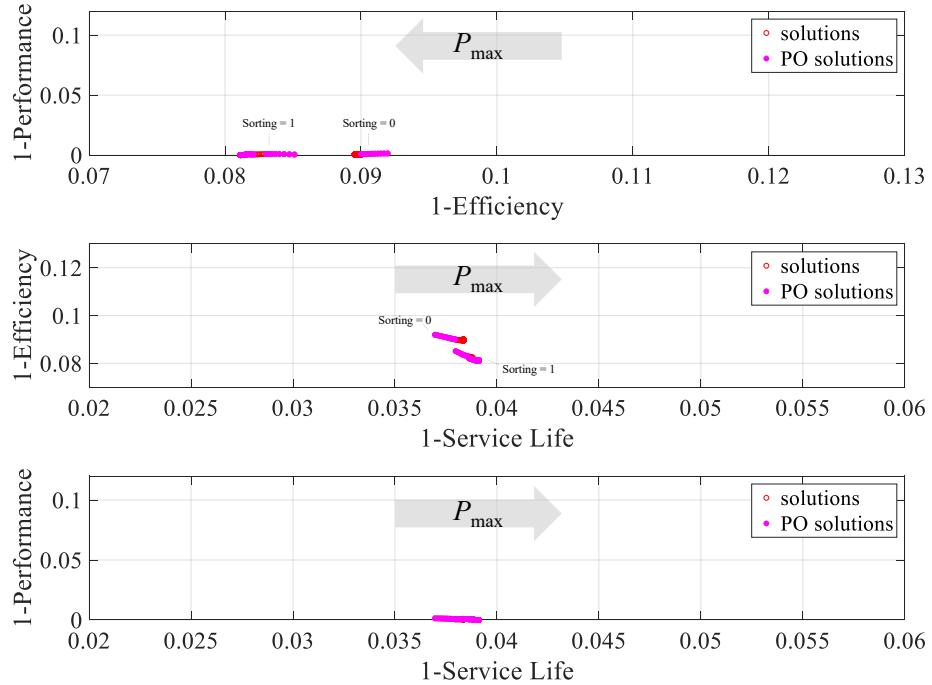
Figure 6.12: Pairwise target indicator trade-off analysis for the specified frequency regulation use case emphasizing PO solutions concerning the sequential PFCS (PFCS Pseq). The heterogeneity was set to 1.5 and the profile scaling factor amounted to 20 %.

Generally, the solution space was divided into two parts due to the design variable "sorting," as the pairwise target indicator trade-off analysis revealed. An ascending order of the BESSs (Sorting = 0) led to lower efficiency and performance. In contrast, the target indicator "service life" could be slightly enhanced. Moreover, the design variable P_{max} influenced both solution spaces similarly, as demonstrated by the arrows in the plots. An increasing value of P_{max} improved both performance and efficiency of the system slightly. The target indicator "service life," on the other hand, was worsened with an increasing value of P_{max}. Thus, PO solutions were observed for performances close to 100 %, efficiencies higher than 90.8 %, and a service life in the range of 96.1 % and 96.3 %. The interpretation of these results is given in Section 7.3.

6.3 Summary of the simulation studies

Thus far, the simulation studies have been separated into the two use cases and further into the two PFCSs to investigate several aspects individually. The following part of this section moves on to describe in greater detail the results of the potential analysis for all PFCSs applied. Therefore, the results of the potential analysis for the peak shaving scenario are put together and compared with the state-of-the-art PFCS (PFCS SoC).[3] For each PFCS, the parameter ranges of the design variables are chosen to represent physically and technically reasonable values. Figure 6.13 summarizes the results of the three PFCSs for the peak shaving scenario.
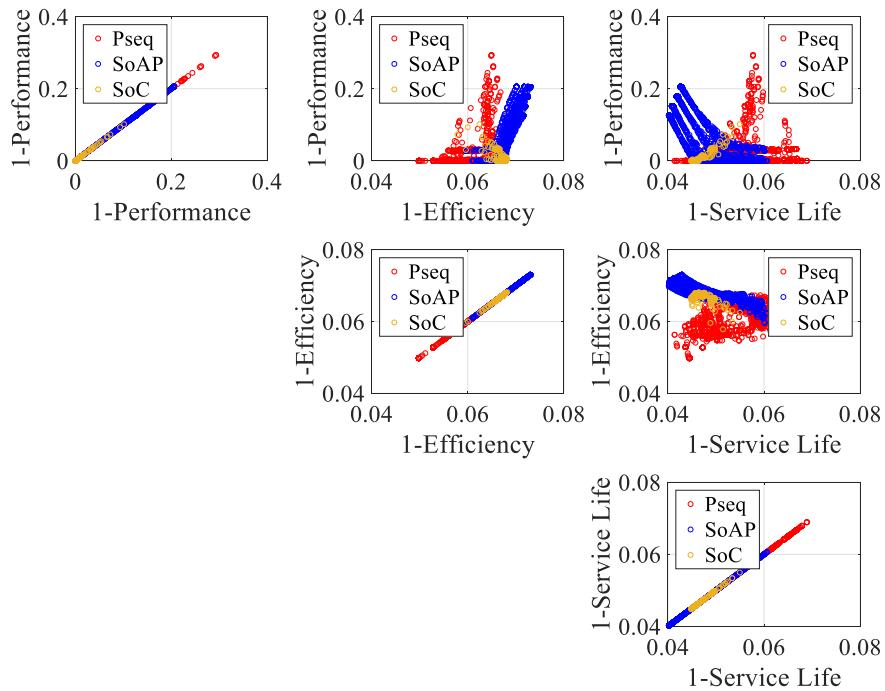
Figure 6.13: Summarized results of the potential analysis for the peak shaving scenario within the specified design space, use case space, and target indicator space.

It can be observed from the data in the matrix plot's main diagonal that the potentials of each of the three PFCSs were entirely different. The SoC-balancing PFCS tended to achieve high performance for each design variable combination,

---

[3]Design variables: convergence factor: 1–5, compensation function: linear, power, exponential, hyp. sine, logarithmic

whereas a broader range of performance was found for the other two PFCSs. In the case of efficiency, high efficiencies were found using the sequential PFCS (PFCS Pseq). In contrast, slightly lower efficiencies were noticed using the parametric and state-of-the-art PFCSs. An inverted effect was observed in terms of the target indicator "service life," indicating that the sequential PFCS (PFCS Pseq) led to lower service life in numerous cases. What is interesting about the data in the matrix plot's main diagonal is that the potentials of the SoC-balancing PFCS could be covered by adapting the design variables of the parametric PFCS (PFCS SoAP). Closer inspection of the upper triangular matrix gives access to this observation. It is apparent from these plots that higher efficiencies for similar performances were achieved when using the parametric PFCS (PFCS SoAP). As far as the target indicator "service life" is concerned, this is not necessarily the case since the specific use case must be considered. Thus, lower service life for similar performance was found in most cases when using the parametric PFCS (PFCS SoAP). In contrast, the sequential PFCS (PFCS Pseq) tended to achieve both higher performance and higher efficiency in most cases compared to the other two PFCSs. However, this PFCS could not necessarily enhance the target indicator "service life." The interpretation of results for a specified design and use case combination is given in Section 7.1.

Likewise to the peak shaving scenario, the results of the potential analysis for the frequency regulation scenario are put together and compared with the state-of-the-art PFCS (PFCS SoC). The results are summarized in Figure 6.14. The interpretation of results for a specified design and use case combination is given in Section 7.1.
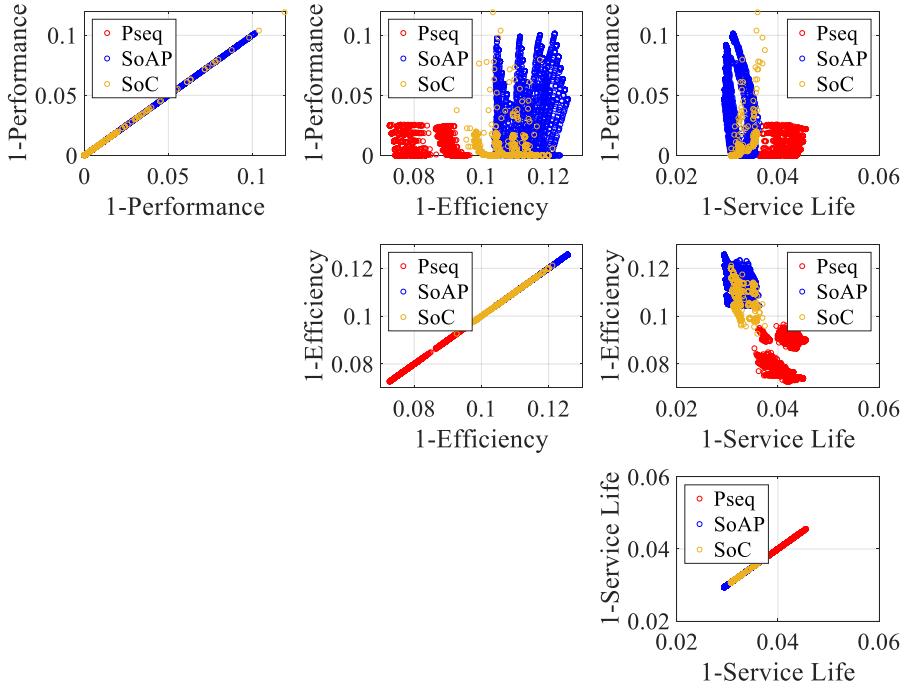
Figure 6.14: Summarized results of the potential analysis for the frequency regulation scenario within the specified design space, use case space, and target indicator space.

The matrix plot's main diagonal data shows that some similarities to the peak shaving scenario were found. In most cases, high performances for different design variable combinations were achieved using the SoC-balancing PFCS. In contrast, high efficiencies were found using the sequential PFCS (PFCS Pseq). Using the parametric and state-of-the-art PFCSs, lower efficiencies were observed. Again, an inverted effect was noticed concerning the target indicator "service life." The sequential PFCS (PFCS Pseq) led to lower service life in numerous cases, whereas for the other two PFCSs a higher service life was found. In contrast to the peak shaving scenario, the potentials of the SoC-balancing PFCS could not be covered at all when adapting the design variables of the parametric PFCS (PFCS SoAP). As the upper triangular matrix shows, higher efficiencies for similar performances were achieved using the state-of-the-art PFCS (PFCS SoC). On the other hand, higher service life for similar performance was found in most cases when using the parametric PFCS (PFCS SoAP). In the case of the sequential PFCS (PFCS Pseq), higher efficiencies were observed in almost all cases. However, the exact opposite was noticed for the target indicator "service life."

Together, the results obtained in this work provide essential insights into the causal relationships between the inputs and the outputs in complex heterogeneous BESSs. The two most striking aspects emerging from the simulation studies are that the potentials of the PFCSs and the correlations between the target indicators, design variables, and use case variables were precisely quantified. The experimental research design based on simulations to investigate the potentials and sensitivities of different PFCSs for heterogeneous BESSs was used. Based on this approach, the methodological framework offered a generic process to solve the MOO on a black-box function problem effectively and efficiently by using surrogate models. However, the accuracy of the performance surrogate model in the case of the sequential PFCS (PFCS Pseq) for the frequency regulation scenario was slightly too weak yet acceptable. Therefore, an additional sensitivity analysis based on the real data is shown in Appendix C Figure C.24, confirming the validity of the performance surrogate model. The next chapter discusses the findings in more detail and checks whether the research questions are answered.

7 Evaluation of the power flow control strategies

The results presented in the previous chapter indicate that this work's methodological framework quantifies the potentials and sensitivities of different PFCSs for heterogeneous BESSs effectively and efficiently. Therefore, the methodological framework provides sensitive information for analyzing the causal relationships between the inputs and the outputs of heterogeneous BESSs to enable the sustainable operation of such systems. Especially the analysis of the sensitivities fundamentally improves the understanding of the relationships between design variables, use case variables, and the target indicators. In general, revealing aspects emerged from the data, and insights into the multi-objective black-box function problem were provided. It is possible to hypothesize that the power distribution within the system is a key issue for sustainable operation. Thus, this chapter moves on to evaluate and discuss these findings in more detail. In Section 7.1, the evaluation based on the potential analysis is presented. The evaluation based on the sensitivity analysis is outlined in Section 7.2. Section 7.3 continues to evaluate the results of the use case-specific potential analysis before Section 7.4 summarizes the evaluation process. It should be noted that the following discussion of the results is partly based on my published works [11, 12, 14].

It is important to reiterate that MOO problems for BESSs have already been studied in the literature (cf. Section 2.2). However, these studies have either turned the MOO problem into a single-objective optimization problem, i.e., weighting the objectives or using heuristics, or have not focused on a thorough analysis of the multiple objectives to provide information about conflicting target indicators. Moreover, especially in the field of DC MGs, an SoC-balancing PFCS is often applied without a comprehensive analysis of its applicability. In this work, the potentials of PFCSs in different use cases were evaluated, and the sensitivities on target indicators were systematically analyzed to improve the understanding

of the correlations between the PFCSs, use case, and target indicators. It was found that trade-offs between the multiple objectives occurred and no single solution, e.g., weighting, existed that concurrently optimizes multiple objectives adequately. Furthermore, it was observed that in many cases, either the parametric PFCS (PFCS SoAP) and the sequential PFCS (PFCS Pseq) achieved better results concerning the target indicators than the state-of-the-art PFCS (PFCS SoC). Unlike existing studies, this work provides a new approach to analyze MOO problems for BESS applications without simplifying the problem itself. The results obtained are in contradiction to the assumptions of several authors that the SoC-balancing PFCS generally constitutes a reasonable operational strategy of BESSs. On the whole, the presented methodological framework and the findings put, for example, the recommendations of Li and Wang [8] into practice, developing an innovative control and operation method for BESSs considering several requirements, e.g., efficient operation or multi-objective control and management [8]. In addition, the methodological framework applies to other PFCSs, use cases, and target indicators, allowing fellow researchers to compare their PFCSs, use cases, and objectives using this framework. So far, the discussion has focused on where this work fits into the research map and how it affects it. The rest of this chapter provides a detailed look into the meaning of the results and explains how these results relate to the research questions.

7.1 Evaluation based on the potential analysis

With respect to the first subordinate research question, a systematic analysis of the target indicators is examined. The results suggest that the potentials of each of the three PFCSs were dependent on the resulting power distribution within the system. In my published work [14], it has been concluded that a PFCS, in which not necessarily all BESSs are in operation, could achieve improvement. In some cases, the results of the potential analysis found support for this hypothesis, as discussed in the following. Concerning the peak shaving scenario, a maximum performance of $100\,\%$ (1-Performance$\,=0$) was observed for each PFCS, as shown in Figure 6.13. This was due to the use case space, which was defined in such a way as to achieve performances around $100\,\%$. However, closer inspection of the results (see Figure 7.1) revealed that both the parametric and the sequential PFCS (PFCS Pseq) gained a higher performance with an increasing (discrete) profile scaling factor than the state-of-the-art PFCS (PFCS SoC).
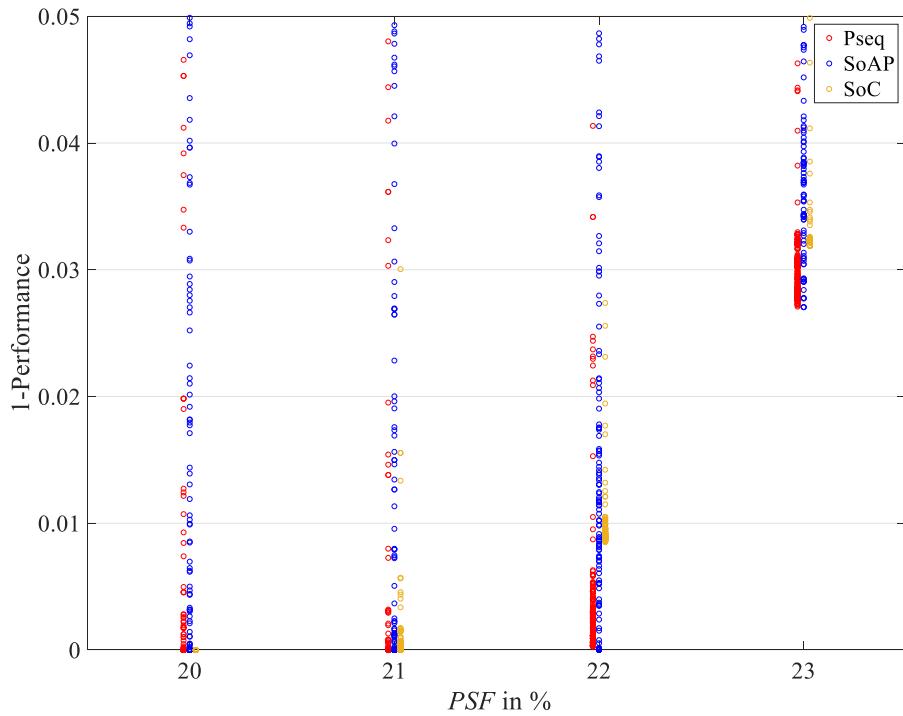
Figure 7.1: Analysis of the target indicator "performance" for an increasing profile scaling factor in the case of the peak shaving scenario. The PFCSs are illustrated in groups and refer to the respective discrete profile scaling factor.

This is attributable to the fact that all BESSs are charged/discharged equally concerning their capacity when using the SoC-balancing PFCS. Consequently, the SoCs remain balanced, and all batteries hit their operating limits equally, resulting in instant performance loss. In contrast, the batteries hit their operating limits differently due to equal power-sharing for the other two PFCSs. Although a single battery might hit operating limits prematurely, another battery can take over a larger share of the power but is not yet limited by the derating. Consequently, performance loss is delayed and slowed down. Deeper analysis with different PFCSs can be found in my published work [11].

Concerning the target indicator "efficiency," differences between the three PFCSs were identified. One interesting finding is that generally, high efficiencies were found using the sequential PFCS (PFCS Pseq) while lower efficiencies were noticed using the parametric and state-of-the-art PFCSs. These differences can be explained by showing the energy losses over one specific simulation run. Therefore,

the same design and use case combination[1] as previously used for the sensitivity analysis (see Section 6.1) serves as an example. For all PFCSs, a performance of 100 % was achieved, and therefore the energy throughput was identical.
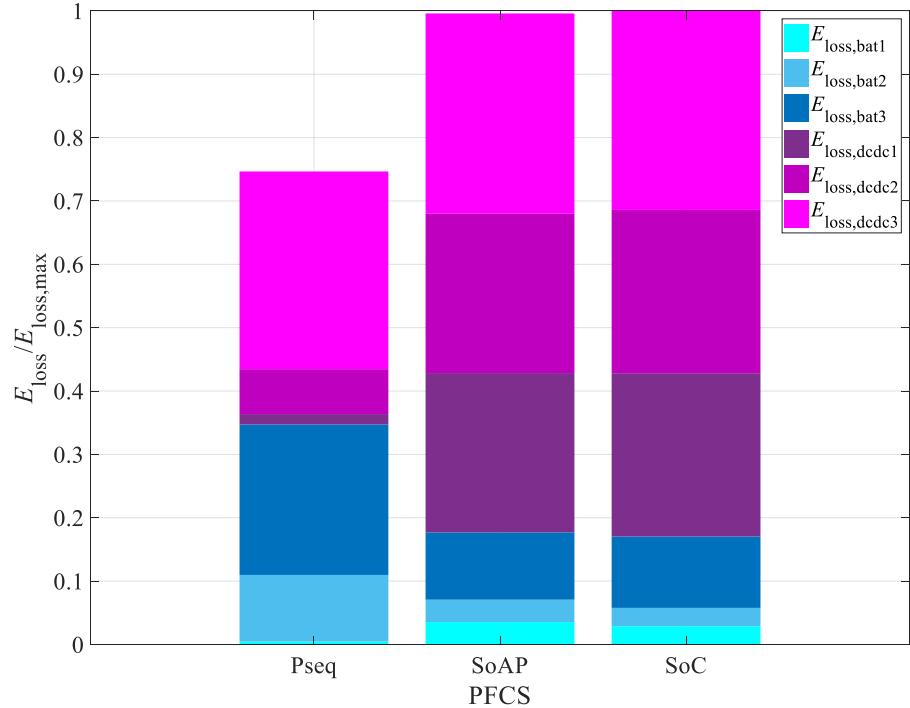
Figure 7.2: Analysis of the target indicator "efficiency" showing the normalized energy losses when using different PFCSs in the case of the peak shaving scenario.

As can be seen in the diagram, the total energy losses were around 25 % lower using the sequential PFCS (PFCS Pseq). An explanation for this can also be found in Figure 7.2. In the case of the other two PFCSs, the batteries are charged/discharged equally with respect to their capacity. Considering the systems' heterogeneity, two BESSs operate at low power ($P_{\mathrm{loss,bat}}$ is low) resulting, however, in lower efficiencies due to the part-load operation of the DC/DC converters ($P_{\mathrm{loss,dcdc}}$ is high). It should be noted that there are some design and use case combinations where the energy losses using the sequential PFCS (PFCS Pseq) are equal or even higher compared with the other two PFCSs. This is especially the case when using the BESSs in ascending order, i.e., the smallest battery first.

---

[1] $H_{\mathrm{C}} = 1.5$, $PSF = 20\,\%$, PFCS Pseq: $P_{\max} = 400\,\mathrm{W}$, Sorting $= 1$, PFCS SoAP: $t_{\mathrm{pred,p}} = 20\,\mathrm{s}$, $t_{\mathrm{pred,e}} = 1500\,\mathrm{s}$, PFCS SoC: convergence factor: 3, compensation function: power

Another important finding was that an inverted effect was observed in terms of the target indicator "service life." The data suggests that the sequential PFCS (PFCS Pseq) led to lower service life in numerous cases. This has been investigated by applying the same design and use case combination again, except that the design variable "sorting" was varied. The results are summarized in Table 7.1.

Table 7.1: Analysis of the target indicator "service life" showing the capacity losses when using different PFCSs in the case of the peak shaving scenario.

PFCS	Q_{loss}^{cal}	Q_{loss}^{cyc}	Q_{loss}
Pseq (Sorting = 0)	0.75 %	0.62 %	1.38 %
Pseq (Sorting = 1)	0.62 %	0.27 %	0.89 %
SoAP	0.70 %	0.28 %	0.98 %
SoC	0.67 %	0.24 %	0.91 %

The data in the table shows that there are design and use case combinations where the sequential PFCS (PFCS Pseq) leads to lower service life, i.e., increased capacity loss. In these cases, the capacity loss due to cycle aging is often enhanced drastically. Analysis has shown that this can be explained by the fact that smaller BESSs are forced to be operated at high C-rates or with great DoDs. Furthermore, a slight increase of the capacity loss due to calendar aging is present. This is due to the slightly higher SoCs after recharging the smaller BESSs. The BESSs remain constant at a high SoC, resulting in an increased capacity loss since the batteries degrade faster at higher SoCs (cf. Section 4.2). Please note that cases exist where the sequential PFCS (PFCS Pseq) leads to higher service life, as indicated in the table. This is especially the case when using the BESSs in descending order, in which the largest battery is operated first, and therefore stress factors are comparably low.

Concerning the frequency regulation scenario, similar investigations were made. In contrast to the peak shaving scenario, the results presented in Figure 7.3 suggest that both the parametric and the state-of-the-art PFCS gained higher performance with an increasing (discrete) profile scaling factor than the sequential PFCS (PFCS Pseq).
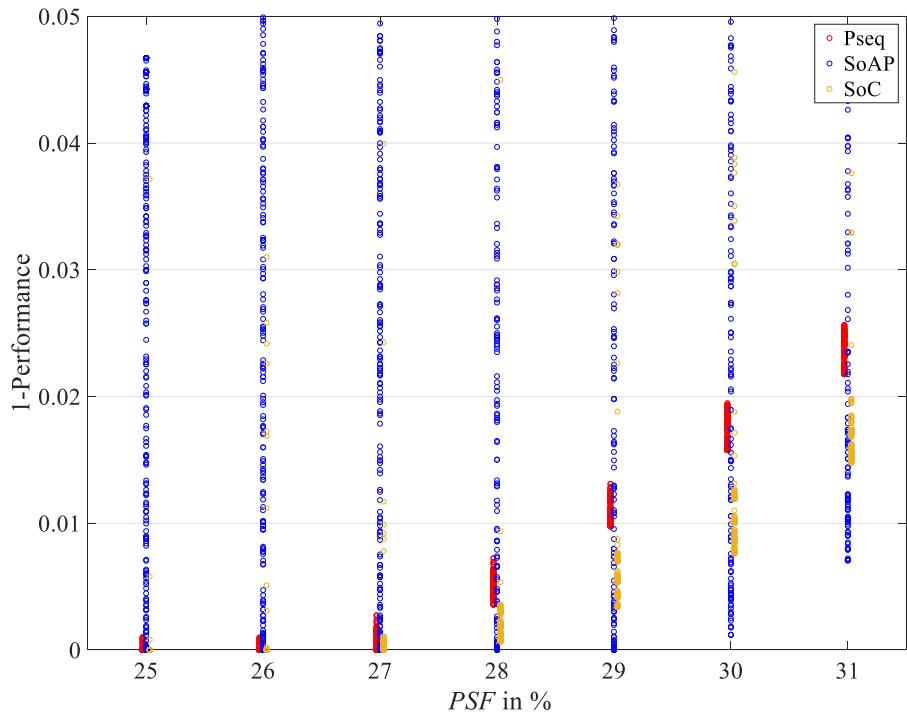
Figure 7.3: Analysis of the target indicator "performance" for an increasing discrete profile scaling factor in the case of the frequency regulation scenario. The PFCSs are illustrated in groups and refer to the respective discrete profile scaling factor.

This can be explained by considering the power distribution. In the case of the sequential PFCS (PFCS Pseq), BESSs hit their operating limits progressively, resulting in instant performance loss when the last BESS hits its limits. By using the parametric PFCS (PFCS SoAP), for example, the power is shared more regularly compared to the sequential PFCS (PFCS Pseq). Although smaller BESSs might hit operating limits prematurely, the largest BESS is still away from its limits. It can take over a larger share of the power and is not yet limited by the derating. Consequently, performance loss is delayed and slowed down.

As far as the target indicator "efficiency" is concerned, increased efficiency was noticed in almost every case using the sequential PFCS (PFCS Pseq), as can be seen in Figure 6.14. Looking at the energy losses over one specific simulation run provides insights into this. Here, the same design and use case combination[2] as previously used for the sensitivity analysis (see Section 6.2) serves as an example.

---

[2] $H_C = 0.75$, $PSF = 27\%$, PFCS Pseq: $P_{max} = 400\,W$, Sorting $= 1$, PFCS SoAP: $t_{pred,p} = 5\,s$, $t_{pred,e} = 700\,s$, PFCS SoC: convergence factor: 3, compensation function: power

Again, for all PFCSs, a performance of 100 % was achieved. Therefore, the energy throughput was identical. The total energy losses were around 40 % lower using the sequential PFCS (PFCS Pseq). An explanation for this can be derived from Figure 7.4.
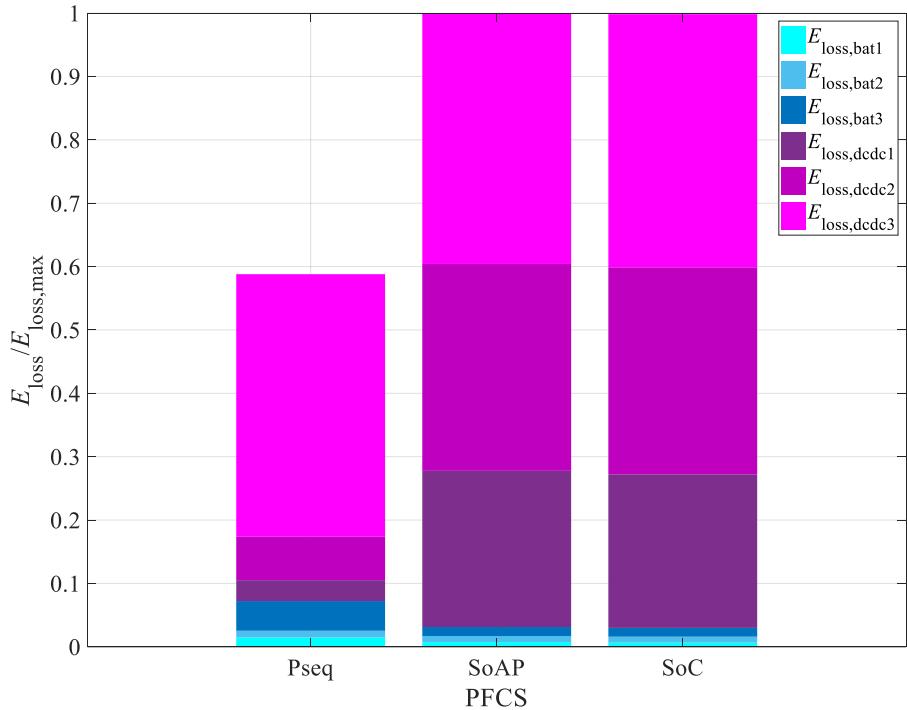
Figure 7.4: Analysis of the target indicator "efficiency" showing the normalized energy losses when using different PFCSs in the case of the frequency regulation scenario.

Generally, the respective power-shares, especially for smaller BESSs, are comparably low using the parametric and state-of-the-art PFCSs. Consequently, all DC/DC converters are forced to operate under part-load conditions, resulting in lower efficiencies, i.e., higher accumulated losses.

Regarding the target indicator "service life," it was found that an inverted effect occurred in almost every case, and the sequential PFCS (PFCS Pseq) led to lower service life. This has been investigated applying the same design and use case combination again. The results are presented in Table 7.2.

Table 7.2: Analysis of the target indicator "service life" showing the capacity losses when using different PFCSs in the case of the frequency regulation scenario.

PFCS	$Q_{\text{loss}}^{\text{cal}}$	$Q_{\text{loss}}^{\text{cyc}}$	Q_{loss}
Pseq	0.73 %	0.05 %	0.78 %
SoAP	0.63 %	0.01 %	0.64 %
SoC	0.62 %	0.01 %	0.63 %

The data in the table indicates that the sequential PFCS (PFCS Pseq) leads to lower service life, i.e., increased capacity loss. The observed increase of the capacity loss can be attributed to the combination of the scenario and the PFCS. The scenario is characterized by more of a charging behavior initially and more of a discharging behavior towards the end. After the charging, two batteries remain constant at a high SoC as only one BESS is needed for almost the rest of the time. Consequently, these batteries degrade faster at higher SoCs, resulting in lower overall service life.

All these findings confirm that the first subordinate research question has been answered conclusively. The methodological framework enables the conduct of a comprehensive potential analysis of different PFCSs for heterogeneous BESSs by systematically performing simulations to identify the Pareto-front for each PFCS. In addition, its results have important implications for developing a PFCS to enable the sustainable operation of such systems. Although a suitable PFCS depends on the specific use case and the objectives of the system operator, the results suggest that economic, environmental, and social benefits can be accomplished in every case. For example, using the sequential PFCS (PFCS Pseq) in peak shaving scenarios, higher performances could be achieved for an increasing profile scaling factor. This means the system could be designed smaller to achieve the same results using other PFCSs, resulting in an economic benefit. On the other hand, using the sequential PFCS (PFCS Pseq) in peak shaving scenarios might lead to a premature replacement of a single battery. In contrast, other PFCSs reduce the capacity loss, leading to longer service life and an environmental benefit.

In the previous section, a deeper analysis of the results has made it clear that the potentials of the PFCSs are related to the individually applied power and consequently to the energy throughput of each BESS. However, the results indicate that the individual applied power, in turn, depends mainly on the design variables

and the specific use case. Further analysis of the triangular matrix's results is necessary to quantify the target indicators' trade-offs adequately (second subordinate research question). Therefore, the potential analysis has been used further to identify and quantify the different trade-offs between the target indicators concerning the design and use case variables. Moreover, the correlations between the target indicators have been analyzed likewise. In the following, both aspects are discussed in more detail through the example of the peak shaving scenario and the parametric PFCS (PFCS SoAP). It should be noted that the identical procedure could be applied to the other use cases and PFCSs. In the case mentioned above, the two most important findings were that, first, pseudo-grouped data sets were observed, and second, positive as well as negative correlations were found. Figure 7.5 illustrates the results of the potential analysis considering the influence of the design variable $t_{\mathrm{pred,p}}$.
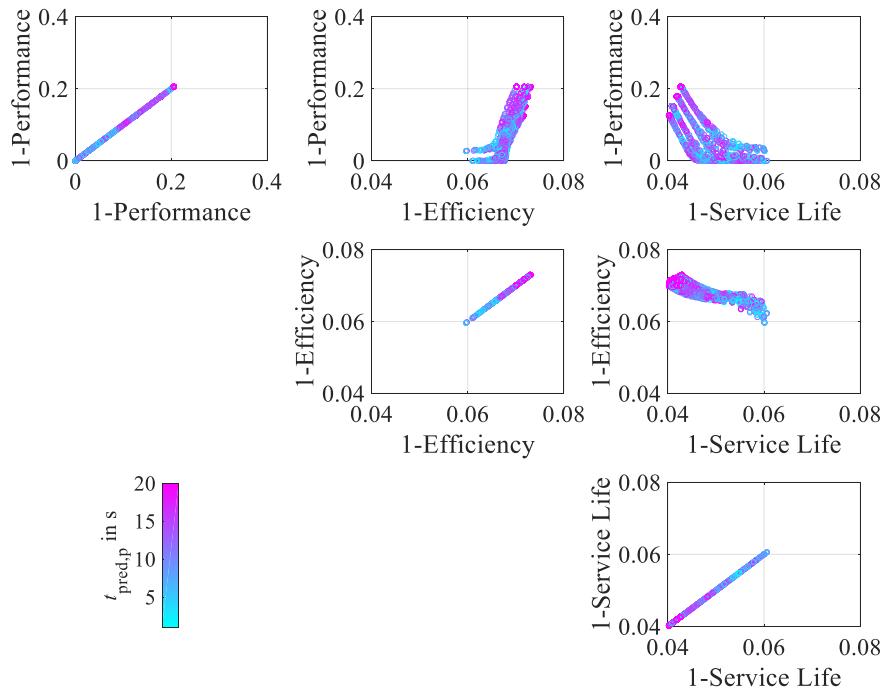
Figure 7.5: Results of the parametric PFCS (PFCS SoAP) potential analysis for the peak shaving scenario within the specified design space, use case space, and target indicator space. The results consider the influence of the design variable $t_{\mathrm{pred,p}}$ (see color bar).

This analysis suggests that the design variable $t_{\mathrm{pred,p}}$ did not significantly affect the trade-offs and correlations. There may be a minor influence on the correla-

tions concerning efficiency, but no significant impact can be identified. A possible explanation for this might be that this design variable influences a battery's predicted charge/discharge power only slightly, resulting in barely unaffected power distribution. Therefore, the second design variable $t_{\mathrm{pred,e}}$ has been investigated in more detail. The results of the potential analysis considering the influence of this design variable are shown in Figure 7.6.
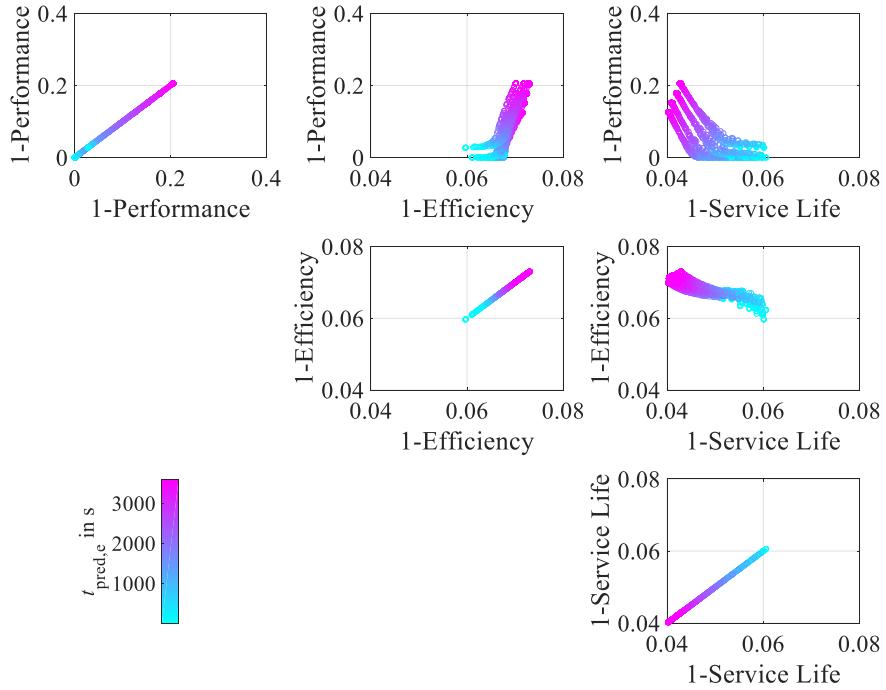

Figure 7.6: Results of the parametric PFCS (PFCS SoAP) potential analysis for the peak shaving scenario within the specified design space, use case space, and target indicator space. The results consider the influence of the design variable $t_{\mathrm{pred,e}}$ (see color bar).

The analysis of the design variable $t_{\mathrm{pred,e}}$ gives an unambiguous indication that the correlations between the target indicators are related to this design variable. Regarding the performance-efficiency trade-off, an efficiency in the range of 92.7 % and 94.0 % and a performance of 79.0 % to 100 % can be expected for the specified design space. Reducing the design variable $t_{\mathrm{pred,e}}$ caused higher efficiency and higher performance at the same time. In contrast, an inverse behavior can be identified concerning the trade-off between performance and service life. A decreasing value of $t_{\mathrm{pred,e}}$ also entails higher performance but severely lower service life. Here, the trade-off ranges from 94.0 % to 96.0 % in the case of service life and

again from 79.0 % to 100 % for the target indicator "performance." Consequently, for the trade-off between efficiency and service life, increasing efficiency and a decreasing service life were identified with a decreasing value of $t_{\mathrm{pred,e}}$. All these findings are likely to be related to the resulting power-sharing within the system. Depending on the value of the design variable, the PFCS strives to balance the power or the state of energy/charge among all BESSs. The former may enhance efficiency due to lower accumulated losses of the DC/DC converters. For the latter, the largest BESS is supposed to take over the applied power's largest share, resulting in proportional power-sharing. In this case, service life is likely to show improvements since no BESS is forced to be operated at high C-rates or with great DoDs. However, a too aggressive state of energy/charge balancing might lead to performance losses as power requirements cannot be fulfilled anymore.

The first part of the analysis has shown that most of the trade-offs are quantifiable and reasonable explanations for the correlations can be provided. However, interactions between the design variables might occur and may affect the results to different extents. Furthermore, the use case variables are also likely to influence the trade-offs and correlations between the target indicators. For this reason, the second part of the analysis deals with the influence of the use case variables on the trade-offs and correlations of the target indicators. Figure 7.7 illustrates the results of the potential analysis, however, now considering the influence of the use case variable "heterogeneity."
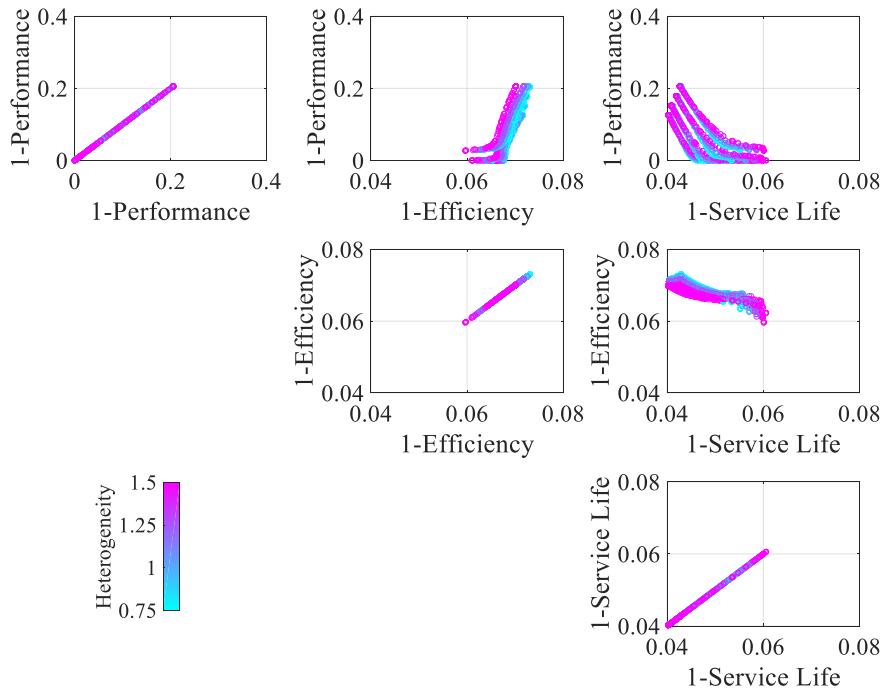
Figure 7.7: Results of the parametric PFCS (PFCS SoAP) potential analysis for the peak shaving scenario within the specified design space, use case space, and target indicator space. The results consider the influence of the use case variable "heterogeneity" (see color bar).

The analysis indicates that the use case variable "heterogeneity" affected the trade-offs considerably, yielding higher or lower target indicator values. In contrast, the correlations themselves were not directly influenced by the heterogeneity. In the case of the performance-efficiency trade-off, a lower heterogeneity caused noticeably lower efficiency but not necessarily lower performance. Differences of up to several tenths of a percent occurred. This relationship may be explained by the fact that the power-sharing within the system might be disadvantageous for efficiency, but the total energy throughput remains constant. Similar results were found regarding the performance-service life trade-off. In some cases, a less heterogeneous system can enhance service life. The explanation for it may be similar. The power-sharing within the system might change favorably concerning the target indicator "service life," but the total energy throughput is still identical. Regarding the trade-off between efficiency and service life, a more heterogeneous system resulted in higher efficiency and higher service life. This contrary effect may be interfered with using a design variable combination where performance is

128

reduced, resulting in higher service life due to a lower energy throughput. However, this effect changed, as can be seen on the right-hand side of the plot. Here, a more heterogeneous system resulted in higher efficiency but lower service life. This may be due to a less equal power-sharing, leading to a shorter part-load operation of the DC/DC converters as operating limits might be reached earlier, yet concurrently, to a more stressful operation for a single battery.

Since the use case variables were changed independently, a closer look into the influence of the use case variable "profile scaling factor" is required. Figure 7.8 shows the results of the potential analysis, considering the effects of the use case variable "profile scaling factor."
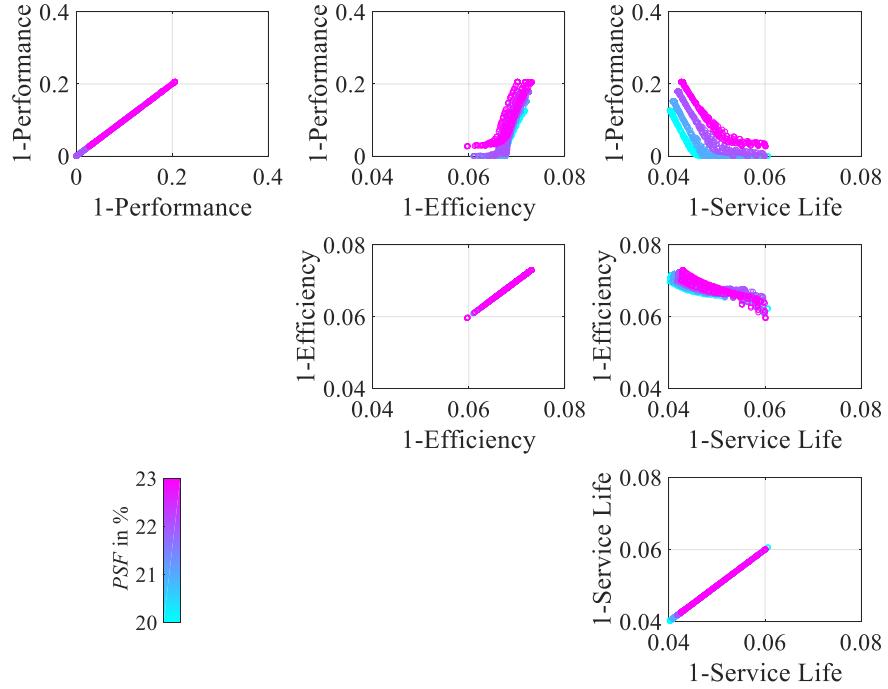

Figure 7.8: Results of the parametric PFCS (PFCS SoAP) potential analysis for the peak shaving scenario within the specified design space, use case space, and target indicator space. The results consider the influence of the use case variable "profile scaling factor" (see color bar).

The most obvious finding to emerge from the analysis is that the pseudo-grouped data resulted from the discrete profile scaling factor, as can be seen in the upper right plot. The analysis further suggests that the use case variable "profile scaling factor" also influenced the trade-offs, but the correlations were not directly

affected. As far as the trade-off between performance and efficiency is concerned, a higher profile scaling factor reduced performance to some extent. However, efficiency was not imperatively enhanced as expected.[3] This aspect may be explained by the interactions between the use case variable and the design variables. A high value of $t_{\mathrm{pred,e}}$ leads to a too aggressive state of energy/charge balancing, resulting in a curtailment of the power. Consequently, DC/DC converters are forced to operate in part-load operation, which, in turn, reduces the target indicator "efficiency." The trade-off between performance and service life indicated that with an increasing profile scaling factor, a high service life can still be achieved but only at the expense of the target indicator "performance." For example, to achieve a service life in the range of 94.0 % to 95.5 %, a performance in the range of 97.5 % to 100 % can be expected for a smaller profile scaling factor. In contrast, to achieve the same service life for the highest profile scaling factor, a performance between 84.0 % and 97.5 % must be accepted. A possible explanation for these results may be that a higher profile scaling factor results in increased energy throughput. This indicates both the reduction in performance and the battery's service life due to higher stress factors. A note of caution is due here since a performance loss implies a lower energy throughput, resulting in possibly higher service life. Concerning the trade-off between efficiency and service life, a higher profile scaling factor resulted in lower efficiency and possibly lower service life. A possible interference of the other design and use case variables cannot be ruled out and is yet likely, as a first analysis has shown. Nevertheless, this behavior seems to vanish at some point, as can be seen on the right-hand side of the plot. In this case, efficiency increases with an increasing profile scaling factor, but at the same time, service life gets worse in most cases. This may be explained by the fact that the required power and thus the energy throughput increases, which yields higher individual powers, i.e., higher efficiencies of the DC/DC converters but enhanced stress for the batteries. However, clear exceptions to this exist in some cases. A higher energy throughput, for example, may yield a lower SoC in the resting periods, resulting in a lower calendar aging. In such cases, service life could be enhanced depending on the aging characteristics of the battery.

In sum, the second subordinate research question has been answered based on the example of the peak shaving scenario and the parametric PFCS (PFCS SoAP). The trade-offs between the target indicators can be quantified accurately consid-

---

[3]A higher profile scaling factor should enhance efficiency due to higher efficiencies of the DC/DC converters.

ering the design and use case variables. One of the issues that emerges from these findings is the interactions between them. Due to superimposed effects, individual influences of the design and use case variables cannot always be clearly assigned. It can be concluded that only a potential analysis is not sufficient to adequately analyze the causal relationships between the inputs and the outputs of heterogeneous BESSs. For this reason, the surrogate model-based sensitivity analysis has been conducted to gain knowledge about the target indicator versus design or use case variables sensitivities. A major benefit of this analysis is that individual influences can be analyzed separately, enabling a detailed evaluation of the explanations stated in the potential analysis.

7.2 Evaluation based on the sensitivity analysis

In this section, the results of the sensitivity analysis are discussed, considering the third and fourth subordinate research questions. In general, they suggest that the concrete impacts of the design and use case variables on the target indicators vary significantly depending on the specific PFCS or applied scenario. Furthermore, as presented in the previous section, individual influences are hardly assignable due to the interactions between the design and use case variables. The goal here is to improve the understanding of the causal relationships, i.e., the relations between design variables, use case variables, and target indicators, by analyzing the results of the sensitivity analysis in the time domain. However, a thorough evaluation of all results obtained by the surrogate model-based sensitivity analysis presented in Section 6.1 and Section 6.2 is not feasible within the scope of this work. Therefore, the focus is on a comprehensive analysis of two different examples that offer unique insight. The first one is continuing the evaluation of the results of the parametric PFCS (PFCS SoAP) in the peak shaving scenario. In contrast, the second one focuses on the results of the sequential PFCS (PFCS Pseq) in the frequency regulation scenario. Referring to Section 5.4, the surrogate model-based sensitivity analysis was done by investigating the relations between each target indicator and each design and use case variable for only one given design and use case combination. It should be noted that for other design and use case combinations, different relationships may occur.

Concerning the first example, an interesting finding of the sensitivity analysis was that the impact of the design variable $t_{\mathrm{pred,p}}$ on each target indicator was

negligible. In contrast, the influence of the design variable $t_{\text{pred,e}}$ on the target indicators was severe. Furthermore, different correlations were noticed between the use case variables and the target indicators. In the following, six exemplary simulation runs of the parametric PFCS (PFCS SoAP) in the case of the peak shaving scenario are presented in the time domain. These simulation runs consider the set values of the sensitivity analysis (see Figure 6.3) as a reference case and the minimum and maximum values of the design and use case space (cf. Table 5.1). The exact design and use case variables and the results for the six exemplary simulation runs are summarized in Table 7.3.

Table 7.3: Design variables, use case variables, and target indicator values for the six exemplary simulation runs of the parametric PFCS (PFCS SoAP) in the case of the peak shaving scenario.

	$t_{\text{pred,p}}$ in s	$t_{\text{pred,e}}$ in s	H_{C}	*PSF* in %
a)	20	1500	1.5	20
b)	1	1500	1.5	20
c)	20	1	1.5	20
d)	20	3600	1.5	20
e)	20	1500	0.75	20
f)	20	1500	1.5	23

	1-Performance	1-Efficiency	1-Service life
a)	0.000	0.066	0.049
b)	0.000	0.066	0.049
c)	0.000	0.062	0.061
d)	0.126	0.070	0.040
e)	0.000	0.067	0.046
f)	0.053	0.066	0.054

As can be seen in the table, the design and use case variables were varied individually concerning the minimum or maximum values of the defined design or use case space. Case a) serves as a reference case, and the respective set values are in line with the ones applied in the sensitivity analysis (see Section 6.1) to ensure easy comparability and, most of all, comprehensibility. In cases b) to f), each design and use case variable was varied individually compared to the reference case. Moreover, the target indicator values were also consistent with those obtained in the surrogate model-based sensitivity analysis, confirming the high accuracy of the surrogate models. For reasons of clarity, Figure 7.9 shows the results of the parametric PFCS (PFCS SoAP) potential analysis for the peak shaving scenario again, however, now emphasizing the results of the six exemplary simulation runs.
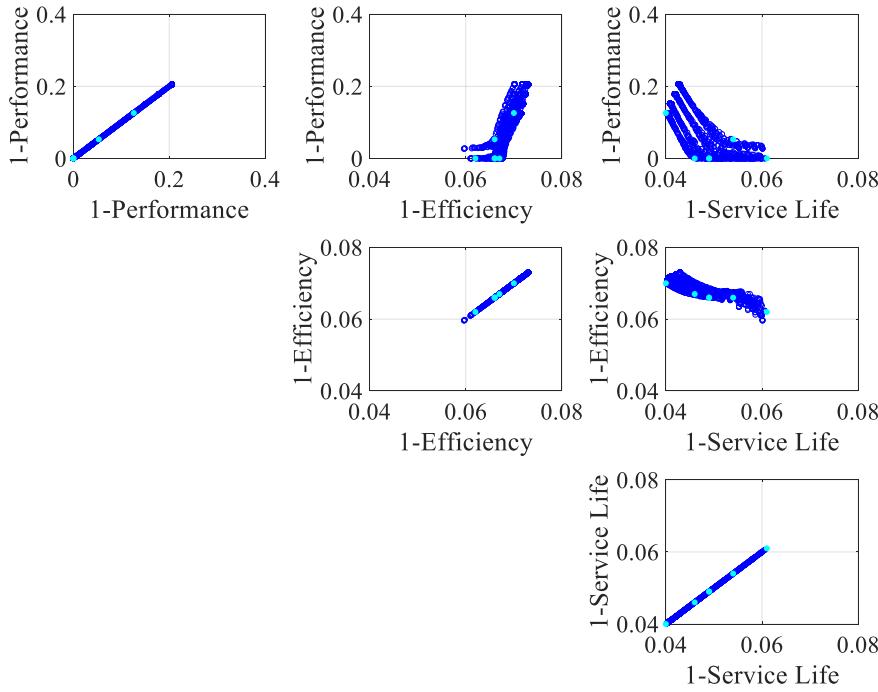
Figure 7.9: Results of the parametric PFCS (PFCS SoAP) potential analysis for the peak shaving scenario emphasizing the results of the six exemplary simulation runs (cyan markers).

It is apparent from Figure 7.9 that the results of the exemplary simulation runs cover the target indicator space essentially. The target indicator "performance" ranged between 87.4 % and 100 %, efficiency between 93.0 % and 93.8 %, and the target indicator "service life" between 93.9 % and 96.0 %. Therefore, different aspects of the sensitivities of the design and use case variables on the target indicators can be examined unambiguously as noticeable differences result from the variation that was carried out. In Figure 7.10, the analysis of the six exemplary simulation runs of the parametric PFCS (PFCS SoAP) in the case of the peak shaving scenario is presented. The power distributions over time are shown on the left side, whereas, on the right side, the respective SoCs over time are provided. The set values of the design and use case variables for each simulation run can be found in Table 7.3.
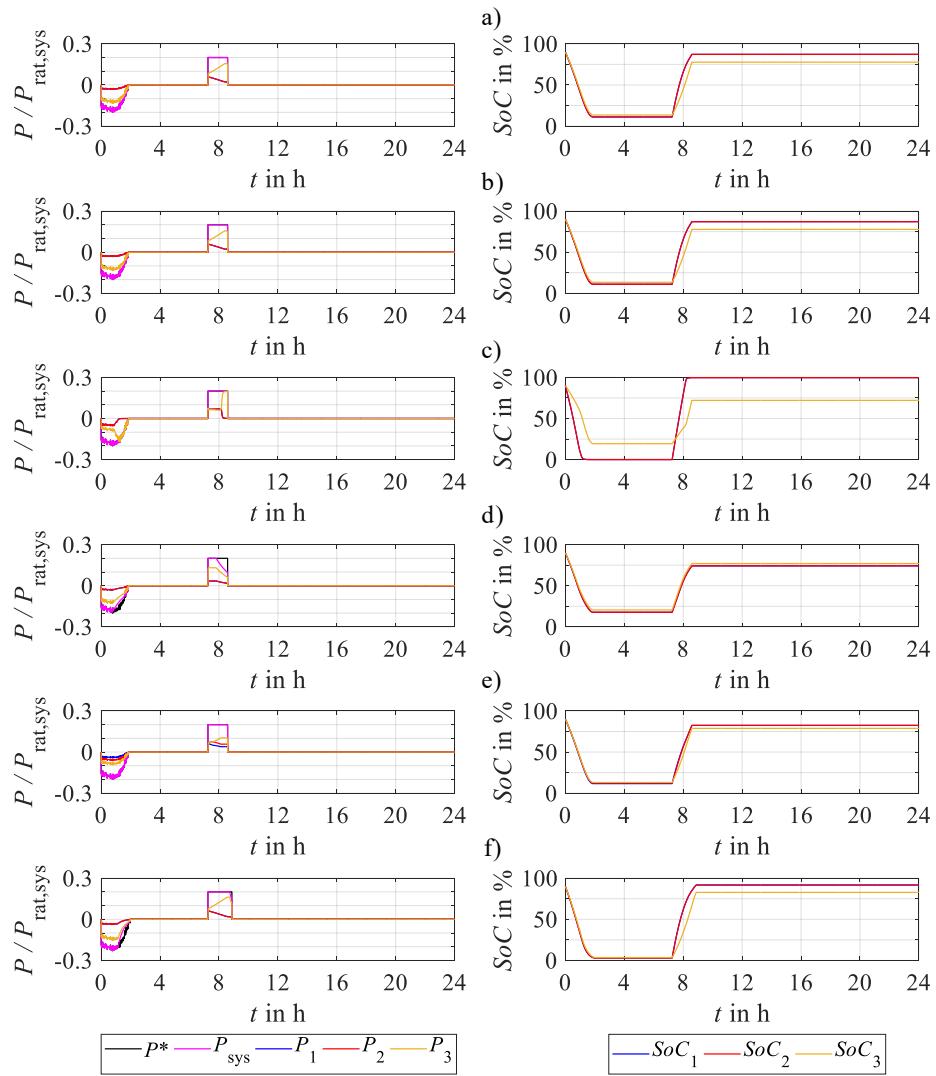
Figure 7.10: Analysis of six exemplary simulation runs of the parametric PFCS (PFCS SoAP) in the case of the peak shaving scenario showing the power distribution (left side) and the SoCs (right side) over time. The set values of the design and use case variables for each simulation run can be found in Table 7.3.

In general, the requested charge/discharge power is represented by P^* (black line) and the total charged/discharged power of the entire system is indicated by P_sys (pink line), as previously described in Section 4.1. The latter considers the efficiencies of each DC/DC converter and the direction of the power flow. The individual charged/discharged power P_i (BESS 1: blue line, BESS 2: red line, BESS 3: yellow line) of a string adds up to the total system power. Furthermore, the SoC of

each battery is denoted as, for example, SoC_1 (battery 1: blue line, battery 2: red line, battery 3: yellow line). With the exception of the fifth simulation run, BESS 1 and BESS 2 are always identical (cf. Table 7.3). Consequently, the behavior of both BESSs is similar and only the red lines (BESS 2) are visible in the graphs.

The first simulation run (reference case) suggests that the set values of the design variables led to a mostly proportional power-sharing, resulting in a moderate state of energy/charge balancing, as shown in graphs a). In this case, the power requirements could be fulfilled, and the target indicator "performance" amounted to 100 %. The target indicator "efficiency" was 93.4 %, and the target indicator "service life" was 95.1 %.

For the second simulation run b), the design variable $t_{\mathrm{pred,p}}$ was changed from its maximum value to its minimum value of 1 s. As both graphs b) reveal, the power distribution and the SoCs virtually did not change compared to the reference case. An explanation for this may be that this design variable influences a battery's predicted charge/discharge power only slightly, resulting in barely unaffected power distribution, as explained in the previous section. Thus, all target indicator values remain de facto identical, and it can be concluded that this design variable is without any influence on the system.

For the third and fourth exemplary simulation runs c) and d), only the design variable $t_{\mathrm{pred,e}}$ was varied to its minimum value of 1 s, displayed in graphs c), and to its maximum value of 3600 s, shown in graphs d). A small design variable $t_{\mathrm{pred,e}}$ of about one second led to full performance and an increase of efficiency (93.8 %) on the one hand, but a decrease of the target indicator "service life" (93.9 %) on the other hand. In contrast, a design variable $t_{\mathrm{pred,e}}$ of about one hour resulted in severely lower performance (87.4 %) and a reduced target indicator "efficiency" (93.0 %), but also noticeably higher service life (96.0 %). Consequently, the calculation of the energy limits cannot be neglected. These findings are explained by the current, voltage, and energy limits of each battery and the operating point of each BESS. Within a specific operating range around an average SoC, the voltage limit is basically non-effective compared with the other limits. Moreover, a small design variable $t_{\mathrm{pred,e}}$ of, e.g., one second practically disables the energy limit additionally due to a comparatively high charge/discharge power. Consequently, the matched current limits of the batteries define the maximum available power, which in turn

leads to a more balanced power distribution among all BESSs, as can be seen in graph c) on the left side. In a heterogeneous system, smaller BESSs (here BESS 1 and BESS 2) hit their voltage limits prematurely during a charge/discharge process, causing a redistribution of the individual power shares. Larger BESSs are then supposed to take over a larger share of the requested power to still fulfill the power requirements. This behavior can be observed after roughly one hour, as the plot on the left side illustrates. Consequently, the SoCs become more balanced outside the normal operating range, and the performance remains constant or increases. Regarding efficiency, a balanced power distribution enhances efficiency due to lower accumulated losses of the DC/DC converters when each converter stage operates at comparably higher efficiencies. However, service life decreases at the same time since BESSs are forced to operate at higher C-rates and with greater DoDs. In contrast, a prediction horizon $t_{\mathrm{pred,e}}$ of one hour leads to unbalanced power distribution, yielding a balanced state of energy/charge, as graphs d) indicate. In this case, the largest BESS is supposed to take over the largest share. However, a too aggressive state of energy/charge balancing often leads to performance losses as power requirements cannot be fulfilled anymore. This behavior was found, e.g., after roughly one hour, as the plot on the left side demonstrates. Furthermore, the accumulated losses of the DC/DC converters are higher due to the extreme part-load operation of two BESSs, resulting in a decreased target indicator "efficiency." Contrary to the third exemplary simulation run c), here, service life increases as two BESSs are operated at lower C-rates and with greater DoDs. However, these results must be interpreted with caution since reduced performance yields a lower energy throughput, resulting in higher service life at the same time. On the whole, this analysis suggests that the target indicators are highly sensitive to the design variable $t_{\mathrm{pred,e}}$.

In the case of the fifth exemplary simulation run e), the use case variable "heterogeneity" was changed to its minimum value of 0.75. The decrease of the heterogeneity, i.e., BESS 1 and BESS 2 were scaled up and BESS 3 was scaled down, resulted in marginally lower efficiency (93.3 %) and higher service life (95.4 %). The target indicator "performance" was not affected as the power requirements did not change and no aggressive state of energy/charge balancing was applied. As can be seen in graphs e), the observed decrease in efficiency can be attributed to the resulting power-sharing between the BESSs. A more homogeneous system results in a more equal distribution, as can be seen in the graph on the left side.

Consequently, all DC/DC converters operate in part-load operation, yielding lower efficiency. On the other hand, an increase was found for the target indicator "service life." An explanation for this is that the influence of the aging stress factors, for example the C-rate, on the capacity fade due to cycle aging becomes lower for larger BESSs. The findings suggest that the system's heterogeneity constitutes an important factor in this case as the power distribution is directly affected by this use case variable. However, as defined in this work, the heterogeneity is not bijective, meaning that a similar heterogeneity could lead to slightly different results (cf. Section 5.1).

An increase of the use case variable "profile scaling factor" to its maximum value of 23 % suggests different behavior, as the sixth exemplary simulation run revealed. Graphs f) provide information about the power distribution and the SoCs for this case. First, a discrepancy between the desired power P^* and the system power P_{sys} was observed. The power curtailment started after not even one and a half hours to keep the SoCs balanced. After roughly two hours, the batteries were fully discharged, resulting in performance loss (94.7 %). Second, almost no change was noticed for the target indicator "efficiency" (93.4 %). This somewhat contradictory result (at least in this specific case) is due to a rapidly decreasing efficiency of the DC/DC converters after the power requirements cannot be fulfilled anymore, even if higher efficiencies were observed initially. Third, the increase of the profile scaling factor led to lower service life (94.6 %). This can be attributed to the recharge process after seven hours. Due to the increased energy throughput, the influence of the aging stress factors, such as the DoD, on the capacity fade (cycle aging) gets higher for smaller BESSs. Furthermore, the SoCs of the batteries are noticeably higher after the recharging process, as can be seen in graph f) on the right side, causing a higher capacity fade due to increased calendar aging. It can be concluded that the use case variable "profile scaling factor" is also decisive for a sustainable operation of the overall system. However, it is important to bear in mind that such systems will often be designed to fulfill the power requirements at any time. Exceptions are, e.g., home storage applications.

In general, all these findings helped improve the understanding of the causal relationships in the peak shaving scenario and the parametric PFCS (PFCS SoAP). Influencing design or use case variables were identified and the individual impact was quantified. The second example moves on to identify and quantify the sensi-

tivities in the case of the frequency regulation scenario and the sequential PFCS (PFCS Pseq), seeking to similarly reveal the causal relationships.

As far as the second example is concerned, the most surprising finding of the sensitivity analysis was that the correlations between each design and use case variable and a specific target indicator were quite similar. However, deeper analysis is necessary to evaluate these results correctly. Therefore, six exemplary simulation runs of the sequential PFCS (PFCS Pseq) in the case of the frequency scenario are presented in the time domain. The simulation runs consider the set values of the sensitivity analysis (see Figure 6.10) as a reference case and the minimum and maximum values of the design and use case space (cf. Table 5.1). Detailed information about the design and use case variables as well as the results for the six exemplary simulation runs is provided in Table 7.4.

Table 7.4: Design variables, use case variables, and target indicator values for the six exemplary simulation runs of the sequential PFCS (PFCS Pseq) in the case of the frequency regulation scenario.

	P_{max} in W	Sorting	H_{C}	PSF in %
a)	400	1	0.75	27
b)	100	1	0.75	27
c)	400	0	0.75	27
d)	400	1	1.5	27
e)	400	1	0.75	25
f)	400	1	0.75	31

	1-Performance	1-Efficiency	1-Service life
a)	0.000	0.081	0.039
b)	0.000	0.085	0.038
c)	0.000	0.090	0.038
d)	0.000	0.075	0.043
e)	0.000	0.083	0.036
f)	0.023	0.078	0.040

The data in the table indicates that the design and use case variables were variegated individually concerning their minimum or maximum values. The respective set values are parallel to those applied in the sensitivity analysis (see Section 6.2) and therefore ensure easy comparability. Again, case a) serves as a reference case, whereas in cases b) to f) each design and use case variable was varied individually compared to the reference case. The target indicator values were mainly consistent with the ones obtained in the surrogate model-based sensitivity analysis. Although

the accuracy of the performance surrogate model was somewhat less, only a slight difference of 0.1 percentage points between the value obtained by the surrogate model and the one obtained here in case f) was observed. Regarding the other target indicators, the high accuracy of the surrogate models was confirmed. Figure 7.11 shows the results of the sequential PFCS (PFCS Pseq) potential analysis for the frequency regulation scenario, emphasizing the results of the six exemplary simulation runs (cyan markers).
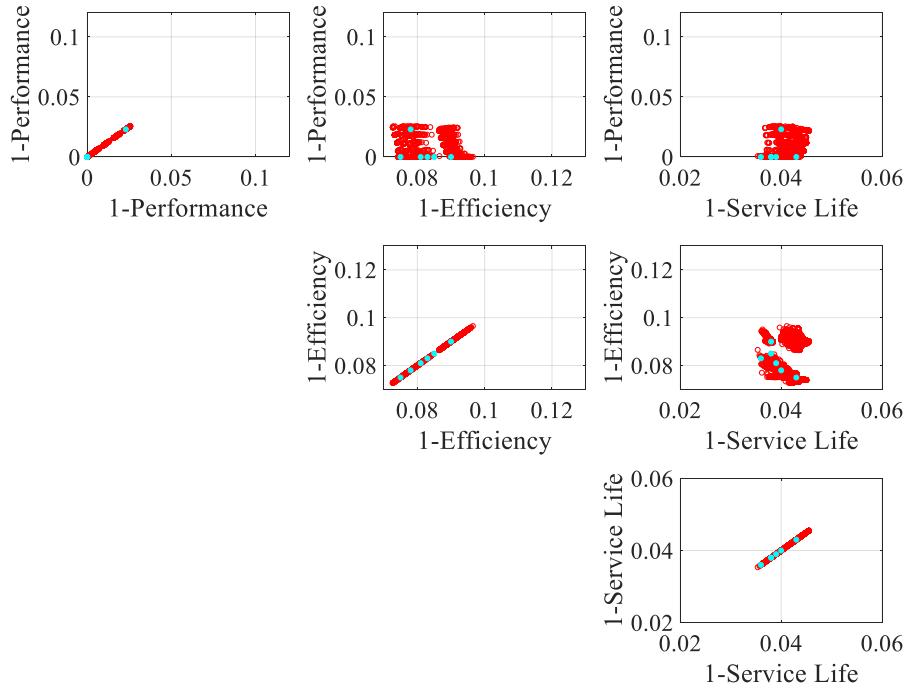
Figure 7.11: Results of the sequential PFCS (PFCS Pseq) potential analysis for the frequency regulation scenario emphasizing the results of the six exemplary simulation runs (cyan markers).

The results of the exemplary simulation runs indicate that, in contrast to the first example, less broad coverage of the target indicator space was achieved, as can be seen in Figure 7.11. The target indicator "performance" amounted to either 97.7 % or 100 %, efficiency ranged between 91.0 % and 92.5 %, and the target indicator "service life" was between 95.7 % and 96.4 %. Nevertheless, the individual effects of the design and use case variables on the target indicators can be examined since relevant information about the sensitivities resulted from the variation carried out. Figure 7.12 illustrates the analysis of the six exemplary simulation runs of the sequential PFCS (PFCS Pseq) in the case of the frequency regulation scenario.

The graphs on the left side show the power distribution over time, whereas the graphs on the right side present the respective SoCs over time. The set values of the design and use case variables for each simulation run can be found in Table 7.4.
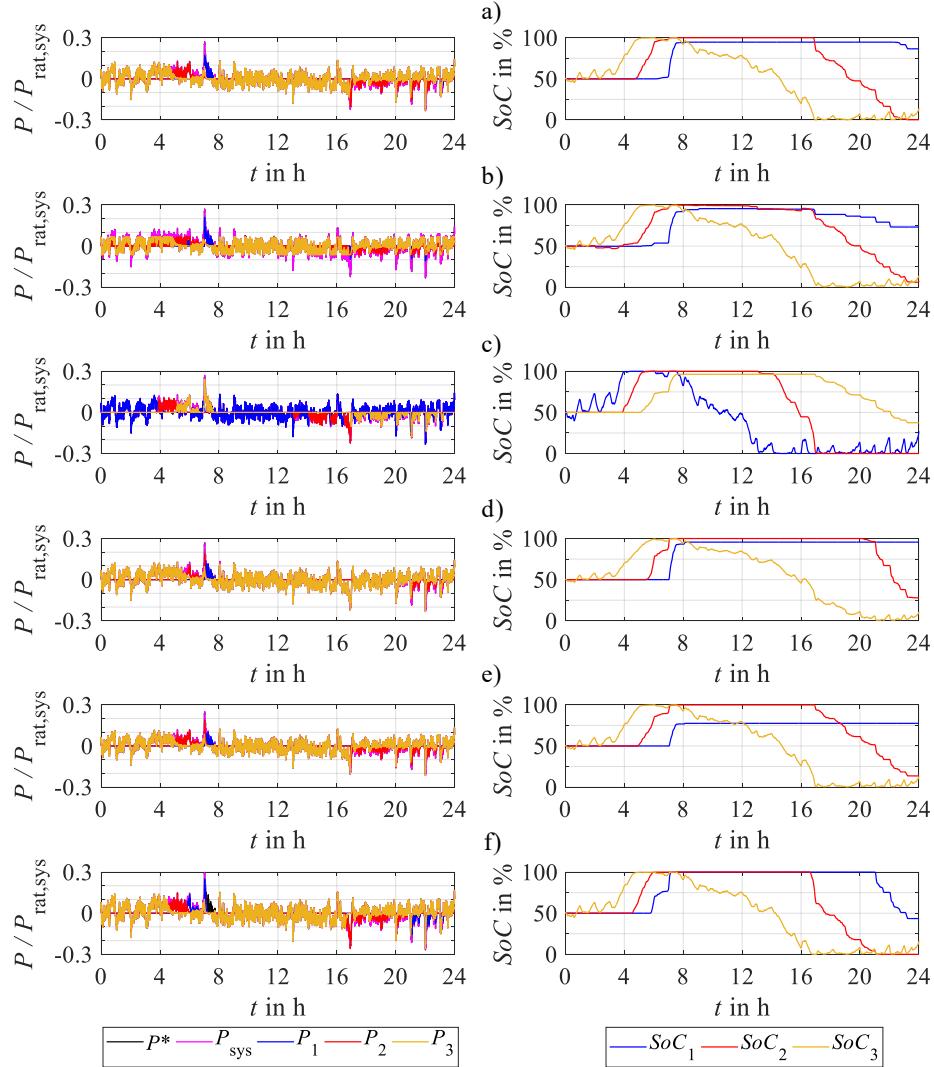
Figure 7.12: Analysis of six exemplary simulation runs of the sequential PFCS (PFCS Pseq) in the case of the frequency regulation scenario showing the power distribution (left side) and the SoCs (right side) over time. The set values of the design and use case variables for each simulation run can be found in Table 7.4.

Again, P^* (black line) displays the requested charge/discharge power and P_{sys} (pink line) shows the total charged/discharged power of the entire system, as previously described in Section 4.1. P_{sys} takes into account the efficiencies of

each DC/DC converter and the direction of the power flow. The individual charged/discharged power P_i (BESS 1: blue line, BESS 2: red line, BESS 3: yellow line) of a BESS adds up to P_{sys}. Moreover, the batteries' SoCs are denoted as SoC_i (battery 1: blue line, battery 2: red line, battery 3: yellow line).

The reference case (first simulation run) indicates that the set values of the design variables led to a power-limited sequential use with the BESSs deployed in descending order. As can be seen in graphs a), BESS 3 was charged/discharged as long as P_{max} was less or equal to 400 W ($P\,/\,P_{\mathrm{rat,sys}}\,=\,0.2\overline{6}$) or operating limits were not exceeded. In this case, the comparable low power requirements were fulfilled, and performance amounted to 100 %. The target indicator "efficiency" accounted for 91.9 % and the target indicator "service life" was 96.1 %.

In the case of the second exemplary simulation run b), the design variable P_{max} was changed to its minimum value of 100 W. No performance loss was observed here, and therefore the target indicator "performance" accounted for 100 %. However, graphs b) illustrate that the power distribution was different as the first two BESSs deployed were limited to a charge/discharge power[4] of 100 W. Through this power limitation, another BESS is forced to operate at low power, resulting in a decreased target indicator "efficiency" of about 91.5 % due to the part-load operation of both DC/DC converters. In contrast, the target indicator "service life" was slightly improved (96.2 %). The explanation for this is twofold. First, the calendar aging is improved marginally as the batteries did not remain at high SoCs for such a long time. Second, the deployed BESSs were operated at lower C-rates and with greater DoDs, resulting in a slightly lower capacity fade due to cycle aging. It can be concluded that this design variable influences the system. In this specific case, however, the effects on the target indicators were rather low. Nevertheless, interactions between the use case variables and this design variable might reinforce the influence considerably. With regard to efficiency, this design variable should not be selected too small in practice, as this would lead to a shorter operating time and an aggravated part-load operation of one BESS. Consequently, other BESSs would be forced to be on standby, resulting in additional energy losses.

For the third exemplary simulation run c), the design variable "sorting" was varied, causing deployment of the BESSs in ascending order with respect to their rated

---

[4]According to the algorithm of the sequential PFCS (PFCS Pseq), only the last BESS is not limited by P_{max}.

capacity. This resulted in significantly lower efficiency (91.0 %) and marginally higher service life (96.2 %). Although the power distribution was different from the reference case, the target indicator "performance" was not affected as the power requirements did not change, resulting in a performance of 100 %. As can be concluded from graphs c), the observed decrease in efficiency can mainly be attributed to the power losses of the smaller BESS in operation. Even if the losses through the DC/DC converters are quite similar to the reference case, the power losses of the smaller batteries are significantly higher due to an increased resistance. On the other hand, for the target indicator "service life," a slight increase was noticed. Although the capacity loss of battery 1 due to cycle aging was drastically enhanced (esp. higher C-rates and greater DoDs), the overall capacity loss due to calendar aging was somewhat less compared to the reference case. As a result, marginally higher service life was noticed here. The findings suggest that the sorting of the BESSs is particularly decisive for the target indicator "efficiency" in this case.

Regarding the fourth exemplary simulation run d), the use case variable "heterogeneity" was changed to its maximum value of 1.5. The increase of the heterogeneity, i.e., BESS 1 and BESS 2 were scaled down and BESS 3 was scaled up, resulting in considerable efficiency gain (92.5 %) and noticeably lower service life (95.7 %). Again, the target indicator "performance" was not biased as the power requirements were identical and therefore rather low. As far as the target indicator "efficiency" is concerned, the significant increase can be explained considering both the power losses of the batteries and the DC/DC converters. From graphs d), it can be seen that mainly BESS 3 was operated due to the set values of the design variables and the increase of this BESS. Thus, the losses of the battery were comparably low (low resistance), and the DC/DC converter was operated at higher powers, yielding higher efficiency. Concerning the target indicator "service life," however, a notable decrease was found. An explanation for this can be found in the plot on the right side and relates to the capacity fade due to calendar aging. Batteries 1 and 2 remain almost unused at high SoCs for a long time, resulting in a comparatively higher capacity loss. Battery 3 is also operated at a higher SoC, as can be seen when comparing graphs a) and d). Compared to the calendar aging, a rather minor yet enhanced capacity loss due to cycle aging was observed as a result of the two down-scaled BESSs. All these findings indicate that the system's heterogeneity is an essential factor in the case of the frequency regulation scenario as the power distribution is directly affected by this use case variable.

For the fifth and sixth exemplary simulation runs e) and f), only the use case variable "profile scaling factor" was varied to its minimum value of 25 %, displayed in graphs e), and to its maximum value of 31 %, illustrated in graphs f). A small profile scaling factor of about 25 % led to full performance and a slight decrease in efficiency (91.7 %) on the one hand, but an increase of the target indicator "service life" (96.4 %) on the other hand. In contrast, a higher profile scaling factor of about 31 % resulted in a considerably lower target indicator "performance" (97.7 %) and a marginally reduced target indicator "service life" (96.0 %), but also somewhat higher efficiency (92.2 %). Regarding the target indicator "performance," the power requirements were lower in the fifth simulation run, resulting in no performance loss. However, in the sixth simulation run f), the power requirements were higher, leading to a discrepancy between the desired power P^* and the system power P_{sys}, as can be seen in the plot on the left side. After roughly seven hours, the batteries were fully charged, yielding performance loss. As far as the target indicator "efficiency" is concerned, it correlates almost in direct proportion to the profile scaling factor in this case since mainly only one BESS is in operation at the same time, resulting in a higher or lower efficiency of the respective DC/DC converter, respectively. In terms of the target indicator "service life," the plots showing the SoC over time are very revealing in several ways. The variation of the profile scaling factor affects the time batteries remaining at high SoCs, leading to an enhanced capacity fade due to calendar aging and the energy throughput of each battery, resulting in an enhanced capacity fade due to cycle aging. However, a non-linear decrease of the target indicator "service life" can be observed for decreasing profile scaling factors. An explanation for this constitutes the combination of both aspects mentioned before. In this case, batteries remain at lower SoCs, and the energy throughput is concurrently lower for small profile scaling factors. From these findings, it can be concluded that the use case variable "profile scaling factor" is again decisive for a sustainable operation of the overall system.

To sum up the second example, the findings also improved the understanding of the causal relationships for the frequency regulation scenario and the sequential PFCS (PFCS Pseq). Influencing design or use case variables were identified and their individual impact was quantified.

In general, the impacts of the design and use case variables on the target indi-

cators were thoroughly examined based on two specific examples. Consequently, the third and the fourth subordinate research questions have been answered profoundly. In both cases, essential causal relationships have been revealed, analyzing the target indicator versus design or use case variables sensitivities in the time domain. This combination of findings supports the conceptual premise that sustainable operation depends on the resulting power distribution within the system. As the results have shown, the resulting power distribution, in turn, is mainly dependent on the design and use case variables. One important implication of this is the possibility to design and operate heterogeneous BESSs more beneficially using this work's methodological framework. The surrogate model-based sensitivity analysis especially helps to improve the understanding of the causal relationships using an interactive plot to experience the sensitivities by changing the values of the design and use case variables independently.

7.3 Evaluation based on the use case-specific potential analysis

Having discussed the potentials and sensitivities of heterogeneous BESSs utilizing different PFCSs in different scenarios, this section moves on to derive specific and general design rules for PFCSs. Therefore, the results of the use case-specific potential analysis are discussed, considering the fifth subordinate research question (design rules). This analysis expanded on using surrogate models for a fixed use case combination. Assigning fixed values to the use case variables limited the degrees of freedom to the two design variables. Dominated as well as non-dominated solutions (PO solutions) were then calculated on a surrogate model basis for all design variable parameters within the defined boundaries.

In the case of the peak shaving scenario and the parametric PFCS (PFCS SoAP), considerable differences between the minimum and maximum values of the target indicators were noticed, as previously presented in Figure 6.5. As extensively discussed in the previous sections, the resulting correlations can be attributed to the design variable $t_{\mathrm{pred,e}}$. Furthermore, it was observed that both dominated solutions and PO solutions lay close together. An explanation for this is that the impact of the design variable $t_{\mathrm{pred,p}}$ on the target indicators was somewhat marginally yet existent, resulting in only minor differences. The evaluation of the design space of the PO solutions revealed PO design variables across the entire

defined range for both design variables. Concerning the design variable $t_{\mathrm{pred,e}}$, most of the PO design variables were identified in the range between roughly $1200\,\mathrm{s}$ and $3600\,\mathrm{s}$. No clear trend could be observed for the other design variable $t_{\mathrm{pred,p}}$, strengthening the argument that both dominated solutions and PO solutions are hardly distinguishable. In sum, for the selected use case combination and PFCS, the following design rules can be derived:

- focus on target indicator "efficiency": $t_{\mathrm{pred,p}}$ arbitrary, $t_{\mathrm{pred,e}}$ low

- focus on target indicator "performance": $t_{\mathrm{pred,p}}$ arbitrary, $t_{\mathrm{pred,e}} < 1500\,\mathrm{s}$

- focus on target indicator "service life": $t_{\mathrm{pred,p}}$ arbitrary, $t_{\mathrm{pred,e}}$ high

Turning to the peak shaving scenario and the sequential PFCS (PFCS Pseq) illustrated in Figure 6.6, the two most important findings were that the solution space was disconnected and the influence of P_{max} on those two disconnected solution spaces was entirely different. The design variable "sorting" can explain the former. Depending on this design variable, either the smaller BESSs or the larger BESSs are forced to operate first, resulting in two distinct effects. Although there was almost no difference in terms of the target indicator "performance" here, operating the BESSs in an ascending order resulted in both lower efficiency and lower service life in most cases. In combination with an increasing design variable P_{max}, an ascending order caused lower efficiency due to increased battery losses, especially for the smaller ones. Simultaneously, the capacity loss due to calendar and cycle aging was enhanced as the smaller batteries remained unused at higher SoCs and were operated with greater DoDs. For a descending order and an increasing design variable P_{max}, contrary effects were observed. Thus, PO design variables were only identified for the BESSs operated in descending order and for values of P_{max} greater than roughly $300\,\mathrm{W}$, resulting mainly in an operation of the larger BESSs. This means there are no trade-offs between the target indicators. Altogether, for the selected use case combination and PFCS, the following design rules can be derived:

- focus on target indicator "efficiency": descending order, P_{max} high

- focus on target indicator "performance": descending order, P_{max} high

- focus on target indicator "service life": descending order, P_{max} high

The main finding in the case of the frequency regulation scenario and the parametric PFCS (PFCS SoAP) (see Figure 6.11) was that the correlation between the target indicator "efficiency" and the other two changed at some point. As the design variable $t_{\text{pred,e}}$ is the most influential one, this can be mainly attributed to the fact that this design variable directly affects the power distribution within the system. For this use case combination, values greater than roughly 700 s shifted the priority of the PFCS towards balancing the SoCs instead of fulfilling the power requirements. Consequently, the target indicator "performance" might be decreased, and the losses of the DC/DC converters may rise due to an increasing part-load operation. As explained in the previous sections, service life might be enhanced when balancing the SoCs. However, performance loss also means a lower energy throughput, which also positively affects the service life. Interestingly, PO design variables were found in the range between roughly 700 s and 3600 s concerning the design variable $t_{\text{pred,e}}$, yielding more balanced SoCs during operation. Again, no clear trend could be observed for the design variable $t_{\text{pred,p}}$. For the selected use case combination and PFCS, the following design rules can be derived:

- focus on target indicator "efficiency": $t_{\text{pred,p}}$ arbitrary, $t_{\text{pred,e}}$ roughly 700 s

- focus on target indicator "performance": $t_{\text{pred,p}}$ arbitrary, $t_{\text{pred,e}} < 700\,\text{s}$

- focus on target indicator "service life": $t_{\text{pred,p}}$ arbitrary, $t_{\text{pred,e}}$ high

In terms of the frequency regulation scenario and the sequential PFCS (PFCS Pseq), the results shown in Figure 6.12 indicated that the solution space was also disconnected due to the design variable "sorting". However, the influence of P_{max} on those two disconnected solution spaces was similar in this case. As a result of the use case combination, almost no difference was observed concerning the target indicator "performance," regardless of the design variable values. As far as the target indicators "efficiency" and "service life" are concerned, a decreasing value of P_{max} decreases efficiency but enhances service life at the same time. As explained in the previous sections, limiting the maximum power of a BESS forces another one to operate at low power as well. This results in a decreased target indicator "efficiency" due to the part-load operation of both DC/DC converters. On the other hand, when reducing the value of P_{max}, the calendar aging may be improved as the batteries do not remain at high SoCs for such a long time. Moreover, the deployed BESSs are operated at lower C-rates and with smaller DoDs, resulting in a slightly lower capacity fade due to cycle aging. Altogether, PO design variables were found across the entire defined range for the design variable P_{max}. In the

case of the design variable "sorting," PO design variables were noticed for an ascending order but mainly for descending order. Therefore, for the selected use case combination and PFCS, the following design rules can be derived:

- focus on target indicator "efficiency": descending order, P_{max} high

- focus on target indicator "performance": descending order, P_{max} high

- focus on target indicator "service life": ascending order, P_{max} low

In general, the results suggest that the individual analysis of the PFCSs supports identifying the overall potential of the applied PFCS for a fixed use case. Even though the methodological framework successfully identifies PO solutions, it suffers from the limitation that no global optimum for a specific use case can be found. As a remedy, one approach to classify the potential of a specific PFCS is to compare different PFCSs. For this reason, the results of the use case-specific potential analysis were combined for a particular use case, and a common Pareto-front was identified. Consequently, general design rules can be derived. Figure 7.13 shows the surrogate model-based results of the parametric and sequential PFCSs for the peak shaving scenario. As an exemplary use case combination, the set values for the heterogeneity and the profile scaling were set to 1.5 and 20 %, respectively. Pink markers emphasize PO solutions.
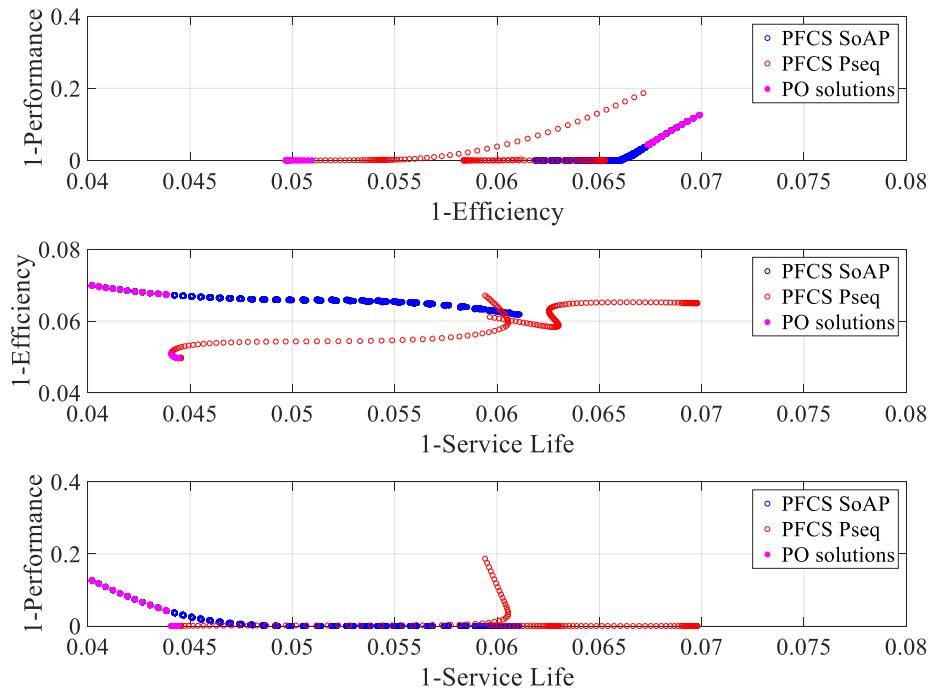
Figure 7.13: Pairwise target indicator trade-off analysis for the specified peak shaving use case emphasizing PO solutions concerning the parametric and sequential PFCSs. The heterogeneity was set to 1.5 and the profile scaling factor amounted to 20 %.

As can be seen in Figure 7.13, both PFCSs covered somewhat different areas of the target indicator space, suggesting that switching between the PFCSs might be favorable in some cases. The parametric PFCS (PFCS SoAP) yielded possibly higher service life but suffered from decreased efficiency. The sequential PFCS (PFCS Pseq), on the other hand, increased efficiency significantly, but the potential of the target indicator "service life" was strongly dependent on the design variable "sorting." Explanations for that have already been provided. Nevertheless, PO solutions for both PFCSs were found. The evaluation of the design space suggests that PO design variables can be identified in the range between roughly 2600 s and 3600 s concerning the design variable $t_{\text{pred,e}}$, i.e., in the case of the parametric PFCS (PFCS SoAP). For the sequential PFCS (PFCS Pseq), PO design variables can be found for values of P_{max} greater than approximately 300 W and in the case of a descending order of the deployed BESSs. However, PO solutions with full performance were only observed in the case of the sequential PFCS (PFCS Pseq). At least for this specific use case combination, these observations support the

hypothesis that a PFCS, where not necessarily all BESSs are in operation, achieves improvement. For reasons of clarity, a spatial representation of the results can be found in Figure C.25 in Appendix C. For the selected use case combination and both PFCSs combined, the following design rules can be derived:

- focus on target indicator "efficiency": descending order, P_{max} high

- focus on target indicator "performance": descending order, P_{max} high

- focus on target indicator "service life": $t_{\mathrm{pred,p}}$ arbitrary, $t_{\mathrm{pred,e}}$ high

With regard to the surrogate model-based results of the parametric and sequential PFCSs for the frequency regulation scenario, these are presented in Figure 7.14, emphasizing PO solutions (pink markers). As an exemplary use case combination, the values for the heterogeneity and profile scaling factor were set to 0.75 and 27 %, respectively.
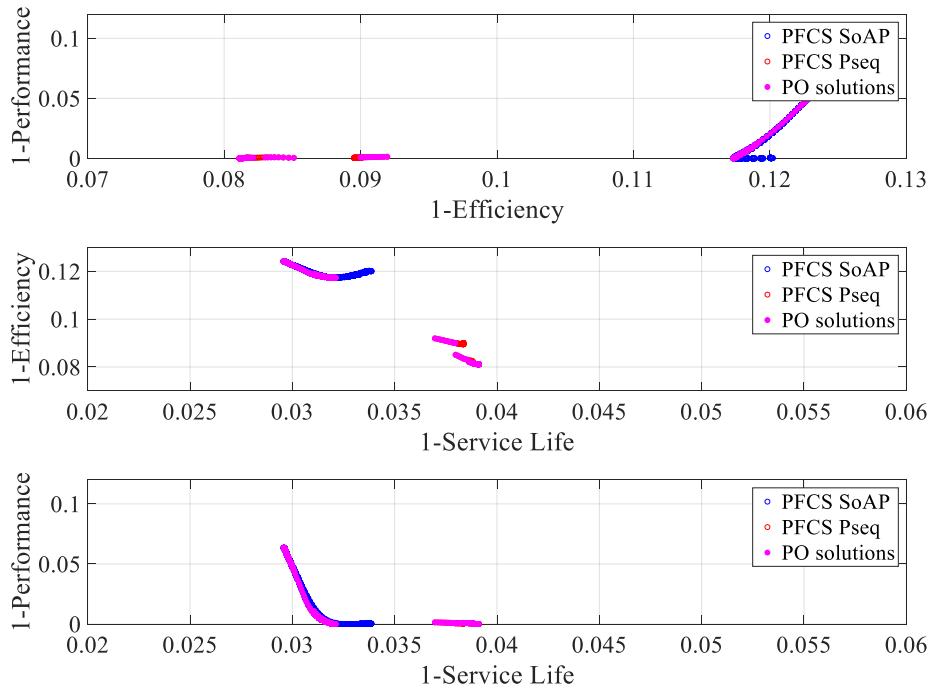
Figure 7.14: Pairwise target indicator trade-off analysis for the specified frequency regulation use case emphasizing PO solutions concerning the parametric and sequential PFCSs. The heterogeneity was set to 0.75 and the profile scaling factor amounted to 27 %.

According to the results shown in Figure 7.14, different areas of the target indicator space were covered using the parametric and sequential PFCSs for the frequency regulation scenario. The results indicate that PO solutions for both PFCSs were found, and switching between the PFCSs may again be advantageous in some cases. Similar to the peak shaving scenario, the parametric PFCS (PFCS SoAP) caused slightly higher service life than the sequential PFCS (PFCS Pseq) but suffered significantly decreased efficiency. In this case, the differences due to the design variable "sorting" were rather minimal. These relationships have already been discussed in the previous sections. Evaluating the design space reveals that PO design variables were found in the range between approximately 700 s and 3600 s regarding the design variable $t_{\mathrm{pred,e}}$, yielding more balanced SoCs during operation. In the case of the sequential PFCS (PFCS Pseq) and the BESSs deployed in ascending order, PO solutions were found for values of P_{max} lower than 130 W. In contrast, for BESSs deployed in descending order, PO solutions were observed across the whole defined range. Contrary to the peak shaving scenario,

PO solutions with full performance were observed for both PFCSs. The observations clearly indicate that possible trade-off decisions between the target indicators can be handled by, e.g., switching between different PFCSs. A spatial representation of the results can be found in Figure C.26 in Appendix C for reasons of clarity. For the selected use case combination and both PFCSs combined, the following design rules can be derived:

- focus on target indicator "efficiency": descending order, $P_{\max}$ high

- focus on target indicator "performance": descending order, $P_{\max}$ high

- focus on target indicator "service life": $t_{\mathrm{pred,p}}$ arbitrary, $t_{\mathrm{pred,e}}$ high

Although a PO-PFCS depends on the specific use case and the objectives of the system operator, economic, environmental, and social benefits can be accomplished by means of PO solutions. Except in the case of the peak shaving scenario and the sequential PFCS (PFCS Pseq), trade-offs between the target indicators have to be accepted. The findings of this section have important implications for designing a PO-PFCS for a specific use case combination. Therefore, three general design rules have been derived from these findings, supporting operators of such systems to enable sustainable and reliable operation.

First, clarification is required whether the target indicator "performance" will be treated as a constraint. In the case of this work, a performance of $100\,\%$ should be ensured as both exemplary applications usually require full performance. However, in the case of residential photovoltaic BESSs, for example, full performance is not mandatory. In general, this design rule may yield economic as well as social benefits. Under consideration of the target indicator "performance," profits can be enhanced by sizing BESSs appropriately, and a reliable and secure power supply might be guaranteed.

Second, often a trade-off between the target indicators "efficiency" and "service life" exists, requiring, therefore, a decision on a more equal or a more individual power-sharing, as the results showed. In this work, for example, a more individual power-sharing might be beneficial in the case of the peak shaving scenario,[5] especially in terms of efficiency. However, using the sequential PFCS (PFCS Pseq)

---

[5]Without consideration of the power requirements after the defined period of $24\,\mathrm{h}$.

might lead to a premature replacement of a single battery. In contrast, other PFCSs reduce the capacity loss, leading to longer service life and an environmental benefit. On the whole, decision-making here strongly depends on the applied use case and the overall objectives of the operator.

Third, the operator has to select preferable trade-offs between non-dominated target indicator trade-offs to match system requirements most favorably. However, decision-making based on the target indicator trade-offs requires quantitative knowledge about the significance of each target indicator. Therefore, as proposed in the literature, concepts of proper optimality might not be the favored solution in most cases. As a remedy, another approach is to analyze the differences between the target indicator values pragmatically. For example, the performance-service life trade-off, presented in Figure 7.14, indicates that a gain of about 0.3 percentage points in terms of the target indicator "service life" can only be achieved at the expense of a performance loss of about six percentage points. Consequently, it can be presumed that the positive effects on service life will not outweigh the severe negative effects on performance.

In general, the use case-specific potential analysis proved to be worthwhile. Non-dominated solutions (PO solutions) were identified on a surrogate model basis, yielding the overall potential of the applied PFCSs for a fixed use case. In this case, however, benefits are comparably low as no conclusions can be drawn about the potentials of the applied PFCS relative to other PFCSs. Further analysis has shown that comparing different PFCSs may increase the benefits gained by deriving a common Pareto-front. Consequently, design rules to support operators enabling sustainable and reliable operation of BESSs can be provided, answering the fifth subordinate research question.

7.4 Summary of the evaluation process

This chapter has provided a detailed look into the meanings of the results and has explained how these results relate to the research questions. In the first step, the methodological framework enabled the conduct of a comprehensive potential analysis of different PFCSs for heterogeneous BESSs by systematically performing simulations to identify the Pareto-front for each PFCS. Thus, the trade-offs between the target indicators were quantified accurately, considering the design and

use case variables. However, the findings suggest that only a potential analysis is not sufficient to adequately analyze the causal relationships between the inputs and the outputs of heterogeneous BESSs. Therefore, the surrogate model-based sensitivity analysis was conducted to learn about the target indicator versus design or use case variables sensitivities. A major benefit of this analysis is that individual influences can be analyzed separately, improving the understanding of the causal relationships considerably. Based on the findings, the conceptual premise that sustainable operation depends on the resulting power distribution within the system is supported. In the last step, non-dominated solutions (PO solutions) were identified on a surrogate model basis, yielding the overall potential of the applied PFCSs for a fixed use case. Analysis revealed that comparing different PFCSs may increase the benefits gained by deriving a common Pareto-front. As a result, design rules to support operators enabling sustainable and reliable operation of BESSs can be provided. This work, therefore, indicates that the benefits gained from the methodological framework may address BESS-operator needs across a wide range of different use cases. Most notably, this is the first work to the best of the authors' knowledge to provide a methodological framework to analyze, quantify, and classify PFCSs in heterogeneous BESSs systematically.

8 Conclusion and future perspectives

This research addressed the question of how the potentials and sensitivities of power flow control strategies for heterogeneous battery energy storage systems can be quantified. Based on a quantitative analysis of the causal relationships between the inputs and the outputs of heterogeneous battery energy storage systems, it can be concluded that the applied power flow control strategy and the use case are essential factors to consider when designing and operating heterogeneous battery energy storage systems. The results indicate that both factors influence the resulting power distribution within the system, which is, in turn, a decisive point for sustainable operation of heterogeneous battery energy storage systems. This work has shown that the developed methodological framework is able to quantify the potentials and sensitivities of power flow control strategies for heterogeneous battery energy storage systems effectively and efficiently. It further contributes to the analysis of multi-objective optimization problems and specifically power flow control strategies for battery energy storage system applications. In the following, a reflective summary of the main points of this work is given, limitations of the work are presented, and future perspectives are outlined. Note that some limitations and future perspectives are based on my published work [14].

Summary

In Chapter 1, an introductory presentation of battery energy storage systems and their operating strategies was provided. This topic was motivated by the idea of operating battery energy storage systems sustainably, yielding economic, environmental, and social benefits. Enabling the sustainable operation of such systems requires knowledge about causal relationships. However, these relationships are not immediately apparent as no simple logical procedures to operate battery energy storage systems sustainably exist. According to the *Cynefin for engineers framework* [9], this assigns the given problem to a complex problem, requesting a

trade-off comparison among potential solutions to select an operating strategy for the sustainable operation of battery energy storage systems. The question thus emerged as to how the inputs can be influenced systematically, effects become perceptible and quantifiable, and the resulting power distribution within battery energy storage systems affects a sustainable operation.

After examining the fundamentals of battery energy storage systems, appropriate use cases and power flow control strategies for battery energy storage system applications were identified and developed in Chapter 2. Furthermore, suitable target indicators representing the three dimensions of sustainability (economic, environmental, and social) were defined. This approach was expected to provide a fundamental basis to quantify the causal relationships by influencing the battery energy storage system systematically through different power flow control strategies and use cases. However, achieving sustainable operation requires solving a multi-objective optimization problem as the different target indicators should be optimized simultaneously. Lacking an analytically closed form of the functional correlation between the inputs and the outputs, the multi-objective optimization problem is further characterized as a multi-objective optimization on a black-box function problem. Therefore, the fundamentals of multi-objective (black-box) optimization and state-of-the-art approaches to solve such problems were presented in Chapter 3. The Hyper Space Exploration methodology as proposed by Palm and Holzmann [159] was identified as a useful tool to solve the multi-objective black-box optimization problem.

Referring to the research question, an appropriate methodological framework that includes the Hyper Space Exploration methodology and a simulation model of a battery energy storage system was required to quantify the potentials and sensitivities of power flow control strategies for heterogeneous battery energy storage systems. Thus, the battery energy storage system simulation model, including the generic aging model, the Hyper Space Exploration process flow, and the battery energy storage system-adapted Hyper Space Exploration toolchain were described in Chapters 4 and 5. The entire framework was expected to solve the multi-objective black-box optimization problem and profoundly analyze the causal relationships. However, two crucial points arise using the presented framework. First, when applying the Hyper Space Exploration methodology, it is challenging to ensure validity of the results due to the extensive parameter variation. Therefore, the

transferability of each submodule of the battery energy storage system simulation model (battery, DC/DC converter, and control scheme) was examined for varying input variables, confirming its validity. Second, proper methods for evaluating and visualizing the results were required for the unambiguous interpretation of the results. Thus, the methods either provided insights into existing target indicator trade-offs to reveal the potentials of power flow control strategies, analyzed the causal relationships between the inputs and the outputs for different power flow control strategies, or identified Pareto-optimal solutions for a fixed use case to derive design rules. Moreover, each method was closely related to subordinate research questions, answering them thoroughly.

The methodological framework thus provided the necessary foundation for comprehensive analysis. However, understanding the causal relationships in complex battery energy storage systems to enable sustainable operation required analyzing different power flow control strategies systematically. Therefore, in Chapter 6, the results of two power flow control strategies were presented for two distinct use cases. Following the structure of the methodological framework and its methods for evaluation, a threefold analysis for each power flow control strategy was carried out to answer the research questions profoundly. The results suggested that the methodological framework offered a generic process to adequately solve the multi-objective black-box optimization problem. The two most striking aspects that emerged from the simulation studies were that, first, the potentials of the power flow control strategies and, second, the correlations between the target indicators and the input variables were precisely quantified. Moreover, the results obtained provided essential insights into the causal relationships between the inputs and the outputs in complex heterogeneous battery energy storage systems. Consequently, a sustainable operation of battery energy storage systems was enabled, strengthening the initial idea.

The discussion in Chapter 7 revealed that the methodological framework quantified the potentials and sensitivities of different power flow control strategies for heterogeneous battery energy storage systems effectively and efficiently, answering the research questions profoundly. First, the methodological framework enabled a comprehensive potential analysis to quantify the existing target indicator trade-offs accurately. Second, the surrogate model-based sensitivity analysis improved the understanding of the causal relationships considerably. Third, Pareto-optimal so-

lutions were identified on a surrogate model basis, deriving design rules to support operators enabling sustainable and reliable operation of battery energy storage systems. Thus, these findings indicated that both the fundamental basis, e.g., suitable target indicators, and the methods for evaluating and visualizing the results are sufficient to gain the required knowledge about causal relationships to operate heterogeneous battery energy storage systems sustainably. Moreover, the conceptual premise that sustainable operation depends on the resulting power distribution within the system was supported. The benefits gained from the methodological framework may address battery energy storage system operator needs across a wide range of different use cases.

Limitations and future perspectives

Nevertheless, this work is subject to certain limitations which should be addressed in future works. During the course of this work, three noticeable limitations have been identified:

First, each multi-objective optimization process necessitates decision-making at some point. However, in this work, decision-making on a power-sharing level was set aside to focus on the implementation of the methodological framework, proper methods for evaluation and visualization, and analysis of the potentials and sensitivities of power flow control strategies. Especially in practice or in the case of application-oriented case studies, it is indispensable as battery energy storage system operator's needs have to be addressed. Referring back to the survey of Marler and Arora [137], three categories are known to model a decision-maker's preferences: *a priori*, *a posteriori*, and *no articulation of preferences*. This work's methodological framework basically entails the *a posteriori* decision-making method, as this work focuses on the analysis of all solutions identified in the multi-objective optimization process. However, this requires a) adaptive sampling approaches with an enhanced search efficiency to effectively and efficiently identify Pareto-optimal solutions and b) selecting one Pareto-optimal solution from a set of mathematically equivalent Pareto-optimal solutions after the optimization process. While this work successfully identifies Pareto-optimal solutions among various power flow control strategies, it did not offer an explicit approach for the required *a posteriori* decision-making, i.e., selecting one Pareto-optimal solution to meet the operator's needs and preferences. Further research should be carried out to establish an (automated) approach for *a posteriori* articulation of preferences relative to the ideas of the third general design rule presented in Section 7.3.

Second, this work is limited by the lack of information on a global optimum for a specific use case. The chosen power flow control strategies limit the solutions in the target space, i.e., better solutions might exist with other power flow control strategies. It would at least be possible to find a near-global optimum if all target indicators were combined into a single one, i.e., if the total cost of ownership, or heuristics, such as particle swarm optimization or genetic algorithms, were applied. However, this approach usually entails a substantial computational expense, requires further assumptions, and most importantly, provides only one near-global optimal solution. Even though heuristics may provide a near-global optimal solution, no clear statement can be made about how good the identified solution is [188], as the actual global optimum is unknown and cannot be proved. Most importantly, it does not allow for the consideration of the shape of the Pareto-front, which is an important aspect for both analyzing the causal relationships and enabling sustainable operation of battery energy storage systems. Thus, the approach of comparing different power flow control strategies was used in this work. Notwithstanding the lack of globally optimal solutions, this work offers valuable insights into the causal relationships between the inputs and the outputs of heterogeneous battery energy storage systems. Further research should be undertaken to explore how to a) implement heuristics in the methodological framework and simultaneously consider the shape of the Pareto-front and b) develop a global optimal power flow control strategy as a reference. Reasonable approaches to tackle, for example, the latter issue could be to deploy dynamic programming methods or machine learning techniques, such as reinforcement learning.

Third, this work focuses, among other things, on the successful implementation of the methodological framework for heterogeneous battery energy storage systems. However, most battery energy storage systems are included in higher-level systems, resulting in new challenges to be addressed. Since the simulation study, i.e., the battery energy storage system simulation model, was limited to heterogeneous battery energy storage systems for reasons of expediency, it is unknown how the presented methodological framework and, therefore, the analysis of power flow control strategies applies to other systems. Microgrids, for example, have a similar basic architecture compared with the heterogeneous battery energy storage system presented in this work. In addition to storage systems, renewable energy sources and loads are interconnected via a common (DC) bus, forming a small (islanded) distribution network. Operating strategies considering

intermittent power generation and irregular consumption in microgrids could be implemented into the methodological framework, targeting the challenge of a balanced system. Moreover, multi-use applications such as simultaneously equalizing power fluctuations and charging electric vehicles are gaining popularity but require thorough analysis to achieving sustainable operation of such systems. Although the current work is based on heterogeneous battery energy storage systems, the methodological framework is basically capable of adjustment to other systems. Even if no power distribution is possible, free parameters (design variables) could be derived from, e.g., the scenario to influence the charging and discharging behavior of the system. Therefore, a further study could assess the potentials and sensitivities of power flow control strategies for microgrids or other higher-level systems, enabling sustainable operation of those. This requires an extension of the validated battery energy storage system model by additional system components, such as renewable energy sources. Furthermore, application-oriented power flow control strategies and use cases should be developed and implemented into the methodological framework to address the challenges adequately.

References

[1] W. F. Schulz, ed. *Lexikon Nachhaltiges Wirtschaften.* Lehr- und Handbücher zur ökologischen Unternehmensführung und Umweltökonomie. Munich and Vienna: Oldenbourg, 2001. ISBN: 978-3-486-24523-3.

[2] C. Andrey, P. Barberi, L. Lacombe, L. Van Nuffel, F. Gérard, J. Gorenstein Dedecca, K. Rademakers, Y. El Idrissi, M. Crenes, and European Commission. Directorate General for Energy. *Study on energy storage - Contribution to the security of the electricity supply in Europe.* Tech. rep. Luxembourg, 2020. DOI: 10.2833/077257.

[3] IRENA. *Innovation landscape for a renewable-powered future: Solutions to integrate variable renewables.* Tech. rep. ISBN: 978-92-9260-111-9. Abu Dhabi, 2019.

[4] H. Hesse, M. Schimpe, D. Kucevic, and A. Jossen. "Lithium-Ion Battery Storage for the Grid - A Review of Stationary Battery Storage System Design Tailored for Applications in Modern Power Grids". *Energies* 10.12 (Dec. 2017). DOI: 10.3390/en10122107.

[5] T. Morstyn, B. Hredzak, and V. G. Agelidis. "Control Strategies for Microgrids With Distributed Energy Storage Systems: An Overview". *IEEE Transactions on Smart Grid* 9.4 (2018), p. 15. DOI: 10.1109/TSG.2016.2637958.

[6] A. Khodadoost Arani, G. B. Gharehpetian, and M. Abedi. "Review on Energy Storage Systems Control Methods in Microgrids". *International Journal of Electrical Power & Energy Systems* 107 (May 2019), pp. 745–757. DOI: 10.1016/j.ijepes.2018.12.040.

[7] C. Goebel, H. Hesse, M. Schimpe, A. Jossen, and H.-A. Jacobsen. "Model-Based Dispatch Strategies for Lithium-Ion Battery Energy Storage Applied to Pay-as-Bid Markets for Secondary Reserve". *IEEE Transactions on Power Systems* 32.4 (July 2017), pp. 2724–2734. DOI: 10.1109/TPWRS.2016.2626392.

[8]   X. Li and S. Wang. "A review on energy management, operation control and application methods for grid battery energy storage systems". *CSEE Journal of Power and Energy Systems* (June 2019). DOI: 10.17775/CSEEJPES.2019.00160.

[9]   J. Vollmar, M. Gepp, H. Palm, and A. Cala. "Engineering framework for the future: Cynefin for engineers". *2017 IEEE International Systems Engineering Symposium (ISSE)*. Vienna, Austria: IEEE, Oct. 2017, pp. 1–5. DOI: 10.1109/SysEng.2017.8088286.

[10]   D. J. Snowden and M. E. Boone. "A leader's framework for decision making". *Harvard Business Review* 85(11) (Nov. 2007), pp. 68–76.

[11]   M. Mühlbauer, O. Bohlen, and M. A. Danzer. "Analysis of power flow control strategies in heterogeneous battery energy storage systems". *Journal of Energy Storage* 30 (Aug. 2020), p. 101415. DOI: 10.1016/j.est.2020.101415.

[12]   M. Muehlbauer, S. Klier, H. Palm, O. Bohlen, and M. A. Danzer. "A Novel Power Flow Control Strategy for Heterogeneous Battery Energy Storage Systems Based on Prognostic Algorithms for Batteries". *22nd European Conference on Power Electronics and Applications (EPE '20 ECCE Europe)*. Lyon, 2020. DOI: 10.23919/EPE20ECCEEurope43536.2020.9215818.

[13]   M. Mühlbauer and O. Bohlen. "Verfahren zum Bestimmen eines Leistungsanteils, Betriebsverfahren, Steuereinheit, Energiespeicheranordnung und Stromnetz". Pat. DE 10 2019 212 762 A1. Mar. 2021.

[14]   M. Mühlbauer, F. Rang, H. Palm, O. Bohlen, and M. A. Danzer. "Pareto-optimal power flow control in heterogeneous battery energy storage systems". en. *Journal of Energy Storage* 48 (Apr. 2022), p. 103803. DOI: 10.1016/j.est.2021.103803.

[15]   M. Anderson and D. Carr. "Battery energy storage technologies". *Proceedings of the IEEE* 81.3 (Mar. 1993), pp. 475–479. DOI: 10.1109/5.241482.

[16]   A. Joseph and M. Shahidehpour. "Battery storage systems in electric power systems". *2006 IEEE Power Engineering Society General Meeting*. Montreal, Canada: IEEE, 2006, 8 pp. DOI: 10.1109/PES.2006.1709235.

[17]   K. Divya and J. Østergaard. "Battery energy storage technology for power systems - An overview". *Electric Power Systems Research* 79.4 (Apr. 2009), pp. 511–520. DOI: 10.1016/j.epsr.2008.09.017.

[18] M. Stecca, L. Ramirez Elizondo, T. Batista Soeiro, P. Bauer, and P. Palensky. "A Comprehensive Review of the Integration of Battery Energy Storage Systems into Distribution Networks". *IEEE Open Journal of the Industrial Electronics Society* (2020), pp. 46–65. DOI: 10.1109/OJIES.2020.2981832.

[19] M. Müller, L. Viernstein, C. N. Truong, A. Eiting, H. C. Hesse, R. Witzmann, and A. Jossen. "Evaluation of grid-level adaptability for stationary battery energy storage system applications in Europe". *Journal of Energy Storage* 9 (Feb. 2017), pp. 1–11. DOI: 10.1016/j.est.2016.11.005.

[20] M. Schimpe, N. Becker, T. Lahlou, H. C. Hesse, H.-G. Herzog, and A. Jossen. "Energy efficiency evaluation of grid connection scenarios for stationary battery energy storage systems". *Energy Procedia* 155 (Nov. 2018), pp. 77–101. DOI: 10.1016/j.egypro.2018.11.065.

[21] G. Wang, G. Konstantinou, C. D. Townsend, J. Pou, S. Vazquez, G. D. Demetriades, and V. G. Agelidis. "A Review of Power Electronics for Grid Connection of Utility-Scale Battery Energy Storage Systems". *IEEE Transactions on Sustainable Energy* 7.4 (Oct. 2016), pp. 1778–1790. DOI: 10.1109/TSTE.2016.2586941.

[22] V. Fernão Pires, E. Romero-Cadaval, D. Vinnikov, I. Roasto, and J. Martins. "Power converter interfaces for electrochemical energy storage systems – A review". *Energy Conversion and Management* 86 (Oct. 2014), pp. 453–475. DOI: 10.1016/j.enconman.2014.05.003.

[23] M. Bauer. "System Design and Power Flow of Stationary Energy Storage Systems". PhD thesis. ETH Zurich, 2019. DOI: 10.3929/ETHZ-B-000374736.

[24] D. Strickland and N. Mukherjee. "Second Life Battery Energy Storage Systems: Converter Topology and Redundancy Selection". *7th IET International Conference on Power Electronics, Machines and Drives (PEMD 2014)*. Manchester, UK: Institution of Engineering and Technology, 2014. DOI: 10.1049/cp.2014.0256.

[25] E. Chatzinikolaou and D. J. Rogers. "A Comparison of Grid-Connected Battery Energy Storage System Designs". *IEEE Transactions on Power Electronics* 32.9 (Sept. 2017), pp. 6913–6923. DOI: 10.1109/TPEL.2016.2629020.

[26] M. Bauer, J. Wiesmeier, and J. Lygeros. "A comparison of system architectures for high-voltage electric vehicle batteries in stationary applications". *Journal of Energy Storage* 19 (Oct. 2018), pp. 15–27. DOI: 10.1016/j.est.2018.06.007.

[27] E. Martinez-Laserna, I. Gandiaga, E. Sarasketa-Zabala, J. Badeda, D.-I. Stroe, M. Swierczynski, and A. Goikoetxea. "Battery second life: Hype, hope or reality? A critical review of the state of the art". *Renewable and Sustainable Energy Reviews* 93 (Oct. 2018), pp. 701–718. DOI: 10.1016/j.rser.2018.04.035.

[28] B. K. Bose. "Power Electronics, Smart Grid, and Renewable Energy Systems". *Proceedings of the IEEE* 105.11 (Nov. 2017), pp. 2011–2018. DOI: 10.1109/JPROC.2017.2745621.

[29] I. Batarseh and A. Harb. *Power Electronics: Circuit Analysis and Design.* 2nd ed. 2018. Cham: Springer International Publishing : Imprint: Springer, 2018. ISBN: 978-3-319-68366-9.

[30] P. T. Krein. *Elements of power electronics.* Second edition. New York: Oxford University Press, 2015. ISBN: 978-0-19-938841-7.

[31] R. W. Erickson and D. Maksimović. *Fundamentals of power electronics.* Second edition. New York, NY: Springer Science+Business Media, LLC, 2001. ISBN: 978-0-306-48048-5.

[32] S. Vazquez, S. M. Lukic, E. Galvan, L. G. Franquelo, and J. M. Carrasco. "Energy Storage Systems for Transport and Grid Applications". *IEEE Transactions on Industrial Electronics* 57.12 (Dec. 2010), pp. 3881–3895. DOI: 10.1109/TIE.2010.2076414.

[33] L. Maharjan, S. Inoue, and H. Akagi. "A Transformerless Energy Storage System Based on a Cascade Multilevel PWM Converter With Star Configuration". *IEEE Transactions on Industry Applications* 44.5 (Sept. 2008), pp. 1621–1630. DOI: 10.1109/TIA.2008.2002180.

[34] H. Akagi. "Classification, Terminology, and Application of the Modular Multilevel Cascade Converter (MMCC)". *IEEE Transactions on Power Electronics* 26.11 (Nov. 2011), pp. 3119–3130. DOI: 10.1109/TPEL.2011.2143431.

[35] S. Waffler and J. W. Kolar. "A Novel Low-Loss Modulation Strategy for High-Power Bidirectional Buck + Boost Converters". *IEEE Transactions on Power Electronics* 24.6 (June 2009), pp. 1589–1599. DOI: 10.1109/TPEL.2009.2015881.

[36] S. Inoue and H. Akagi. "A Bidirectional DC-DC Converter for an Energy Storage System With Galvanic Isolation". *IEEE Transactions on Power Electronics* 22.6 (Nov. 2007), pp. 2299–2306. DOI: 10.1109/TPEL.2007.909248.

[37] S. A. Gorji, H. G. Sahebi, M. Ektesabi, and A. B. Rad. "Topologies and Control Schemes of Bidirectional DC-DC Power Converters: An Overview". *IEEE Access* 7 (2019), pp. 117997–118019. DOI: 10.1109/ACCESS.2019.2937239.

[38] M. S. Whittingham. "Electrointercalation in transition-metal disulphides". *Journal of the Chemical Society, Chemical Communications* 9 (1974), p. 328. DOI: 10.1039/c39740000328.

[39] M. S. Whittingham. "Electrical Energy Storage and Intercalation Chemistry". *Science* 192.4244 (June 1976), pp. 1126–1127. DOI: 10.1126/science.192.4244.1126.

[40] K. Mizushima, P. Jones, P. Wiseman, and J. Goodenough. "LixCoO2 (0<x<-1): A new cathode material for batteries of high energy density". *Materials Research Bulletin* 15.6 (June 1980), pp. 783–789. DOI: 10.1016/0025-5408(80)90012-4.

[41] A. Yoshino, K. Sanechikat, and T. Nakajima. "Secondary battery". Pat. 4668595. 1985.

[42] G. L. Plett. *Battery management systems: battery modeling. Volume 1.* Boston : London: Artech House, 2015. ISBN: 978-1-63081-023-8.

[43] C. R. Birkl, M. R. Roberts, E. McTurk, P. G. Bruce, and D. A. Howey. "Degradation diagnostics for lithium ion cells". *Journal of Power Sources* 341 (Feb. 2017), pp. 373–386. DOI: 10.1016/j.jpowsour.2016.12.011.

[44] J. Lu, Z. Chen, F. Pan, Y. Cui, and K. Amine. "High-Performance Anode Materials for Rechargeable Lithium-Ion Batteries". *Electrochemical Energy Reviews* 1.1 (Mar. 2018), pp. 35–53. DOI: 10.1007/s41918-018-0001-4.

[45]   N. Nitta, F. Wu, J. T. Lee, and G. Yushin. "Li-ion battery materials: present and future". *Materials Today* 18.5 (June 2015), pp. 252–264. DOI: `10.1016/j.mattod.2014.10.040`.

[46]   J. Kalhoff, G. G. Eshetu, D. Bresser, and S. Passerini. "Safer Electrolytes for Lithium-Ion Batteries: State of the Art and Perspectives". *ChemSusChem* 8.13 (July 2015), pp. 2154–2175. DOI: `10.1002/cssc.201500284`.

[47]   V. Deimede and C. Elmasides. "Separators for Lithium-Ion Batteries: A Review on the Production Processes and Recent Developments". *Energy Technology* 3.5 (May 2015), pp. 453–468. DOI: `10.1002/ente.201402215`.

[48]   J. Vetter, P. Novak, M. Wagner, C. Veit, K.-C. Moeller, J. Besenhard, M. Winter, M. Wohlfahrt-Mehrens, C. Vogler, and A. Hammouche. "Ageing mechanisms in lithium-ion batteries". *Journal of Power Sources* 147.1-2 (Sept. 2005), pp. 269–281. DOI: `10.1016/j.jpowsour.2005.01.006`.

[49]   M. Broussely, P. Biensan, F. Bonhomme, P. Blanchard, S. Herreyre, K. Nechev, and R. Staniewicz. "Main aging mechanisms in Li ion batteries". *Journal of Power Sources* 146.1-2 (Aug. 2005), pp. 90–96. DOI: `10.1016/j.jpowsour.2005.03.172`.

[50]   M. Dubarry, B. Y. Liaw, M.-S. Chen, S.-S. Chyan, K.-C. Han, W.-T. Sie, and S.-H. Wu. "Identifying battery aging mechanisms in large format Li ion cells". *Journal of Power Sources* 196.7 (Apr. 2011), pp. 3420–3425. DOI: `10.1016/j.jpowsour.2010.07.029`.

[51]   A. Barré, B. Deguilhem, S. Grolleau, M. Gérard, F. Suard, and D. Riu. "A review on lithium-ion battery ageing mechanisms and estimations for automotive applications". *Journal of Power Sources* 241 (Nov. 2013), pp. 680–689. DOI: `10.1016/j.jpowsour.2013.05.040`.

[52]   M. Woody, M. Arbabzadeh, G. M. Lewis, G. A. Keoleian, and A. Stefanopoulou. "Strategies to limit degradation and maximize Li-ion battery service lifetime - Critical review and guidance for stakeholders". *Journal of Energy Storage* 28 (Apr. 2020), p. 101231. DOI: `10.1016/j.est.2020.101231`.

[53]   M. Dubarry, N. Qin, and P. Brooker. "Calendar aging of commercial Li-ion cells of different chemistries - A review". *Current Opinion in Electrochemistry* 9 (June 2018), pp. 106–113. DOI: `10.1016/j.coelec.2018.05.023`.

[54] T. Gewald, A. Candussio, L. Wildfeuer, D. Lehmkuhl, A. Hahn, and M. Lienkamp. "Accelerated Aging Characterization of Lithium-ion Cells: Using Sensitivity Analysis to Identify the Stress Factors Relevant to Cyclic Aging". *Batteries* 6.1 (Jan. 2020), p. 6. DOI: 10.3390/batteries6010006.

[55] R. Rao, S. Vrudhula, and D. Rakhmatov. "Battery modeling for energy-aware system design". *Computer* 36.12 (Dec. 2003), pp. 77–87. DOI: 10.1109/MC.2003.1250886.

[56] T. M. Bandhauer, S. Garimella, and T. F. Fuller. "A Critical Review of Thermal Issues in Lithium-Ion Batteries". *Journal of The Electrochemical Society* 158.3 (2011), R1. DOI: 10.1149/1.3515880.

[57] J. P. Schmidt. "Verfahren zur Charakterisierung und Modellierung von Lithium-Ionen Zellen". PhD thesis. Karlsruhe: KIT Scientific Publishing, 2013.

[58] U. Krewer, F. Röder, E. Harinath, R. D. Braatz, B. Bedürftig, and R. Findeisen. "Review-Dynamic Models of Li-Ion Batteries for Diagnosis and Operation: A Review and Perspective". *Journal of The Electrochemical Society* 165.16 (2018), A3656–A3673. DOI: 10.1149/2.1061814jes.

[59] K. Uddin, S. Perera, W. Widanage, L. Somerville, and J. Marco. "Characterising Lithium-Ion Battery Degradation through the Identification and Tracking of Electrochemical Battery Model Parameters". *Batteries* 2.2 (Apr. 2016), p. 13. DOI: 10.3390/batteries2020013.

[60] M. Doyle, T. F. Fuller, and J. Newman. "Modeling of Galvanostatic Charge and Discharge of the Lithium/Polymer/Insertion Cell". *Journal of The Electrochemical Society* 140.6 (June 1993), pp. 1526–1533. DOI: 10.1149/1.2221597.

[61] A. Jokar, B. Rajabloo, M. Désilets, and M. Lacroix. "Review of simplified Pseudo-two-Dimensional models of lithium-ion batteries". *Journal of Power Sources* 327 (Sept. 2016), pp. 44–55. DOI: 10.1016/j.jpowsour.2016.07.036.

[62] J. M. Reniers, G. Mulder, and D. A. Howey. "Unlocking extra value from grid batteries using advanced models". *Journal of Power Sources* 487 (Mar. 2021). DOI: 10.1016/j.jpowsour.2020.229355.

[63] M. Ecker, T. K. D. Tran, P. Dechent, S. Käbitz, A. Warnecke, and D. U. Sauer. "Parameterization of a Physico-Chemical Model of a Lithium-Ion Battery: I. Determination of Parameters". *Journal of The Electrochemical Society* 162.9 (2015), A1836–A1848. DOI: 10.1149/2.0551509jes.

[64] M. Ecker, S. Käbitz, I. Laresgoiti, and D. U. Sauer. "Parameterization of a Physico-Chemical Model of a Lithium-Ion Battery: II. Model Validation". *Journal of The Electrochemical Society* 162.9 (2015), A1849–A1857. DOI: 10.1149/2.0541509jes.

[65] A. Eddahech, O. Briat, H. Henry, J.-Y. Delétage, E. Woirgard, and J.-M. Vinassa. "Ageing monitoring of lithium-ion cell during power cycling tests". *Microelectronics Reliability* 51.9-11 (Sept. 2011), pp. 1968–1971. DOI: 10.1016/j.microrel.2011.07.013.

[66] J. Schmitt, A. Maheshwari, M. Heck, S. Lux, and M. Vetter. "Impedance change and capacity fade of lithium nickel manganese cobalt oxide-based batteries during calendar aging". *Journal of Power Sources* 353 (June 2017), pp. 183–194. DOI: 10.1016/j.jpowsour.2017.03.090.

[67] S. Käbitz, J. B. Gerschler, M. Ecker, Y. Yurdagel, B. Emmermacher, D. André, T. Mitsch, and D. U. Sauer. "Cycle and calendar life study of a graphite | LiNi1/3Mn1/3Co1/3O2 Li-ion high energy system. Part A: Full cell characterization". *Journal of Power Sources* 239 (Oct. 2013), pp. 572–583. DOI: 10.1016/j.jpowsour.2013.03.045.

[68] M. Ecker, N. Nieto, S. Käbitz, J. Schmalstieg, H. Blanke, A. Warnecke, and D. U. Sauer. "Calendar and cycle life study of Li(NiMnCo)O2-based 18650 lithium-ion batteries". *Journal of Power Sources* 248 (Feb. 2014), pp. 839–851. DOI: 10.1016/j.jpowsour.2013.09.143.

[69] J. Schmalstieg, S. Käbitz, M. Ecker, and D. U. Sauer. "A holistic aging model for Li(NiMnCo)O2 based 18650 lithium-ion batteries". *Journal of Power Sources* 257 (July 2014), pp. 325–334. DOI: 10.1016/j.jpowsour.2014.02.012.

[70] E. Sarasketa-Zabala, E. Martinez-Laserna, M. Berecibar, I. Gandiaga, L. Rodriguez-Martinez, and I. Villarreal. "Realistic lifetime prediction approach for Li-ion batteries". *Applied Energy* 162 (Jan. 2016), pp. 839–852. DOI: 10.1016/j.apenergy.2015.10.115.

[71] M. Naumann, M. Schimpe, P. Keil, H. C. Hesse, and A. Jossen. "Analysis and modeling of calendar aging of a commercial LiFePO4/graphite cell". *Journal of Energy Storage* 17 (June 2018), pp. 153–169. DOI: `10.1016/j.est.2018.01.019`.

[72] M. Naumann, F. B. Spingler, and A. Jossen. "Analysis and modeling of cycle aging of a commercial LiFePO4/graphite cell". *Journal of Power Sources* 451 (Mar. 2020), p. 227666. DOI: `10.1016/j.jpowsour.2019.227666`.

[73] M. Hossain Lipu, M. Hannan, A. Hussain, A. Ayob, M. H. Saad, T. F. Karim, and D. N. How. "Data-driven state of charge estimation of lithium-ion batteries: Algorithms, implementation factors, limitations and future trends". *Journal of Cleaner Production* 277 (Dec. 2020), p. 124110. DOI: `10.1016/j.jclepro.2020.124110`.

[74] Y. Li, K. Liu, A. M. Foley, A. Zülke, M. Berecibar, E. Nanini-Maury, J. Van Mierlo, and H. E. Hoster. "Data-driven health estimation and lifetime prediction of lithium-ion batteries: A review". *Renewable and Sustainable Energy Reviews* 113 (Oct. 2019), p. 109254. DOI: `10.1016/j.rser.2019.109254`.

[75] *ISO 12405-1:2011. Electrically propelled road vehicles - Test specification for lithium-ion traction battery packs and systems - Part 1: High-power applications.*

[76] G. L. Plett. *Battery management systems. Vol. 2: Equivalent-circuit methods.* Artech House power engineering and power electronics. Boston: Artech House, 2016. ISBN: 978-1-63081-027-6.

[77] A. J. Smith, J. C. Burns, and J. R. Dahn. "A High Precision Study of the Coulombic Efficiency of Li-Ion Batteries". *Electrochemical and Solid-State Letters* 13.12 (2010), A177. DOI: `10.1149/1.3487637`.

[78] M. Naumann. "Techno-economic evaluation of stationary battery energy storage systems with special consideration of aging". PhD thesis. Technische Universität München, 2018.

[79] G. Fitzgerald, J. Mandel, J. Morris, and H. Touati. *The economics of battery energy storage - How multi-use, customer-sited batteries deliver the most services and value to customers and the grid.* Tech. rep. Rocky Mountain Institute, Sept. 2015. URL: `https://rmi.org/wp-content/uploads/2017/03/RMI-TheEconomicsOfBatteryEnergyStorage-FullReport-FINAL.pdf`.

[80] G. Reid and J. Julve. "Second Life-Batterien als flexible Speicher für Erneuerbare Energien". *Bundesverband Erneuerbare Energie e.V.* (2016).

[81] M. García-Plaza, J. Eloy-García Carrasco, J. Alonso-Martínez, and A. Peña Asensio. "Peak shaving algorithm with dynamic minimum voltage tracking for battery storage systems in microgrid applications". *Journal of Energy Storage* 20 (Dec. 2018), pp. 41–48. DOI: 10.1016/j.est.2018.08.021.

[82] M. Uddin, M. Romlie, M. Abdullah, C. Tan, G. Shafiullah, and A. Bakar. "A novel peak shaving algorithm for islanded microgrid using battery energy storage system". *Energy* 196 (Apr. 2020), p. 117084. DOI: 10.1016/j.energy.2020.117084.

[83] M. Uddin, M. F. Romlie, M. F. Abdullah, S. Abd Halim, A. H. Abu Bakar, and T. C. Kwang. "A review on peak load shaving strategies". *Renewable and Sustainable Energy Reviews* 82.3 (2018), pp. 3323–3332. DOI: 10.1016/j.rser.2017.10.056.

[84] J. Fleer and P. Stenzel. "Impact analysis of different operation strategies for battery energy storage systems providing primary control reserve". *Journal of Energy Storage* 8 (Nov. 2016), pp. 320–338. DOI: 10.1016/j.est.2016.02.003.

[85] D.-I. Stroe, V. Knap, M. Swierczynski, A.-I. Stroe, and R. Teodorescu. "Operation of a Grid-Connected Lithium-Ion Battery Energy Storage System for Primary Frequency Regulation: A Battery Lifetime Perspective". *IEEE Transactions on Industry Applications* 53.1 (Jan. 2017), pp. 430–438. DOI: 10.1109/TIA.2016.2616319.

[86] D. Zhu and Y.-J. A. Zhang. "Optimal Coordinated Control of Multiple Battery Energy Storage Systems for Primary Frequency Regulation". *IEEE Transactions on Power Systems* 34.1 (Jan. 2019), pp. 555–565. DOI: 10.1109/TPWRS.2018.2868504.

[87] Z. A. Obaid, L. M. Cipcigan, L. Abrahim, and M. T. Muhssin. "Frequency control of future power systems: reviewing and evaluating challenges and new control methods". *Journal of Modern Power Systems and Clean Energy* 7.1 (Jan. 2019), pp. 9–25. DOI: 10.1007/s40565-018-0441-1.

[88] D. Kucevic, B. Tepe, S. Englberger, A. Parlikar, M. Mühlbauer, O. Bohlen, A. Jossen, and H. Hesse. "Standard battery energy storage system profiles: Analysis of various applications for stationary energy storage systems using

a holistic simulation framework". *Journal of Energy Storage* 28 (Apr. 2020), p. 101077. DOI: 10.1016/j.est.2019.101077.

[89] G. T. Doran. "There's a S.M.A.R.T. way to write management's goals and objectives". *Management Review* 70 (11) (1981), pp. 35–36.

[90] M. Bauer, M. Muehlbauer, O. Bohlen, M. A. Danzer, and J. Lygeros. "Power flow in heterogeneous battery systems". *Journal of Energy Storage* 25 (Oct. 2019), p. 100816. DOI: 10.1016/j.est.2019.100816.

[91] D. E. Olivares et al. "Trends in Microgrid Control". *IEEE Transactions on Smart Grid* 5.4 (July 2014), pp. 1905–1919. DOI: 10.1109/TSG.2013.2295514.

[92] T. Dragicevic, X. Lu, J. Vasquez, and J. Guerrero. "DC Microgrids–Part I: A Review of Control Strategies and Stabilization Techniques". *IEEE Transactions on Power Electronics* (2015), pp. 1–1. DOI: 10.1109/TPEL.2015.2478859.

[93] L. Meng, Q. Shafiee, G. Ferrari Trecate, H. Karimi, D. Fulwani, X. Lu, and J. M. Guerrero. "Review on Control of DC Microgrids". *IEEE Journal of Emerging and Selected Topics in Power Electronics* (2017). DOI: 10.1109/JESTPE.2017.2690219.

[94] J. Kumar, A. Agarwal, and V. Agarwal. "A review on overall control of DC microgrids". *Journal of Energy Storage* 21 (Feb. 2019), pp. 113–138. DOI: 10.1016/j.est.2018.11.013.

[95] J. M. Guerrero, J. C. Vasquez, and R. Teodorescu. "Hierarchical control of droop-controlled DC and AC microgrids - a general approach towards standardization". *2009 35th Annual Conference of IEEE Industrial Electronics*. Porto: IEEE, Nov. 2009, pp. 4305–4310. DOI: 10.1109/IECON.2009.5414926.

[96] Z. Jiang and R. Dougal. "Control Strategies for Active Power Sharing in a Fuel-Cell-Powered Battery-Charging Station". *IEEE Transactions on Industry Applications* 40.3 (May 2004), pp. 917–924. DOI: 10.1109/TIA.2004.827467.

[97] X. Lu, K. Sun, J. M. Guerrero, J. C. Vasquez, L. Huang, and R. Teodorescu. "SoC-based droop method for distributed energy storage in DC microgrid applications". *International Symposium on Industrial Electronics (ISIE)*. IEEE, 2012, pp. 1640–1645. DOI: 10.1109/ISIE.2012.6237336.

[98] X. Lu, K. Sun, J. M. Guerrero, J. C. Vasquez, and L. Huang. "State-of-Charge Balance Using Adaptive Droop Control for Distributed Energy Storage Systems in DC Microgrid Applications". *IEEE Transactions on Industrial Electronics* 61.6 (June 2014), pp. 2804–2815. DOI: `10.1109/TIE.2013.2279374`.

[99] X. Lu, K. Sun, J. M. Guerrero, J. C. Vasquez, and L. Huang. "Droop-control-based state-of-charge balancing method for charging and discharging process in autonomous DC microgrids". *Industrial Electronics (ISIE), 2014 IEEE 23rd International Symposium on*. IEEE, 2014, pp. 2359–2364. DOI: `10.1109/ISIE.2014.6864988`.

[100] X. Lu, K. Sun, J. M. Guerrero, J. C. Vasquez, and L. Huang. "Double-Quadrant State-of-Charge-Based Droop Control Method for Distributed Energy Storage Systems in Autonomous DC Microgrids". *IEEE Transactions on Smart Grid* 6.1 (Jan. 2015), pp. 147–157. DOI: `10.1109/TSG.2014.2352342`.

[101] N. L. Diaz, T. Dragicevic, J. C. Vasquez, and J. M. Guerrero. "Fuzzy-logic-based gain-scheduling control for state-of-charge balance of distributed energy storage systems for DC microgrids". *Twenty-Ninth Annual IEEE Applied Power Electronics Conference and Exposition (APEC)*. IEEE, 2014, pp. 2171–2176. DOI: `10.1109/APEC.2014.6803606`.

[102] N. L. Diaz, T. Dragicevic, J. C. Vasquez, and J. M. Guerrero. "Intelligent Distributed Generation and Storage Units for DC Microgrids - A New Concept on Cooperative Control Without Communications Beyond Droop Control". *IEEE Transactions on Smart Grid* 5.5 (Sept. 2014), pp. 2476–2485. DOI: `10.1109/TSG.2014.2341740`.

[103] C. Li, T. Dragicevic, M. G. Plaza, F. Andrade, J. C. Vasquez, and J. M. Guerrero. "Multiagent based distributed control for state-of-charge balance of distributed energy storage in DC microgrids". *Industrial Electronics Society, IECON 2014-40th Annual Conference of the IEEE*. IEEE, 2014, pp. 2180–2184. DOI: `10.1109/IECON.2014.7048804`.

[104] C. Li, T. Dragicevic, N. L. Diaz, J. C. Vasquez, and J. M. Guerrero. "Voltage scheduling droop control for State-of-Charge balance of distributed energy storage in DC microgrids". *2014 IEEE International Energy Conference (ENERGYCON)*. Cavtat, Croatia: IEEE, May 2014, pp. 1310–1314. DOI: `10.1109/ENERGYCON.2014.6850592`.

[105]   C. Li, T. Dragicevic, J. M. Guerrero, and E. A. A. Coelho. "Multi-Agent-Based Distributed State of Charge Balancing Control for Distributed Energy Storage Units in AC Microgrids". *Applied Power Electronics Conference and Exposition (APEC), 2015 IEEE* (2015). DOI: 10.1109/APEC.2015.7104773.

[106]   F. L. Marcelino, H. H. Sathler, W. W. Silva, T. R. de Oliveira, and P. F. Donoso-Garcia. "A comparative study of Droop Compensation Functions for State-of-Charge based adaptive droop control". *8th International Symposium on Power Electronics for Distributed Generation Systems (PEDG)*. IEEE, 2017, pp. 1–8. DOI: 10.1109/PEDG.2017.7972492.

[107]   M. Mobarrez, S. Bhattacharya, and D. Fregosi. "Implementation of distributed power balancing strategy with a layer of supervision in a low-voltage DC microgrid". Tampa, FL, USA: IEEE, Mar. 2017, pp. 1248–1254. DOI: 10.1109/APEC.2017.7930855.

[108]   Q. Wu, R. Guan, X. Sun, Y. Wang, and X. Li. "SoC Balancing Strategy for Multiple Energy Storage Units With Different Capacities in Islanded Microgrids Based on Droop Control". *IEEE Journal of Emerging and Selected Topics in Power Electronics* 6.4 (Dec. 2018), pp. 1932–1941. DOI: 10.1109/JESTPE.2018.2789481.

[109]   A. Y. Ali, A. Basit, T. Ahmad, A. Qamar, and J. Iqbal. "Optimizing coordinated control of distributed energy storage system in microgrid to improve battery life". *Computers & Electrical Engineering* 86 (Sept. 2020), p. 106741. DOI: 10.1016/j.compeleceng.2020.106741.

[110]   N. Li, F. Gao, T. Hao, Z. Ma, and C. Zhang. "SOH Balancing Control Method for MMC Battery Energy Storage System". *IEEE Transactions on Industrial Electronics* (2017). DOI: 10.1109/TIE.2017.2733462.

[111]   M. Schimpe, C. Piesch, H. Hesse, J. Paß, S. Ritter, and A. Jossen. "Power Flow Distribution Strategy for Improved Power Electronics Energy Efficiency in Battery Storage Systems: Development and Implementation in a Utility-Scale System". *Energies* 11.3 (Mar. 2018), p. 533. DOI: 10.3390/en11030533.

[112]   J.-Y. Choi, I.-S. Choi, G.-H. Ahn, and D.-J. Won. "Advanced Power Sharing Method to Improve the Energy Efficiency of Multiple Battery Energy Storages System". *IEEE Transactions on Smart Grid* 9.2 (Mar. 2018), pp. 1292–1300. DOI: 10.1109/TSG.2016.2582842.

[113]   M. Masih-Tehrani and M. Dahmardeh. "A Novel Power Distribution System Employing State of Available Power Estimation for a Hybrid Energy Storage System". *IEEE Transactions on Industrial Electronics* 65.8 (Aug. 2018), pp. 6676–6685. DOI: 10.1109/TIE.2017.2774721.

[114]   T. Morstyn, B. Hredzak, and V. G. Agelidis. "Dynamic optimal power flow for DC microgrids with distributed battery energy storage systems". *2016 IEEE Energy Conversion Congress and Exposition (ECCE)*. Milwaukee, WI, USA: IEEE, Sept. 2016, pp. 1–6. DOI: 10.1109/ECCE.2016.7855059.

[115]   L. K. Vedulla and M. K. Mishra. "PSO based power sharing scheme for an islanded DC microgrid system". *IECON 2017 - 43rd Annual Conference of the IEEE Industrial Electronics Society*. Beijing: IEEE, Oct. 2017, pp. 392–397. DOI: 10.1109/IECON.2017.8216070.

[116]   L. Meng, T. Dragicevic, J. Vasquez, J. Guerrero, and E. R. Sanseverino. "Hierarchical Control with Virtual Resistance Optimization for Efficiency Enhancement and State-of-Charge Balancing in DC Microgrids". *2015 IEEE First International Conference on DC Microgrids*. IEEE, 2015, pp. 1–6. DOI: 10.1109/ICDCM.2015.7152000.

[117]   A. J. Jones and W. W. Weaver. "Optimal droop surface control of dc microgrids based on battery state of charge". Milwaukee, WI, USA: IEEE, Sept. 2016, pp. 1–8. DOI: 10.1109/ECCE.2016.7855317.

[118]   R. Wang, H. Tang, and Y. Xu. "Distributed cooperative optimal control of Energy Storage Systems in a microgrid". *2016 IEEE Power and Energy Society General Meeting (PESGM)*. Boston, MA, USA: IEEE, July 2016, pp. 1–5. DOI: 10.1109/PESGM.2016.7741398.

[119]   X. Li and D. Zhang. "Coordinated Control and Energy Management Strategies for Hundred Megawatt-level Battery Energy Storage Stations Based on Multi-agent Theory". *2018 International Conference on Advanced Mechatronic Systems (ICAMechS)*. Zhengzhou: IEEE, Aug. 2018, pp. 1–5. DOI: 10.1109/ICAMechS.2018.8506868.

[120]   S. Jinlei, P. Lei, L. Ruihang, M. Qian, T. Chuanyu, and W. Tianru. "Economic Operation Optimization for 2nd Use Batteries in Battery Energy Storage Systems". *IEEE Access* 7 (2019), pp. 41852–41859. DOI: 10.1109/ACCESS.2019.2902402.

[121] P. Fortenbacher, J. L. Mathieu, and G. Andersson. "Modeling, identification, and optimal control of batteries for power system applications". *2014 Power Systems Computation Conference*. Wrocław, Poland: IEEE, Aug. 2014, pp. 1–7. DOI: 10.1109/PSCC.2014.7038360.

[122] P. Fortenbacher, G. Andersson, and J. L. Mathieu. "Optimal real-time control of multiple battery sets for power system applications". *2015 IEEE Eindhoven PowerTech*. Eindhoven, Netherlands: IEEE, June 2015, pp. 1–6. DOI: 10.1109/PTC.2015.7232763.

[123] Z. Wu, H. Tazvinga, and X. Xia. "Demand side management of photovoltaic-battery hybrid system". *Applied Energy* 148 (June 2015), pp. 294–304. DOI: 10.1016/j.apenergy.2015.03.109.

[124] S.-K. Kim, J.-Y. Kim, K.-H. Cho, and G. Byeon. "Optimal Operation Control for Multiple BESSs of a Large-Scale Customer Under Time-Based Pricing". *IEEE Transactions on Power Systems* 33.1 (Jan. 2018), pp. 803–816. DOI: 10.1109/TPWRS.2017.2696571.

[125] W. Kang, M. Chen, Q. Li, W. Lai, Y. Luo, and P. J. Tavner. "Distributed optimization model and algorithms for virtual energy storage systems using dynamic price". *Journal of Cleaner Production* 289 (Mar. 2021), p. 125440. DOI: 10.1016/j.jclepro.2020.125440.

[126] F. Sanchez Gorostiza and F. M. Gonzalez-Longatt. "Deep Reinforcement Learning-Based Controller for SOC Management of Multi-Electrical Energy Storage System". *IEEE Transactions on Smart Grid* 11.6 (Nov. 2020), pp. 5039–5050. DOI: 10.1109/TSG.2020.2996274.

[127] H. Chaoui, H. Gualous, L. Boulon, and S. Kelouwani. "Deep Reinforcement Learning Energy Management System for Multiple Battery Based Electric Vehicles". *2018 IEEE Vehicle Power and Propulsion Conference (VPPC)*. Chicago, IL: IEEE, Aug. 2018, pp. 1–6. DOI: 10.1109/VPPC.2018.8605023.

[128] F. Tuchnitz, N. Ebell, J. Schlund, and M. Pruckner. "Development and Evaluation of a Smart Charging Strategy for an Electric Vehicle Fleet Based on Reinforcement Learning". *Applied Energy* 285 (Mar. 2021), p. 116382. DOI: 10.1016/j.apenergy.2020.116382.

[129] O. Bohlen and M. Roscher. "Verfahren zur Bestimmung und/oder Vorhersage der maximalen Leistungsfähigkeit einer Batterie". Pat. DE 10 2009 049 589 A1. Apr. 2011.

[130] N. Gunantara. "A review of multi-objective optimization: Methods and its applications". *Cogent Engineering* 5.1 (Jan. 2018). Ed. by Q. Ai, p. 1502242. DOI: 10.1080/23311916.2018.1502242.

[131] K. Deb. "Multi-objective Optimization". *Search Methodologies.* Ed. by E. K. Burke and G. Kendall. Boston, MA: Springer US, 2014, pp. 403–449. ISBN: 978-1-4614-6939-1.

[132] M. Ehrgott. *Multicriteria optimization.* 2nd ed. Berlin ; New York: Springer, 2005. ISBN: 978-3-540-21398-7.

[133] C.-L. Hwang and A. S. M. Masud. *Multiple Objective Decision Making – Methods and Applications A State-of-the-Art Survey.* 1979. ISBN: 978-3-642-45511-7.

[134] J. Villemonteix, E. Vazquez, M. Sidorkiewicz, and E. Walter. "Global optimization of expensive-to-evaluate functions: an empirical comparison of two sampling criteria". *Journal of Global Optimization* 43.2-3 (Mar. 2009), pp. 373–389. DOI: 10.1007/s10898-008-9313-y.

[135] K. K. Vu, C. D'Ambrosio, Y. Hamadi, and L. Liberti. "Surrogate-based methods for black-box optimization: Surrogate-based methods for black-box optimization". *International Transactions in Operational Research* 24.3 (May 2017), pp. 393–424. DOI: 10.1111/itor.12292.

[136] D. Golovin, B. Solnik, S. Moitra, G. Kochanski, J. Karro, and D. Sculley. "Google Vizier: A Service for Black-Box Optimization". *Proceedings of the 23rd ACM SIGKDD International Conference on Knowledge Discovery and Data Mining.* Halifax NS Canada: ACM, Aug. 2017, pp. 1487–1495. DOI: 10.1145/3097983.3098043.

[137] R. Marler and J. Arora. "Survey of multi-objective optimization methods for engineering". *Structural and Multidisciplinary Optimization* 26.6 (Apr. 2004), pp. 369–395. DOI: 10.1007/s00158-003-0368-6.

[138] G. G. Wang and S. Shan. "An Efficient Pareto Set Identification Approach for Multi-Objective Optimization on Black-Box Functions". *Volume 1: 30th Design Automation Conference.* Salt Lake City, Utah, USA: ASMEDC, Jan. 2004, pp. 279–291. DOI: 10.1115/DETC2004-57194.

[139] M. J. Kochenderfer and T. A. Wheeler. *Algorithms for optimization.* Cambridge, Massachusetts: The MIT Press, 2019. ISBN: 978-0-262-03942-0.

[140] P. I. Frazier. "A Tutorial on Bayesian Optimization". *arXiv:1807.02811* (July 2018). URL: http://arxiv.org/abs/1807.02811.

[141] B. Shahriari, K. Swersky, Z. Wang, R. P. Adams, and N. de Freitas. "Taking the Human Out of the Loop: A Review of Bayesian Optimization". *Proceedings of the IEEE* 104.1 (Jan. 2016), pp. 148–175. DOI: 10.1109/JPROC.2015.2494218.

[142] J. A. Nelder and R. Mead. "A Simplex Method for Function Minimization". *The Computer Journal* 7.4 (Jan. 1965), pp. 308–313. DOI: 10.1093/comjnl/7.4.308.

[143] J. Larson, M. Menickelly, and S. M. Wild. "Derivative-free optimization methods". *Acta Numerica* 28 (May 2019), pp. 287–404. DOI: 10.1017/S0962492919000060.

[144] M. Ahmed and N. Qin. "Surrogate-Based Aerodynamic Design Optimization: Use of Surrogates in Aerodynamic Design Optimization". *International Conference on Aerospace Sciences and Aviation Technology* 13 (May 2009), pp. 1–26. DOI: 10.21608/asat.2009.23442.

[145] A. Sóbester, A. I. J. Forrester, D. J. J. Toal, E. Tresidder, and S. Tucker. "Engineering design applications of surrogate-assisted optimization techniques". *Optimization and Engineering* 15.1 (Mar. 2014), pp. 243–265. DOI: 10.1007/s11081-012-9199-x.

[146] Z. Zhou, Y. S. Ong, M. H. Nguyen, and D. Lim. "A Study on Polynomial Regression and Gaussian Process Global Surrogate Model in Hierarchical Surrogate-Assisted Evolutionary Algorithm". *2005 IEEE Congress on Evolutionary Computation.* Vol. 3. Edinburgh, Scotland, UK: IEEE, 2005, pp. 2832–2839. DOI: 10.1109/CEC.2005.1555050.

[147] N. Dyn, D. Levin, and S. Rippa. "Numerical Procedures for Surface Fitting of Scattered Data by Radial Functions". *SIAM Journal on Scientific and Statistical Computing* 7.2 (Apr. 1986), pp. 639–659. DOI: 10.1137/0907043.

[148] H. Fang and M. F. Horstemeyer. "Global response approximation with radial basis functions". *Engineering Optimization* 38.4 (June 2006), pp. 407–424. DOI: 10.1080/03052150500422294.

[149] N. Cressie. "Spatial prediction and ordinary kriging". *Mathematical Geology* 20.4 (May 1988), pp. 405–421. DOI: 10.1007/BF00892986.

[150] C. E. Rasmussen and C. K. I. Williams. *Gaussian processes for machine learning*. Adaptive computation and machine learning. Cambridge, Mass: MIT Press, 2006. ISBN: 978-0-262-18253-9.

[151] R. A Fisher. *The design of experiments*. Ninth Edition. New York: Hafner Press, 1974. ISBN: 978-0-02-844690-5.

[152] M. D. McKay, R. J. Beckman, and W. J. Conover. "Comparison of Three Methods for Selecting Values of Input Variables in the Analysis of Output from a Computer Code". *Technometrics* 21.2 (May 1979), pp. 239–245. DOI: 10.1080/00401706.1979.10489755.

[153] D. Chicco, M. J. Warrens, and G. Jurman. "The coefficient of determination R-squared is more informative than SMAPE, MAE, MAPE, MSE and RMSE in regression analysis evaluation". *PeerJ Computer Science* 7 (July 2021), e623. DOI: 10.7717/peerj-cs.623.

[154] S. Chatterjee and J. S. Simonoff. *Handbook of Regression Analysis*. Hoboken, NJ, USA: John Wiley & Sons, Inc., Dec. 2012. ISBN: 978-1-118-53284-3.

[155] M. Palesi and T. Givargis. "Multi-objective design space exploration using genetic algorithms". *Proceedings of the tenth international symposium on Hardware/software codesign - CODES '02*. Estes Park, Colorado: ACM Press, 2002, p. 67. DOI: 10.1145/774789.774804.

[156] A. M. Ross and D. E. Hastings. "The Tradespace Exploration Paradigm". *INCOSE International Symposium* 15.1 (July 2005), pp. 1706–1718. DOI: 10.1002/j.2334-5837.2005.tb00783.x.

[157] Y. Xie, G. H. Loh, B. Black, and K. Bernstein. "Design space exploration for 3D architectures". *ACM Journal on Emerging Technologies in Computing Systems* 2.2 (Apr. 2006), pp. 65–103. DOI: 10.1145/1148015.1148016.

[158] E. Kang, E. Jackson, and W. Schulte. "An Approach for Effective Design Space Exploration". *Foundations of Computer Software. Modeling, Development, and Verification of Adaptive Systems*. Ed. by R. Calinescu and E. Jackson. Vol. 6662. Berlin, Heidelberg: Springer Berlin Heidelberg, 2011, pp. 33–54. ISBN: 978-3-642-21291-8.

[159] H. Palm and J. Holzmann. "Hyper Space Exploration A Multicriterial Quantitative Trade-Off Analysis for System Design in Complex Environment". *2018 IEEE International Systems Engineering Symposium (ISSE)*. Rome: IEEE, Oct. 2018, pp. 1–6. DOI: 10.1109/SysEng.2018.8544435.

[160] L. Zhang, H. Peng, Z. Ning, Z. Mu, and C. Sun. "Comparative Research on RC Equivalent Circuit Models for Lithium-Ion Batteries of Electric Vehicles". *Applied Sciences* 7.10 (Sept. 2017). DOI: 10.3390/app7101002.

[161] M. Abdel-Monem, O. Hegazy, N. Omar, K. Trad, P. Van den Bossche, and J. Van Mierlo. "Lithium-ion batteries: Comprehensive technical analysis of second-life batteries for smart grid applications". *2017 19th European Conference on Power Electronics and Applications (EPE'17 ECCE Europe)*. Warsaw: IEEE, Sept. 2017, pp. 1–16. DOI: 10.23919/EPE17ECCEEurope.2017.8099385.

[162] D.-I. Stroe, M. Swierczynski, A.-I. Stroe, and S. Knudsen Kær. "Generalized Characterization Methodology for Performance Modelling of Lithium-Ion Batteries". *Batteries* 2.4 (Dec. 2016), p. 37. DOI: 10.3390/batteries2040037.

[163] A. Barai, W. D. Widanage, J. Marco, A. McGordon, and P. Jennings. "A study of the open circuit voltage characterization technique and hysteresis assessment of lithium-ion cells". *Journal of Power Sources* 295 (Nov. 2015), pp. 99–107. DOI: 10.1016/j.jpowsour.2015.06.140.

[164] S. N. Motapon, E. Lachance, L.-A. Dessaint, and K. Al-Haddad. "A Generic Cycle Life Model for Lithium-Ion Batteries Based on Fatigue Theory and Equivalent Cycle Counting". *IEEE Open Journal of the Industrial Electronics Society* 1 (2020), pp. 207–217. DOI: 10.1109/OJIES.2020.3015396.

[165] B. Xu, A. Oudalov, A. Ulbig, G. Andersson, and D. S. Kirschen. "Modeling of Lithium-Ion Battery Degradation for Cell Life Assessment". *IEEE Transactions on Smart Grid* 9.2 (Mar. 2018), pp. 1131–1140. DOI: 10.1109/TSG.2016.2578950.

[166] D. Magnor, J. Gerschler, M. Ecker, P. Merk, and D. Sauer. "Concept of a Battery Aging Model for Lithium-Ion Batteries Considering the Lifetime Dependency on the Operation Strategy". *24th European Photovoltaic Solar Energy Conference* 21-25 September 2009 (2009). DOI: 10.4229/24THEUPVSEC2009-4BO.11.3.

[167] Y. Preger, H. M. Barkholtz, A. Fresquez, D. L. Campbell, B. W. Juba, J. Romàn-Kustas, S. R. Ferreira, and B. Chalamala. "Degradation of Commercial Lithium-Ion Cells as a Function of Chemistry and Cycling Conditions". *Journal of The Electrochemical Society* 167.12 (Sept. 2020), p. 120532. DOI: 10.1149/1945-7111/abae37.

[168] J. Wang, J. Purewal, P. Liu, J. Hicks-Garner, S. Soukazian, E. Sherman, A. Sorenson, L. Vu, H. Tataria, and M. W. Verbrugge. "Degradation of lithium ion batteries employing graphite negatives and nickel-cobalt-manganese oxide + spinel manganese oxide positives: Part 1, aging mechanisms and life estimation". *Journal of Power Sources* 269 (Dec. 2014), pp. 937–948. DOI: `10.1016/j.jpowsour.2014.07.030`.

[169] J. de Hoog, J.-M. Timmermans, D. Ioan-Stroe, M. Swierczynski, J. Jaguemont, S. Goutam, N. Omar, J. Van Mierlo, and P. Van Den Bossche. "Combined cycling and calendar capacity fade modeling of a Nickel-Manganese-Cobalt Oxide Cell with real-life profile validation". *Applied Energy* 200 (Aug. 2017), pp. 47–61. DOI: `10.1016/j.apenergy.2017.05.018`.

[170] F. Schaeufl. *Stabilitätsuntersuchungen einer hierarchischen Regelstruktur für heterogene Batteriespeichersysteme*. Bachelor thesis, Munich University of Applied Sciences. 2019.

[171] B. W. Boehm. "Guidelines for Verifying and Validating Software Requirements and Design Specifications". *Euro IFIP 79*. North Holland, 1979, pp. 711–719.

[172] "IEEE Standard for System, Software, and Hardware Verification and Validation". *IEEE Std 1012-2016 (Revision of IEEE Std 1012-2012/ Incorporates IEEE Std 1012-2016/Cor1-2017* (2017), pp. 1–260. DOI: `DOI:10.1109/IEEESTD.2017.8055462`.

[173] USABC. *FreedomCAR Battery Test Manual For Power-Assist Hybrid Electric Vehicles*. Oct. 2003. URL: `https://avt.inl.gov/sites/default/files/pdf/battery/freedomcar_manual_04_15_03.pdf`.

[174] H. Zhang, H. W. Mu, Y. Zhang, and J. Han. "Calculation and Characteristics Analysis of Lithium Ion Batteries' Internal Resistance Using HPPC Test". *Advanced Materials Research* 926-930 (May 2014), pp. 915–918. DOI: `10.4028/www.scientific.net/AMR.926-930.915`.

[175] Y. Huang, Y. Li, L. Jiang, X. Qiao, Y. Cao, and J. Yu. "Research on Fitting Strategy in HPPC Test for Li-ion battery". *2019 IEEE Sustainable Power and Energy Conference (iSPEC)*. Beijing, China: IEEE, Nov. 2019, pp. 1776–1780. DOI: `10.1109/iSPEC48194.2019.8975264`.

[176] E. Zitzler and L. Thiele. "Multiobjective optimization using evolutionary algorithms — A comparative case study". *Parallel Problem Solving from Nature — PPSN V*. Ed. by G. Goos, J. Hartmanis, J. van Leeuwen, A. E. Eiben, T. Bäck, M. Schoenauer, and H.-P. Schwefel. Vol. 1498. Berlin, Heidelberg: Springer Berlin Heidelberg, 1998, pp. 292–301. ISBN: 978-3-540-65078-2.

[177] K. Deb, S. Agrawal, A. Pratap, and T Meyarivan. "A Fast Elitist Nondominated Sorting Genetic Algorithm for Multi-objective Optimization: NSGA-II". *Parallel Problem Solving from Nature PPSN VI*. Ed. by G. Goos, J. Hartmanis, J. van Leeuwen, M. Schoenauer, K. Deb, G. Rudolph, X. Yao, E. Lutton, J. J. Merelo, and H.-P. Schwefel. Vol. 1917. Berlin, Heidelberg: Springer Berlin Heidelberg, 2000, pp. 849–858. DOI: `10.1007/3-540-45356-3_83`.

[178] S. Peitz and M. Dellnitz. "A Survey of Recent Trends in Multiobjective Optimal Control-Surrogate Models, Feedback Control and Objective Reduction". *Mathematical and Computational Applications* 23.2 (June 2018), p. 30. DOI: `10.3390/mca23020030`.

[179] V. Strijov and G. W. Weber. "Nonlinear regression model generation using hyperparameter optimization". *Computers & Mathematics with Applications* 60.4 (Aug. 2010), pp. 981–988. DOI: `10.1016/j.camwa.2010.03.021`.

[180] K. Amouzgar and N. Strömberg. "Radial basis functions as surrogate models with a priori bias in comparison with a posteriori bias". *Structural and Multidisciplinary Optimization* 55.4 (Apr. 2017), pp. 1453–1469. DOI: `10.1007/s00158-016-1569-0`.

[181] M. D. Buhmann. *Radial Basis Functions: Theory and Implementations*. Cambridge University Press, July 2003. DOI: `10.1017/CBO9780511543241`.

[182] D. Eriksson, D. Bindel, and C. A. Shoemaker. "pySOT and POAP: An event-driven asynchronous framework for surrogate optimization" (July 2019). URL: `http://arxiv.org/abs/1908.00420`.

[183] J. Müller. "SOCEMO: Surrogate Optimization of Computationally Expensive Multiobjective Problems". *INFORMS Journal on Computing* 29.4 (Nov. 2017), pp. 581–596. DOI: `10.1287/ijoc.2017.0749`.

[184] C. R. Rao, ed. *Linear Statistical Inference and its Applications*. Wiley Series in Probability and Statistics. Hoboken, NJ, USA: John Wiley & Sons, Inc., Apr. 1973. DOI: `10.1002/9780470316436`.

[185]   J. Rodriguez, A. Perez, and J. Lozano. "Sensitivity Analysis of k-Fold Cross Validation in Prediction Error Estimation". *IEEE Transactions on Pattern Analysis and Machine Intelligence* 32.3 (Mar. 2010), pp. 569–575. DOI: 10.1109/TPAMI.2009.187.

[186]   A. Burkov. *The hundred-page machine learning book.* 2019. ISBN: 978-1-9995795-0-0.

[187]   M. Kuhn and K. Johnson. *Applied Predictive Modeling.* New York, NY: Springer New York, 2013. ISBN: 978-1-4614-6848-6.

[188]   D. Scholz. *Optimierung interaktiv: Grundlagen verstehen, Modelle erforschen und Verfahren anwenden.* Berlin, Germany [Heidelberg]: Springer Spektrum, 2018. ISBN: 978-3-662-57953-4.

Appendix

A Abbreviations

AC   alternating current

BESS   battery energy storage system

BMS   battery management system

BOL   beginning-of-life

DC   direct current

DoD   depth of discharge

DovE   design of virtual experiments

ECM   equivalent circuit model

EMS   energy management system

EOL   end-of-life

FEC   full equivalent cycle

HPPC   hybrid pulse power characterization

HSE   Hyper Space Exploration

ISES   Institute for Sustainable Energy Systems

IT   isolé-terre

LCO   lithium cobalt oxide

LFP   lithium iron phosphate

LV   low voltage

MG   microgrid

MOO	multi-objective optimization
MPC	model predictive control
MV	medium voltage
NCA	lithium nickel cobalt aluminium oxide
NMC	lithium nickel manganese cobalt oxide
OCV	open-circuit voltage
PCC	point of common coupling
PI	proportional integral
PFCS	power flow control strategy
PO	Pareto-optimal
PSO	particle swarm optimization
RBF	radial basis function
RC	resistor-capacitor
SCADA	supervisory control and data aquisition
SEI	solid electrolyte interphase
SoAP	state of the available power
SoC	state of charge
SoH	state of health

B Nomenclature

accuracy	model's accuracy
α_i	power-sharing factor of the ith BESS
$\alpha_{\text{SoAP},i}$	power-sharing factor of the ith BESS (PFCS SoAP)
$\alpha_{\text{SoC},i}$	power-sharing factor of the ith BESS (PFCS SoC)
BOL_{c}	(relative) initial capacity
C	capacitance
C_{act}	actual discharge capacity
C_{p}	parallel capacitance
C_{rat}	rated (or nominal) capacity
$C\text{-}rate$	C-rate
$C\text{-}rate_{\text{ref}}$	reference value (C-rate)
δv	control signal of PI-controller
ΔFEC	full equivalent cycle interval
d	design space vector
d'	another design space vector
$d_{\text{SoC}}^{\text{cal}}$	calendar aging stress factor (SoC)
$d_{\text{T}}^{\text{cal}}$	calendar aging stress factor (temperature)
$d_{\text{C-rate}}^{\text{cyc}}$	cycle aging stress factor (C-rate)
$d_{\text{DoD}}^{\text{cyc}}$	cycle aging stress factor (DoD)
$d_{\text{SoC}}^{\text{cyc}}$	cycle aging stress factor (SoC)
$d_{\text{T}}^{\text{cyc}}$	cycle aging stress factor (temperature)
D	design space
D_{Pseq}	design space for the sequential PFCS
D_{SoAP}	design space for the parametric PFCS
DoD	depth of discharge
DoD_{ref}	reference value (DoD)
E_{loss}	system losses
$E_{\text{loss,bat}}$	battery losses
$E_{\text{loss,dcdc}}$	DC/DC converter losses

$E_{\text{loss,max}}$	maximum system losses
E_{pred}	maximum available charging/discharging energy
$E_{\text{pred,ch}}$	maximum available charging energy
$E_{\text{pred,dch}}$	maximum available discharging energy
Efficiency	efficiency
Efficiency$_{\text{act}}$	actual value of the target indicator "efficiency"
EOL_{c}	(relative) remaining capacity at end-of-life
$f(x)$	objective vector
FEC	full equivalent cycle
FEC^*	virtual full equivalent cycle
FEC_{end}	end-of-life criterion (full equivalent cycles)
η_{c}	coulombic efficiency
η_{rt}	round-trip efficiency
H_{C}	heterogeneity (use case variable)
i_{bat}	battery current
i_{lim}	current limit
$i_{\text{pred,V}}$	current response (voltage limit)
k_{i}	integral gain coefficient
k_{p}	proportional gain coefficient
K	folds
L	inductance
m_i	droop coefficient of the ith BESS
n_{BESS}	number of applied BESSs
n_{cal}	number of applied stress factors (calendar aging)
n_{cyc}	number of applied stress factors (cycle aging)
OCV	open-circuit voltage
p	convergence factor
P^*	requested power
P_{bat}	output power of the battery
$P_{\text{bat},i}$	output power of the ith battery
$P_{\text{bat,meas}}$	measured battery power
$P_{\text{bat,sim}}$	simulated battery power
P_{err}	model power error
P_i^*	desired output power of the ith BESS
P_i	output power of the ith BESS
P_{loss}	system losses

$P_{\text{loss,bat}}$	battery losses
$P_{\text{loss,dcdc}}$	DC/DC converter losses
P_{max}	maximum allowed charging/discharging power (design variable)
$P_{\text{max},i}$	maximum output power of the ith BESS
P_{pred}	maximum available charging/discharging power
$P_{\text{pred},i}$	maximum available charging/discharging power of the ith BESS
$P_{\text{pred,E}}$	maximum available charging/discharging power (energy limit)
$P_{\text{pred,I}}$	maximum available charging/discharging power (current limit)
$P_{\text{pred,V}}$	maximum available charging/discharging power (voltage limit)
P_{rat}	rated power
$P_{\text{rat,sys}}$	rated system power
P_{ref}	reference variable (system power or output power of the battery)
P_{sys}	system power
$P(u)$	Pareto-front
PE	performance
Performance	performance
Performance$_{\text{act}}$	actual value of the target indicator "performance"
PSF	profile scaling factor (use case variable)
q_{loss}	differential capacity loss
$q_{\text{loss}}^{\text{cal}}$	differential capacity loss (calendar aging)
$q_{\text{loss}}^{\text{cyc}}$	differential capacity loss (cycle aging)
$q_{\text{loss,min}}$	minimum differential capacity loss
$q_{\text{loss,min}}^{\text{cal}}$	minimum differential capacity loss (calendar aging)
Q_{err}	model capacity loss error
Q_{loss}	capacity loss
Q_{loss}^*	accumulated value of the differential capacity losses
$Q_{\text{loss,max}}$	maximum permitted capacity loss
$Q_{\text{loss}}^{\text{cal}}$	capacity loss (calendar aging)
$Q_{\text{loss}}^{*\text{cal}}$	accumulated differential capacity loss (calendar aging)
$Q_{\text{loss}}^{\text{cyc}}$	capacity loss (cycle aging)
$Q_{\text{loss}}^{*\text{cyc}}$	accumulated differential capacity loss (cycle aging)
R_{s}	ohmic resistance
R^2	coefficient of determination
R_k^2	k^{th} coefficient of determination
R_{p}	parallel resistance
S	sorting (design variable)

Service Life	service life
SL	service life
SoC	state of charge
SoC_{end}	state of charge at the end of a charging or discharging process
SoC_i	state of charge of the ith battery
SoC_{max}	maximum state of charge
SoC_{min}	minimum state of charge
SoC_{ref}	reference value (SoC)
SoC_{start}	state of charge at the beginning of a charging or discharging process
SoH	state of health
Sorting	merit order of BESSs (design variable)
Δt	time interval
τ	time interval (integration variable)
t	time
t	solution space (target indicator) vector
t^*	virtual time
t'	another solution space (target indicator) vector
$\hat{t}$	surrogate model
t_0	starting time
t_{end}	end-of-life criterion (time)
$t_{\text{pred,e}}$	prediction horizon (energy limit)
$t_{\text{pred,p}}$	prediction horizon (current and voltage limit)
t_{sim}	simulation time
T	temperature
T	target indicator space or solution space
T_{E}	target indicator "efficiency"
T_{P}	target indicator "performance"
T_{ref}	reference value (temperature)
T_{s}	sampling period
T_{SL}	target indicator "service life"
TiS_2	titanium disulfide
u	use case space vector
U	use case space
U_{UC1}	use case space for the peak shaving scenario
U_{UC2}	use case space for the frequency regulation scenario
v_{bat}	terminal voltage of the battery

v_{dc}	DC bus voltage
v_{err}	model voltage error
v_{lim}	voltage limit
v_{meas}	measured terminal voltage
$v_{\text{pred,I}}$	voltage response (current limit)
v_{rc}	voltage drop (RC-circuit)
v_{ref}^*	reference DC voltage
v_{s}	ohmic voltage drop
v_{sim}	simulated terminal voltage
x	vector of feasible decisions
X	feasible decision space
x_{11}	calendar aging pre-factor (temperature)
x_{12}	calendar aging pre-factor (SoC)
x_{13}	cycle aging pre-factor (temperature)
x_{14}	cycle aging pre-factor (SoC)
x_{15}	cycle aging pre-factor (C-rate)
x_{16}	cycle aging pre-factor (DoD)
z^{cal}	exponential factor (time)
z^{cyc}	exponential factor (FEC)
$\gamma_{\text{SoC}}^{\text{cal}}$	calendar aging stress exponent (SoC)
$\gamma_{\text{T}}^{\text{cal}}$	calendar aging stress exponent (temperature)
$\gamma_{\text{C-rate}}^{\text{cyc}}$	cycle aging stress exponent (C-rate)
$\gamma_{\text{DoD}}^{\text{cyc}}$	cycle aging stress exponent (DoD)
$\gamma_{\text{SoC}}^{\text{cyc}}$	cycle aging stress exponent (SoC)
$\gamma_{\text{T}}^{\text{cyc}}$	cycle aging stress exponent (temperature)
$\lambda(k)$	k^{th} weighting factor (calendar aging)
$\lambda(j)$	j^{th} weighting factor (cycle aging)
ω	weighting factor between calendar and cycle aging

C Supplementary material
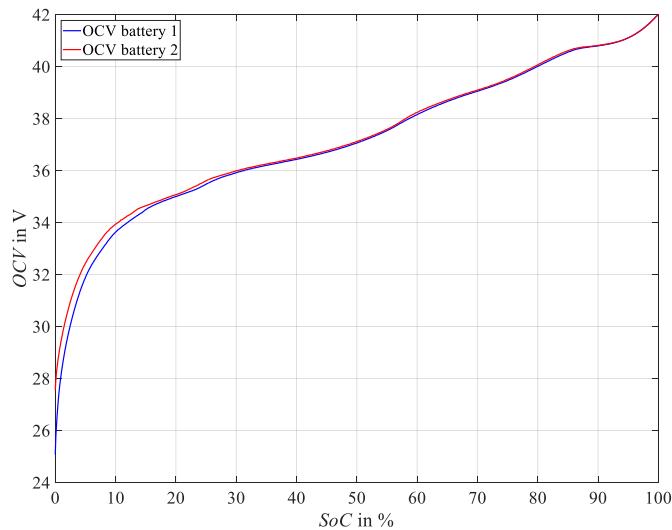
Figure C.1: Experimental OCV curve of the battery model at 20 °C.

Table C.2: Median absolute model error of the terminal voltage of the battery model for the verification case.

	Battery 1			Battery 2		
	0RC	1RC	2RC	0RC	1RC	2RC
Median absolute model error	66 mV	59 mV	45 mV	48 mV	47 mV	47 mV
Computational complexity	+	0	-	+	0	-

Table C.3: Look-up table of the battery model (battery 1) showing the ohmic resistance (in Ohm) over the SoC (in %) at different currents (in A).

	10	20	30	40	50	60	70	80	90
-40	0.109	0.103	0.101	0.099	0.098	0.097	0.097	0.098	0.099
-20	0.112	0.107	0.103	0.102	0.101	0.100	0.101	0.101	0.103
-10	0.114	0.107	0.106	0.103	0.104	0.103	0.103	0.104	0.105
-4	0.122	0.111	0.104	0.104	0.102	0.102	0.103	0.107	0.110
-1	0.129	0.115	0.106	0.108	0.104	0.110	0.112	0.111	0.107
0	0.111	0.101	0.093	0.097	0.093	0.098	0.091	0.094	0.094
1	0.093	0.086	0.079	0.086	0.081	0.085	0.070	0.076	0.080
2	0.098	0.095	0.091	0.089	0.088	0.085	0.089	0.089	0.089
3	0.105	0.100	0.100	0.094	0.094	0.094	0.094	0.094	0.094
5	0.107	0.101	0.099	0.096	0.097	0.096	0.095	0.096	0.096
8	0.108	0.101	0.098	0.098	0.097	0.094	0.096	0.097	0.097

Table C.4: Look-up table of the battery model (battery 1) showing the polarization resistance (in Ohm) over the SoC (in %) at different currents (in A).

	10	20	30	40	50	60	70	80	90
-40	0.327	0.148	0.064	0.054	0.050	0.054	0.053	0.054	0.050
-20	0.229	0.071	0.072	0.061	0.058	0.063	0.065	0.070	0.058
-10	0.233	0.066	0.076	0.069	0.066	0.080	0.086	0.090	0.063
-4	0.216	0.072	0.082	0.075	0.076	0.108	0.106	0.104	0.066
-1	0.184	0.083	0.103	0.082	0.089	0.131	0.100	0.127	0.065
0	0.182	0.077	0.082	0.069	0.077	0.107	0.095	0.114	0.065
1	0.180	0.070	0.062	0.056	0.065	0.083	0.090	0.101	0.066
2	0.172	0.068	0.071	0.061	0.063	0.103	0.085	0.088	0.063
3	0.168	0.068	0.070	0.064	0.065	0.095	0.077	0.086	0.062
5	0.161	0.066	0.070	0.061	0.063	0.084	0.069	0.077	0.060
8	0.118	0.070	0.065	0.060	0.060	0.071	0.061	0.070	0.056

Table C.5: Look-up table of the battery model (battery 1) showing the polarization capacitance over the SoC (in %) at different currents (in A).

	10	20	30	40	50	60	70	80	90
-40	78	190	149	157	151	141	135	125	146
-20	88	156	158	158	150	121	122	118	140
-10	97	147	162	167	161	119	124	121	135
-4	103	155	170	167	170	119	135	131	142
-1	101	145	184	87	146	123	124	201	106
0	96	155	160	123	197	118	114	168	99
1	92	164	136	159	247	114	103	134	93
2	93	131	185	176	144	141	137	105	139
3	94	148	132	118	158	117	120	133	114
5	101	151	153	157	155	123	121	129	121
8	105	164	143	161	151	121	143	133	140

Table C.6: Factors to consider the heterogeneity H_{C} of the system. The capacity, capacitive ECM elements, rated power, and energy of each BESS are multiplied by these factors, resistive ECM elements of each BESS are divided by these factors. Battery 1 serves as the reference data set and is thus the equivalent of a factor of one.

H_{C}	BESS 1	BESS 2	BESS 3
0.75	0.65	0.95	1.4
1	0.6	0.8	1.6
1.25	0.55	0.65	1.8
1.5	0.5	0.5	2
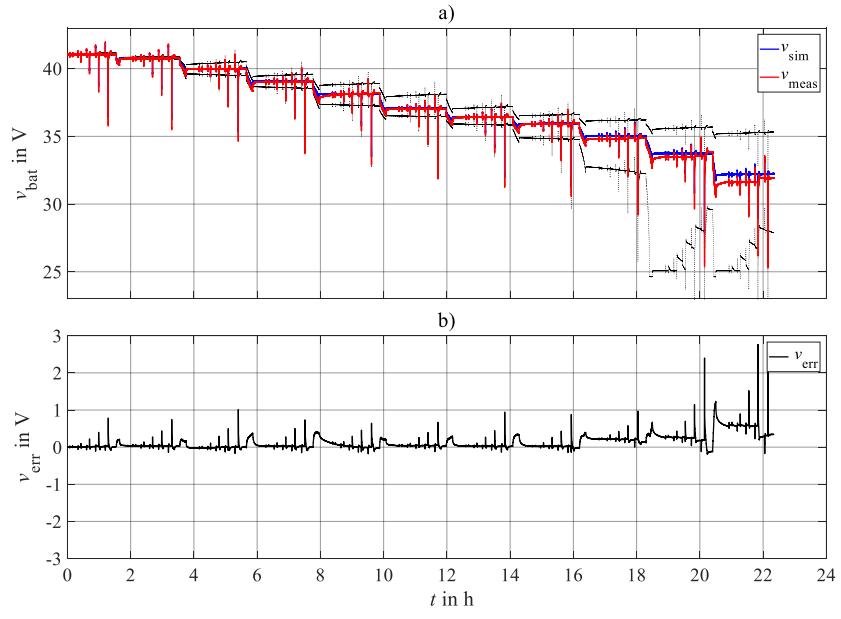
Figure C.2: Comparison of the simulated terminal voltage (blue) and the measured terminal voltage (red) of battery 2. The dotted lines show exemplary simulations with the maximum specified current measurement error of the battery test system. a) terminal voltages, b) model error. Adapted from a previous work [12].
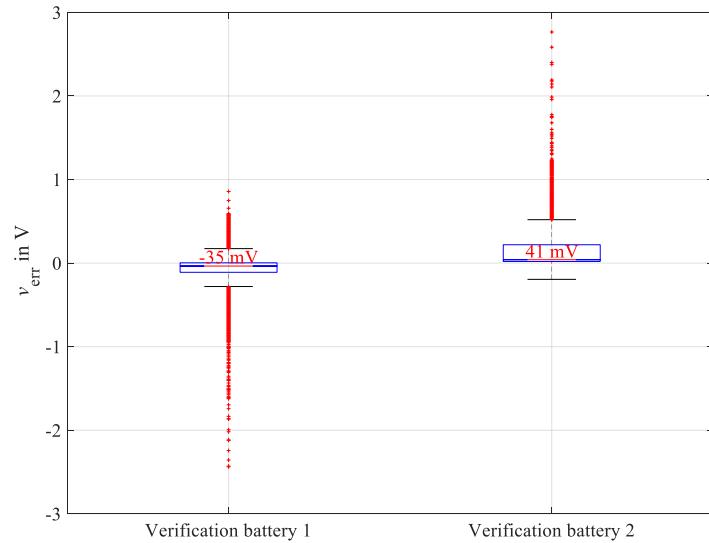
Figure C.3: Model error of the terminal voltage of the battery model. The red central mark indicates the median value and the box indicates the 25th and 75th percentiles, respectively. Adapted from a previous work [12].
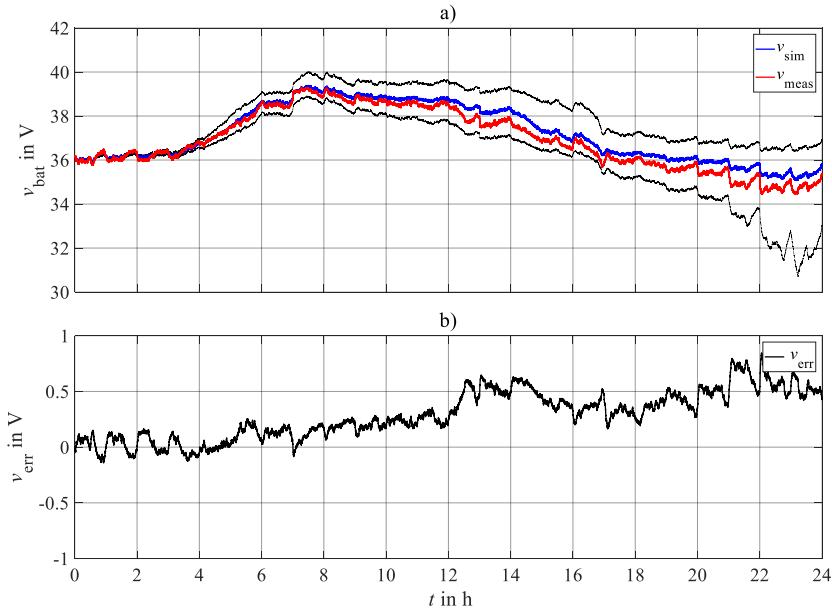
Figure C.4: Comparison of the simulated terminal voltage (blue) and the measured terminal voltage (red) of battery 2 for the frequency regulation scenario. The dotted lines show exemplary simulations with the maximum specified current measurement error of the battery test system. a) terminal voltages, b) model error.
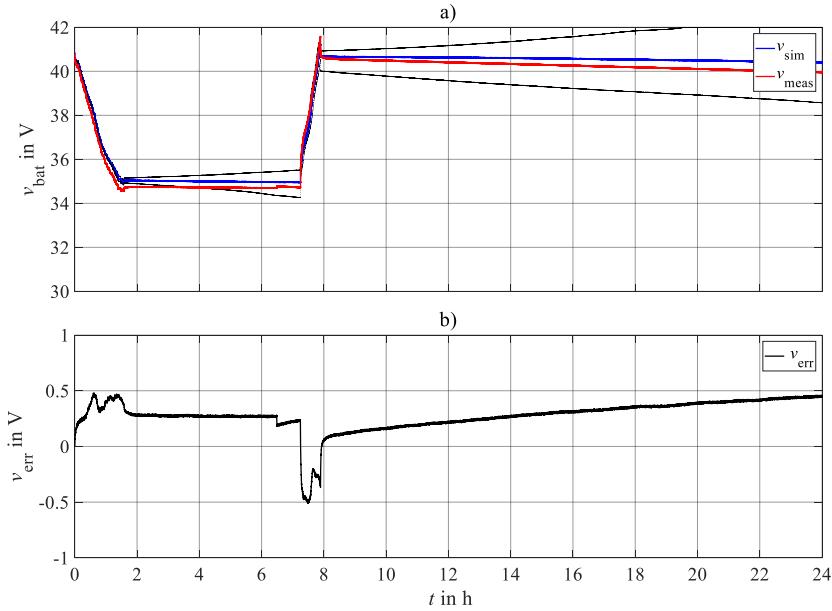
Figure C.5: Comparison of the simulated terminal voltage (blue) and the measured terminal voltage (red) of battery 2 for the peak shaving scenario. The dotted lines show exemplary simulations with the maximum specified current measurement error of the battery test system. a) terminal voltages, b) model error.

XIII
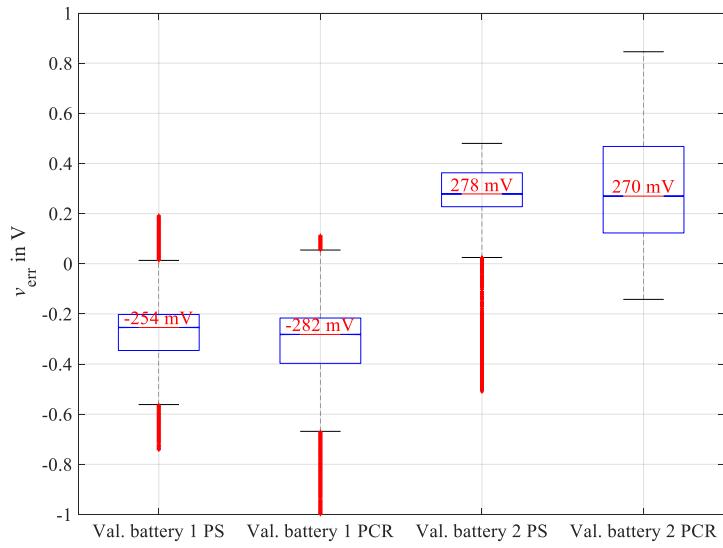
Figure C.6: Model error of the terminal voltage of the battery model. The red central mark indicates the median value and the box indicates the 25th and 75th percentiles, respectively.
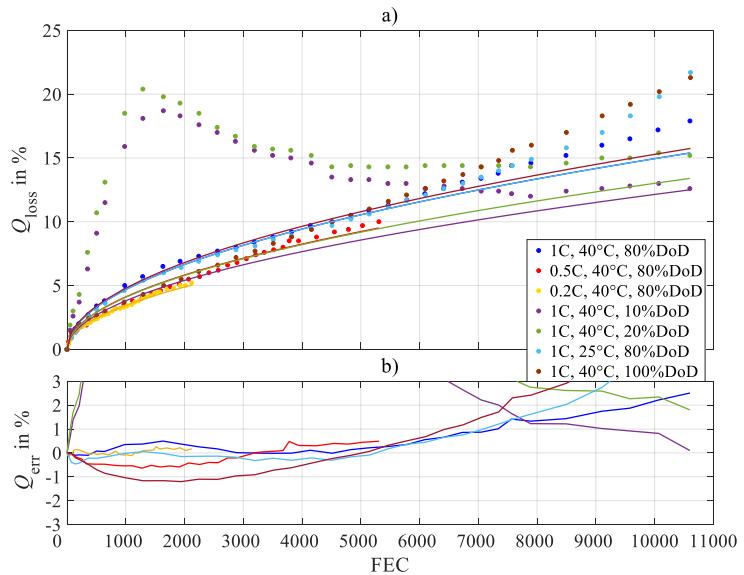

Figure C.7: Results of the generic aging model using the data of the cycle aging experiment presented in [72]. a) loss of relative discharge capacity, b) model error.
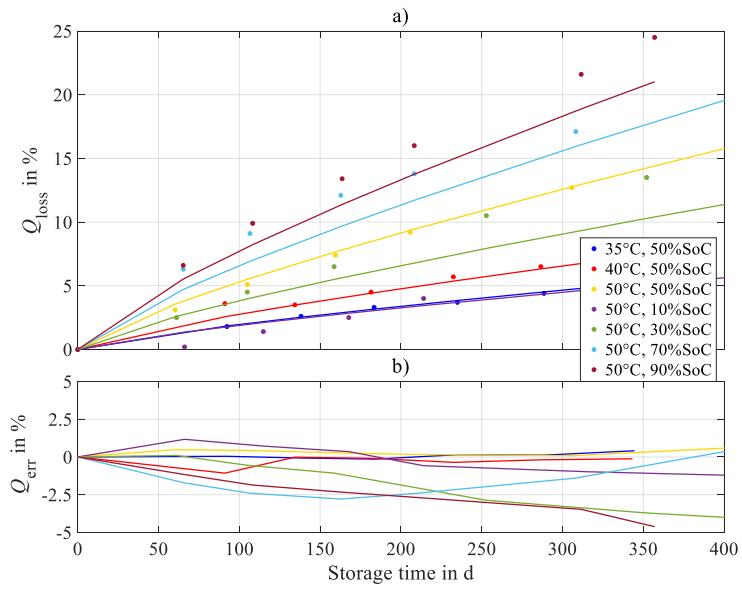
Figure C.8: Results of the generic aging model using the data of the calendar aging experiment presented in [68]. a) loss of relative discharge capacity, b) model error.
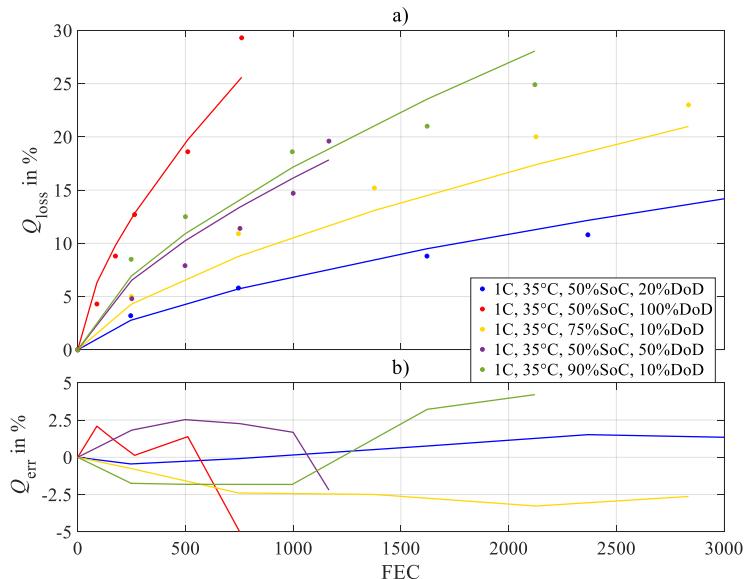
Figure C.9: Results of the generic aging model using the data of the cycle aging experiment presented in [68]. a) loss of relative discharge capacity, b) model error.
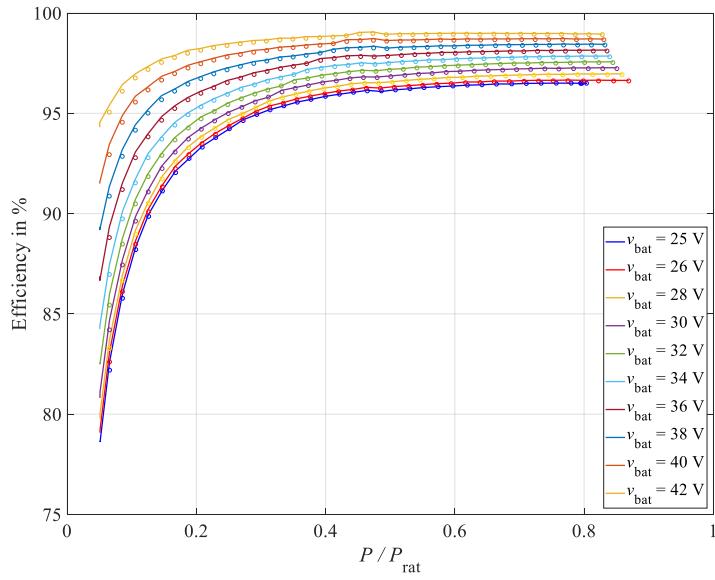
Figure C.10: Efficiency curves of the applied bidirectional dynamic synchronous buck-boost converter at a primary side voltage of 45 V. The solid lines show the measured efficiencies at different secondary side voltages, and the markers represent the corresponding simulated efficiencies.
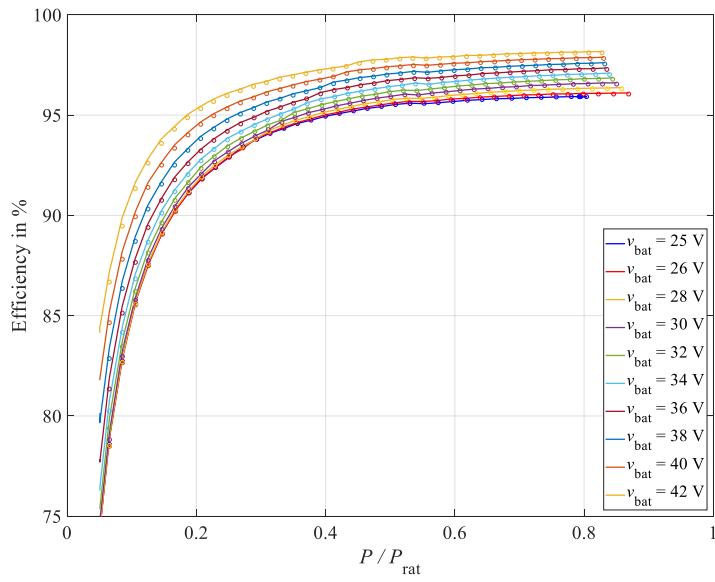
Figure C.11: Efficiency curves of the applied bidirectional dynamic synchronous buck-boost converter at a primary side voltage of 52 V. The solid lines show the measured efficiencies at different secondary side voltages, and the markers represent the corresponding simulated efficiencies.
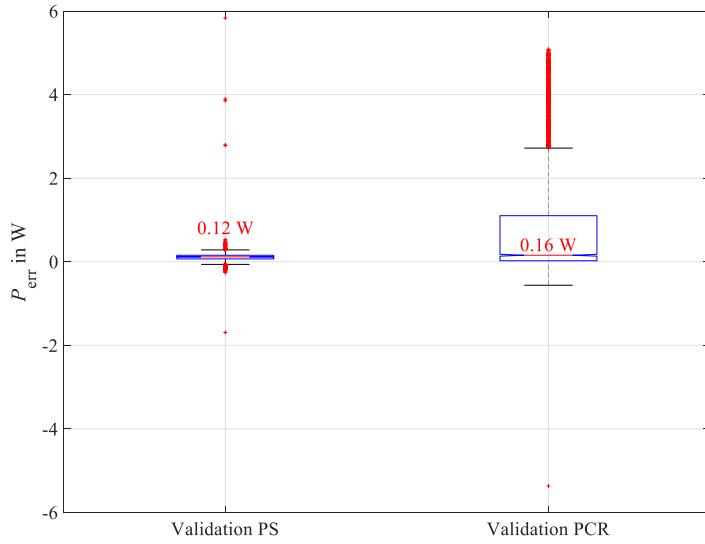
Figure C.12: Model error of the output power of the simulation model. The red central mark indicates the median value and the box indicates the 25th and 75th percentiles, respectively.
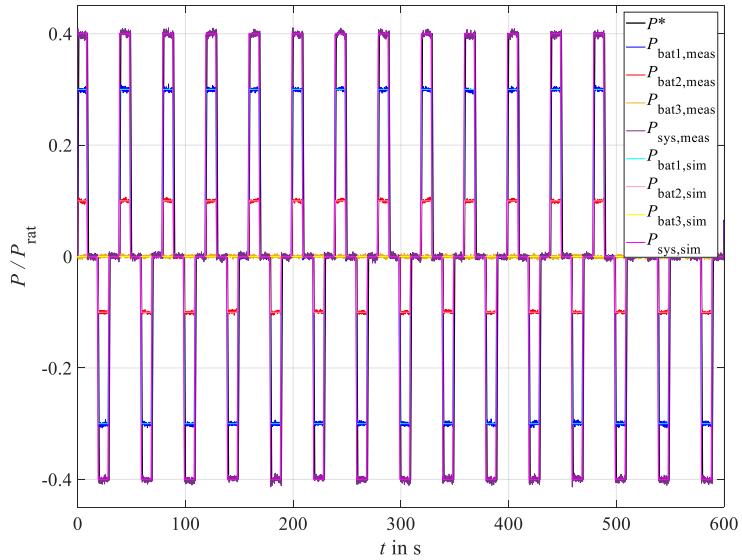

Figure C.13: Test case for verification of the control scheme. Dynamic load profile with a requested power P^* of 40 % of the rated BESS power and the sequential PFCS (PFCS Pseq) with the two design variables $P_{\max} = 150\,\mathrm{W}$ and $Sorting = 0$.
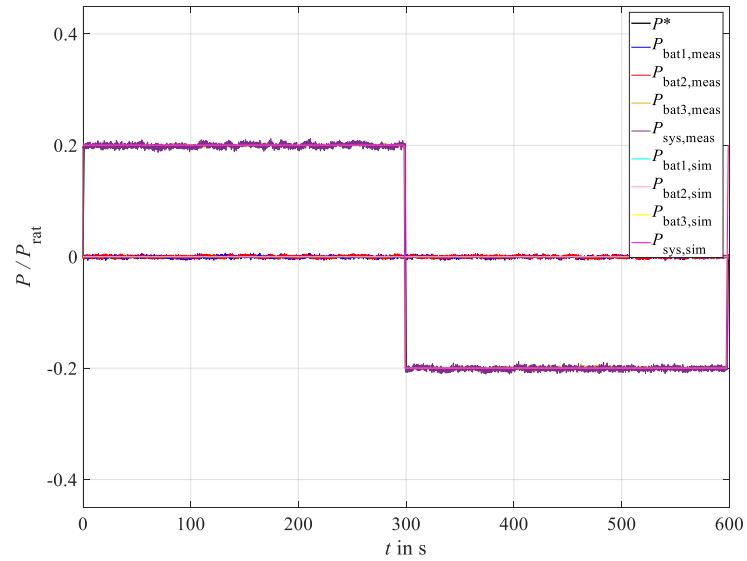
Figure C.14: Test case for verification of the control scheme. Static load profile with a requested power P^* of 20 % of the rated BESS power and the sequential PFCS (PFCS Pseq) with the two design variables $P_{\max} = 500\,\mathrm{W}$ and $Sorting = 1$.
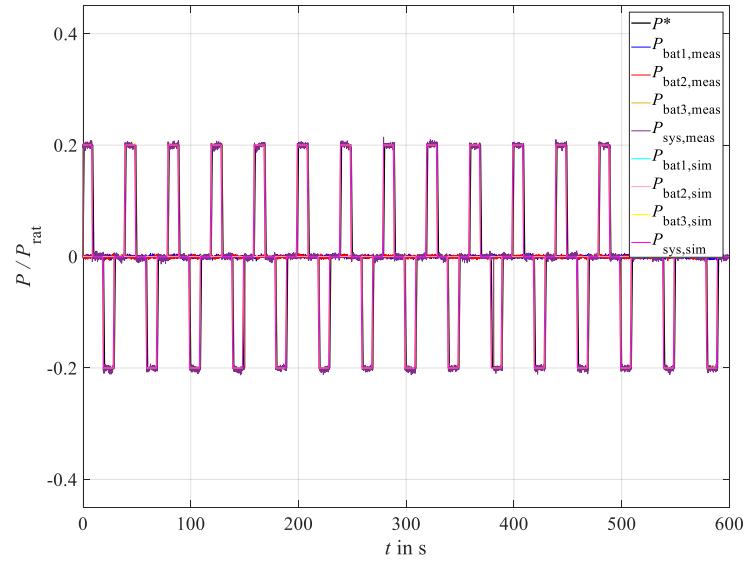
Figure C.15: Test case for verification of the control scheme. Dynamic load profile with a requested power P^* of 20 % of the rated BESS power and the sequential PFCS (PFCS Pseq) with the two design variables $P_{\max} = 500\,\mathrm{W}$ and $Sorting = 1$.
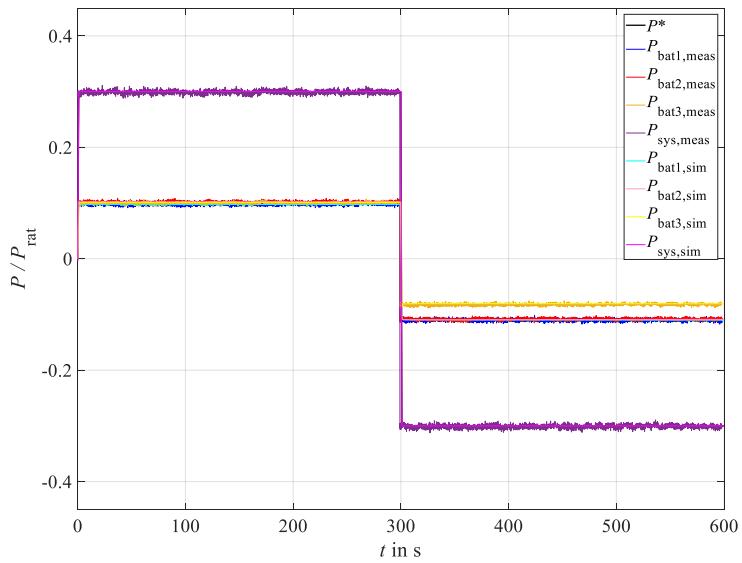
Figure C.16: Test case for verification of the control scheme. Static load profile with a requested power P^* of 30 % of the rated BESS power and the parametric PFCS (PFCS SoAP) with the two design variables $t_{\mathrm{pred,p}} = 1\,\mathrm{s}$ and $t_{\mathrm{pred,e}} = 1\,\mathrm{s}$.
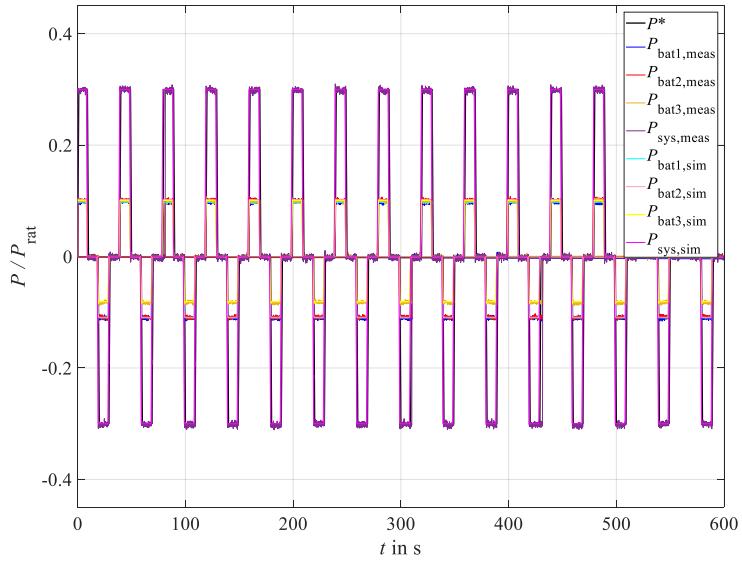
Figure C.17: Test case for verification of the control scheme. Dynamic load profile with a requested power P^* of 30 % of the rated BESS power and the parametric PFCS (PFCS SoAP) with the two design variables $t_{\mathrm{pred,p}} = 1\,\mathrm{s}$ and $t_{\mathrm{pred,e}} = 1\,\mathrm{s}$.
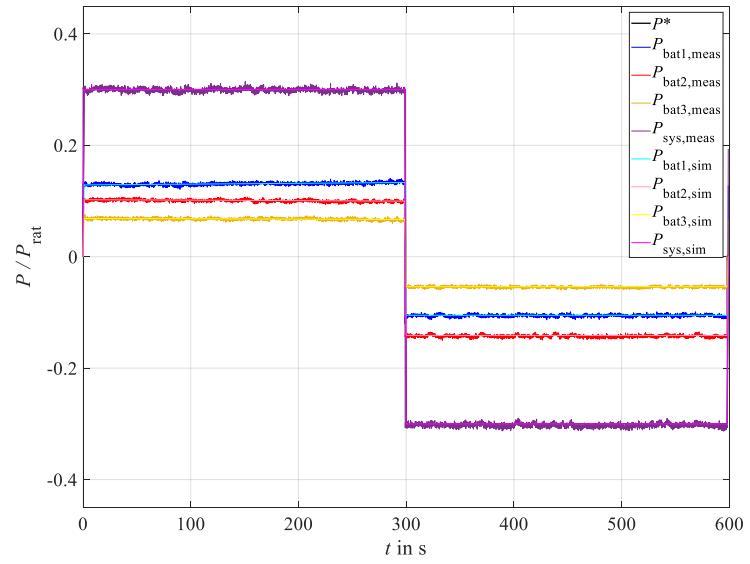
Figure C.18: Test case for verification of the control scheme. Static load profile with a requested power P^* of 30% of the rated BESS power and the parametric PFCS (PFCS SoAP) with the two design variables $t_{\mathrm{pred,p}} = 10\,\mathrm{s}$ and $t_{\mathrm{pred,e}} = 1200\,\mathrm{s}$.
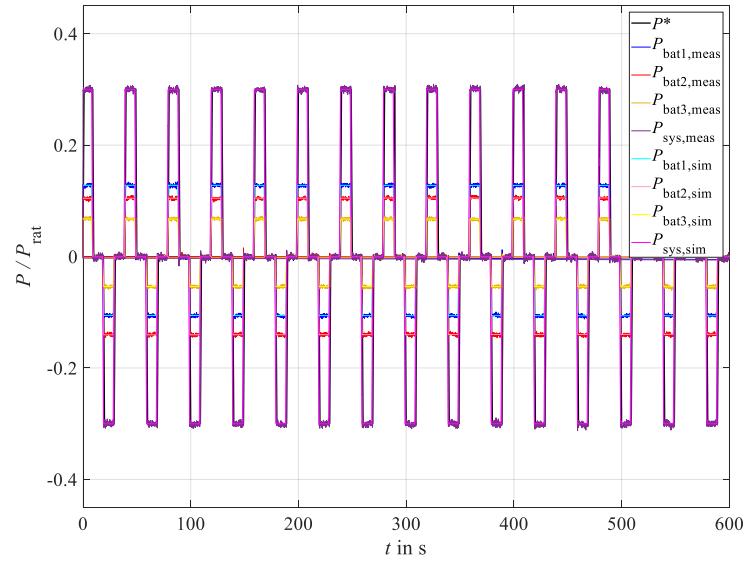
Figure C.19: Test case for verification of the control scheme. Dynamic load profile with a requested power P^* of 30% of the rated BESS power and the parametric PFCS (PFCS SoAP) with the two design variables $t_{\mathrm{pred,p}} = 10\,\mathrm{s}$ and $t_{\mathrm{pred,e}} = 1200\,\mathrm{s}$.
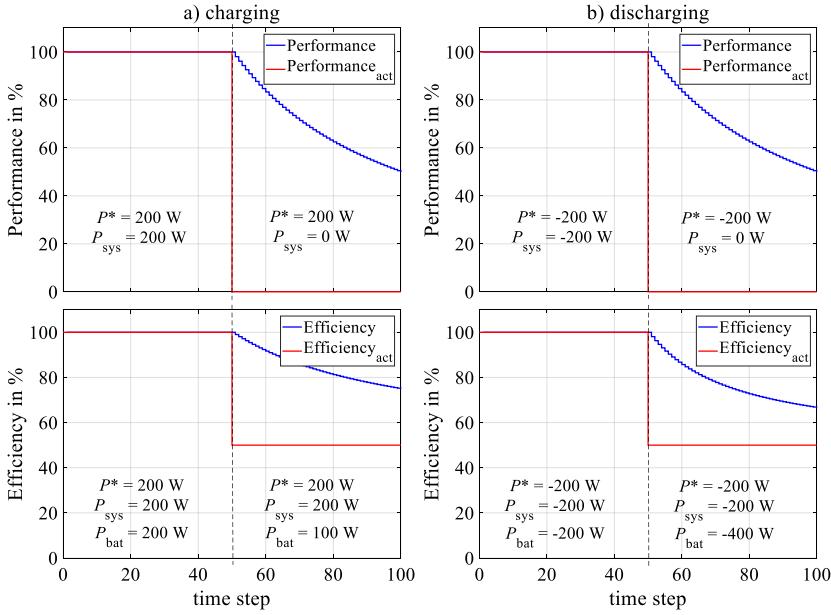
Figure C.20: Formal verification of the target indicators "performance" and "efficiency" for a) charging and b) discharging. Within the first 50 time steps, the requested power P^* was fulfilled at any time. After 50 time steps, the system power P_{sys} was set to 0 in the case of the performance criterion. Thus, the overall performance was reduced to 50 %. In the case of the efficiency criterion, after 50 time steps, only the battery power P_{bat} was changed to 100 W and -400 W, respectively. Consequently, the overall efficiency was reduced to 75 % and 66.7 %, respectively. These results prove the correct implementation.
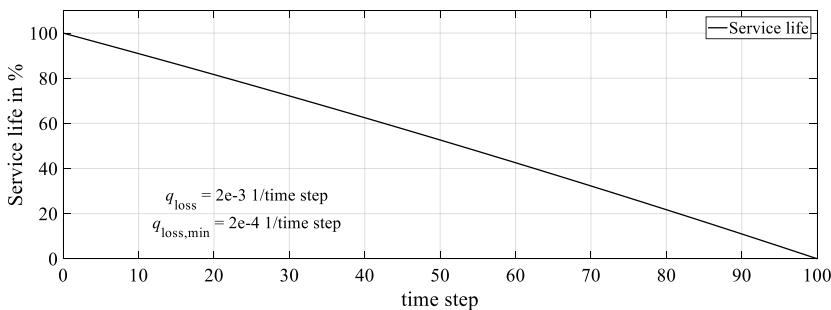
Figure C.21: Formal verification of the target indicator "service life." The differential capacity loss q_{loss} was set to 2e-3 1/time step, the minimum differential capacity loss due to calendar aging $q_{\mathrm{loss,min}}$ to 2e-4 1/time step, and the maximum allowed capacity loss $Q_{\mathrm{loss,max}}$ to 0.2 within the 100 time steps. Thus, service life was reduced to 0 % within the 100 time steps. These results prove the correct implementation.
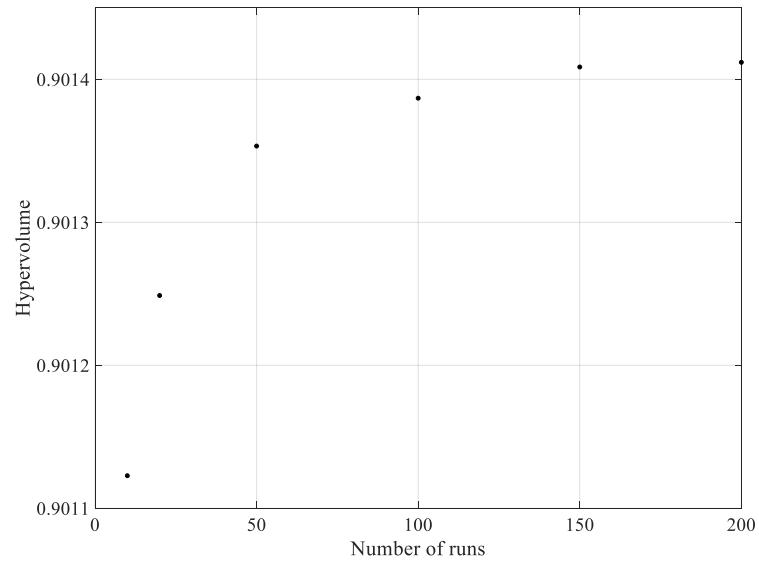
Figure C.22: Preliminary analysis to determine the number of simulation runs. The heterogeneity was set to 1.5 and the profile scaling factor amounted to 20 %. The results indicate that 100 simulation runs are reasonable as this constitutes an acceptable cost-benefit ratio.
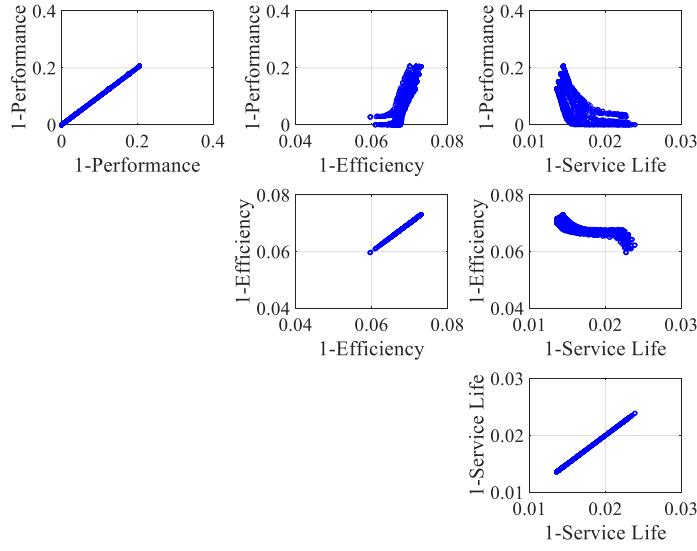
Figure C.23: Results of the parametric PFCS (PFCS SoAP) potential analysis for the peak shaving scenario within the specified design space, use case space, and target indicator space. The target indicator "service life" was considered the worst service life among all BESSs here.
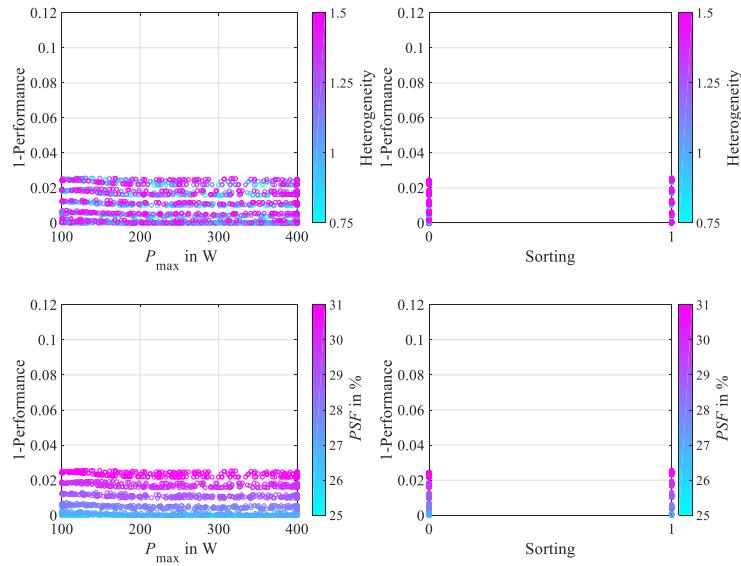

Figure C.24: Real data sensitivity analysis of the target indicator "performance" concerning the design variables of the sequential PFCS (PFCS Pseq) and the use case variables of the frequency regulation scenario. The correlations are comparable to the ones described in Section 6.2.
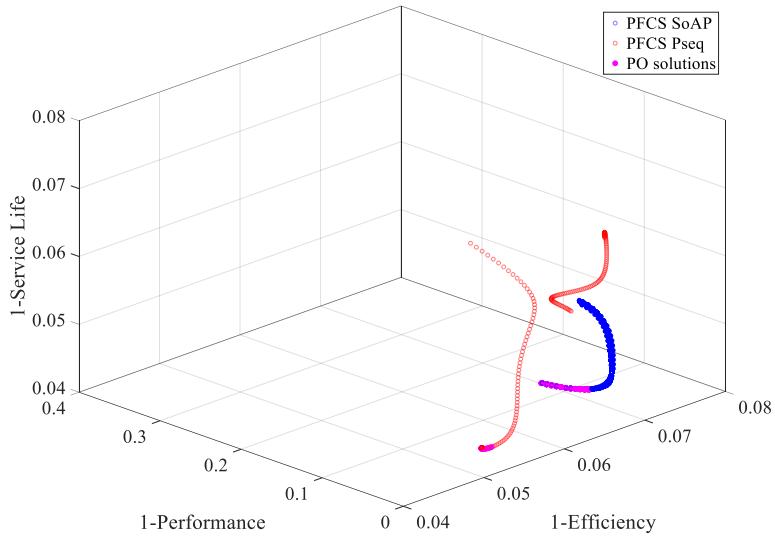
Figure C.25: Analysis of the surrogate model-based results concerning the parametric and sequential PFCS for the specified peak shaving scenario, emphasizing PO solutions (pink markers). The heterogeneity was set to 1.5 and the profile scaling factor amounted to 20 %.
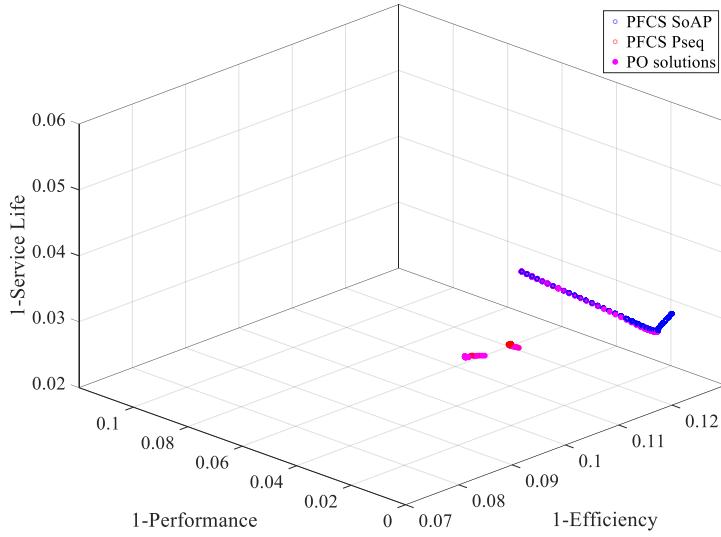

Figure C.26: Analysis of the surrogate model-based results concerning the parametric and sequential PFCS for the specified frequency regulation scenario, emphasizing PO solutions (pink markers). The heterogeneity was set to 0.75 and the profile scaling factor amounted to 27 %.

D Deutsche Zusammenfassung

In den vergangenen Jahren hat sich durch die Integration erneuerbarer Energien in vielen Ländern weltweit eine rasche Umgestaltung der Stromnetze vollzogen. Die damit verbundene und zunehmend volatile Stromerzeugung sowie auch der unregelmäßigere Verbrauch zwingen die Netzbetreiber dazu resultierende Stromschwankungen auszugleichen. Batteriespeichersysteme sind dafür prädestiniert eine reibungslose Integration erneuerbarer Energien zu gewährleisten, erfordern aber ein entsprechendes Energiemanagement. Forschungsarbeiten in diesem Gebiet haben gezeigt, dass ein koordinierter Betrieb einen wesentlichen Beitrag zur Zuverlässigkeit von Energiespeichersystemen und somit von Stromnetzen leistet. Die Entwicklung von Batteriespeichersystemen erfordert unter anderem Betriebsstrategien zur effizienten Leistungsflusssteuerung bei sich schnell und kontinuierlich ändernden Leistungsanforderungen. Daher zielt diese Arbeit darauf ab, die Potenziale und Sensitivitäten von, teilweise in dieser Arbeit entwickelten, Betriebsstrategien für heterogene Batteriespeichersysteme in verschiedenen Anwendungen und Systemkonfigurationen zu identifizieren, zu quantifizieren und schließlich zu bewerten.

In Kapitel 1 wird dazu zu Beginn eine Einführung in das Themengebiet der Batteriespeichersysteme und deren Betriebsstrategien gegeben. Diese Thematik wird durch die Idee motiviert, Batteriespeichersysteme nachhaltig zu betreiben, um wirtschaftliche, ökologische und soziale Vorteile zu erzielen. Jedoch sind Kenntnisse über die Wirkungszusammenhänge erforderlich, um den nachhaltigen Betrieb solcher Systeme zu ermöglichen. Diese Zusammenhänge sind meist nicht unmittelbar ersichtlich, da es keine einfachen logischen Verfahren für den nachhaltigen Betrieb von Batteriespeichersystemen gibt. Gemäß dem *Cynefin Framework für Ingenieure* [9] wird damit die gegebene Problemstellung zu einem komplexen Problem. Komplexe Probleme wiederum erfordern bei der Auswahl einer nachhaltigen Betriebsstrategie einen Vergleich zwischen identifizierten möglichen Lösungen.

Im Anschluss zur Aufarbeitung der Grundlagen von Batteriespeichersystemen werden in Kapitel 2 geeignete Betriebsstrategien und Anwendungsfälle für Batteriespeichersysteme identifiziert und entwickelt. Darüber hinaus werden geeignete Zielindikatoren definiert, die die drei genannten Dimensionen der Nachhaltigkeit repräsentieren. Diese Ansätze liefern eine Grundlage für die Quantifizierung der Wirkungszusammenhänge, bei der das Batteriespeichersystem durch eine systematische Variation der verschiedenen Betriebsstrategien und Anwendungsfälle unterschiedlich beeinflusst wird. Dies erfordert das Lösen eines multi-kriteriellen Optimierungsproblems, bei dem die verschiedenen Zielindikatoren gleichzeitig optimiert werden. Aufgrund des nicht vorhandenen analytischen Zusammenhangs zwischen Ein- und Ausgangsgrößen, wird das vorliegende Optimierungsproblem als multi-kriterielles Black-Box Optimierungsproblem betrachtet. Dementsprechend werden in Kapitel 3 die Grundlagen der Mehrzieloptimierung, der multi-kriteriellen Black-Box Optimierung sowie Ansätze zur Lösung solcher Probleme vorgestellt. Die Recherche ergibt, dass die von Palm und Holzmann [159] vorgeschlagene Methode der Hyper Space Exploration als nützliches Werkzeug zur Lösung des vorhandenen Optimierungsproblems gilt.

Um die Wirkungszusammenhänge von heterogenen Batteriespeichersystemen zu analysieren, wird ein experimentelles Forschungsdesign auf der Grundlage von Simulationen verwendet. Dafür ist wiederum ein geeigneter methodischer Rahmen erforderlich, der ein validiertes Simulationsmodell eines Batteriespeichersystems und die Hyper Space Exploration umfasst. Zu diesem Zweck wird in Kapitel 4 ein Simulationsmodell entwickelt und dessen Module verifiziert bzw. validiert. Weiterhin wird in Kapitel 5 ein an das Batteriespeichersystem angepasster Prozessablauf der Hyper Space Exploration als Teil einer gesamtheitlichen Werkzeugkette beschrieben. Die Erwartungshaltung dabei ist, dass dadurch das multi-kriterielle Black-Box Optimierungsproblem gelöst wird und die Wirkungszusammenhänge tiefgreifend analysiert werden. Bei der Anwendung des vorgestellten methodischen Rahmens sind zwei entscheidende Punkte von großer Bedeutung. Erstens ist es bei der Anwendung der Hyper Space Exploration aufgrund der umfangreichen Parametervariation schwierig, die Gültigkeit jedes erzielten Ergebnisses zu gewährleisten. Dementsprechend muss die Übertragbarkeit jedes Teilmoduls des Simulationsmodells (Batterie, DC/DC-Wandler und Regelungskonzept) bei variierenden Eingangsvariablen untersucht und so die Validität der Ergebnisse bestätigt werden. Zweitens sind geeignete Methoden zur Auswertung und Visualisierung der Ergeb-

nisse erforderlich, um diese eindeutig interpretieren zu können. Demnach liefern diese Methoden entweder Einblicke in einzugehende Kompromisse zwischen den Zielindikatoren, analysieren die Wirkungszusammenhänge bei verschiedenen Betriebsstrategien oder identifizieren Pareto-optimale Lösungen für einen bestimmten Anwendungsfall.

Der methodische Rahmen bietet somit die notwendige Grundlage für eine umfassende Analyse. Um die Wirkungszusammenhänge in komplexen Batteriespeichersystemen zu verstehen und einen nachhaltigen Betrieb zu ermöglichen, müssen verschiedene Betriebsstrategien systematisch analysiert werden. Daher werden in Kapitel 6 die Ergebnisse von zwei Betriebsstrategien für zwei unterschiedliche Anwendungsfälle vorgestellt. Entsprechend der Struktur des methodischen Rahmens und seiner Bewertungsmethoden wird für jede Betriebsstrategie eine dreiteilige Analyse durchgeführt, um die Forschungsfragen umfassend zu beantworten. Die Ergebnisse legen nahe, dass der methodische Rahmen einen generischen Prozess zur Lösung des multi-kriteriellen Black-Box Optimierungsproblems bietet. Weiterhin zeigen sie, dass die einzugehenden Kompromisse zwischen den Zielindikatoren „Funktionserfüllung", „Effizienz" und „Lebensdauer" genau quantifiziert werden können. Darüber hinaus werden die einzelnen Einflüsse der Betriebsstrategien und Anwendungen auf die Zielindikatoren bewertet und visualisiert. Dadurch kann gezeigt werden, dass z.B. die Heterogenität eines Batteriespeichersystems je nach verwendeter Betriebsstrategie die Lebensdauer der Batterien unterschiedlich beeinflusst. Zusammengefasst verdeutlichen die Ergebnisse, dass sowohl die grundlegende Basis (z.B. geeignete Zielindikatoren) als auch die Methoden zur Auswertung und Visualisierung der Ergebnisse ausreichen, um das erforderliche Wissen über Wirkungszusammenhänge für den nachhaltigen Betrieb heterogener Batteriespeichersysteme zu gewinnen.

Die Diskussion in Kapitel 7 verdeutlicht, dass der methodische Rahmen die Potenziale und Sensitivitäten verschiedener Betriebsstrategien für heterogene Batteriespeichersysteme effektiv und effizient quantifiziert und damit die Forschungsfragen fundiert beantwortet. Der methodische Rahmen ermöglicht eine umfassende Potenzialanalyse zur genauen Quantifizierung der bestehenden Kompromisse zwischen den Zielindikatoren. Weiterhin verbessert die auf einem Surrogatmodell basierende Sensitivitätsanalyse das Verständnis der Wirkungszusammenhänge erheblich. Mit Hilfe des Surrogatmodells können zudem Pareto-optimale Lösungen

ermittelt werden, aus denen sich Designregeln ableiten lassen, die den Betreibern einen nachhaltigen und zuverlässigen Betrieb von Batteriespeichersystemen ermöglichen. Die Ergebnisse dieser Studie legen demnach dar, dass die Betriebsstrategie und der Anwendungsfall wesentliche Faktoren sind, die beim Betrieb heterogener Batteriespeichersysteme zu berücksichtigen sind. Beide Faktoren sind für die resultierende Leistungsaufteilung innerhalb des Systems essenziell. Die Leistungsaufteilung wiederum ist der entscheidende Punkt für einen zuverlässigen und nachhaltigen Betrieb. Somit wird die konzeptionelle Prämisse unterstützt, dass ein nachhaltiger Betrieb von der resultierenden Leistungsverteilung innerhalb des Systems abhängt.

Abschließend werden in Kapitel 8 nochmal die Hauptpunkte der einzelnen Kapitel in reflektierender Form wiedergegeben, die wesentlichen Limitierungen dieser Arbeit aufgezählt und gleichzeitig die Themen adressiert, die zukünftig behandelt werden sollten. Die drei genannten Kernpunkte sind die Entscheidungsfindung nach dem Optimierungsprozess, die Entwicklung einer global optimalen Betriebsstrategie und die Übertragung des methodischen Rahmens auf weitere Systeme, bei denen Batteriespeichersysteme eingesetzt werden.

Zusammengefasst leistet diese Arbeit einen wesentlichen Beitrag zum aktuellen Wissensstand von Betriebsstrategien für Batteriespeichersysteme, indem sie einen methodischen Rahmen für die Analyse und Entwicklung von Batteriespeichersystemen für Forschung und Industrie bietet. Die Vorteile, die sich aus dem methodischen Rahmen ergeben, können die Anforderungen von Systembetreibern in einem breiten Spektrum unterschiedlicher Anwendungen erfüllen.

E List of publications

The research presented in this work results from close collaboration with colleagues and is partly based on the following scientific contributions:

Conference presentations

M. Mühlbauer, D. Goldmann, M. A. Danzer, S. Schramm, and O. Bohlen. "UnABESA - Universelle Anbindung von Batteriespeichern aus Elektrofahrzeugen für Stationäre Anwendungen." *25. DESIGN&ELEKTRONIK Entwickler- und Anwenderforum Batterien und Ladekonzepte.* München, 2018.

M. Muehlbauer, M. A. Danzer, and O. Bohlen. "Analysis and Control of Heterogeneous Battery Systems." *Advanced Battery Power Conference 2018.* Münster, 2018.

M. Muehlbauer, M. A. Danzer, and O. Bohlen. "Comparison of Power Flow Control Strategies in Heterogeneous Battery Energy Storage Systems." *Advanced Battery Power Conference 2019.* Aachen, 2019.

M. Muehlbauer, S. Klier, H. Palm, O. Bohlen, and M. A. Danzer, "A Novel Power Flow Control Strategy for Heterogeneous Battery Energy Storage Systems Based on Prognostic Algorithms for Batteries." *22nd European Conference on Power Electronics and Applications (EPE '20 ECCE Europe).* Lyon, 2020.

M. Mühlbauer, O. Bohlen, and M. A. Danzer. "Impact of Power Flow Control Strategies on the Degradation of Lithium-Ion Batteries in Heterogeneous Battery Energy Storage Systems." *Advanced Battery Power Conference 2021.* 2021.

Conference proceedings

M. Muehlbauer, S. Klier, H. Palm, O. Bohlen, and M. A. Danzer, "A Novel Power Flow Control Strategy for Heterogeneous Battery Energy Storage Systems Based on Prognostic Algorithms for Batteries." *22nd European Conference on Power Electronics and Applications (EPE '20 ECCE Europe).* Lyon, 2020.

Journal articles

M. Bauer, M. Muehlbauer, O. Bohlen, M. A. Danzer, and J. Lygeros. "Power Flow in Heterogeneous Battery Systems." *Journal of Energy Storage 25*, p. 100816. 2019.

D. Kucevic, B. Tepe, S. Englberger, A. Parlikar, M. Mühlbauer, O. Bohlen, A. Jossen, and H. Hesse. "Standard battery energy storage system profiles: Analysis of various applications for stationary energy storage systems using a holistic simulation framework." *Journal of Energy Storage 28*, p. 101077. 2020.

M. Mühlbauer, O. Bohlen, and M. A. Danzer. "Analysis of Power Flow Control Strategies in Heterogeneous Battery Energy Storage Systems." *Journal of Energy Storage 30*, p. 101415. 2020.

M. Mühlbauer, F. Rang, H. Palm, O. Bohlen, and M. A. Danzer. "Pareto-optimal power flow control in heterogeneous battery energy storage systems." *Journal of Energy Storage 48*, p. 103803. 2022.

T. Rüther, P. Mößle, M. Mühlbauer, O. Bohlen, and M. A. Danzer. "An iterative dynamic programming approach for the validation of power flow control strategies in heterogeneous multi-state battery systems." (submitted 2021)

Patents

M. Mühlbauer and O. Bohlen. "Verfahren zum Bestimmen eines Leistungsanteils, Betriebsverfahren, Steuereinheit, Energiespeicheranordnung und Stromnetz." Pat. DE 10 2019 212 762. 2021.

F Curriculum vitae

Professional experience

02/2022 - **Research assistant**
11/2017   Munich University of Applied Sciences

01/2020 - **Visiting scholar**
09/2019   North Carolina State University - FREEDM Systems Center

10/2017 - **Master thesis**
04/2017   BMW AG

04/2017 - **Student assistant - Energy systems**
04/2016   Munich University of Applied Sciences

03/2016 - **Bachelor thesis**
10/2015   Vispiron Energy GmbH & Co. KG

01/2015 - **Internship - Energy**
08/2014   Vispiron Energy GmbH & Co. KG

05/2012 - **Vocational training - Electronics technician**
09/2009   Zollner Elektronik AG

Education

02/2022 - **Doctoral researcher (Dr.-Ing.)**
01/2018   University of Bayreuth and Munich University of Applied Sciences

10/2017 - **Master (M. Sc.) - Electrical Engineering**
03/2016   Munich University of Applied Sciences

03/2016 - **Bachelor (B. Eng.) - Renewable Energies**
10/2012   Munich University of Applied Sciences